LEABHARLANN CHOLÁISTE NA TRÍONÓIDE, BAILE ÁTHA CLIATH | TRINITY COLLEGE LIBRARY DUBLIN
Ollscoil Átha Cliath | The University of Dublin

Terms and Conditions of Use of Digitised Theses from Trinity College Library Dublin

Copyright statement

All material supplied by Trinity College Library is protected by copyright (under the Copyright and Related Rights Act, 2000 as amended) and other relevant Intellectual Property Rights. By accessing and using a Digitised Thesis from Trinity College Library you acknowledge that all Intellectual Property Rights in any Works supplied are the sole and exclusive property of the copyright and/or other IPR holder. Specific copyright holders may not be explicitly identified. Use of materials from other sources within a thesis should not be construed as a claim over them.

A non-exclusive, non-transferable licence is hereby granted to those using or reproducing, in whole or in part, the material for valid purposes, providing the copyright owners are acknowledged using the normal conventions. Where specific permission to use material is required, this is identified and such permission must be sought from the copyright holder or agency cited.

Liability statement

By using a Digitised Thesis, I accept that Trinity College Dublin bears no legal responsibility for the accuracy, legality or comprehensiveness of materials contained within the thesis, and that Trinity College Dublin accepts no liability for indirect, consequential, or incidental, damages or losses arising from use of the thesis for whatever reason. Information located in a thesis may be subject to specific use constraints, details of which may not be explicitly described. It is the responsibility of potential and actual users to be aware of such constraints and to abide by them. By making use of material from a digitised thesis, you accept these copyright and disclaimer provisions. Where it is brought to the attention of Trinity College Library that there may be a breach of copyright or other restraint, it is the policy to withdraw or take down access to a thesis while the issue is being resolved.

Access Agreement

By using a Digitised Thesis from Trinity College Library you are bound by the following Terms & Conditions. Please read them carefully.

I have read and I understand the following statement: All material supplied via a Digitised Thesis from Trinity College Library is protected by copyright and other intellectual property rights, and duplication or sale of all or part of any of a thesis is not permitted, except that material may be duplicated by you for your research use or for educational purposes in electronic or print form providing the copyright owners are acknowledged using the normal conventions. You must obtain permission for any other use. Electronic or print copies may not be offered, whether for sale or otherwise to anyone. This copy has been supplied on the understanding that it is copyright material and that no quotation from the thesis may be published without proper acknowledgement.

Passive mechanical properties of skeletal muscle in compression

by

Mélanie Van Loocke

A thesis submitted to the University of Dublin in partial fulfilment of the requirements for the degree of

Doctor in philosophy

Trinity College Dublin

July 2007

Supervisors

Mr. Garry Lyons and Dr. Ciaran Simms

External examiner

Prof. Peter McHugh

(National University of Ireland, Galway)

Internal examiner

Prof. Henry Rice

(Department of Mechanical Engineering)

TRINITY COLLEGE
16 JAN 2008
LIBRARY DUBLIN
THESIS
8304

Declaration

I declare that I am the sole author of this thesis and that the work presented in it, unless otherwise referenced, is entirely my own. I also declare that the work has not been submitted, in whole or in part, to any other University as an exercise for a degree or other qualification.

I agree that the library of Trinity College Dublin may lend or copy this thesis upon request.



Mélanie Van Loocke

September 2007

Acknowledgements

I first came to Dublin for my final year project in college and was supposed to stay there for five months. This was four years and a half ago and my fantastic adventure in Dublin only comes to an end.

First, I would like to thank Prof. Patrick Prendergast who is the first person I contacted in Dublin and without whom this journey would not have started.

I would like to express my most profound gratitude to my supervisors, Mr. Garry Lyons and Dr. Ciaran Simms, who gave me the opportunity to realise this project. From the start, they both provided constant advice, encouragements and guidance, which made this experience so pleasant. I would like to thank them both for their time; Garry for the hours spent in the workshop, designing and building the experimental setup; and Ciaran for the hours spent trying to make sense of experimental results and working on mathematical developments.

Special thanks are due to all the postgrads (past and present) of the Mechanical Engineering department. Being away from home was not always easy but they managed to make me feel at home in Ireland and a lot of them have become really good friends. I won't mention names to make sure I don't forget anyone; i'm sure they will recognise themselves.

I also would like to thank Sheena Brown, the administator of the centre for her availability, her kindness and efficiency in organising conferences, meetings and sorting out all the paperwork.

Many thanks are due to Peter O'Reilly, the chief technicien of the department who was always available when help was needed in the lab.

I wish to thank most sincerely my parents, who always supported and encouraged my choices. And I would like to thank my whole family, specially my sisters, for the "long distance" support they provided during my stay in Dublin.

Finaly, my deepest thanks go to Pierre-François. I admire his patience, his trust and his permanent support during these last four years. I would like to thank him for accepting to travel constantly, organising his life between weekends in Dublin and weekends in Belgium. I hope he realises how much of this achievement is due to him.

Contents

Abstract iii

List of publications resulting from this study v

List of tables vii

List of figures ix

Nomenclature xv

Chapter 1 Introduction 1

This chapter introduces the rationale and objectives of the thesis.

Chapter 2 Literature review 7

This chapter provides background information on which the thesis is based. Skeletal muscle structure and function are first briefly described. A review of experimental data published on skeletal muscle mechanical properties is then provided, outlining the lack of experimental studies investigating muscle compressive properties. A review of constitutive models developed to characterise soft tissues elastic and viscoelastic properties is then provided. These models have rarely been applied to describe skeletal muscle behaviour. This lack of experimental and theoretical data helps understand the need to further investigate skeletal muscle behaviour.

Chapter 3 Muscle elastic properties 53

This chapter describes the procedure developed to characterise skeletal muscle elastic properties. Results from tests performed on animal muscle tissues are presented and a nonlinear transversely isotropic model is proposed to reproduce the observed experimental behaviour; parameters of the model are also provided. The experimental and theoretical

procedures developed to characterise muscle elastic behaviour under compressive loading are then discussed.

Chapter 4 Muscle viscoelastic properties 95

This section investigates the viscoelastic properties of the tissue. Experimental results from relaxation and cyclic tests performed on porcine muscle tissue are presented. A mathematical model based on a discretised form of the quasi-linear theory of viscoelasticity is proposed to represent skeletal muscle properties and parameters of the model are provided. A discussion of experimental and theoretical results obtained is provided.

Chapter 5 Conclusions 179

In this chapter, the main results of this thesis are summarised and guidelines for further improving the understanding of skeletal muscle mechanical properties are provided.

References 191

Appendices Electronic format - cd attached to the thesis. 201

Abstract

The compressive properties of skeletal muscle are of prime interest in applications where muscle tissue is submitted to compressive loads; e.g., to improve the design of protective equipment for vehicular occupants, to improve the biofidelity of simulation tools for surgical procedures or to investigate pressure sore formation. However, little data is available to characterise muscle tissue in compression. The aim of this study was therefore to advance the knowledge of passive skeletal muscle compressive behaviour using a combined experimental and theoretical approach.

Uniaxial unconfined compression experiments were conducted on animal skeletal muscle in order to characterise the elastic and viscoelastic properties of the tissue. The experimental protocol consisted of quasi-static ramps, stress-relaxation and cyclic compression tests performed at various rates and various orientations of the muscle fibres.

Results from the tests performed at a quasi-static rate showed that skeletal muscle has nonlinear, transversely isotropic elastic properties. A transversely isotropic model including strain dependent Young's moduli (SYM model) was developed to represent this behaviour. The SYM model successfully fitted experimental data and also yielded good prediction of muscle behaviour in various orientations of the muscle fibres.

Results from relaxation tests demonstrated that muscle viscoelastic behaviour is also anisotropic; the viscoelastic component being more influential in directions closer to the muscle fibres. Stiffening of the tissue was also observed with an increase in compression rate.

Using a quasi-linear viscoelastic approach, the SYM model was extended with Prony series to account for the tissue viscoelastic properties. This model successfully fitted and predicted the behaviour observed at various rates and orientations of the muscle fibres.

Finally, during low amplitude cyclic tests muscle tissue displayed a linear viscoelastic behaviour and good agreement was obtained between model predictions and experimental results. During higher amplitude tests however, nonlinearity was observed in the tissue behaviour and a nonlinear viscoelastic formulation was required to fit the experimental data. These results represent a unique set of data on skeletal muscle elastic and viscoelastic properties under compressive loading. The model and the parameters proposed provide a powerful tool to improve the biofidelity of future numerical models of the human body.

List of publications resulting from this study

Van Loocke, M., Lyons, C. G., Simms, C. K., 2004. The three-dimensional mechanical properties of skeletal muscle: experiments and modelling. In: Prendergast, P. J., McHugh, P. E., Topics in Bio-Mechanical Engineering. Trinity Centre for Bioengineering & the National Centre for Biomedical Engineering Science: Dublin & Galway, pp. 216-234.

Van Loocke, M., Simms, C. K., Lyons, C. G., 2005. Three dimensional passive properties of muscle tissue in compression. In: Gilchrist, M. D. (Ed.), IUTAM Symposium on Impact Biomechanics: From Fundamental Insights to Applications. Springer, New York, pp. 313-320.

Van Loocke, M., Lyons, C. G., Simms, C. K., 2007. A validated model of passive muscle in compression. Journal of Biomechanics, 39 (16) 2999-3009.

To be submitted:

Van Loocke, M., Lyons, C. G., Simms, C. K. Viscoelastic properties of passive skeletal muscle in compression. Stress-relaxation behaviour and mathematical modeling. Journal of Biomechanics.

Van Loocke, M., Simms, C. K., Lyons, C. G. Viscoelastic properties of passive skeletal muscle in compression. Cyclic behaviour and model predictions. Journal of Biomechanics.

List of tables

Table 2-1: Comparison of muscle fat, collagen and water contents in control patients and patients with progressive muscular distrophy (from Vignos *et al.*, 1959) 11

Table 2-2: Values of Young's modulus used in residual limb models for relaxed bulk muscular tissues 21

Table 2-3: Parameters for Martins' model representing the tensile and compressive behaviour of passive porcine muscle tissue. 36

Table 2-4: Parameters for the Ogden viscoelastic model representing passive rat muscle behaviour in compression (Bosboom *et al.*, 2001a, b) 45

Table 3-1: Values of stress at 30% compression for fresh porcine samples compressed in various fibre orientations - mean ± SD 64

Table 3-2: Parameters for Martins' model fitted to aged bovine and aged porcine data (see equation 3-8). 69

Table 3-3: Parameters (in kPa) for the SYM model fitted to aged bovine and aged porcine data (see equation 3-15) - mean ± standard error. 74

Table 3-4: Correlation coefficients and max error ($\lambda < 0.95$) for SYM model fitted to aged bovine and aged porcine data. 76

Table 3-5: Parameters for Martins' model fitted to fresh porcine data (equation (3-8)) 77

Table 3-6: values of Poisson's ratios - mean ± standard deviation 80

Table 3-7: Parameters (in kPa) for the SYM model fitted on fresh porcine and ovine data - mean ± standard error. 82

Table 3-8: Parameters (in kPa) resulting from the fitting of fresh porcine and ovine data at 45° from the muscle fibre direction - mean ± standard error. 83

Table 3-9: Correlation coefficients and maximum error ($\lambda < 0.95$) for fresh ovine and porcine data 85

Table 3-10: Mean values (± SD) of Young's and shear moduli calculated for aged and fresh porcine muscle tissue (in kPa). 86

Table 4-1: Evolution with deformation rate of the stress reached after 30% compression in various orientations of the muscle fibres - mean ± SD. 105

Table 4-2: Relative contribution of the viscoelastic component to the total stress reached at 30% compression at various strain rates and fibre orientations. 107

Table 4-3: Amount of stress relaxation following compressive ramps at various rates and orientations of the muscle fibres – values taken 300s after the ramp. 110

Table 4-4: Values of stress at 30% compression in quasi-static and relaxation tests (values taken after 300s relaxation) 110
Table 4-5: Relative contribution of the viscoelastic component to the total stress reached at 30% compression at various strain rates. 113
Table 4-6: Parameters m and a for power-law fitting of stress-relaxation curves obtained at various levels of compression in fibre and cross-fibre directions. 116
Table 4-7: Hysteresis ratio (h_r) and stress cycle amplitude calculated after 240s for low amplitude, low frequency tests. 138
Table 4-8: Hysteresis ratio (h_r) and cycles amplitude calculated after 240s for high amplitude, low frequency tests. 143
Table 4-9: Hysteresis ratio (h_r) and stress cycles amplitude calculated after 240s for high amplitude, high frequency tests. 149
Table 4-10: Parameters for the nonlinear viscoelastic SYM model fitted to high amplitude cyclic data obtained at 0.44Hz on fresh porcine muscle tissue in fibre (left) and cross-fibre (right) directions. 160
Table 4-11: Numerical values used to characterise the increase in stress with compression rate for skeletal muscle tissue. 173
Table 5-1: Parameters for the SYM model fitted on fresh porcine data 185
Table 5-2: Parameters for the quasi-linear SYM model fitted on fresh porcine data 186
Table 5-3: Parameters for the nonlinear viscoelastic SYM model fitted on fresh porcine data 187

List of figures

Figure 2-1: General structure of skeletal muscle 9
Figure 2-2: Bovine semitendinosus muscle - Extracellular network shown by scanning electron micrographs after removal of the muscle proteins 10
Figure 2-3: Electron micrograph of a cross section through a tendon from the finger of the squirrel monkey, 13000X 11
Figure 2-4: Theoretical normalised force-length curves of skeletal muscle. 14
Figure 2-5: Comparison of published passive (a) and active (b) muscle force-length characteristics 15
Figure 2-6: Stress-strain curves obtained during unconfined compression of porcine muscle tissue (reproduced from Grieve and Armstrong, 1988). 16
Figure 2-7: Results of compression tests on rat muscle tissue (Bosboom *et al.*, 2001b). 17
Figure 2-8: Typical results from compression tests performed on bovine muscle tissue at various strain rates (reproduced from Van Sligtenhorst *et al.*, 2006) 19
Figure 2-9: Results from compression tests performed on porcine muscle at various strain rates, in the cross-fibre direction (reproduced from Song *et al.*, Article in press). 20
Figure 2-10: Comparison of muscle compressive properties published in the literature. 22
Figure 2-11: Continuum homogeneous deformation. 26
Figure 2-12: Stress components acting on a cube. 29
Figure 2-13: Uniaxial definition of commonly used stresses 30
Figure 2-14: Hill's functional muscle model; parallel elastic element (PE), contractile element (CE), series elastic element (SE). 32
Figure 2-15: Representation of a unidirectional composite. 34
Figure 2-16: Theoretical behaviour of passive porcine muscle under tension and compression along the fibre direction. 37
Figure 2-17: Specimens used to characterise linear elastic, transversely isotropic materials. 38
Figure 2-18: (a) Maxwell model, (b) Kelvin model, (c) Generalised Maxwell model. 40
Figure 3-1: Schematic of specimens used for testing 55
Figure 3-2: Custom made cutting bench. 56
Figure 3-3: Experimental setup used for compression tests 57
Figure 3-4: Compression tests on (left) aged bovine and (right) aged porcine samples. 60
Figure 3-5: Compression tests on (left) aged bovine and (right) aged porcine samples. 61

Figure 3-6: Illustration of the change in shape during compression of a porcine muscle sample in (top) cross-fibre and (bottom) fibre directions. 61
Figure 3-7: Compression tests on fresh ovine samples. 62
Figure 3-8: Compression tests on fresh porcine samples. 63
Figure 3-9: Comparison between original and modified data sets for tests on fresh porcine muscle samples in the cross-fibre direction 64
Figure 3-10: Compression tests on fresh porcine samples. 65
Figure 3-11: Deformation of a porcine sample with fibres oriented at 45° from the direction of testing. 65
Figure 3-12: Evolution of the maximum compressive stress with time after death for fresh ovine (left) and porcine (right) samples. 66
Figure 3-13: Relationship between stretch ratios in directions 1, 2 and 3 70
Figure 3-14: Compression tests on (a) aged bovine and (b) aged porcine samples fitted with Martins' model. 71
Figure 3-15: Residual errors between experimental data and Martins' model for (a) aged bovine and (b) aged porcine muscle. 72
Figure 3-16: Compression tests on (a) aged bovine and (b) aged porcine samples fitted with the SYM model. 75
Figure 3-17: Residual error between experimental data and SYM model for (a) aged bovine and (b) aged porcine muscle. 76
Figure 3-18: Compression tests on fresh porcine samples fitted with Martins' model. 77
Figure 3-19: Residual errors between experimental data and Martins' model for fresh porcine muscle 78
Figure 3-20: Markers displacements during compression tests 79
Figure 3-21: Illustration of the method used to calculate the values of Poisson's ratios v_{ij} (i,j = L,T *or* T'). 80
Figure 3-22: Box and whiskers plot for Poisson's ratios of fresh porcine muscle tissue. 81
Figure 3-23: Schematic explaining the values of Poisson's ratios for muscle tissue in compression. 81
Figure 3-24: Compression tests on fresh ovine muscle samples fitted with the SYM model. 83
Figure 3-25: Compression tests on fresh porcine muscle samples fitted with the SYM model. 84
Figure 3-26: Compression tests on fresh porcine samples - Comparison between experimental data and theoretical predictions using the SYM model. 84
Figure 3-27: Residual error between experimental data and SYM model for fresh porcine muscle 85

Figure 3-28: Evolution with the stretch ratio of the shear modulus and Young's moduli (in fibre, cross-fibre and 45° from the fibre direction) for (a) aged and (b) fresh porcine muscle. 86
Figure 3-29: Elastic properties of skeletal muscle tissue in compression - comparison between data obtained in this study and data published in the literature. 90
Figure 4-1: Deformation history applied to samples during relaxation tests at 1%str.s^{-1} up to 10, 20 and 30% compression. 99
Figure 4-2: Deformation history applied to samples during cyclic tests with (a) 2% and (b) 10% amplitude. 100
Figure 4-3: Custom built high speed cyclic testing rig. 101
Figure 4-4: Stress-stretch curves comparing porcine muscle compressive behaviour at various rates and various orientations of the muscle fibres. 104
Figure 4-5: Evolution with deformation rate of the stress reached after 30% compression in various orientations of the muscle fibres. 105
Figure 4-6: Stress-stretch curves comparing muscle compression behaviour at 0.05, 5 and 10%str.s^{-1} in fibre and cross-fibre directions. 106
Figure 4-7: Typical stress-relaxation curve illustrating the contribution to the total stress (σ_{tot}) of elastic (σ_e) and viscoelastic (σ_v) components. 106
Figure 4-8: Relative contribution of the viscoelastic component to the total stress reached at 30% compression at various strain rates and fibre orientations. 107
Figure 4-9: Stress-relaxation curves obtained at various compression rates and orientations of the muscle fibres. 108
Figure 4-10: Evolution with time of the amount of stress relaxation. Comparison between results obtained at various compression rates. 109
Figure 4-11: Comparison between mean values of stress obtained during quasi-static tests and relaxed values obtained after compressive ramps performed at various rates. 111
Figure 4-12: Evolution with time of the amount of stress relaxation. Comparison between results obtained at various orientations of the muscle fibres 112
Figure 4-13: Relative contribution of the viscoelastic component to the total stress reached at 30% compression at various strain rates and fibre orientations. 113
Figure 4-14: Stress relaxation curves in fibre and cross-fibre directions after 10, 20 and 30% compression at a rate of 1%s^{-1}. 114
Figure 4-15: Evolution with time of the amount of stress relaxation obtained in the fibre and the cross-fibre directions after 10, 20 and 30% compression; compression rate of 1%s^{-1}. 115
Figure 4-16: Stress-relaxation curves on logarithmic scales illustrating the linear trend of the stress decay. 115

Figure 4-17: Evolution of the relaxation rate (m) with compression level..... 116
Figure 4-18: Comparison between experimental data and viscoelastic SYM model fitting - Individual fitting at each rate..... 119
Figure 4-19: Comparison between experimental stress-relaxation results and viscoelastic SYM model fitting in fibre direction..... 122
Figure 4-20: Comparison between experimental stress-relaxation results and viscoelastic SYM model fitting at 45° from the fibre direction..... 123
Figure 4-21: Comparison between experimental stress-relaxation results and viscoelastic SYM model fitting at 60° from the fibre direction..... 124
Figure 4-22: Comparison between experimental stress-relaxation results and viscoelastic SYM model fitting in cross-fibre direction..... 125
Figure 4-23: Comparison between experimental and theoretical relaxed stresses..... 126
Figure 4-24: Comparison between experimental and theoretical peak stresses..... 127
Figure 4-25: Percentage errors between experimental and theoretical (a) relaxed stresses, (b) peak stresses..... 128
Figure 4-26: Comparison between experimental and theoretical stress-relaxation behaviour at 10, 20 and 30% compression..... 129
Figure 4-27: Comparison between experimental stress-relaxation results and viscoelastic SYM model predictions at 60° from the fibre direction..... 132
Figure 4-28: Comparison between experimental and theoretical (a) relaxed stresses, (b) peak stresses..... 133
Figure 4-29: Percentage errors between experimental and theoretical relaxed and peak stresses..... 133
Figure 4-30: (a) and (c) Deformation history applied to porcine samples during low amplitude cyclic compression tests performed respectively at 0.22 and 0.4Hz. (b) and (d) Corresponding cyclic stress-relaxation curves obtained in fibre and cross-fibre directions..... 135
Figure 4-31: (a) and (c) Stress-stretch curves obtained during low amplitude cyclic compression tests of porcine muscle samples performed respectively at 0.22 and 0.4Hz (cross-fibre results). (b) and (d) Corresponding plots of the first two and last twenty cycles..... 136
Figure 4-32: Definition of the hysteresis ratio h_r. A_l and A_u represent respectively the loading and unloading areas..... 137
Figure 4-33: (a) Deformation history applied to fresh porcine samples during high amplitude cyclic compression tests performed at 0.22 Hz. (b) and (c) Corresponding cyclic stress-relaxation curves obtained in fibre and cross-fibre directions..... 139

Figure 4-34: (a) Deformation history applied to fresh porcine samples during high amplitude cyclic compression tests performed at 0.44 Hz. (b) to (e) Corresponding cyclic stress-relaxation curves obtained in fibre and cross-fibre directions. 140
Figure 4-35: Close-up comparing stress-time curves at various orientations of the muscle fibres for high amplitude, low frequency cyclic tests. 141
Figure 4-36: (a) and (c) Stress-stretch curves obtained during high amplitude cyclic compression tests of porcine muscle samples performed respectively at 0.22 and 0.44 Hz (cross-fibre results). (b) and (d) Corresponding plots of the first two and last twenty cycles..... 142
Figure 4-37: Comparison between cyclic relaxation tests with 2, 10, 20 and 30% amplitude. 144
Figure 4-38: Cyclic stress-relaxation curves obtained during high amplitude cyclic compression tests performed at 5Hz, at 0°, 45°, 60° and 90° from the fibre direction. 145
Figure 4-39: Cyclic stress-relaxation curves obtained during high amplitude cyclic compression tests performed at 20Hz, at 0°, 45°, 60° and 90° from the fibre direction. 146
Figure 4-40: Cyclic stress-relaxation curves obtained during high amplitude cyclic compression tests performed at 80Hz, at 0°, 45°, 60° and 90° from the fibre direction. 147
Figure 4-41: Close-up comparing stress-time curves at various orientations of the muscle fibres for high amplitude, high frequency cyclic tests. 148
Figure 4-42: Evolution of the stress cycle amplitude with frequency for 10% amplitude cyclic tests performed on fresh porcine muscle samples. 150
Figure 4-43: Evolution of the hysteresis with frequency for 10% amplitude cyclic tests performed on fresh porcine muscle samples. 151
Figure 4-44: Comparison between experimental results and viscoelastic SYM model predictions for low amplitude cyclic compression tests performed in (left) fibre and (right) cross-fibre directions at 0.22Hz. 153
Figure 4-45: Comparison between experimental results and viscoelastic SYM model predictions for low amplitude cyclic compression tests performed in (left) fibre and (right) cross-fibre directions at 0.4Hz. 154
Figure 4-46: Comparison between experimental results and viscoelastic SYM model predictions for high amplitude cyclic compression tests performed in (left) fibre and (right) cross-fibre directions at 0.44Hz. 155
Figure 4-47: Comparison between experimental results and viscoelastic SYM model predictions for high amplitude cyclic compression tests performed in (left) fibre and (right) cross-fibre directions at 5Hz. 156

Figure 4-48: Comparison between experimental results and viscoelastic SYM model predictions (—) for high amplitude cyclic compression tests performed in (left) fibre and (right) cross-fibre directions at 20Hz. 157
Figure 4-49: Comparison between experimental results and nonlinear viscoelastic SYM model fitting for high amplitude cyclic compression tests performed in fibre (left) and cross-fibre (right) directions at 0.44Hz. 161
Figure 4-50: Comparison between experimental results and nonlinear viscoelastic SYM model predictions for high amplitude cyclic compression tests performed in the fibre direction at 5Hz. 162
Figure 4-51: Evolution with stretch ratio of expressions h_j and a_j, $j \equiv XF$ (see equation 4-21) obtained from fitting to cyclic data in the cross-fibre direction. 163
Figure 4-52: Comparison between experimental stress-relaxation results and nonlinear viscoelastic SYM model predictions in the cross- fibre direction. 164
Figure 4-53: Evolution with deformation rate of the stress reached after 30% compression in various orientations of the muscle fibres. 166
Figure 4-54: Illustration of the influence of the fluid component on muscle viscoelastic behaviour during compression in (a) cross-fibre and (b) fibre directions. 166
Figure 4-55: Relative contribution of the viscoelastic component to the total stress reached at 30% compression at various strain rates and fibre orientations. 167
Figure 4-56: Evolution of (a) the stress cycle amplitude and (b) the hysteresis with frequency for 10% amplitude cyclic tests performed on fresh porcine muscle samples. 169
Figure 4-57: Results from compression tests performed on porcine muscle tissue at various strain rates, in fibre and cross-fibre directions (reproduced from Song *et al.*, Article in press). 172
Figure 4-58: Relative increase in stress with compression rate for skeletal muscle tissue. . 174
Figure 5-1: Elastic properties of fresh porcine muscle tissue under compressive loading in three orientations of the muscle fibres 181
Figure 5-2: Evolution with deformation rate of the stress reached after 30% compression in various orientations of the muscle fibres. 182
Figure 5-3: Relative contribution of the viscoelastic component to the total stress reached at 30% compression at various compression rates and fibre orientations. 182
Figure 5-4: Evolution of the stress cycle amplitude with frequency for 10% amplitude cyclic tests performed on fresh porcine muscle samples (values taken after cyclic relaxation). 183
Figure 5-5: Relative increase in stress with compression rate for skeletal muscle tissue. ... 184

Nomenclature

Roman symbols

Boldface is used for tensors.

a	Amplitude parameter for power-law fitting of stress-relaxation curves
a_j ; j=L,T,45,60	Strain-dependent term in direction j in the nonlinear SYM model
a_{ij} ; i=1,2 ; j=L,T,45,60	Parameters of a_j
a_0	Vector representing the material preferred direction
$\boldsymbol{A} = A_{i_1 i_2 \ldots i_n} e_{i_1} \otimes e_{i_2} \otimes \ldots \otimes e_{i_n}$	Tensor of order n
$[\boldsymbol{A}]$	Matrix notation of tensor $\boldsymbol{A}$
A_{ij}	Components of tensor $\boldsymbol{A}$
$\boldsymbol{A}^T$	Transpose of tensor $\boldsymbol{A}$
$tr(\boldsymbol{A})$	Trace of tensor $\boldsymbol{A}$
A_0, A_t	Respectively initial and current sample areas
A_l, A_u	Respectively loading and unloading areas in a stress cycle
$\boldsymbol{B}$	Left Cauchy-Green dilatation tensor
$\boldsymbol{c}$	Cauchy strain tensor
$\boldsymbol{C}$	Right Cauchy-Green dilatation tensor
c_1, c_2, c_3, *and* c_4	Parameters of Humphrey's and Martins' models
dS, ds	Elementary surfaces respectively in reference and current configurations
du	Elementary displacement
dV, dv	Elementary volumes respectively in reference and current configurations
dX, dx	Elementary segments respectively in reference and current configurations
$\boldsymbol{D}$	Reverse deformation gradient tensor
D_{ijkl}	State variable in Poon's 3D nonlinear viscoelastic model
$\boldsymbol{e}$	Eulerian strain tensor
e_1, e_2, e_3	Orthonormal basis vectors
$e_{\%}$	Error between experimental and theoretical values of stress

E	Young's modulus characterising a linear elastic, isotropic material
$\boldsymbol{E}$	Green-Lagrange (Lagrangian) strain tensor
E_j ; $j=L,T,45,60$	Young's modulus in direction j
E_j^v ; $j=L,T,45,60$	Viscoelastic Young's modulus in direction j.
$E_{S\infty}$ and E_{Si}, $i=1,\ldots,n$	Springs constants in the mechanistic viscoelastic models
$\mathbb{E}$	Euclidean vector space
f_0 , f_t	Respectively the initial and current force in the sample
F_m	Current muscle force
F_{m0}	Maximum isometric muscle force
$\boldsymbol{F}$	Deformation gradient tensor
$\Im$	Functional representing the history of strain in Pioletti's model
$G(t)$	Reduced relaxation function in the QLV
$G_j(t)$	Reduced relaxation function in direction j
$\boldsymbol{G}(t)$	Tensorial reduced relaxation function
$G_l(t)$	Relaxation modulus characterising linear viscoelastic behaviour
G_{LT}	Shear modulus characterising a transversely isotropic material
G_{LT}^v	Viscoelastic shear modulus characterising a transversely isotropic material
$G_n(t)$	Relaxation modulus in Schapery's nonlinear viscoelastic model
G_∞	Equilibrium or final value of $G_n(t)$
$\tilde{G}$	Amplitude of $\Delta G(t)$
$G_{ijkl}(t)$	Components of the relaxation modulus in Poon's 3D nonlinear viscoelastic model
G_{ijkl}^∞	Equilibrium or final value of $G_{ijkl}(t)$
$\tilde{G}_{ijkl}$	Amplitude of $\Delta G_{ijkl}(t)$
h_r	Hysteresis ratio
h_e, h_l, h_2, a_τ	Strain-dependent material properties in Schapery's and Poon's nonlinear viscoelastic models
h_j ; $j=L,T,45,60$	Strain-dependent term in direction j in the nonlinear SYM model
h_{ij} ; $i=1,2$; $j=L,T,45,60$	Parameters of h_j
$\boldsymbol{I}$	Identity tensor
I_1 , I_2 , I_3 , I_4 and I_5	Invariants of the right Cauchy-Green dilatation tensor $\boldsymbol{C}$

J	Jacobian of the deformation gradient tensor $\boldsymbol{F}$
k_1, k_2, k_3, k_4	Li's model parameters
k_{ij}, $i=1,\ldots,3$; $j=L,T,45,60$	Fitting parameters characterising the Young's modulus in direction j
$\boldsymbol{K}$	Compliance matrix relating stress and strain
l_0, l_t	Respectively initial and current sample lengths
L_{i0k} *and* L_{j0k} ; $k=1,2$	Respectively initial horizontal and vertical distances between markers
L_{ik} *and* L_{ik} ; $k=1,2$	Respectively horizontal and vertical distances between markers after compression
L_m	Current muscle length
L_{m0}	Muscle rest length
L^s	External load applied on ds
$L(y_1)$	Exponential integral function
m	Rate of relaxation (slope parameter for power-law fitting of stress-relaxation curves)
N, n	Unit vectors normal to the surface elements dS and ds, respectively in reference and current configurations
p	Lagrange multiplier enforcing incompressibility in Humphrey's and Martins' models
p_i ; $i = 1,..,N$	Amplitude parameters of $G(t)$ (Prony series with N terms)
p_{ij} ; $i = 1,..,N$; $j=L,T,45,60$	Amplitude parameters of $G_j(t)$ (Prony series with N terms)
p_∞	Equilibrium or final value of $G(t)$
$p_{\infty j}$	Equilibrium or final value of $G_j(t)$
P	Material point belonging to Ω
R^2	Correlation coefficient
R_0, R_t	Respectively reference and current configurations
s_i; $i = 1,..,N$	Stress term in the discretised QLV model
s_{ij}; $i = 1,..,N$; $j=L,T,45,60$	Stress term in the discretised QLV model in directon j
$\boldsymbol{S}$	Second Piola-Kirchhoff stress tensor
$\boldsymbol{S}^e$	Instantaneaous elastic (Piola-Kirchhoff second) stress tensor; corresponding to the instantaneous contribution in Pioletti's model
$\boldsymbol{S}^v$	Viscous (Piola-Kirchhoff second) stress tensor; corresponding to the almost immediate contribution in Pioletti's model, i.e. the short time memory
t, t'	Time
t_n	Time at increment n

$\boldsymbol{t}^s$	Current internal stress vector acting along the surface normal n of Ω
T_0	Maximum steady-state stress developed by the muscle under isometric conditions in Martins' model
$\boldsymbol{T}$	First Piola-Kirchhoff stress tensor or Lagrange stress tensor
u	Displacement vector
W	Strain energy function
v, w	Vectors of $\mathbb{E}$
$\lvert v \rvert$	Length of vector v
v_1, v_2, v_3	Components of vector v along the directions e_1, e_2, e_3
$v \otimes w$	Tensor product
v_c	Parameter reflecting the amount of viscoelastic content in Fung's reduced relaxation function
$W_1^{'}$	Derivative of the strain energy function with respect to I_1 in Humphrey's and Martins' models
$W_\alpha^{'}$	Derivative of the strain energy function with respect to α in Humphrey's and Martins' models
X, x	Position vector of point P respectively in the reference and the current configuration

Greek symbols

α	Stretch ratio along the fibre direction
δ_1	Viscoelastic multiplicative parameters in Ogden model
$\Delta G(t)$	Transient component of the relaxation modulus in Schapery's nonlinear viscoelastic model
$\Delta G_{ijkl}(t)$	Transient components of the relaxation modulus in Poon's 3D nonlinear viscoelastic model
Δt; $\Delta\tau$	Time step
∇u	Displacement gradient tensor
$\boldsymbol{\varepsilon}$	Infinitesimal strain tensor
$\tilde{\varepsilon}_i$, $\tilde{\varepsilon}_j$, i,j=L,T,T',45,60	Logarithmic strain respectively in directions i and j for uniaxial tests
ε^t, ε^v	Strains acting respectively on the device and on the dashpot in Kelvin's mechanistic model
η, η_i, i=1,...,n	Dashpots viscosity in the mechanistic viscoelastic models
θ	Angle between vectors v and w
λ	Stretch ratio in the direction of testing in a uniaxial test
λ_i; i = 1,2,3	Principal stretch ratio in direction i

μ_1 *and* μ_2	Elastic parameters in Ogden model
ν	Poisson's ratio characterising a linear elastic, isotropic material
ν_{ij} ; *i,j = L,T or T'*	Poisson's ratios characterising a transversely isotropic material
ξ_{ijkl}	Reduced time in Poon's 3D nonlinear viscoelastic model
ρ, ρ'	Reduced time in Schapery's nonlinear viscoelastic model
σ	Cauchy stress in the direction of testing in a uniaxial test
σ_j	Cauchy stress in direction *j* in a uniaxial definition
$\boldsymbol{\sigma}$	Cauchy stress tensor
σ^e	Instantaneous elastic stress
$\overline{\sigma}_e$	Mean experimental elastic stress used in error evaluation
σ_t	Theoretical elastic stress used in error evaluation
σ_{tot}, σ_e, σ_v	Respectively total, elastic and viscoelastic Cauchy stresses in a uniaxial stress-relaxation test
σ^I, σ^v	Stresses acting respectively on the device and on the dashpot in Kelvin's mechanistic model
$\sigma_{30\%}$	Values of stress at 30% compression
τ	Time
τ_i , *i = 1,..,N*	Relaxation time constants of *G(t)* (Prony series with N terms)
τ_{ij} , *i = 1,..,N;*	Relaxation time constants of $G_j(t)$ (Prony series with N terms)
τ_d	Relaxation time in Kelvin's model, $\tau_d = \eta / E_s$
ω	Angle from the longitudinal (fibre) direction in a muscle sample
Ω	Body in the three-dimensional Euclidean space

Abbreviations

amp	Amplitude of the stress cycles
Def	Deformation applied to the sample
EDL	Extensor digitorum longus
F, 30°, 45°, 60°, XF	Respectively the muscle fibre, 30°, 45°, 60° and cross-fibre directions
L ; also used as a subscript	Longitudinal or fibre direction for a transversely isotropic material
MRI	Magnetic Resonance Imaging
PTFE	Polytetrafluoroethylene

QLV	Quasi-linear viscoelastic
SD	Standard deviation
SHPB	Split Hopkinson pressure bar
SYM	Strain dependent Young's moduli
Str	Strain
T, T'; also used as subscripts	Transverse directions (perpendicular to the muscle fibres) for a transversely isotropic material
TA	Tibialis anterior

Chapter 1 - Introduction

1.1 RATIONALE FOR THE STUDY 2

1.2 OBJECTIVES OF THE STUDY 4

1.3 OUTLINE OF THE THESIS 5

1.1 Rationale for the study

In the last decade, virtual modelling has become a widely used tool in various biomechanical fields. Finite element models of the human body are used in impact biomechanics to assess trauma occurring to the body during road accidents and to improve the design and optimise the effectiveness of safety devices for vehicular occupants (Forbes *et al.*, 2005 ; van Rooij *et al.*, 2003; Verver *et al.*, 2004; Ward *et al.*, 2005). In rehabilitation engineering, human body models are used to improve the design of orthopaedic walking casts or soft tissue support devices for patients with amputation; to investigate pressure sore formation (Oomens *et al.*, 2001) and to improve seat cushion and mattress design for wheelchair or bedridden patients. Virtual environments are also used to model surgical procedures and develop teleoperated systems for surgery (Guccione *et al.*, 2001; Keeve *et al.*, 1998).

The models used in these various applications require both a description of hard and soft tissue geometries as well as the determination of their material properties under large deformations. Powerful imaging techniques have been developed to generate accurate geometries. However, the fundamental mechanical properties of soft tissues remain poorly described in the literature, especially when compressive loading is considered. This observation has also been made by various authors, e.g. Bosboom *et al.* (2001b), Van Sligtenhorst *et al.* (2006). In 1997, the HUMOS project (HUman MOdel for Safety) was launched to develop more accurate mathematical models of the human being for road safety; one of the main difficulties encountered in the model development was to find data (in terms of properties and behaviour) for the different biological tissues of the human body.

In this thesis, focus is upon skeletal muscle, which is the most abundant soft tissue in the human body. It is responsible for the relative motion of the bones and also provides strength and protection to the skeleton by distributing loads and absorbing shocks, both functions of particular interest in the applications mentioned earlier. Coming from the Latin *musculus* "little mouse", the term muscle refers to muscles like the biceps which pop up as though a mouse were scurrying about under the skin. Already in the 17th century scientific research

was aimed at skeletal muscle (Borelli, 1681; Stensen, 1667). Numerous investigations have been conducted to determine muscle structure and function. Experimental studies have also been performed to determine muscle mechanical properties. However, in most experimental studies, muscle has been considered as a force actuator and existing data are mainly limited to the tensile, longitudinal behaviour of the tissue (Davis *et al.*, 2003; Gareis, 1992; Hawkins and Bey, 1994, 1997; Muhl, 1982; Woittiez *et al.*, 1984). The literature review presented in chapter 2 of this thesis shows that information on muscle compressive behaviour is quite sparse; Bosboom *et al.* (2001b) point out that additional information is needed on the transverse mechanical properties of the tissue.

As with most biological soft tissue, muscle presents complex properties; it displays viscoelastic behaviour and has anisotropic properties due to its fibre oriented structure. It is subject to large deformations *in vivo* and the stress state in a given muscle is the result of passive and active contributions. Furthermore, parameters such as age, gender and species are also influential. One-dimensional models have been developed to reproduce muscle global mechanical behaviour observed in the experiments. Most of these models (see for example Best *et al.*, 1994; Cole *et al.*, 1996; de Jager, 2000) are based on the famous mechanistic model proposed by Hill (1938).

Three dimensional constitutive models of nonlinear anisotropic tissue exist (see Humphrey *et al.*, 1990; Li *et al.*, 2001; Limbert *et al.*, 2004; Weiss *et al.* 1996). They have been developed to reproduce the tensile behaviour of soft tissues with fibre-oriented structure such as cardiac muscle, tendons and ligaments. In their review of models used to represent soft tissue behaviour, Maurel *et al.* (1998) pointed out that passive skeletal muscles have rarely been investigated in the biomechanics literature from a constitutive modelling point of view; only a few uniaxial relations are available. However, for three-dimensional modelling, they suggest using one of the strain energy functions developed for ventricles (Humphrey *et al.*, 1990), though skeletal muscles may have slightly different mechanical behaviour in structure, strength and stiffness. The model proposed by Humphrey *et al.* (1990) has been used to reproduce muscle behaviour (Martins *et al.*, 1998); however, the paucity of

experimental data does not permit one to determine the validity of the model. This problem was also outlined by Bosboom *et al.* (2001b) who stated that a problem in formulating constitutive equations to describe the passive behaviour of skeletal muscle is the limited availability of experimental data.

1.2 Objectives of the study

Data concerning skeletal muscle behaviour are clearly missing in applications where muscle tissue is submitted to compressive loads, i.e. impact biomechanics, rehabilitation engineering, etc. This study aimed to provide additional information on muscle properties that could be used to improve the biofidelity of finite element models of the human body. Focus was placed on muscle compressive behaviour which is the relevant deformation mode in human/machine impacts or in seated postures. The stress state of a given muscle results from the passive and active contributions; only the passive properties of muscle tissue were however considered in this thesis. It represents a first, fundamental step in the study of this material with such complex structure and physiological behaviour. Also, during impacts, the time scale of the event does not allow sufficient time for muscles to be activated and so the stress state is mainly due to the passive properties of the tissue.

More specifically, the objectives of the study were to provide an experimental as well as a mathematical characterisation of passive skeletal muscle properties under compressive loading. Elastic and viscoelastic properties of the tissue had to be investigated. For muscle elastic behaviour, the main tasks were to characterise the nonlinearity and the dependency to the fibre orientation, i.e. to characterise muscle anisotropy. For muscle viscoelastic behaviour, the influence of fibre orientation and deformation rate had to be investigated.

From a modelling point of view, the objectives were to provide a three-dimensional model that could appropriately fit the observed experimental data and also had good predictive capabilities concerning muscle behaviour under various loading conditions. Emphasis was placed on simplicity and ease of parameters determination.

1.3 Outline of the thesis

After this introductive chapter, chapter 2 presents a literature review of experimental and theoretical studies conducted on skeletal muscle. Information on muscle structure and composition is provided; experimental data on the tissue mechanical behaviour are summarised and mathematical models relevant to skeletal muscle are also presented.

The approach followed in this study is similar to the approach described by Quaglini (2000); a series of experiments were first conducted to obtain a general knowledge of the tissue mechanical behaviour under compressive loading. The mathematical framework in which a constitutive model representing muscle properties was then set. Finally, further experiments were performed to identify values of the model parameters which are specific to muscle tissue.

Chapter 3 concerns the experimental and theoretical investigation of muscle elastic properties conducted in the study. Results from quasi-static compression experiments performed on animal muscle tissue at various orientations of the muscle fibres are presented; the suitability of two non-linear anisotropic models to reproduce skeletal muscle elastic behaviour in compression is investigated and the results obtained are then discussed.

Chapter 4 focuses on muscle viscoelastic properties. Results from relaxation and cyclic compression experiments conducted on animal muscle tissue at various rates and various orientations of the muscle fibres are presented; the suitability of a quasi-linear and a non-linear viscoelastic model to reproduce skeletal muscle viscoelastic behaviour is investigated and the results obtained are discussed.

Finally, chapter 5 provides a summary of the results obtained, suggests guidelines for further investigation of skeletal muscle mechanical behaviour and concludes the thesis.

Chapter 2 - Literature review

2.1 INTRODUCTION 8

2.2 SKELETAL MUSCLE STRUCTURE AND FUNCTION 8

2.3 PUBLISHED DATA ON SKELETAL MUSCLE MECHANICAL PROPERTIES 13

2.3.1 MUSCLE TENSILE PROPERTIES 13

2.3.2 MUSCLE COMPRESSIVE PROPERTIES – INVASIVE TECHNIQUES 16

2.3.3 NON-INVASIVE MUSCLE CHARACTERISATION 20

2.3.4 GENERAL COMMENT 23

2.4 THEORETICAL FRAMEWORK 24

2.4.1 BASICS OF CONTINUUM MECHANICS 24

2.4.2 MODELLING OF MUSCLE ELASTIC PROPERTIES 32

2.4.2.1 One-dimensional macroscopic models 32

2.4.2.2 Three-dimensional transversely isotropic models 33

2.4.3 MODELLING OF VISCOELASTIC PROPERTIES 38

2.4.3.1 Linear viscoelastic models 39

2.4.3.2 Quasi-linear theory of viscoelasticity 41

2.4.3.3 Discretised QLV theory 44

2.4.3.4 Strain rate effect 47

2.4.3.5 Nonlinear viscoelastic model 48

2.5 CONCLUDING REMARKS 51

2.1 Introduction

As mentioned in the general introduction, skeletal muscle structure, function and mechanical properties have already been extensively investigated in the past. The usefulness of a new study on muscle mechanical behaviour can therefore be questioned. However, this chapter presents a literature review of experimental and theoretical studies conducted on muscle tissue and will demonstrate that our understanding of skeletal muscle under compressive loading is poor.

A brief description of muscle structure is first presented, as understanding the structure of a material is fundamental to the study of its mechanical properties. The second section of the chapter provides a summary of experimental data available in the literature on muscle mechanical behaviour. Finally, the theoretical framework and mathematical developments relevant to the modelling of muscle tissue are presented in the third section of this chapter; elastic and viscoelastic models are considered.

2.2 Skeletal muscle structure and function

Along with cardiac and smooth muscles, skeletal muscle is one of the three types of muscles contained in the human body. It represents the most abundant soft tissue of the body as it accounts for 40% to 45% of its total weight. The term soft tissue refers to tissues that connect, support, or surround other structures and organs. In particular, skeletal muscle's function is to produce force and ensure relative motion between bones, it also provides strength and protection to the skeleton by distributing loads and absorbing shocks. Structure, which is a fundamental aspect in the study of materials' mechanical properties, is closely related to the function biological tissues assume in the body. Skeletal muscle presents a fibre oriented structure in order to fulfil its force producing function. Each muscle is composed of fascicles containing bundles of fibres, themselves composed of parallel bundles of myofibrils (Figure 2-1).

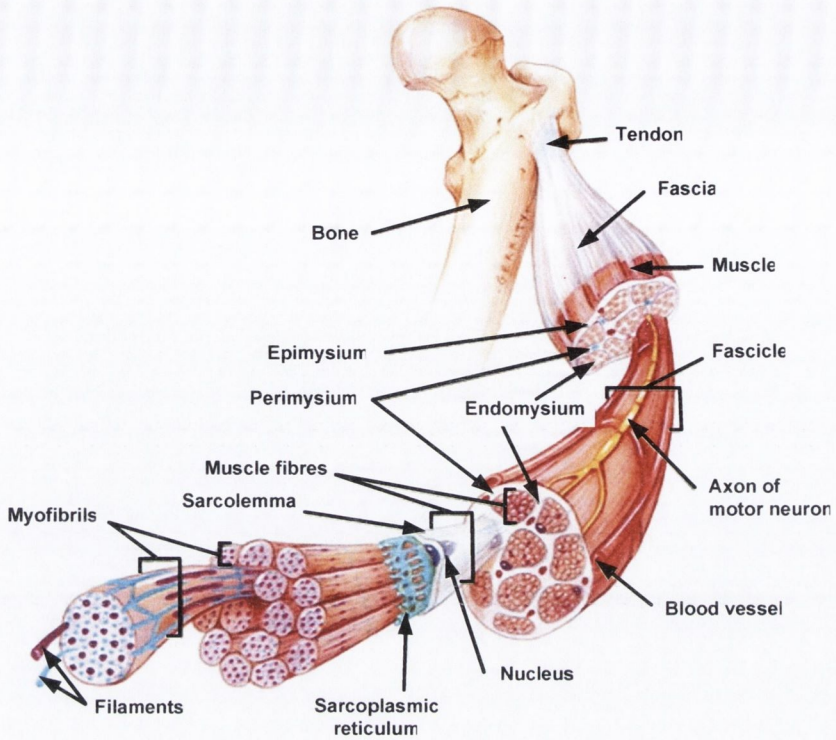


Figure 2-1: General structure of skeletal muscle

Reproduced from http://jan.ucc.nau.edu/~jrc1/exs%20490/EXS%20490%20MusSkRev1.pdf

A myofibril is the basic fibre of the muscle; it consists of series of contractile units, named sarcomeres, composed of arrays of actin and myosin myofilaments. No further details will be provided here on a muscle's contractile mechanism as the present work concerns muscle passive properties. For further details, the reader can refer to Huxley (1980), Squire (1990) or Herzog (2000) to name but a few.

Fibrous connective tissues are supporting tissues, composed mainly of collagenous fibres that surround other tissues and organs. In skeletal muscle, they can be divided into three structural entities: the epimysium which surrounds the whole muscle, the perimysium which surrounds the bundles of muscle fibres and the endomysium which surrounds each muscle fibre individually. The ensemble of these tissue sheaths, called the fascia, encloses the muscles, groups or separates them into layers, and ultimately connects them at their ends to the tendons. Epimysium, perimysium and endomysium are represented schematically in Figure 2-1. Figure 2-2 illustrates their arrangement for bovine muscle tissue after removal of the muscle proteins.

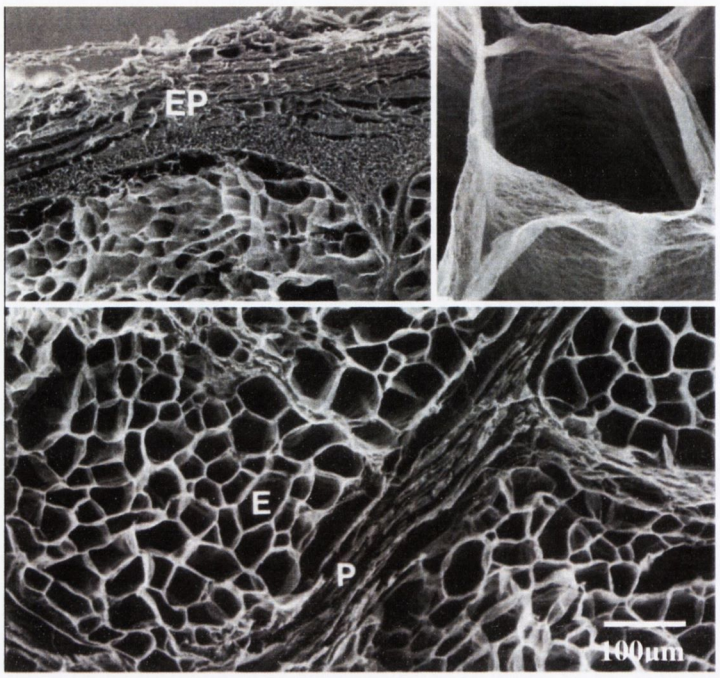


Figure 2-2: Bovine semitendinosus muscle - Extracellular network shown by scanning electron micrographs after removal of the muscle proteins

(EP) epimysium, (P) perimysium and (E) endomysium. The top right picture shows the endomysium surrounding one individual muscle fibre. Reproduced from Kjær, 2004.

About 80% of skeletal muscle mass is made of water, 2 to 3% is made of fatty tissues and collagenous connective tissues account for 1–10% of the muscle mass. These are bulk figures which vary from muscle to muscle and between individuals. Diseases will also affect these values as illustrated in Table 2-1 which presents experimental data by Vignos *et al.* (1959). In this study, muscle fat, collagen and water composition was compared in skeletal muscles of control patients and patients with progressive muscular dystrophy. The most significant difference between the two groups appears to be collagen content which corresponds to an increase in connective tissues as a result of muscle degeneration.

Table 2-1: Comparison of muscle fat, collagen and water contents in control patients and patients with progressive muscular distrophy (from Vignos *et al.*, 1959)

	Fat (as % of wet weight)		Collagen (collagen nitrogen as % of total nitrogen)		Water (as % of wet weight)	
	Normal controls	Juvenile dystrophy	Normal controls	Juvenile dystrophy	Normal controls	Juvenile dystrophy
1	1.4	-	5.0	32.7	80.1	66.4
2	2.1	1.4	4.2	19.4	80.7	77.4
3	2.9	2.0	5.6	15.1	79.7	-
4	2.5	1.7	7.4	26.3	83.1	78.0
5	1.6	6.3	10.2	22.7	83.1	77.7
6	6.2	2.3	5.9	27.5	77.3	78.4
7	0.6	4.5	4.9	31.5	80.5	76.3
8	1.2	5.1	4.6	36.8	81.9	79.5
9	0.6	2.0	5.0	28.4	81.6	77.9
10	1.8	5.7	4.9	14.4	84.3	77.0
11	-	5.1	-	25.6	-	77.2
12	-	4.2	-	24.7	-	77.9
Mean	**2.1**	**3.7**	**5.8**	**26.4**	**81.2**	**76.7**

From a modelling point of view, the passive properties of skeletal muscle are often assumed to be similar to those of other soft tissues such as tendons and ligaments, which also present a hierarchical fibre oriented structure. However, tendons are made of densely packed collagen fibres (Figure 2-3), which account approximately for 86% of their dry weight.

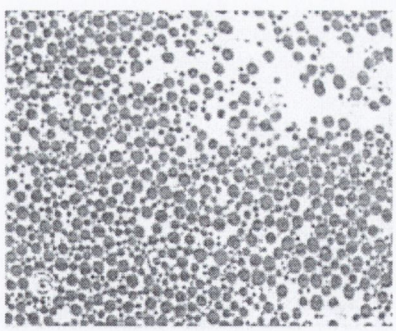


Figure 2-3: Electron micrograph of a cross section through a tendon from the finger of the squirrel monkey, 13000X.

Reproduced from http://www.visualhistology.com/Visual_Histology_Atlas, chapter 3.

Collagen fibres are highly stable and have high mechanical properties. However, due to their high slenderness (length to diameter ratio about 200) collagen fibres, and so tendons, can not withstand compressive forces (Quaglini, 2000).

This brief comparison between skeletal muscle and tendon structures, along with the results of tests that are presented later in the thesis, will help the reader to understand why models developed to represent tendon or ligament properties might not be best suited to describe muscle compressive behaviour; even though they all present a fibre oriented structure.

2.3 Published data on skeletal muscle mechanical properties

Experimental investigation is a fundamental step in the study of a material's mechanical properties. However, experimental characterisation of biological soft tissues may be considered as a challenge. Their complex structure often leads to anisotropic properties; their sensitivity to external parameters such as hydration, temperature, time after death requires *in vivo* testing in order to obtain data representative of the living state; they are often subject to large deformations *in vivo*. Skeletal muscle presents particular difficulties due to its force producing capabilities; the stress state in a given muscle is the result of passive and active contributions. Furthermore, parameters such as age, gender and species are also influential.

Researchers have tried to overcome these difficulties over the years and a significant amount of experimental investigations on skeletal muscle properties is available in the literature. Most of them are however interested in the force producing capability of the tissue and present uniaxial tensile tests performed along the tissue fibre direction (see section 2.3.1). Very few studies have investigated muscle compressive properties, data of particular interest when muscle's protective role to the skeleton is considered (see section 2.3.2). *In vitro* and *in vivo* studies were conducted. However, the use of invasive techniques has limited *in vivo* tests to animal subjects only. A number of studies have investigated the use of non-invasive techniques (elastography and indentation tests) for *in vivo* measurement of human muscle properties (see section 2.3.3).

2.3.1 Muscle tensile properties

When skeletal muscle is considered as a unidirectional actuator, the total force (or tension) that can be developed is considered as the sum of two terms: passive and active tension (Figure 2-4). Passive tension is the tension muscle develops at length greater than its resting length, due to its elastic properties. Active tension is developed when muscle is voluntarily activated. The passive length-tension curve is obtained by stretching the tissue in the absence

of active stimulation. The active curve is usually obtained by subtracting the passive from the total tension muscle develops when activated.

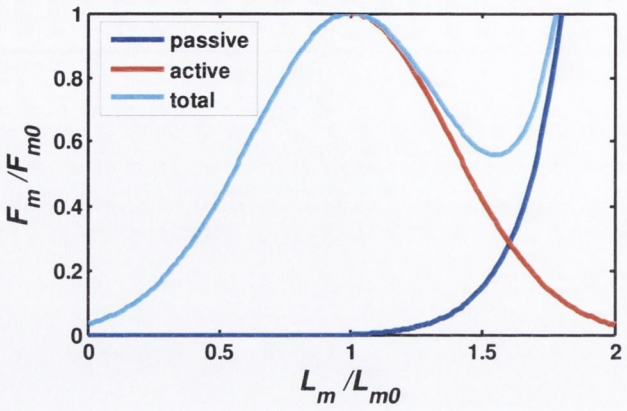


Figure 2-4: Theoretical normalised force-length curves of skeletal muscle.
F_m, current muscle force; F_{m0}, maximum isometric muscle force; L_m, current muscle length; L_{m0}, muscle rest length.

In most published studies, force-length and/or force-velocity relationships are presented. These are respectively determined by performing static isometric tests and dynamic isotonic tests. In isometric tests, muscle contracts without change in overall length. In isotonic tests, muscle shortens against a constant load. A comparison has been established between published data. This task is complicated by the non-uniformity present in the data generation and presentation: use of different specimens and different experimental protocols, different presentation of the results and lack of information to transform them. Figure 2-5 presents (a) passive and (b) active force-length curves obtained by experiments conducted variously on rat, cat or rabbit muscles. These results represent only a small selection within published data; they were however chosen because they were amongst the only studies providing sufficient information to establish a comparison. In Figure 2-5 forces are normalised with respect to the maximum isometric force (F_{m0}) generated by each muscle and lengths are normalised with respect to the muscle rest length (L_{m0}). Even with this geometrical normalisation of the data significant differences are present. When the maximum isometric stress generated by the muscle is chosen for comparison, values ranging from 0.05 to 0.35MPa can be found for rat, cat or rabbit muscles (Close, 1972; Hawkins and Bey, 1994;

Herzorg, 1992; Woittiez, 1984). These large differences due to the use of different animals, different muscles, different experimental protocols, etc. illustrate the variation that is fundamental to biological systems and the difficulty in obtaining a uniform set of data characterising muscle properties.

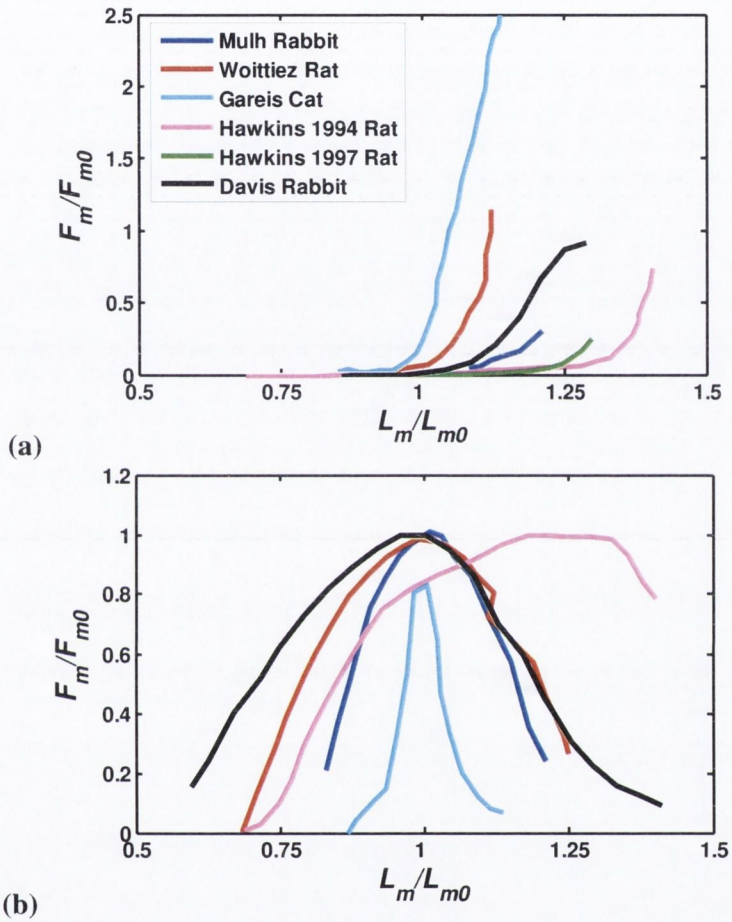


Figure 2-5: Comparison of published passive (a) and active (b) muscle force-length characteristics.

F_m, current muscle force; F_{m0}, maximum isometric muscle force; L_m, current muscle length; L_{m0}, muscle rest length. These observations are based on: Davis et al.,2003; Gareis et al.,1992; Hawkins and Bey,1994 and 1997; Muhl,1982; Woittiez et al., 1984.

The studies listed previously considered only muscle elastic behaviour. Best *et al.* (1994) measured the tensile viscoelastic response of live, innervated rabbit skeletal muscles (tibialis anterior (TA) and extensor digitorum longus (EDL) muscles). The experimental protocol applied to each specimen consisted of one relaxation test (ramp with strain rate of 667%s^{-1}; hold for 300s) and six constant velocity tests at rates ranging from 0.01 to 2Hz. Large

differences were observed between the elastic behaviour of TA and EDL muscles, even after geometric normalisation. This led the authors to suggest that the elastic function of a muscle depends not only on external dimensions but also on internal structure and fibre orientation. Both muscles showed however similar relaxation behaviour; an initial rapid decay followed by a decreasing rate of decay to an asymptotic value. The force-time history exhibited rate sensitivity; peak forces varied by as much as 60% between low- and high-rate tests. Hysteresis was also observed but it appeared to be rate-insensitive.

2.3.2 Muscle compressive properties – invasive techniques

Literature on muscle compressive properties is rather sparse. In a study published in 1988, Grieve and Armstrong performed *in vitro* measurements of porcine adipose and muscle tissues compressive properties. Small uniform specimens of tissue were submitted to confined and unconfined uniaxial compression tests. Figure 2-6 presents stress-strain curves obtained during unconfined compression of muscle specimen at various strain rates (ranging from 0.005 to 2.5%str.s^{-1}).

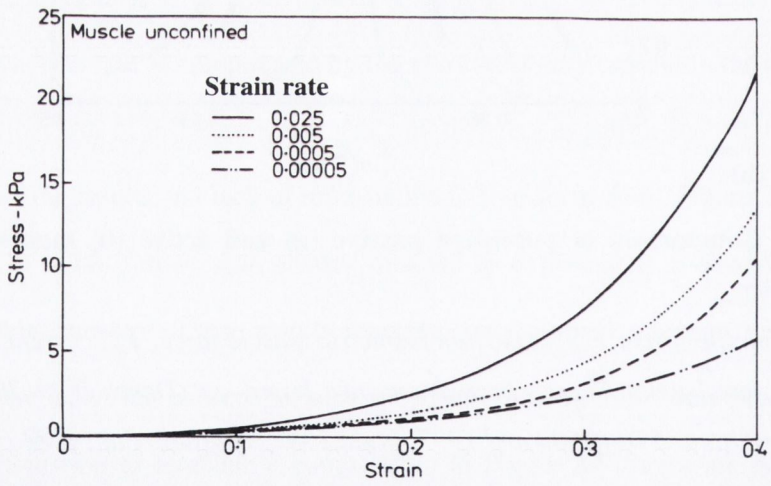


Figure 2-6: Stress-strain curves obtained during unconfined compression of porcine muscle tissue (reproduced from Grieve and Armstrong, 1988).

As expected, skeletal muscle presents a nonlinear behaviour under compressive loading. Stiffening of the tissue is also observed when loading speed is increased. It has to be noted

that specimens were frozen on the day of slaughter and thawed prior to testing; according to the authors, this did not affect the results. Also, no mention is made of fibre orientation with respect to loading direction.

Bosboom *et al.* conducted *in vitro* (2001a) and *in vivo* (2001b) compression tests on rat tibialis anterior muscles (TAs) in the transverse direction. In both types of tests, muscles with intact geometry were used. For *in vitro* tests, TAs were excised and placed in a box containing Ringers solution at 37°C. For *in vivo* experiments, the TAs was bilaterally exposed from the proximal aponeuroses to the distal tendons; sutures were used to preserve muscle's *in vivo* length. Subsequently, the rat was positioned in a mechanical testing device and the muscle was compressed between two plates. Each TA were compressed following a ramp and hold function, with a ramp speed of $0.25mm.s^{-1}$ and a hold phase of 20s. A series of experiments with increasing levels of compression were conducted. Tests were separated by three minutes to allow for relaxation and each series was repeated three times. Results from the experiments are provided by means of force relaxation curves (Figure 2-7).

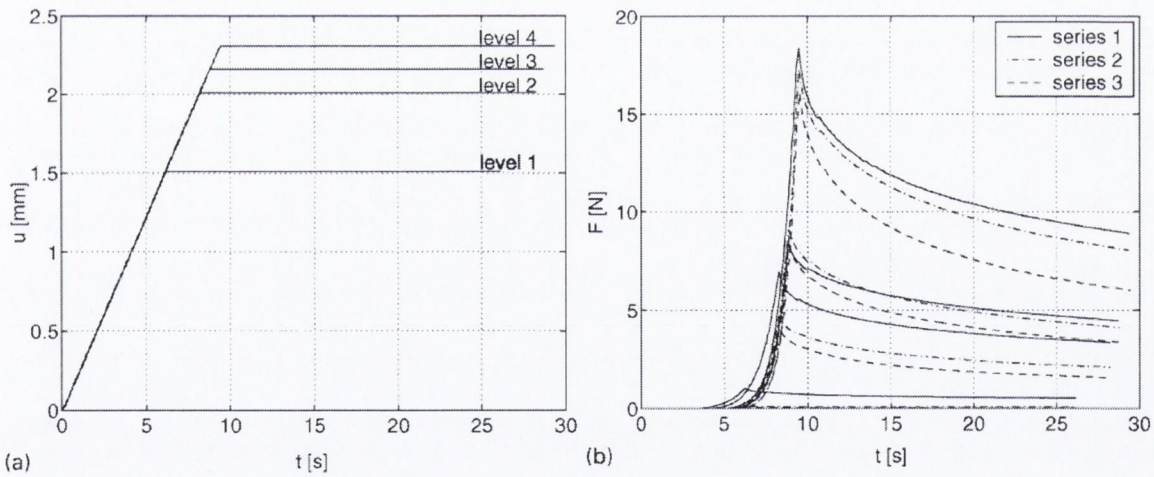


Figure 2-7: Results of compression tests on rat muscle tissue (Bosboom *et al.*, 2001b).
(a) Protocol consisting of four levels of compression, repeated three times; (b) Indentation forces as a function of time.

Due to the non-uniform geometry of the muscle tested, stress-strain curves can not be obtained and the comparison with previously published data is not directly possible. However, Bosboom *et al.* fitted their experimental data with a viscoelastic hyperelastic

model; from the values provided for the model parameters, the theoretical results can be reproduced and used as a means of comparison. This is described in section 2.4.2 and graphically compared to other experimental data in Figure 2-10.

Aimedieu *et al.* (2003) quantified the mechanical properties of the muscles of the buttock using dynamic compression (5-30Hz). Tests were conducted *in vitro* on porcine muscles, using a lever arm device, which applied a dynamic load onto cylindrical samples. Results are presented using a two-parameter mechanical model, which offers limited information. The average stiffness curve showed a monotonous increase: 5 Hz, 8.5 kN/m - 30 Hz, 347 kN/m.

Muscle compressive properties at very high strain rates have been investigated in a few studies. In 1966, McElhaney used an air gun-type testing machine to test the dynamic response of bone and muscle tissue. Cylindrical specimens of bovine muscle were compressed up to 75% strain at rates ranging from 0.001 to $1000s^{-1}$. Nonlinearity and rate sensitivity, characteristic of muscle response, were observed during the tests. The maximum compressive stress measure at 75% strain is multiplied by 2.6 from tests performed at 0.001 to $1000str.s^{-1}$. Muscle fibre orientation during testing is not addressed in this study, nor is the influence of time of death but testing was completed within three days after sacrifice of the animal. Results obtained by McElhaney at 1000 $str.s^{-1}$ are presented in Figure 2-8 along with results obtained in a more recent publication by Van Sligtenhorst et *al.* (2006). In this study, a polymeric split Hopkinson pressure bar (SHPB) apparatus was used to measure the very high strain rate compressive properties of bovine muscle tissue. Cylindrical samples of bovine muscle tissue were submitted to compressive strains up to 80% at rates ranging from 0.1 to $2300s^{-1}$. The main direction of testing is the fibre direction. The authors comment that stress-strain curves were found to be strain rate-sensitive and concave upward, as is typical of muscle tissues; however, Figure 2-8 shows seemingly linear stress-strain curves. The influence of time of test after death was investigated by the authors. It is observed that rigor mortis had a significant impact on the material properties between 5 and 24h post mortem. At longer times however, properties returned essentially to their pre-rigor values. The authors point out that their study presents some of the first published high rate properties of

muscle tissue data that are urgently needed for advanced modelling of the human body and for evaluation of safety systems for the human body.

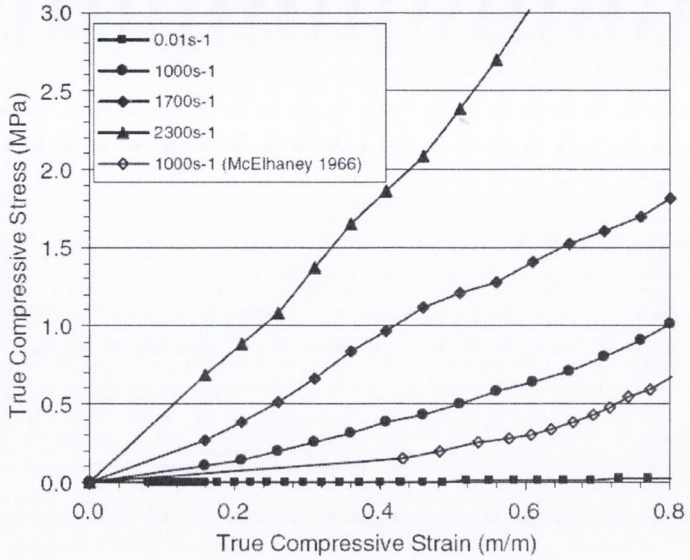


Figure 2-8: Typical results from compression tests performed on bovine muscle tissue at various strain rates (reproduced from Van Sligtenhorst *et al.*, 2006)

Finally, the most recent publication on muscle compressive response has is a study by Song *et al.* (article in press). In this paper, a modified SHPB was used to investigate the compressive stress-strain behaviour of porcine muscle tissue along and perpendicular to the muscle fibre direction at strain rates of 540, 1900 and $3700s^{-1}$. Tests were also performed on a hydraulically driven machine at strain rates of 7.10^{-3} and $6.10^{-2}s^{-1}$. Figure 2-9 presents results obtained perpendicular to the muscle fibre direction. The authors comment that muscle compressive properties are nonlinear and strongly strain-rate sensitive in both directions considered. They also point out that the strain-rate sensitivity is more significant in the cross-fibre than in the fibre direction.

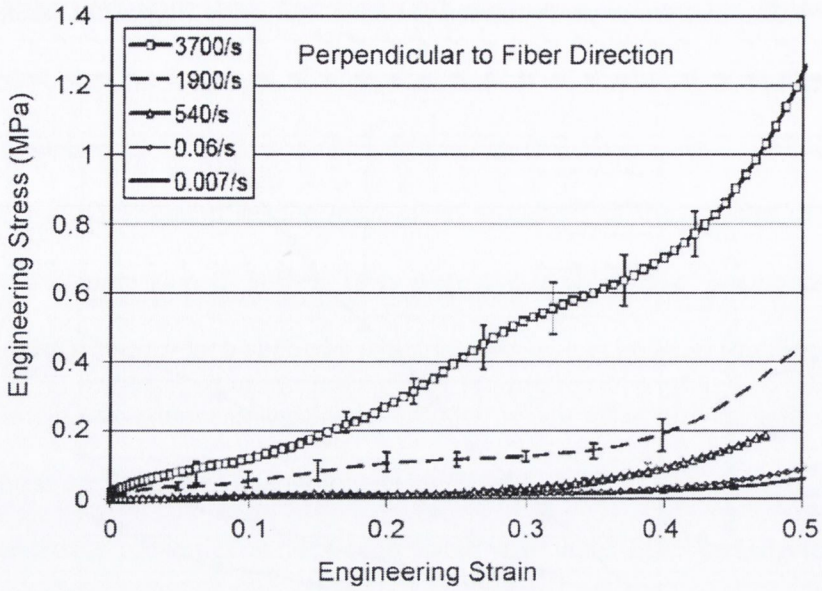


Figure 2-9: Results from compression tests performed on porcine muscle at various strain rates, in the cross-fibre direction (reproduced from Song *et al.*, Article in press).

2.3.3 Non-invasive muscle characterisation

Non-invasive techniques, namely transient elastography and magnetic resonance elastography, have recently been used to investigate skeletal muscle properties. These techniques respectively use ultrasound acquisition and phase contrast MRI method to measure the speed of externally applied shear waves propagating in the tissue. Tissue stiffness is then obtained from shear wave speed through shear or elastic modulus calculation. The techniques offer the advantage of human *in vivo* investigation. However, only limited information is obtained on muscle properties. Linear elasticity is assumed and authors usually report values of shear stiffness (or modulus) measured at rest or under static loading. Discrepancies appear between published values: Gennisson *et al.* (2005) report a mean value of 0.92kPa for biceps brachii shear modulus measured at rest. Bensamoun *et al.* (2006) report values of 3.73kPa, 3.91kPa and 7.53kPa for shear moduli measured at rest in the vastus lateralis, vastus medialis and sartorius muscles respectively. Dresner *et al.* (2001) report values of shear stiffness at rest for human biceps brachii ranging from 15.6 to 39.2kPa. These authors however agree that muscle stiffness increases with mechanical loading.

As mentioned in the introduction, particular interest is placed on soft tissue compressive properties in areas of rehabilitation engineering where soft tissues are supporting loads. An interesting review of numerical and experimental analyses conducted to improve the design of prosthetic sockets for persons with lower limb amputation has been published by Silver-Thorn *et al.* (1996). A number of studies in the field present results of *in vivo* indentation tests performed on human bulk muscular tissues, i.e. tissues surrounding bones and including skin, fat and muscle tissue (Krouskop *et al.* 1987, Reynolds, 1988, Mak *et al.* 1994, Vannah *et al.*, 1996). In these experiments, local indentation tests of subjects limbs are performed perpendicular to the skin surface; indentation displacements and corresponding forces are recorded. In most studies, bulk muscular tissue is considered as isotropic linear elastic and values of Young's modulus are reported (see Table 2-2 for a sample of published values).

Table 2-2: Values of Young's modulus used in residual limb models for relaxed bulk muscular tissues

Reference	Young's modulus
Steege *et al.* (1987)	60kPa
Krouskop *et al.* (1987)	6.2kPa
Reynolds (1988)	50 to 145kPa
Mak *et al.* (1994)	21 to 130kPa

As illustrated in Table 2-2, the range of published values is again quite large. This reflects biological variations present between subjects but also variations between test sites selected on the body. Values reported represent relaxed muscle stiffness. Activation state could however also be of influence as levels of muscle activity are usually only qualitatively determined (relaxed state, mild activation or maximum activation).

The nonlinearity of muscular bulk tissue under compressive loading has been considered by some authors. Vannah *et al.* (1996) conducted *in vivo* indentation tests on the calf of human subjects; Silver-Thorn (1999) performed similar tests on the residual limbs of subjects with trans-tibial amputation and the calf of non-amputees. Zheng *et al.* (1999) performed indentation tests on human forearm *in vivo* using an ultrasound indentation system with a

pen-size hand-held probe. Figure 2-10 presents typical stress-stretch curves calculated from the data published by Vannah *et al.* (1996) and Zheng *et al.* (1999). These are compared with the *in vitro* data obtained by Grieve and Armstrong (1988) on bovine muscle tissue, as well as with the theoretical curves based on *in vitro* and *in vivo* compression of rat muscles (Bosboom *et al.*, 2001a, b). Relaxed muscle state is considered in the *in vivo* tests; however muscle activity was only assessed qualitatively as mentioned previously.

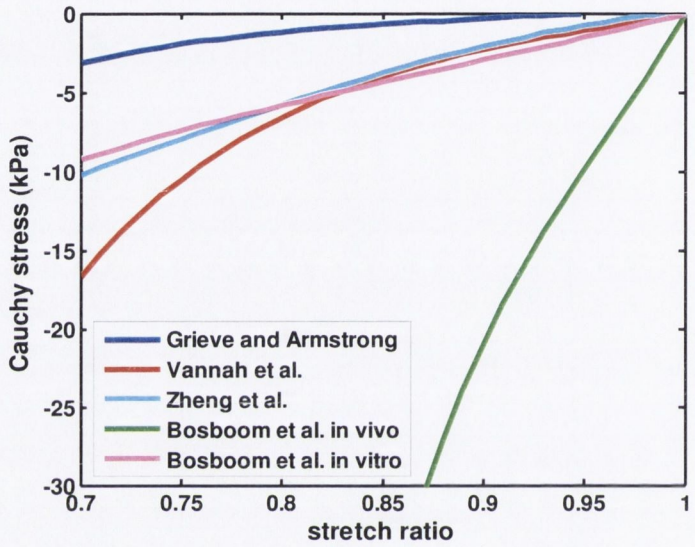


Figure 2-10: Comparison of muscle compressive properties published in the literature. *The following are represented: experimental results from in vitro compression tests on bovine muscle tissues (Grieve and Armstrong, 1988), theoretical curves based on in vivo indentation of human bulk muscular tissues (Vannah et al., 1996, Zheng et al., 1999); theoretical curves based on in vitro and in vivo compression of rat TA muscle (Bosboom et al., 2001a and b).*

Data from Vannah *et al.* (1996) correspond to quasi-static measurements. Zheng *et al.* used indentation speeds ranging from 0.75 to 7.5mm.s^{-1}, corresponding to strain rates ranging approximately from 4 to 40%s^{-1}. They report however that the tissue properties appeared to be rate-insensitive in the range tested. Grieve & Armstrong data were obtained at a rate of 0.05%str.s^{-1}. Results from Bosboom *et al.* correspond to the long term elastic response of the tissue (see section 2.4.3.3 for details).

Relaxation behaviour was also considered by Silver-Thorn *et al.* (1999). They reported that limb bulk soft tissues undergo substantial relaxation: after indenting the tissue at $5mm.s^{-1}$, 55% and 95% relaxation were observed on average respectively for amputee subjects and for non-amputees. The majority of this relaxation (35% for amputees, 85% for non-amputees) occurred within the first five seconds after indentation. Equilibrium was typically reached in less than 60s.

2.3.4 General comment

This review of experimental studies published on skeletal muscle properties, shows that large variations are present in the type of investigations conducted as well as in the experimental results obtained.

Muscle tensile properties have widely been brought under scrutiny. The experimental knowledge of skeletal muscle compressive behaviour remains however unsatisfactory.

2.4 Theoretical framework

2.4.1 Basics of continuum mechanics

This section gives a brief overview of continuum mechanics concepts; this sets the framework and notations used in subsequent sections. For more details, the reader is invited to consult Ogden (1984), Maurel *et al.* (1998) or Holzapfel (2000).

A. Algebra of vectors and tensors

In the following developments, a three-dimensional Euclidean vector space $\mathbb{E}$ will be considered; $\mathbb{E}$ is a real vector space for which the dot product is defined as:

$$v.w = |v||w|\cos\theta \tag{2-1}$$

θ is the angle between vectors v and w when their origins coincide; $|v| = (v \cdot v)^{1/2}$ is the length of vector v. The dot product gives a scalar quantity.

It is often necessary to refer vectors to a basis and express their components (or coordinates) relative to a given basis. An orthonormal basis is introduced as a set of three mutually orthogonal vectors e_1, e_2, e_3 of unit length so that $e_1 \cdot e_2 = e_1 \cdot e_3 = e_2 \cdot e_3 = 0$ and $e_1 \cdot e_1 = e_2 \cdot e_2 = e_3 \cdot e_3 = 1$.

Any vector v in the three-dimensional Euclidean space is represented uniquely by a linear combination of the basis vectors:

$$v = v_1 e_1 + v_2 e_2 + v_3 e_3 \tag{2-2}$$

where the real numbers v_1, v_2, v_3 are the components of vector v along the directions e_1, e_2, e_3 respectively. Using index notation, expression (2-2) can be written as $v = \sum_{i=1}^{3} v_i e_i$ or in abbreviated form:

$$v = v_i e_i, \; i = 1,2,3 \tag{2-3}$$

where the summation convention, invented by Einstein, has been adopted; whenever an index is repeated in the same term, a summation over the range of this index is implied unless otherwise indicated.

A second order tensor $\boldsymbol{A}$ may be thought of mathematically as a linear operator that acts on a vector v to generate another vector w:

$$w = \boldsymbol{A} v \tag{2-4}$$

The tensor product or the dyad of the vectors v and w is denoted by $v \otimes w$. A second-order tensor may be expressed as a linear combination of dyads formed by the basis $\{e_i\}$:

$$\boldsymbol{A} = A_{ij}\, e_i \otimes e_j \tag{2-5}$$

$\boldsymbol{A}$ is called a Cartesian tensor of order two as it is resolved along basis vectors that are orthonormal.

The matrix notation of tensor $\boldsymbol{A}$ is obtained using the nine Cartesian components of $\boldsymbol{A}$ with respect to $\{e_i\}$, represented by A_{ij} :

$$[\boldsymbol{A}] = \begin{bmatrix} A_{11} & A_{12} & A_{13} \\ A_{21} & A_{22} & A_{23} \\ A_{31} & A_{32} & A_{33} \end{bmatrix} \tag{2-6}$$

The components of $v \otimes w$ may be written as:

$$(v \otimes w)_{ij} = \begin{bmatrix} v_1 \\ v_2 \\ v_3 \end{bmatrix} \begin{bmatrix} w_1 & w_2 & w_3 \end{bmatrix} = \begin{bmatrix} v_1 w_1 & v_1 w_2 & v_1 w_3 \\ v_2 w_1 & v_2 w_2 & v_2 w_3 \\ v_3 w_1 & v_3 w_2 & v_3 w_3 \end{bmatrix} \tag{2-7}$$

A tensor of order n may be expressed in the form:

$$\boldsymbol{A} = A_{i_1 i_2 \ldots i_n}\, e_{i_1} \otimes e_{i_2} \otimes \ldots \otimes e_{i_n} \tag{2-8}$$

It has 3^n components $A_{i_1 \ldots i_n}$. In particular, a tensor of order 0 has $3^0 = 1$ component and is simply a scalar; a tensor of order 1 characterises a vector and has 3 components; a tensor of order 2 has 9 components.

B. Deformation gradient tensor

In the continuum approach, a body Ω is imagined as being the composition of a set of particles (or material points) P (Figure 2-11).

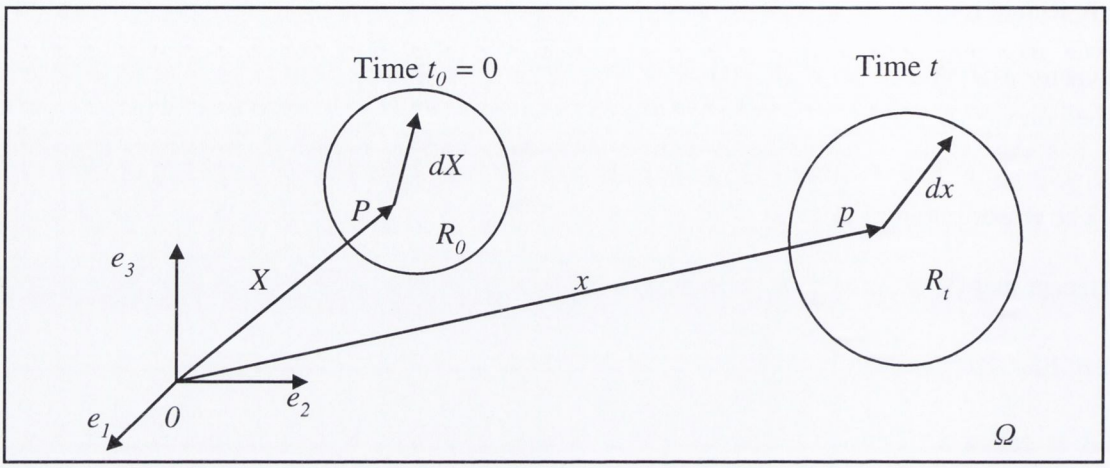


Figure 2-11: Continuum homogeneous deformation.

Ω is embedded in the three-dimensional Euclidean space at a given instant of time t. A reference frame of rectangular coordinate axis is introduced at a fixed origin 0, with basis vectors $\{e_i\}$. The continuous medium is in motion between an initial configuration R_0, defined at time $t_0 = 0$ (reference configuration, named Lagrangian configuration) and any subsequent configuration R_t, defined at time t (current configuration, named Eulerian configuration). X and x are the position vectors of any point P belonging to Ω, defined respectively with respect to the Lagrangian and Eulerian configurations. The motion of a point P is described by:

$$x = x(X,t) \quad \text{or} \quad x_i = x_i(X,t) \tag{2-9}$$

Differentiating with respect to the Lagrangian coordinates leads to:

$$dx = \boldsymbol{F} dX \quad \text{or} \quad dx_i = \sum_j \frac{\partial x_i(X,t)}{\partial X_j} dX_j \tag{2-10}$$

where $\boldsymbol{F} = \left[\frac{\partial x_i}{\partial X_j} \right]$ is the deformation gradient tensor, which transforms any elementary segment dX of Ω (defined with respect to the reference configuration) into a segment dx

(defined with respect to the current configuration). Similarly, the reverse deformation gradient tensor may be defined as $\boldsymbol{F}^{-1} = \boldsymbol{D} = \left[\frac{\partial X_i}{\partial x_j}\right]$.

The elementary volume in the current configuration $dv = dx_1 dx_2 dx_3$, can be expressed as a function of the elementary volume in the reference configuration $dV = dX_1 dX_2 dX_3$ as:

$$dv = JdV \tag{2-11}$$

where $J = \det(\boldsymbol{F})$ represents the Jacobian of the deformation gradient tensor.

Similarly, the elementary surface in the current configuration ds can be expressed as a function of the elementary surface in the reference configuration dS as:

$$nds = J\boldsymbol{D}^T NdS \tag{2-12}$$

where n and N are the unit vectors, normal to the surface elements ds and dS respectively.

C. Strain tensors

The squared lengths of both segments dx and dX may be developed as follows:

$$dx^2 = dx^T dx = dX^T F^T FdX \quad \text{and} \quad dX^2 = dX^T dX = dx^T D^T Ddx \tag{2-13}$$

The tensorial product $\boldsymbol{C} = \boldsymbol{F}^T \boldsymbol{F}$ is defined as the right Cauchy-Green dilatation tensor.

Similarly, the left Cauchy-Green dilatation tensor is defined as $\boldsymbol{B} = \boldsymbol{F}\boldsymbol{F}^T$.

This allows definition of the Cauchy strain tensor as $\boldsymbol{c} = \boldsymbol{D}\boldsymbol{D}^T = (\boldsymbol{F}\boldsymbol{F}^T)^{-1} = \boldsymbol{B}^{-1}$.

The squared length variation of the segments dX and dx may be expressed in Lagrangian coordinates as

$$dx^2 - dX^2 = dX^T(\boldsymbol{C} - \boldsymbol{I})dX = dX^T 2\boldsymbol{E}dX \tag{2-14}$$

where $\boldsymbol{E} = \frac{1}{2}(\boldsymbol{C} - \boldsymbol{I})$ is the Green-Lagrange (Lagrangian) strain tensor.

The squared variation may be expressed in Eulerian coordinates as:

$$dx^2 - dX^2 = dx^T(\boldsymbol{I} - \boldsymbol{c})dx = dx^T 2\boldsymbol{e}dx \tag{2-15}$$

where $\boldsymbol{e} = \frac{1}{2}(\boldsymbol{I} - \boldsymbol{c})$ is the Eulerian strain tensor.

The extension ratios λ_i are related to the principal strain components C_{ii} and E_{ii} by:

$$\lambda_i = F_{ii} = \frac{\partial x_i}{\partial X_i} \qquad C_{ii} = \lambda_i^2 \qquad E_{ii} = \frac{1}{2}(\lambda_i^2 - 1) \qquad i = 1,2,3 \qquad (2\text{-}16)$$

$\boldsymbol{C}$, $\boldsymbol{B}$, $\boldsymbol{c}$, $\boldsymbol{E}$ and $\boldsymbol{e}$ are all second-order symmetric strain tensors. $\boldsymbol{C}$ and $\boldsymbol{E}$ allow the calculation of the length variation of any segment dX known in the reference configuration, whereas $\boldsymbol{c}$ and $\boldsymbol{e}$ allow the calculation of the length variation of any segment dx known in the current configuration.

In practice, the trajectory function of any point of the continuum is unknown; the notion of displacement is thus preferably used. The elementary displacement variation may be defined as:

$$du = dx - dX = (\boldsymbol{F} - \boldsymbol{I})dX = (\boldsymbol{I} - \boldsymbol{D})dx \qquad (2\text{-}17)$$

In terms of displacement gradient tensor, this may be expressed as:

$$du = \nabla u dX \qquad \text{i.e.:} \quad du_i = \sum_j \frac{\partial u_i}{\partial X_j} dX_j \qquad (2\text{-}18)$$

The Green-Lagrange strain tensor is finally expressed as:

$$\boldsymbol{E} = \frac{1}{2}(\nabla u + \nabla u^T + \nabla u^T \nabla u) \qquad (2\text{-}19)$$

When strains are small, the Lagrangian and Eulerian strain tensors are close enough to allow the linear approximation:

$$\boldsymbol{E} = \boldsymbol{e} = \boldsymbol{\varepsilon} = \frac{1}{2}(\nabla u + \nabla u^T) \qquad (2\text{-}20)$$

$\varepsilon_{ii} = (\lambda_i - 1)$ correspond to infinitesimal strains, used when the deformations are small.

Some authors call $\ln(\lambda)$ the "true" strain. This is another useful strain measure defined considering the sum of small incremental deformations.

D. Stress tensors

The continuous medium Ω is assumed to be deforming passively under external loads, from the initial unstressed and undeformed reference state. For continuity reasons, the current

internal stress vector $\boldsymbol{t}^s$ (acting along the surface normal n of Ω) is related to the external load L^s applied on ds by:

$$\boldsymbol{t}^s(x,\mathrm{n}) = \lim_{ds\to 0} \frac{dL^s}{ds} \tag{2-21}$$

According to Cauchy's theorem, the internal stress vector $\boldsymbol{t}^s$ is related to an internal second order stress tensor, corresponding to the physically true stress in the material and named Cauchy stress tensor:

$$\boldsymbol{t}^s(x,\mathrm{n}) = \boldsymbol{\sigma}^T \mathrm{n} \tag{2-22}$$

In matrix notation, the columns of $\boldsymbol{\sigma}$ can be identified as the components of traction vectors acting on planes normal to the coordinate directions:

$$\begin{bmatrix} t_1 \\ t_2 \\ t_3 \end{bmatrix} = \begin{bmatrix} \sigma_{11} & \sigma_{12} & \sigma_{13} \\ \sigma_{21} & \sigma_{22} & \sigma_{23} \\ \sigma_{31} & \sigma_{32} & \sigma_{33} \end{bmatrix} \begin{bmatrix} e_1 \\ e_2 \\ e_3 \end{bmatrix} \tag{2-23}$$

σ_{ij} represent the stress components of the Cauchy stress tensor. There are six independent stress components acting at a certain point of a body as the Cauchy stress tensor is symmetrical for equilibrium reasons; $\sigma_{ij} = \sigma_{ji}$ for $i \neq j$. Figure 2-12 offers a graphical representation.

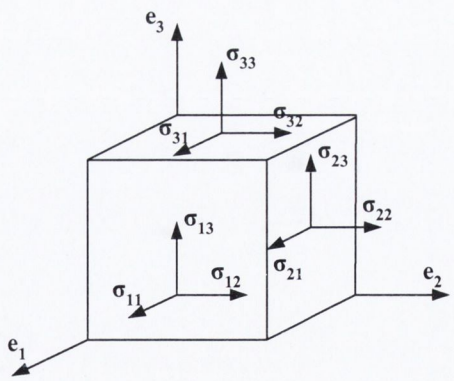


Figure 2-12: Stress components acting on a cube.

Cauchy (true) stress, σ,corresponds to the force per unit area on the current configuration (Eulerian). When the stress is expressed with respect to the known initial configuration

(Lagrangian), reference is made to the Piola-Kirchhoff first stress tensor or Lagrange stress tensor,

$$\boldsymbol{T} = J\boldsymbol{D}\boldsymbol{\sigma} \tag{2-24}$$

which corresponds to the internal stress tensor that would be obtained by applying the current external load onto the initial undeformed configuration. The lagrange stress tensor is not symmetric and so in practice the symmetric second Piola-Kirchhoff stress tensor is preferable:

$$\boldsymbol{S} = \boldsymbol{T}\boldsymbol{D}^T = J\boldsymbol{D}\boldsymbol{\sigma}\boldsymbol{D}^T \tag{2-25}$$

$\boldsymbol{S}$ corresponds to the stress tensor in the initial configuration, equivalent to the stress tensor in the current configuration, i.e. it takes into account all geometrical changes between initial and current configurations.

Uniaxial definitions of commonly used stresses are summarised in Figure 2-13.

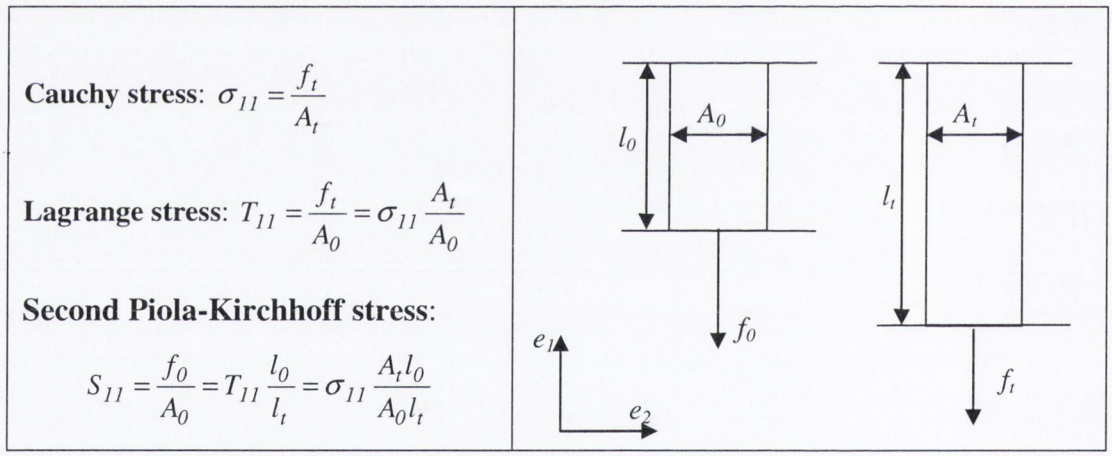


Figure 2-13: Uniaxial definition of commonly used stresses.

E. Elasticity

The definitions and formulae presented in the previous section are valid for every continuous medium, irrespective of its physical properties. The specific deformation response of a material under stress may be described by its constitutive relationship in the form of a function involving the state variables. The theory of elasticity states that the stress at any

time t depends upon only the local deformation at that time and not upon the history of the deformation (Oden, 1972).

Hyperelasticity

The nonlinear theory of elasticity constitutes the theoretical basis for the study of hyperelastic materials such as elastomers. It includes nonlinearities in material properties and takes into account large deformations. A homogeneous continuous material is considered hyperelastic if the Lagrange stress tensor $\boldsymbol{T}$ is derived from an internal strain energy function $W(\boldsymbol{F})$ as:

$$\boldsymbol{T} = \frac{\partial W(\boldsymbol{F})}{\partial \boldsymbol{F}} \tag{2-26}$$

In terms of the second Piola-Kirchhoff stress, this can be written:

$$\boldsymbol{S} = 2\frac{\partial W(\boldsymbol{C})}{\partial \boldsymbol{C}} \tag{2-27}$$

If the material is isotropic, W may be expressed in terms of the three invariants of $\boldsymbol{C}$ only:

$$W(\boldsymbol{C}) = W(I_1, I_2, I_3) \tag{2-28}$$

$$I_1 = \mathrm{tr}\boldsymbol{C} \quad I_2 = 1/2[(\mathrm{tr}\,\boldsymbol{C})^2 - \mathrm{tr}\,\boldsymbol{C}^2] \quad I_3 = \det \boldsymbol{C} = J^2 \tag{2-29}$$

Various forms of W have been developed to account for specific materials behaviour. The Neo-Hookean, Mooney-Rivlin or else Ogden models figure among the most famous (consult Holzapfel, 2000 for further details).

Linear elasticity

When a material presents linear properties and only small deformations are considered (Lagrangian and Eulerian configurations are considered equivalent), the relationship between stress and strain may be expressed in terms of the generalised Hooke's law.

In a form introducing engineering constants, Hooke's law may be expressed as:

$$\begin{bmatrix} \sigma_{11} \\ \sigma_{22} \\ \sigma_{33} \\ \sigma_{12} \\ \sigma_{13} \\ \sigma_{23} \end{bmatrix} = \frac{E}{(1+\nu)(1-2\nu)} \begin{bmatrix} 1-\nu & \nu & \nu & 0 & 0 & 0 \\ \nu & 1-\nu & \nu & 0 & 0 & 0 \\ \nu & \nu & 1-\nu & 0 & 0 & 0 \\ 0 & 0 & 0 & (1-2\nu)/2 & 0 & 0 \\ 0 & 0 & 0 & 0 & (1-2\nu)/2 & 0 \\ 0 & 0 & 0 & 0 & 0 & (1-2\nu)/2 \end{bmatrix} \begin{bmatrix} \varepsilon_{11} \\ \varepsilon_{22} \\ \varepsilon_{33} \\ \varepsilon_{12} \\ \varepsilon_{13} \\ \varepsilon_{23} \end{bmatrix} \quad (2\text{-}30)$$

with E, the Young's modulus and ν, Poisson's ratio.

2.4.2 Modelling of muscle elastic properties

2.4.2.1 One-dimensional macroscopic models

A review of skeletal muscle modelling would not be complete without mentioning the famous one-dimensional active muscle model developed by A.V. Hill (1938). Hill represented the muscle actuator as composed of three elements (Figure 2-14):

- a *contractile element* (CE), which models the active part of the muscle, freely extensible at rest but capable of shortening when activated;
- a *series elastic element* (SE), a nonlinear spring arranged in series with the contractile element, which allows a rapid change of the muscle state from inactive to active and provides an energy storing mechanism;
- a *parallel elastic element* (PE), a nonlinear spring arranged in parallel with the two previous elements, which is responsible for the passive behavior of the muscle when it is stretched, even when the contractile element is not activated.

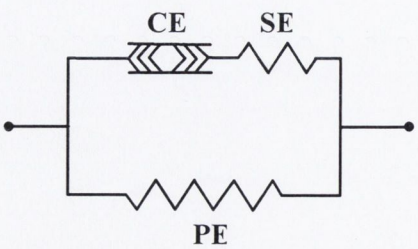


Figure 2-14: Hill's functional muscle model; parallel elastic element (PE), contractile element (CE), series elastic element (SE).

This model leads to the force-length relationships illustrated on Figure 2-4. It has been extensively used in modelling of muscle mechanics and is the basis of most models used for gait analysis (see MADYMO User's Manuals (2001), de Jager (2000), Deng and Goldsmith (1987), Winters and Stark (1988), Winters (1990), Hof and Van den Berg (1981), Cole *et al.* (1996), Forcinito *et al.* (1998), Zajac (1989), Delp *et al.* (1990), Brown *et al.* (1996) for example). The most challenging and limiting aspect of these authors use of the Hill model is parameter estimation and only a few studies present specific parameter values. Moreover, differences appear between the values of these parameters as their determination is based on published experimental data, amongst which variation is present (see Section 2.3.1).

2.4.2.2 Three-dimensional transversely isotropic models

Due to its fibre-oriented structure, skeletal muscle is often considered as a fibre-reinforced composite, consisting of parallel fibres embedded in a matrix (see Figure 2-15 for illustration). Unidirectional composites are transversely isotropic; they possess one axis of rotational symmetry parallel to the fibre direction (L). All properties are the same in planes perpendicular to the fibre direction, i.e. planes TT' are planes of isotropy. However, applying material science technology to biological material is not without difficulty due to the complexity of biological structures. Huijing (1999), describes muscle tissue as a composite consisting of an extracellular matrix with triple reinforcement by fibrous material. The reinforcement is obtained by (1) an active component (myofibres) able to generate force and bear loads actively. The load bearing capacity is shared, but only passively, by (2) the basal lamina (coating the myofibres on one side and interfacing with collagen fibres of the endomysium on its other side) and (3) the passive fascial apparatus of the organ. Only muscle passive properties are considered in the present work. The reader will nonetheless appreciate the difficulties and limitations of the idealized representation consisting of a unidirectional composite with nonlinear, transversely isotropic properties.

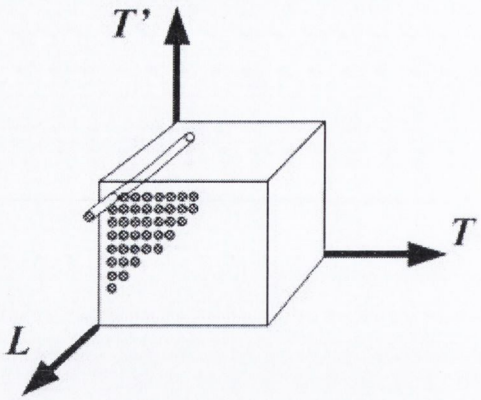


Figure 2-15: Representation of a unidirectional composite.

Direction L is the fibre or longitudinal direction. T & T' are directions perpendicular to fibres (transverse directions). Properties are identical in the plane T T'.

A. Hyperelastic approach

The most popular models developed to characterise nonlinear transverse isotropy are based on the theory developed by Spencer (1984) for fibre-reinforced composites. Spencer developed a constitutive hyperelastic model in which the strain energy function depends on a vector representing the material preferred direction (a_0). The strain energy function is defined in terms of five scalar invariants:

$$W(\boldsymbol{C}, a_0) = W(I_1(\boldsymbol{C}), I_2(\boldsymbol{C}), I_3(\boldsymbol{C}), I_4(\boldsymbol{C}, a_0), I_5(\boldsymbol{C}, a_0)) \tag{2-31}$$

with

$$I_1 = \operatorname{tr} \boldsymbol{C} \quad I_2 = 1/2[(\operatorname{tr} \boldsymbol{C})^2 - \operatorname{tr} \boldsymbol{C}^2] \quad I_3 = \det \boldsymbol{C} = J^2$$
$$I_4 = a_0 \cdot \boldsymbol{C} \cdot a_0 \qquad I_5 = a_0 \cdot \boldsymbol{C}^2 \cdot a_0 \tag{2-32}$$

I_1, I_2 and I_3, are the standard invariants of the right Cauchy-Green deformation tensor and are the complete set of invariants associated with isotropic material behaviour. The invariants I_4, and I_5 arise directly from the anisotropy introduced by the reinforcing fibre. These invariants represent contributions to the strain energy from the properties of the fibres and their interaction with the other material constituents; I_4 for instance, is the square of the stretch along the fibre direction.

Others further developed Spencer's theory to determine particular forms of the strain energy function to accommodate soft tissues with transversely isotropic properties such as tendons and ligaments (Weiss *et al.*, 1996), arterial walls (Holzapfel *et al.*, 2002), cardiac muscle

tissue (Humphrey *et al.*, 1990) to name a few. A common approach to capture the material anisotropy considering a fibre reinforced structure is to formulate the strain energy function as the sum of two terms:

$$W = W_{matrix} + W_{fibres} \tag{2-33}$$

the first term represents the behaviour of the isotropic ground matrix; the second term represents the behaviour of the fibres embedded in the matrix. Humphrey *et al.* (1987) determined a constitutive relation for passive myocardium with a strain energy function (W) depending upon only two invariant measures of the finite deformation, $W = W(I_1, \alpha)$:

$$W = c_1\left(\exp(c_2(I_1 - 3)) - 1\right) + c_3\left(\exp\left(c_4(\alpha - 1)^2\right) - 1\right) \tag{2-34}$$

where α is the stretch ratio along the fibre direction and I_1 is the invariant defined in equation (2-32). c_1, c_2, c_3, and c_4 are parameters of the model. This form was established from biaxial experiments on passive myocardium and the assumption of incompressibility ($I_3 = 0$) and transverse isotropy were made. The Cauchy stress derived from W then takes the form:

$$\boldsymbol{\sigma} = -p\boldsymbol{I} + 2W_1'\boldsymbol{B} + \frac{W_\alpha'}{\alpha}\boldsymbol{F}a_0 \otimes a_0\boldsymbol{F}^T \tag{2-35}$$

where p is a Lagrange multiplier enforcing incompressibility, $W_1' = \partial W/\partial I_1$, $W_\alpha' = \partial W / \partial \alpha$. Parameters for this type of model are usually obtained from biaxial experiments as analytical developments become complicated when uniaxial tests are considered.

Humphrey's model has been used successfully to model cardiac muscle behaviour in tension (Novak *et al.*, 1994; Sacks and Chuong, 1993). Martins *et al.* (2006) also used this formulation to fit data from *in vitro* tensile tests performed on porcine muscular tissues in the muscle fibre direction. A quasi-incompressible generalisation of Humphrey's model had been developed earlier by Martins *et al.* (1998) to include muscle active properties; the model was made compatible with a 1-D mechanical model of the Hill type (Figure 2-14). In this model, the fibres do not bear any load in compression; parameters c_1 and c_2, corresponding to the behaviour of the isotropic matrix, were obtained by fitting to *in vitro*

compression tests on porcine muscle tissues published by Grieve and Armstrong (1988) (see section 2.3.2 for details). Martins *et al.* (1998) considered that these data correspond to tests performed in the muscle fibre direction; fibre orientation during the tests is however not specified in the paper published by Grieve and Armstrong. This reflects the paucity of data available to characterise muscle compressive behaviour. Values of parameters published in Martins *et al.* (1998) and Martins *et al.* (2006) respectively for muscle compressive and tensile behaviour are presented in Table 2-3.

Table 2-3: Parameters for Martins' model representing the tensile and compressive behaviour of passive porcine muscle tissue.

Deformation type	c_1(kPa)	c_2	c_3(kPa)	c_4
Compression – Martins (1998)	0.82	1.79	-	-
Tension – Martins (2006)	-0.22	0.54	0.43	0.79

Figure 2-16 presents theoretical curves obtained with Martins model for passive porcine muscle during tension and compression in the fibre direction. Mathematical developments are presented in section 2.3.1, along with application of the model to compression in the muscle transverse direction.

Overall, good fits are obtained with Martins' model; a correlation coefficient > 0.99 is reported in Martins *et al.* (2006) for fitting to muscle tensile data. Figure 2-16 shows however that the model predicts unrealistic behaviour in the region of small tensile stretches (negative values of stress are observed). Also, the parameters of the model have no physical means.

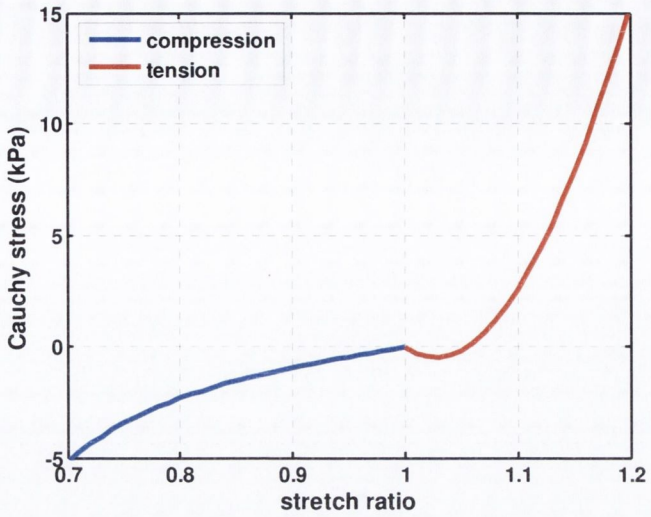


Figure 2-16: Theoretical behaviour of passive porcine muscle under tension and compression along the fibre direction.

Compressive behaviour calculated from Martins et al. (1998); tensile behaviour calculated from Martins et al. (2006).

B. Strain dependent Young's moduli approach

Li *et al.* (2001) used another approach to model nonlinear transverse isotropy in porcine aortic heart valves: they adapted the general theory of linear elasticity for transversely isotropic bodies and introduced nonlinearity by means of strain dependent Young's moduli.

For a linear elastic, transversely isotropic material with the L direction as the axis of transverse isotropy (see Figure 2-15), the relationship between stress (σ) and strain (ε) can be expressed in the following form:

$$\begin{vmatrix} \varepsilon_L \\ \varepsilon_T \\ \varepsilon_{T'} \\ \varepsilon_{LT} \\ \varepsilon_{LT'} \\ \varepsilon_{TT'} \end{vmatrix} = \boldsymbol{K} \begin{vmatrix} \sigma_L \\ \sigma_T \\ \sigma_{T'} \\ \sigma_{LT} \\ \sigma_{LT'} \\ \sigma_{TT'} \end{vmatrix} \tag{2-36}$$

with $$\boldsymbol{K} = \begin{vmatrix} 1/E_L & -\nu_{TL}/E_T & -\nu_{TL}/E_T & 0 & 0 & 0 \\ -\nu_{LT}/E_L & 1/E_T & -\nu_{TT}/E_T & 0 & 0 & 0 \\ -\nu_{LT}/E_L & -\nu_{TT}/E_T & 1/E_T & 0 & 0 & 0 \\ 0 & 0 & 0 & 1/(G_{LT}) & 0 & 0 \\ 0 & 0 & 0 & 0 & 1/(G_{LT}) & 0 \\ 0 & 0 & 0 & 0 & 0 & 2*(1+\nu_{TT})/E_T \end{vmatrix} \tag{2-37}$$

The compliance matrix, $\boldsymbol{K}$, has five independent elastic constants: two Young's moduli (E_L and E_T), two Poisson's ratio ($\nu_{TT'}$ and ν_{LT}) and one shear modulus (G_{LT}). Index L denotes the longitudinal direction, indices T and T' denote the two transverse directions.

As described by Lemaitre *et al.* (1990), the five characteristic coefficients can be obtained by uniaxial tension or compression tests on specimens cut out along (Figure 2-17):

- the cross-fibre direction: need to measure σ_T, ε_T, $\varepsilon_{T'}$; can determine E_T, ν_{TT}
- the fibre direction: need to measure σ_L, ε_L, ε_T ; can determine E_L, ν_{LT}
- at 45° from the fibre direction: need to measure σ_{45}, ε_{45} ; can determine G_{LT}

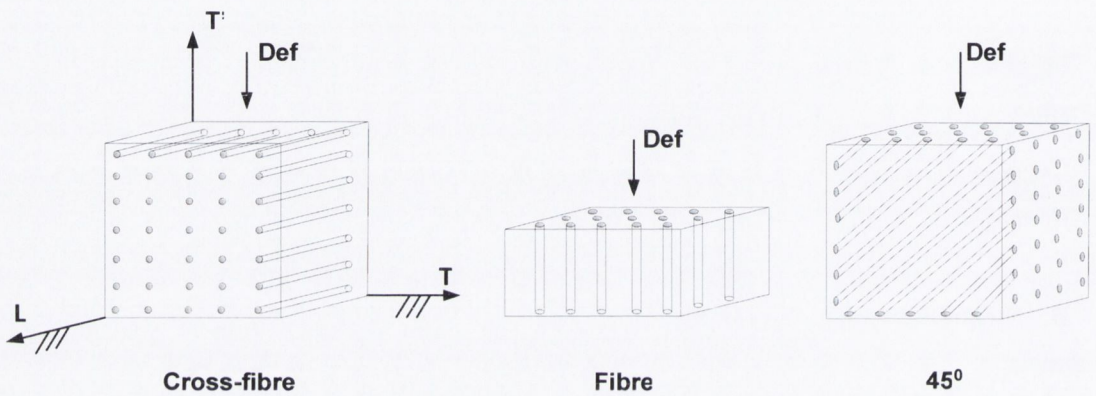


Figure 2-17: Specimens used to characterise linear elastic, transversely isotropic materials.

L is the longitudinal direction. T & T' are the transverse directions. D represents the applied deformation.

Soft tissues usually present a nonlinear relationship between stress and strain and undergo large deformations *in vivo*. To introduce nonlinearity in the model, strain dependent moduli have been introduced by Li *et al.* (2001):

$$E_L = k_1 \exp(k_2 \varepsilon) \quad \text{and} \quad E_T = k_3 \exp(k_4 \varepsilon) \tag{2-38}$$

where k_1, k_2, k_3, k_4 are the model parameters.

2.4.3 Modelling of viscoelastic properties

When a body is suddenly strained and the strain is maintained constant afterwards, the corresponding stresses induced in the body decrease with time: this phenomenon is called

stress relaxation. If the body is suddenly stressed and then the stress is maintained constant afterwards, the body continues to deform: this phenomenon is called *creep*. If the body is subjected to a cyclic loading, the stress-strain relationship in the loading process is usually somewhat different from that in the unloading process, and the phenomenon is known as *hysteresis*. These three features are part of the behaviour of many materials; they are the manifestation of a phenomenon called *viscoelasticity* (Fung, 1993).

Almost all biological soft tissues are viscoelastic. Quaglini (2000) points out that the presence of water within the ground substance of soft tissues is very important for their mechanical properties as the mobility of the fluid affects their viscous properties. In particular, the response of skeletal muscle to tensile load has long been recognised as nonlinear, time-dependent, and viscoelastic (Butchal, 1951).

Numerous models have been developed to represent the viscoelastic properties of engineering and biological materials. In the following sections, three types of approaches commonly used are reviewed: linear, quasi-linear and nonlinear viscoelastic models; focus is placed on models used to characterise soft tissue behaviour.

2.4.3.1 Linear viscoelastic models

The superposition principle proposed by Boltzmann in 1874 is usually used to formulate linear viscoelasticity. It states that the total effect of applying several deformations is the sum of the effects of applying each one separately:

$$\sigma(t) = \int_{-\infty}^{t} G_l(t-\tau)\frac{\partial \varepsilon(\tau)}{\partial \tau} d\tau \tag{2-39}$$

where $G_l(t)$ is the relaxation modulus.

Although the convolution integral expressed in equation (2-39) represents a constitutive relation for a linear viscoelastic material, it does not allow by itself an explicit analytical form of the material function, $G_l(t)$, to be found. Another classical approach to represent linear viscoelasticity uses mechanical models consisting of linear springs and dashpots such as the Maxwell and Kelvin models (Figure 2-18).

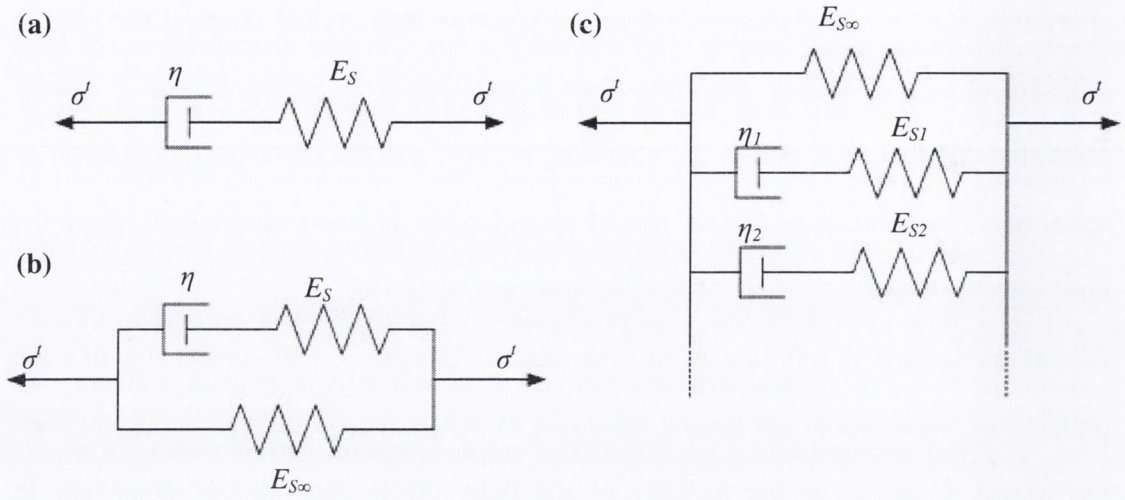


Figure 2-18: (a) Maxwell model, (b) Kelvin model, (c) Generalised Maxwell model.

An ideal linear spring produces instantaneously a deformation proportional to the load. An ideal dashpot produces a velocity proportional to the load at any instant. Different global behaviours are obtained with different arrangements of springs and dashpots. We assume that the devices of Figure 2-18 have unit area and unit length so that force and elongation can be identified with stress and strain respectively.

Considering the Kelvin model (Figure 2-18b), σ^t and ε^t are respectively the total stress and strain applied to the device. σ^v and ε^v are defined as the stress and strain acting on the dashpot. $E_{S\infty}$ and E_S are the springs' constants and η is the viscosity of the dashpot. The following developments are taken from Simo (1998). The constitutive equation characterising the stress response of the model takes the form:

$$\sigma^t = E_{S\infty}\varepsilon^t + E_S(\varepsilon^t - \varepsilon^v) = E_{S0}\varepsilon^t - E_S\varepsilon^v \tag{2-40}$$

where $E_{S0} = E_{S\infty} + E_S$, $\tau_d = \eta / E_S$ and the internal variable, ε^v, satisfies the evolution equation:

$$\frac{\partial \varepsilon^v}{\partial \tau} + \frac{1}{\tau_d}\varepsilon^v = \frac{1}{\tau_d}\varepsilon^t \tag{2-41}$$

By eliminating the internal variable from the constitutive equation (2-40), the stress response of the device can also be formulated by the following convolution integral, equivalent to equation (2-39):

$$\sigma^t(t) = \int_{-\infty}^{t} G_l(t-\tau)\frac{\partial \varepsilon}{\partial \tau} d\tau \tag{2-42}$$

where $G_l(t) = E_{S\infty} + E_s \exp(-t/\tau_d)$, the relaxation function associated with the device.

This elementary model can easily be generalised to include an arbitrary number of Maxwell elements arranged in parallel (Figure 2-18c). This would leads to a continuous relaxation spectrum if the number of elements was infinite. For this model, the stress response is defined by:

$$\sigma^t(t) = E_{S0}\varepsilon^t(t) - \sum_{i=1}^{n} E_{Si}\varepsilon_i^v \tag{2-43}$$

where $E_{S0} = E_{S\infty} + \sum_{i=1}^{N} E_{Si}$, $\tau_i = \eta_i / E_{Si}$, $i=1, \ldots, n$. The internal variable satisfies

$$\frac{\partial \varepsilon_i^v}{\partial \tau} + \frac{\varepsilon_i^v}{\tau_i} = \frac{\varepsilon^t}{\tau_i} \tag{2-44}$$

The relaxation function derived from the generalized Maxwell model is given by:

$$G_l(t) = E_{S\infty} + \sum_{i=1}^{n} E_{Si} \exp(-t/\tau_i) \tag{2-45}$$

where $E_{S\infty}$, E_{Si} and τ_i are all positive constants denoting respectively the equilibrium modulus, relaxation moduli, and relaxation times. The series expression in equation (2-45) is often referred to as Prony series. It is a monotonically decreasing function which assumes that the material depends more on the recent history than on earlier events.

2.4.3.2 Quasi-linear theory of viscoelasticity

As outlined by Fung (1972), it is reasonable to expect that for oscillations of small amplitude about the equilibrium state, the theory of linear viscoelasticity should apply for soft tissues. For finite deformations, however, the nonlinear stress-strain characteristics of the tissues

must be accounted for. In order to account for these nonlinearities, Fung (1972) developed the quasi-linear theory of viscoelasticity (QLV theory) which describes the deformation- and time-dependent stress within a tissue by the following convolution:

$$\sigma(t) = G(t) * \sigma^e(\lambda) \tag{2-46}$$

where $\sigma^e(\lambda)$ is the elastic response, a nonlinear function describing the stress in response to an instantaneous input of stretch (from $\lambda = 1$ to λ). $G(t)$ is the reduced relaxation function that represents the time-dependent stress response of the tissue normalised by the peak stress following a step input of stretch.

To describe a non-instantaneous deformation history, the Boltzmann superposition principle is applied and the stress at time t, $\sigma(t)$, is given by:

$$\sigma(t) = \int_{-\infty}^{t} G(t-\tau) \frac{\partial \sigma^e[\lambda(\tau)]}{\partial \tau} d\tau \tag{2-47}$$

The stress at any time t is the sum of contributions of all the past changes, each governed by the same relaxation function, $G(t)$. This is a generalisation of the linear theory of viscoelasticity, where the instantaneous stress response $\sigma^e[\lambda(t)]$ plays the role assumed by the strain ε in equation (2-39). If the motion starts at $t=0$, equation (2-47) reduces to

$$\sigma(t) = \sigma^e(0+)G(t) + \int_0^t G(t-\tau) \frac{\partial \sigma^e[\lambda(\tau)]}{\partial \tau} d\tau \tag{2-48}$$

and $G(t)$ is referred to as the reduced relaxation function.

For a simple interpretation, this can also be written as

$$\sigma(t) = \sigma^e[\lambda(t)] + \int_0^t \sigma^e[\lambda(t-\tau)] \frac{\partial G(\tau)}{\partial \tau} d\tau \tag{2-49}$$

if $\partial \sigma^e / \partial \tau, \partial G(\tau) / \partial \tau$ are continuous in $0 \le t < \infty$.

Thus the tensile stress at any time t is equal to the instantaneous stress response $\sigma^e[\lambda(t)]$ decreased by an amount depending on the past history, because $\partial G(\tau) / \partial \tau$ is generally of negative value.

As shown by the following non-exhaustive list, the QLV model is probably the most extensively used model to represent soft tissues viscoelasticity: modelling of artery (Tanaka and Fung, 1974), modelling of tendons and ligaments (Lanir, 1980, Woo *et al.*, 1981, Lyon *et al.*, 1988, Kwan *et al.*, 1993, Puso and Weiss, 1998, Abramowitch *et al.*, 2004), modelling of mature myocardium (Pinto and Patitucci, 1980), modelling of cartilage (Mow *et al.*,1980), modelling of porcine aortic valve tissues (Rousseau *et al.*, 1983, Sauren *et al.*, 1983, Doehring *et al.*, 2004), modelling of rabbit skeletal muscle (Best *et al.*, 1994).

Numerous forms have been used for the elastic response within the context of the QLV theory, depending on the underlying material symmetry and the modes of deformation of interest. For the reduced relaxation function, the most common form was designed by Fung (1972) and describes a constant spectrum of relaxation:

$$G(t) = \frac{1 + v_c\left[L(t/\tau_2) - L(t/\tau_1)\right]}{1 + c\ln(\tau_2/\tau_1)} \qquad L(y_1) = \int_{y_1}^{\infty} \frac{e^{-y}}{y}\,dy \qquad \begin{cases} y = \dfrac{1}{\tau} \\ y_1 = \dfrac{1}{\tau_1} \end{cases} \tag{2-50}$$

where v_c is a parameter reflecting the amount of viscoelastic content of the tissue, τ_1 and τ_2 are time constants that regulate the short and long term material responses respectively. Expression (2-50) corresponds to a generalisation of the mechanistic Kelvin model; it combines a large number of Kelvin units in which the sizes of the springs and dampers are varied so that the characteristic frequencies of the successive units form an almost continuous spectrum.

This form for *G(t)* was developed from observations made by Fung on rabbit mesentery showing that the hysteresis loop in the tissue response is almost independent of the strain rate over several orders of magnitude.

Best *et al.* (1994) modelled with success skeletal muscle tensile viscoelastic behaviour using the QLV theory. They adopted a fourth-order polynomial form for the elastic response of the tissue and equation (2-50) was used for the relaxation function.

However, one of the difficulties in the use of the QLV theory is parameters estimation; they have often been estimated by separately fitting an elastic function to the stress-strain data

from the loading phase of a stress-relaxation test, and a reduced relaxation function to the normalised stress-time data from the relaxation phase (Sauren *et al.*, 1983; Dortmans *et al.*, 1984). Ideally, an instantaneous step displacement should be applied to completely separate the nonlinear elastic and time-dependent viscoelastic behavior. This is however impossible to achieve in practice, since real world stress-relaxation experiments are limited to finite time ramp displacements, leading to erroneous parameter estimates and limitations in model performances (Nigul and Nigul, 1987, Myers *et al.*, 1991, Abramowitch and Woo, 2004). Moreover, the use of a continuous spectrum of relaxation makes the QLV theory memory inefficient for finite element implementation.

Equation (2-48) corresponds to a uniaxial state of stress. In a three-dimensional framework, the following tensor equation applies:

$$\boldsymbol{S}(t) = \boldsymbol{G}(t)\boldsymbol{S}^{e}(0) + \int_{0}^{t} \boldsymbol{G}(t-\tau)\frac{\partial \boldsymbol{S}^{e}[\boldsymbol{E}(\tau)]}{\partial \tau} d\tau \tag{2-51}$$

where $\boldsymbol{S}(t)$ is the second Piola-Kirchhoff stress tensor, $\boldsymbol{S}^{e}[\boldsymbol{E}]$ is the instantaneaous elastic response of the material and $\boldsymbol{G}(t)$ is the tensorial reduced relaxation function. Considering the lack of experimental data to fully determine the terms of the tensorial relaxation function, a scalar form is commonly used (Maurel *et al.*, 1998).

2.4.3.3 Discretised QLV theory

A discretised form of the QLV theory, using a Prony series formulation for the relaxation function has been adopted by some authors to represent soft tissues behaviour: modelling of brain tissue in tension and compression (Miller, 1999; Miller and Chinzei, 2002), modelling of kidney in compression (Snedeker *et al.*, 2005), modelling of skeletal muscle in compression (Bosboom *et al.*, 2001a, 2001b).

The formulation used by these authors takes the general form:

$$\boldsymbol{S}(t) = \int_{0}^{t} G(t-\tau)\frac{\partial \boldsymbol{S}^{e}[\boldsymbol{E}(\tau)]}{\partial \boldsymbol{E}}\frac{\partial \boldsymbol{E}}{\partial \tau} d\tau \quad \text{with} \quad G(t) = p_{\infty} + \sum_{i=1}^{N} p_i \exp(-\frac{t}{\tau_i}) \tag{2-52}$$

This leads to

$$\boldsymbol{S}(t) = p_\infty \boldsymbol{S}^e\left(E(t)\right) + \sum_{i=1}^{N} \int_0^t p_i \exp\left(-\frac{t-\tau}{\tau_i}\right) \frac{\partial \boldsymbol{S}^e[\boldsymbol{E}(\tau)]}{\partial \boldsymbol{E}} \frac{\partial \boldsymbol{E}}{\partial \tau} d\tau \tag{2-53}$$

with $p_\infty = 1 - \sum_{i=1}^{N} p_i$. The first term in equation (2-53) represents the long term elastic contribution; the second term is the sum of viscoelastic components.

Bosboom *et al.* (2001a and b) conducted *in vitro* and *in vivo* experiments on rat tibialis anterior muscles (see section 2.3.2). They used an isotropic formulation – incompressible Ogden model (Ogden, 1984) – to describe passive muscle elastic behaviour and implemented viscoelasticity by means of a single term Prony series expansion. The strain energy function W in single mode incompressible Ogden model takes the form

$$W = \frac{\mu_1}{\mu_2}\left(\lambda_1^{\mu_2} + \lambda_2^{\mu_2} + \lambda_3^{\mu_2} - 3\right) \tag{2-54}$$

μ_1 and μ_2 are the material parameters, λ_i, the principal stretch ratios. Considering a uniaxial compression test, the Cauchy stress characterising the long term elastic response of the material can be expressed as

$$\sigma = (1-\delta_1)\mu_1\left(\lambda^{\mu_2} + \lambda^{(-\mu_2/2)}\right) \tag{2-55}$$

with λ representing the stretch ratio in the direction of testing.

Due to inhomogeneous stress and strain distribution in the muscle a two-dimensional plane stress approach was used for parameter estimation. Table 2-4 presents values of parameters obtained for the *in vivo* and the *in vitro* tests.

Table 2-4: Parameters for the Ogden viscoelastic model representing passive rat muscle behaviour in compression (Bosboom *et al.*, 2001a, b)

Type of test	μ_1 (kPa)	μ_2	δ_1	τ_1(s)
in vitro – Bosboom et al. (2001a)	13.5	5	0.7	2.7
in vivo – Bosboom et al. (2001a)	15.6	21.4	0.549	6.01

Using these parameters, the theoretical curves presented in Figure 2-10 were generated. These results are compared to experimental data on muscle compressive properties published by various authors.

Goh *et al.* (2004) presented a simple formulation for computing the strain and the time dependent constants for viscoelastic materials which exhibit separable strain and time dependent behaviours. Their method is based on a recurrence numerical algorithm proposed by Taylor *et al.* (1970). The convolution integral is divided into recursive parts; this allows an incremental formulation and integration for the current stress state from the history variables stored at the previous time step, and the current time and strain increments.

For the time interval (t_n, t_{n+1}), the time step Δt is given as $\Delta t = t_{n+1} - t_n$. The exponential expression in equation (2.52), $\exp(-t_{n+1}/\tau_i)$, can be split into:

$$\exp\left(\frac{-t_{n+1}}{\tau_i}\right) = \exp\left(\frac{-t_n}{\tau_i}\right)\exp\left(\frac{-\Delta t}{\tau_i}\right) \tag{2-56}$$

Using a uniaxial formulation for simplicity of notations, the Cauchy stress can be expressed as:

$$\begin{aligned} \sigma(t) &= p_\infty \sigma^e(t) + \sum_{i=1}^{n} \int_0^t p_i \exp\left(\frac{-(t-\tau)}{\tau_i}\right) \frac{\partial \sigma^e[\varepsilon(\tau)]}{\partial \tau} d\tau \\ \text{or} \quad \sigma(t) &= p_\infty \sigma^e(t) + \sum_{i=1}^{n} s_i \end{aligned} \tag{2-57}$$

The stress term s_i at t_{n+1} can be separated into two components. The first corresponds to the deformation history during the period $0 \le \tau \le t_n$ while the second relates to the time period $t_n \le \tau \le t_{n+1}$. Thus,

$$s_i(t_{n+1}) = \int_0^{t_{n+1}} p_i \exp\left(-\frac{t_{n+1}-\tau}{\tau_i}\right) \frac{\partial \sigma^e(\tau)}{\partial \tau} d\tau \tag{2-58}$$

$$s_i(t_{n+1}) = \exp\left(-\frac{\Delta t}{\tau_i}\right) s_i(t_n) + \int_{t_n}^{t_{n+1}} p_i \exp\left(-\frac{t_{n+1}-\tau}{\tau_i}\right) \frac{\partial \sigma^e(\tau)}{\partial \tau} d\tau \tag{2-59}$$

The differential coefficient, $\frac{d\sigma^e(\tau)}{d\tau}$, can be expressed in terms of discrete time steps,

$$\frac{d\sigma^e(\tau)}{d\tau} = \lim_{\Delta\tau\to 0} \frac{\Delta\sigma^e(\tau)}{\Delta\tau} = \lim_{\Delta t\to 0} \frac{\sigma^e_{n+1} - \sigma^e_n}{\Delta t} \tag{2-60}$$

Substituting equation (2-60) into equation (2-59) and solving the integral analytically leads to the recursive formula for updating the stress $\sigma(t_{n+1})$:

$$\sigma(t_{n+1}) = p_\infty \sigma^e(t_{n+1}) + \sum_{i=1}^{N} \left(\exp\left(-\frac{\Delta t}{\tau_i}\right) s_i(t_n) + p_i \frac{1-\exp\left(-\frac{\Delta t}{\tau_i}\right)}{\frac{\Delta t}{\tau_i}} \left[\sigma^e(t_{n+1}) - \sigma^e(t_n)\right] \right) \tag{2-61}$$

This recursive approach greatly minimizes the storage required to perform the constitutive integration. The formulation will be used in chapter 4 to fit a quasi-linear viscoelastic model to experimental data obtained on skeletal muscle.

2.4.3.4 Strain rate effect

A limitation of the QLV theory is that it does not explicitly take into account the loading rate which, according to some authors, influences the viscoelastic behaviour of soft tissues (Chiba and Komatsu, 1993; Pioletti *et al.*, 1998; Ticker *et al.*, 1996). The QLV model has been modified to incorporate the strain-rate dependency (Haut and Little, 1972; Woo *et al.*, 1981). As reported by Pioletti *et al.* (1998), this gives good results at low strain rates (0.06-0.75%s^{-1}) but gives inaccurate results for higher strain rates (up to 10%s^{-1}). Pioletti *et al.* (2000) proposed a model in which stress-relaxation and the strain rate effect are discriminated according to the time scale of their effects: the stress relaxation corresponds to the long time memory while the strain rate dependence corresponds to the short time memory. In the proposed constitutive law, the second Piola-Kirchhoff stress tensor is separated into three parts (equation 2-62).

$$\boldsymbol{S}(t)=\boldsymbol{S}^{e}[\boldsymbol{C}(t)]+\boldsymbol{S}^{v}\left[\overset{\circ}{\boldsymbol{C}}(t);\boldsymbol{C}(t)\right]+\Im_{s=\delta}^{\infty}\{\boldsymbol{G}(t-\tau);\boldsymbol{C}(t)\} \tag{2-62}$$

where $\boldsymbol{S}^{e}$ is the immediate contribution (elastic behaviour) as it supports the contribution of the deformation at the actual time t. $\boldsymbol{S}^{v}$ represents the almost immediate contribution (viscous behaviour), i.e. the short time memory. Finally, the third term represents the delayed contribution (relaxation behaviour), i.e. the long time memory. $\Im$ is a functional representing the history of strain, $\boldsymbol{G}(t-s)=\boldsymbol{C}(t-\tau)-\boldsymbol{C}(t)$. The long time memory can be described with the quasi-linear viscoelastic theory of Fung (1993) for example.

Compared to the QLV theory, the model developed by Pioletti *et al.* includes explicitly a strain rate dependent term, which might be required to represent soft tissues behaviour at high strain rates.

2.4.3.5 Nonlinear viscoelastic model

Some materials present nonlinearity not only in their elastic but also in their viscoelastic behaviour. To account for this, Schapery (1969) derived a nonlinear viscoelastic formulation from thermodynamic principles. The constitutive equations developed have a single-integral form, which is very similar to the Boltzmann superposition principle used in linear viscoelastic theory (equation 2-39). When strain is treated as the independent state variable and uniaxial loading is considered, Schapery's theory takes the form:

$$\sigma(t)=h_e G_\infty \varepsilon(t)+h_1\int_0^t \Delta G(\rho-\rho')\frac{dh_2\varepsilon(\tau)}{d\tau}d\tau \tag{2-63}$$

with the reduced time, ρ, defined as

$$\rho=\int_0^t \frac{dt'}{a_\tau[\varepsilon(t')]} \quad \text{and} \quad \rho'=\rho(\tau)=\int_0^\tau \frac{dt'}{a_\tau[\varepsilon(t')]} \tag{2-64}$$

The terms h_e, h_1, h_2, and a_τ are strain-dependent material properties; they introduce nonlinearities in the elastic (h_e and h_2) and in the viscoelastic (h_1 and a_τ) behaviour. Thermal

effects can also be included in a_τ; these are not taken into account in the following developments.

As a means of illustrating the type of behaviour described by these equations, the form relevant to a relaxation (constant strain) test is considered. Substituting a constant strain, ε, into equation (2-63), and recognizing that $\frac{dh_2\varepsilon}{dt}=0$ is zero except at $t=0$, yields

$$\int_0^t \Delta G(\rho-\rho')\frac{dh_2\varepsilon}{d\tau}d\tau = \Delta G(\rho)\int_0^t \frac{dh_2\varepsilon}{d\tau}d\tau = \Delta G\left(\frac{t}{a_\tau}\right)h_2\varepsilon \tag{2-65}$$

The nonlinear relaxation modulus, $G_n(t)$, is then defined as:

$$G_n(t)\equiv\frac{\sigma}{\varepsilon}=h_e G_\infty + h_1 h_2 \Delta G\left(\frac{t}{a_\tau}\right) \tag{2-66}$$

with $G_\infty = G_n(\infty)$, equilibrium or final value of the modulus and $\Delta G(t)=\tilde{G}\exp(-t/\tau)$, transient component of the modulus. The long term elastic stress is thus multiplied by the strain dependent term h_e; the transient stress is multiplied by h_1 and h_2 and the time constant charaterising the transient decay is multiplied by a_τ.

Poon *et al.* (1998) extended Shapery's nonlinear model to a three-dimensional anisotropic formulation. A method to perform the integration and implement the model into a finite element analysis is also provided in this paper. Their method is based on a judicious choice of state variables and a stable backward Euler integration step.

Three-dimensional anisotropic linear viscoelasticity can be formulated as:

$$\sigma_{ij}(t)=\left[\sum_k\sum_l G^\infty_{ijkl}\varepsilon_{kl}\right]+\int_0^t\sum_k\sum_l\left[\Delta G_{ijkl}(t-\tau)\frac{d}{d\tau}\varepsilon_{kl}\right]d\tau \tag{2-67}$$

where G^∞_{ijkl} are the equilibrium moduli, $\Delta G_{ijkl}(t)$ the transient decay.

Following Schapery's one-dimensional pattern given in equation (2-63), nonlinearity is introduced into the constitutive relation of equation (2-67), resulting in

$$\sigma_{ij}(t)=h_e\left[\sum_k\sum_l G^\infty_{ijkl}\varepsilon_{kl}\right]+h_1\int_0^t\sum_k\sum_l\left[\Delta G_{ijkl}(\xi_{ijkl}-\xi'_{ijkl})\frac{d}{dt'}(h_2\varepsilon_{kl})\right]dt' \tag{2-68}$$

The scalar functions h_e, h_1, h_2 are dependent on the strain tensor. The reduced time is influenced by the mechanical strain via

$$\xi_{ijkl} = \int_0^t \frac{dt}{a_{\tau ijkl}(\boldsymbol{E}(t'))} \tag{2-69}$$

Using a single term Prony series to describe the stress relaxation behaviour $G_{ijkl}(\xi_{ijkl}) = G^{\infty}_{ijkl} + \tilde{G}_{ijkl}\exp(-\xi_{ijkl}/\tau_{ijkl})$, equation (2-68) becomes:

$$\sigma_{ij}(t) = h_e\left[\sum_k\sum_l G^{\infty}_{ijkl}\varepsilon_{ijkl}\right] + h_1\int_0^t\sum_k\sum_l\left[\tilde{G}_{ijkl}\exp(-\frac{\xi_{ijkl}-\xi'_{ijkl}}{\tau_{ijkl}})\frac{d}{dt'}(h_2\varepsilon_{ijkl})\right]dt' \tag{2-70}$$

Defining the following state variable,

$$D_{ijkl} = \int_0^t \tilde{G}_{ijkl}\left[1-\exp\left(-\frac{\xi_{ijkl}-\xi'_{ijkl}}{\tau_{ijkl}}\right)\right]\frac{d}{dt'}(h_2\varepsilon_{kl})dt' \tag{2-71}$$

and developing a special differentiation formula to derive an evolution law for D_{ijkl}, the following recursive formula is obtained for the stress during the time period $t_n \le \tau \le t_{n+1}$

$$\sigma^{n+1}_{ij} = h^{n+1}_e\left[\sum_k\sum_l G^{\infty}_{ijkl}\varepsilon^{n+1}_{kl}\right] + h^{n+1}_1\sum_k\sum_l\left[\tilde{G}_{ijkl}h^{n+1}_2\varepsilon^{n+1}_{kl} - D^{n+1}_{ijkl}\right] \tag{2-72}$$

with

$$D^{n+1}_{ijkl} = \left(\frac{1}{\Delta t}+\frac{1}{\tau_{ijkl}a^{n+1}_{ijkl}}\right)^{-1}\left[\frac{D^n_{ijkl}}{\Delta t}+\frac{\tilde{G}_{ijkl}h^{n+1}_2\varepsilon^{n+1}_{kl}}{\tau_{ijkl}a^{n+1}_{ijkl}}\right] \tag{2-73}$$

This recursive formulation will be used in chapter 4 to test the suitability of a nonlinear viscoelastic model to represent skeletal muscle properties.

2.5 Concluding remarks

It should now be clear to the reader that past scientific research on skeletal muscle has mainly considered the tissue as a force actuator and has been centred on its force producing capabilities. The recent advancements of virtual modelling in impact biomechanics, rehabilitation engineering, etc. led to the observation that experimental data on muscle load bearing capabilities are missing. The literature on muscle compressive properties remains quite sparse. A few *in vivo* studies have been carried out on animal muscle tissues; however, different experimental protocols have been used in these studies (different species, samples, strain rates, etc.) and large variations are noticed between the data published. Non-invasive techniques have also been used to measure human muscle properties; however, linear elasticity is often assumed and only limited information is obtained on muscle properties.

As a result of this, muscle tissue has also been poorly characterised from a modelling point of view; most models suitable to represent muscle properties have been developed for other soft tissues with fibre oriented structure, such as tendons and ligaments.

This study aims to further advance the knowledge on the mechanical properties of this fundamental but structurally complex constituent of the human body. Elastic and viscoelastic behaviour of the tissue have been brought under scrutiny; for both types of properties, an experimental investigation has first been conducted and this was followed by a theoretical approach.

Chapter 3 - Study of muscle elastic properties

3.1 INTRODUCTION 54

3.2 MATERIALS AND METHODS 54

3.3 EXPERIMENTAL RESULTS 59

3.3.1 AGED TISSUE 59

3.3.2 FRESH TISSUE 62

3.4 MATHEMATICAL MODELLING 67

3.4.1 AGED TISSUE 67

3.4.1.1 Martins' model 67

3.4.1.2 SYM model 74

3.4.2 FRESH TISSUE 77

3.4.2.1 Martins' model 77

3.4.2.2 SYM model 79

3.5 DISCUSSION 87

3.5.1 GENERAL REMARKS 87

3.5.2 CHOICE OF EXPERIMENTAL PARAMETERS AND TISSUE TESTED 87

3.5.3 COMPARISON OF EXPERIMENTAL RESULTS WITH PUBLISHED DATA 89

3.5.4 DIFFERENCES OBSERVED BETWEEN THE VARIOUS TISSUES TESTED 92

3.5.5 CHOICE OF A MODEL 93

3.5.6 TENSILE BEHAVIOUR OF THE TISSUE 94

3.1 Introduction

The first step undertaken in this study to investigate skeletal muscle compressive behaviour was the measurement of the tissue long term elastic properties. Given the fibre oriented structure of muscle tissue, compression tests were performed at various orientations of the muscle fibres. Results from theses tests, performed at a low compression rate ($0.05\%.s^{-1}$) on animal muscle tissues, are presented in this chapter.

In view of the results obtained, the hypothesis of transverse isotropy was formulated and the applicability of two nonlinear transversely isotropic models was investigated to mathematically represent skeletal muscle compressive behaviour.

3.2 Materials and methods

Uniaxial unconfined compression experiments were conducted on porcine, bovine and ovine muscle samples. The bovine and a first set of porcine samples were obtained from a local butcher and had therefore been bled and hung after slaughtering. No control over age, gender, time of death or methods of storage was available for these samples and they will be referred to as "aged" samples. In contrast, the ovine and the second set of porcine samples were obtained immediately after death from unbled animals. The ovine samples were excised from the thoracic limb of male sheep aged 10 months. The porcine fresh samples were excised from the pelvic limb of male pigs aged 3 months. These will be referred to as fresh samples. Aged tissues have the advantage that they are readily available; they were used to conduct preliminary experiments and obtain a general idea of skeletal muscle behaviour under compressive loading. The experimental protocol used to characterise muscle properties in three-dimensions was then established from these tests. However, most results were obtained from tests performed on fresh porcine tissues - tests conducted after death of the animal show a significant influence of time of death on muscle mechanical properties as detailed later in this chapter.

Cubic specimens of characteristic length between 5 and 10mm were used for testing. Samples with regular shape were chosen in order to determine more easily and more accurately their dimensions as well as the stress distribution; this will lead to more repeatability in the results. Tests specimens were mainly cut out along the cross-fibre, the fibre and at 45° from the fibre direction (Figure 3-1). As discussed in the theoretical section (section 2.3.2), tests performed in these three directions are sufficient to determine the five coefficients characteristic of transversely isotropic materials. Samples used for compression in the fibre direction had a smaller height than the two other types of samples. This was adopted in order to diminish buckling of the muscle fibres that was observed in samples compressed in the fibre direction. Samples with a ratio (height/transverse dimension) approximating ½ were used.

Muscle tissue is quite mobile and manual cutting leads to specimens with inconsistent geometry and orientation, increasing scatter and error in subsequent calculations of mechanical properties. Therefore a cutting bench was developed in order to improve the cutting process and increase repeatability in samples preparation (Figure 3-2).

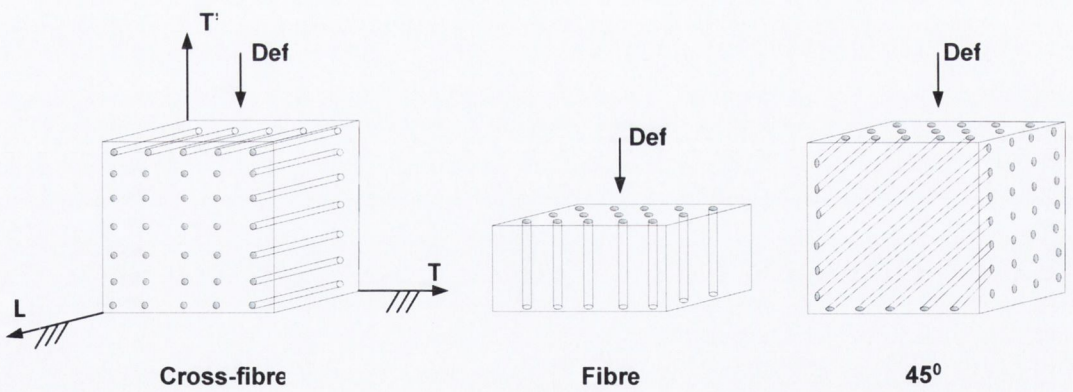


Figure 3-1: Schematic of specimens used for testing.

L is the longitudinal direction. T & T' are the transverse directions. Def represents the applied deformation.

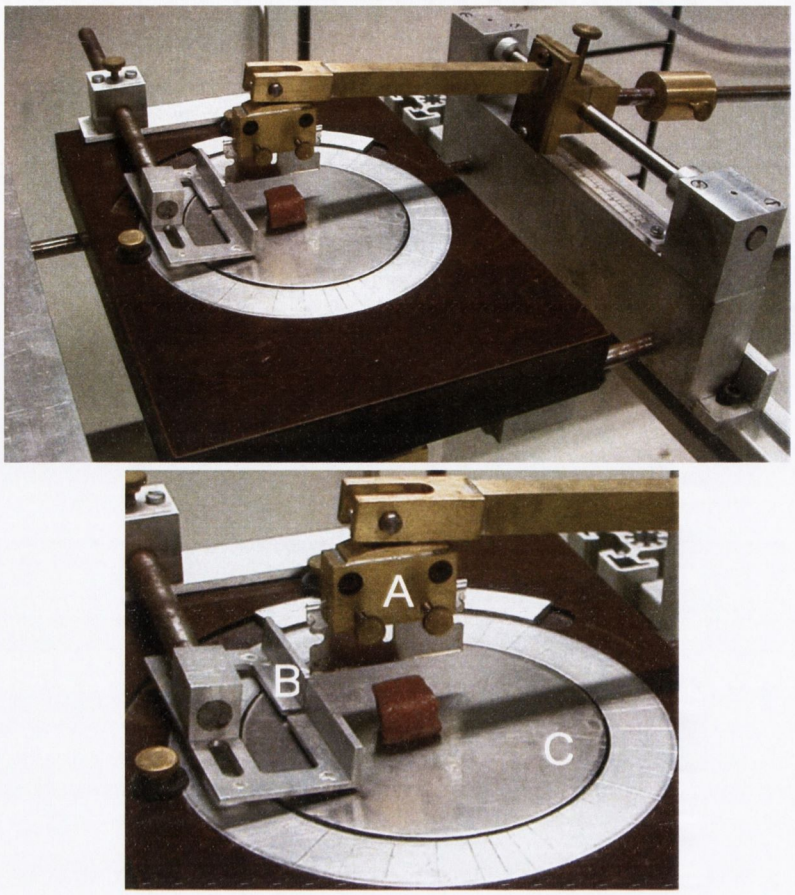


Figure 3-2: Custom made cutting bench.

(A) Blade; (B) Support fence; (C) Rotary table.

The bench is equipped with a cutting blade (disposable single edge razor blade) mounted perpendicular to a stainless steel rotary table, on which samples are held in place by superficial freezing (Peltier Effect device mounted on the obverse of the table). Rotation of the table allows control of the relative orientation of the cuts that need to be performed in order to obtain a cubic specimen. A support 'fence' positioned against the sample reduces its mobility which is exacerbated during cutting. Using the device, a specimen with correct geometry and orientation can be obtained in a few steps. It has to be noted that the specimens obtained are not perfect cubes in the engineering sense as muscle tissue remains a soft and mobile material.

The compression tests were performed on a uniaxial test machine, Zwick Z005 (Zwick GmbH & Co. Ulm, Germany). A 5N load cell was used for force measurement. Samples

were positioned on a static platen and deformation was applied via a platen attached to the moving crosshead of the machine. To reduce friction between platens and samples, a sheath of PTFE was applied on both platens.

Samples were compressed up to 30% of their original length at a rate of $0.05\%str.s^{-1}$. This was considered as a good compromise between test duration and the measurement of truly elastic properties. Further comments on this point are made in the discussion section. Displacement and force were recorded with a time resolution of 0.05s. Each sample was tested once as the high strain level leads to some permanent tissue deformation. Tests were performed at room temperature and samples were placed in airtight containers after cutting to avoid dehydration. No fluid was seen to express from the specimens during the tests.

Displacement and force were measured uniaxially; however, biaxial information on deformation was obtained by recording the displacement of markers placed on the samples with quick drying ink. Images were acquired every second for the duration of the tests using a CCD camera. The experimental setup is illustrated in Figure 3-3.

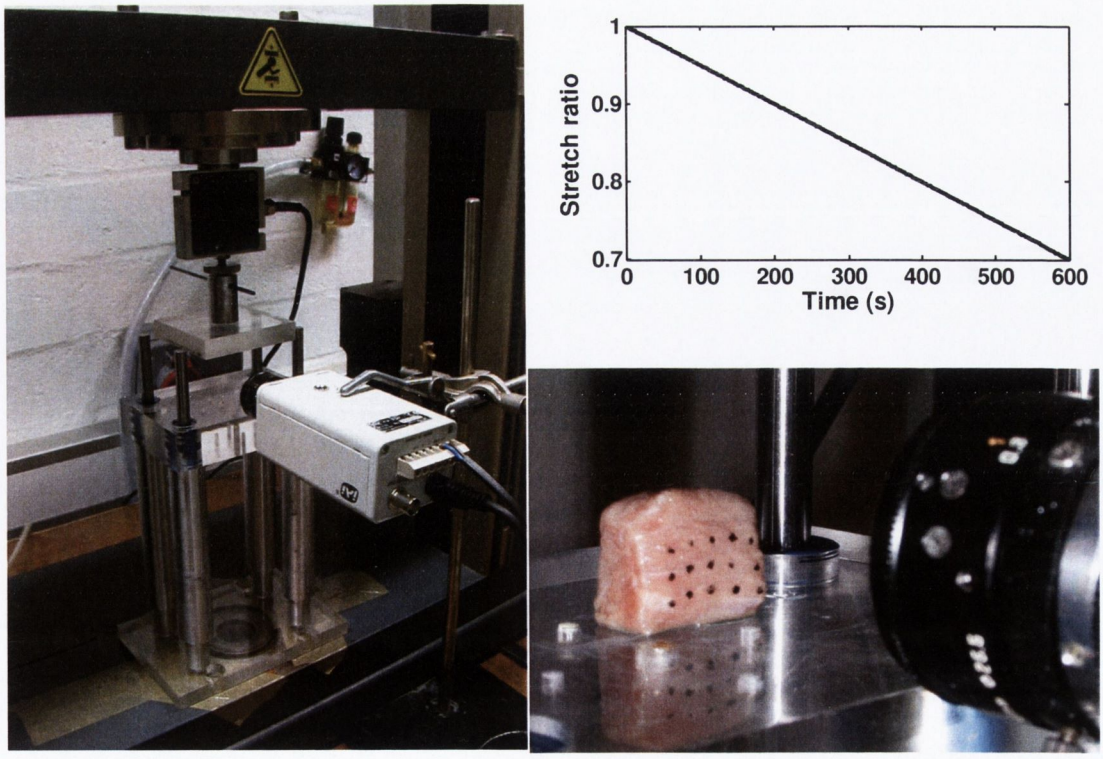


Figure 3-3: Experimental setup used for compression tests.

Finally, to investigate the sensitivity of muscle mechanical properties to time of test after death, repeated low strain tests were also performed on fresh ovine and porcine samples at regular intervals after death of the animal. Samples kept at room temperature in airtight containers were compressed up to 10% of their original length at regular intervals post mortem.

3.3 Experimental results

Results are presented using Cauchy stress (σ) and stretch ratio (λ). These were obtained by conversion of the load displacement data acquired during the tests:

$$\lambda = \frac{l_t}{l_0} \quad \text{and} \quad \sigma = \frac{f_t}{A_t} = \frac{f_t}{(A_0/\lambda)} \tag{3-1}$$

with l_0, the original length of the sample; l_t, its current (measured) length; A_0, the original area of the sample; A_t, the current (calculated) area; f_t, the measured force.

The following colour convention is adopted throughout this chapter: blue for cross-fibre direction, red for fibre direction, green for 30° direction, cyan for 45° direction and magenta for 60° direction. For clarity of presentation, only mean experimental results are presented. Complete data sets from which these mean results are derived are presented in Appendix A. Statistical analyses were performed using the Graphpad Prism software.

3.3.1 Aged tissue

Figure 3-4 presents experimental stress-strain curves obtained by compression of aged bovine and aged porcine samples. Tests were performed in the cross-fibre direction, the fibre direction and at 45° from the fibre direction. Three and four samples were respectively tested in each direction for the bovine and for the porcine tissue. Mean curves with one standard deviation are presented. Different scales are adopted on these graphs in order to clearly show results in each direction. Results in the three directions of testing are compared in Figure 3-5; it shows that for both types of muscle the cross-fibre direction is stiffer than the 45° direction, which in turn is stiffer than the fibre direction.

These results clearly illustrate that skeletal muscle presents a nonlinear and anisotropic behaviour when submitted to high levels of compressive deformation. Tests show an increase in stiffness with an increase in angle from the muscle fibre direction.

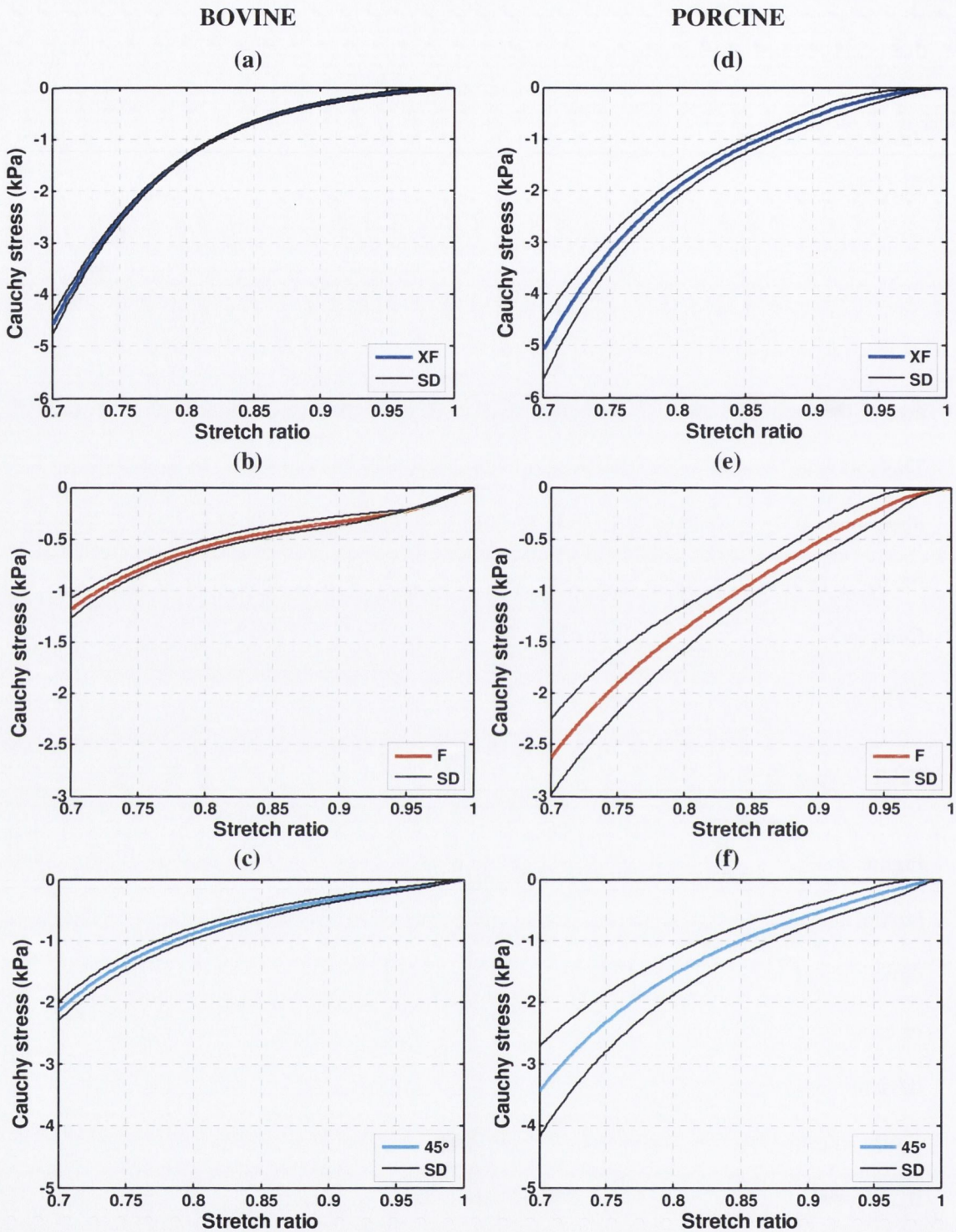


Figure 3-4: Compression tests on (left) aged bovine and (right) aged porcine samples.
(a) and (d) cross-fibre direction, (b) and (e) fibre direction and (c) and (f) 45° from the fibre direction - mean curves with one standard deviation.

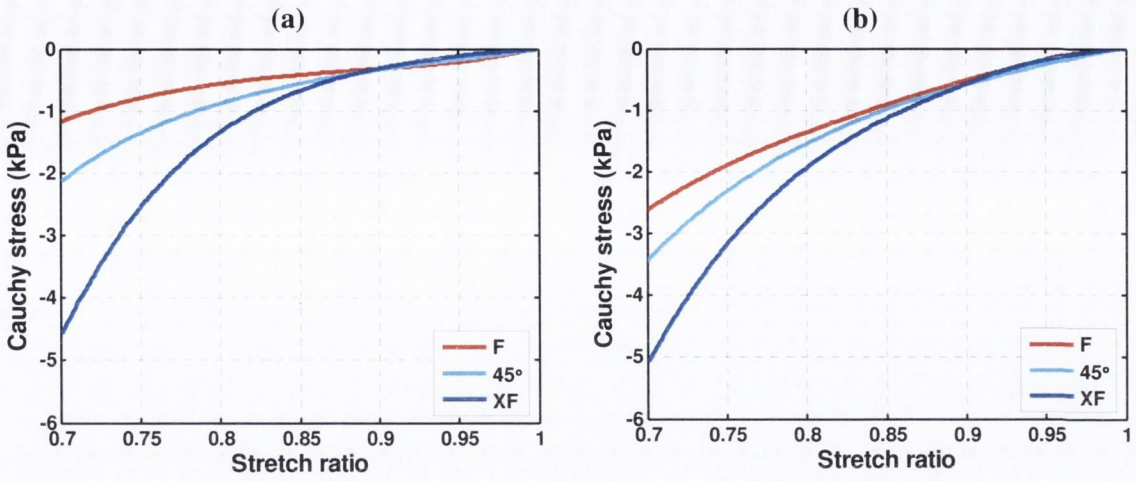


Figure 3-5: Compression tests on (left) aged bovine and (right) aged porcine samples. *Mean curves for the three directions of testing.*

Figure 3-5(a) shows that, within the first 10% of compression, the fibre direction is stiffer than the other two directions of testing. No significance was however attributed to this observation regarding muscle compressive behaviour. As mentioned previously, numerous parameters (hydration, storage of the muscle, age of the animal, etc.) could not be controlled with aged tissue and only a few samples were tested. These tests were conducted to obtain preliminary information and globally characterise skeletal muscle compressive behaviour.

Figure 3-6 illustrates the deformation of a sample during compression.

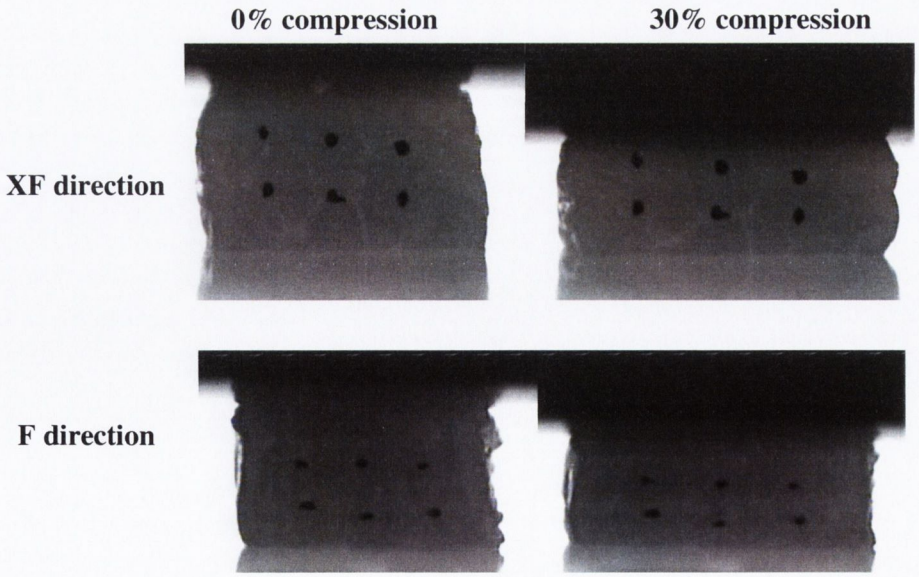


Figure 3-6: Illustration of the change in shape during compression of a porcine muscle sample in (top) cross-fibre and (bottom) fibre directions.

Apart from a small amount of barrelling due to friction between samples and compression platens, the cuboid appearance of the sample is preserved and markers placed on the samples preserve their relative horizontal and vertical arrangement. From these results, the hypothesis was made that skeletal muscle is transversely isotropic with the axis of symmetry running along the direction of the muscle fibres.

3.3.2 Fresh tissue

Data obtained from compression tests performed on fresh ovine muscle tissues show a markedly different behaviour of the tissue. Figure 3-7 presents results obtained after compression of samples oriented in the cross-fibre, the fibre and at 45° from the fibre direction. Anisotropy and nonlinearity still characterise muscle behaviour. The cross-fibre direction remains the stiffest of all directions; however the 45° direction is this time the least stiff of all three. Only two samples were tested in each direction and one series of tests was performed using ovine muscles due to the impracticality of obtaining tissues quickly enough after death of the animal. However, further tests performed on fresh porcine tissues confirmed these preliminary data.

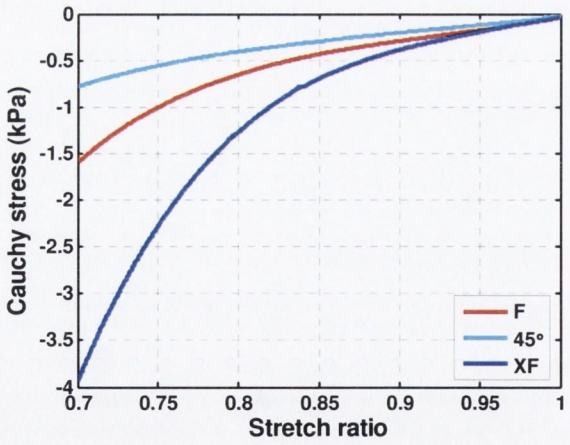


Figure 3-7: Compression tests on fresh ovine samples.
Mean curves for the three directions of testing.

Figure 3-8 presents experimental stress-strain curves obtained by compression of fresh porcine samples oriented in cross-fibre, fibre, 45°, 30° and 60° from the fibre direction. Tests

were performed on four pigs, aged 10-12 weeks. 15 samples were tested in each direction and mean curves with standard deviation are presented. Tests were started within two hours after animal death.

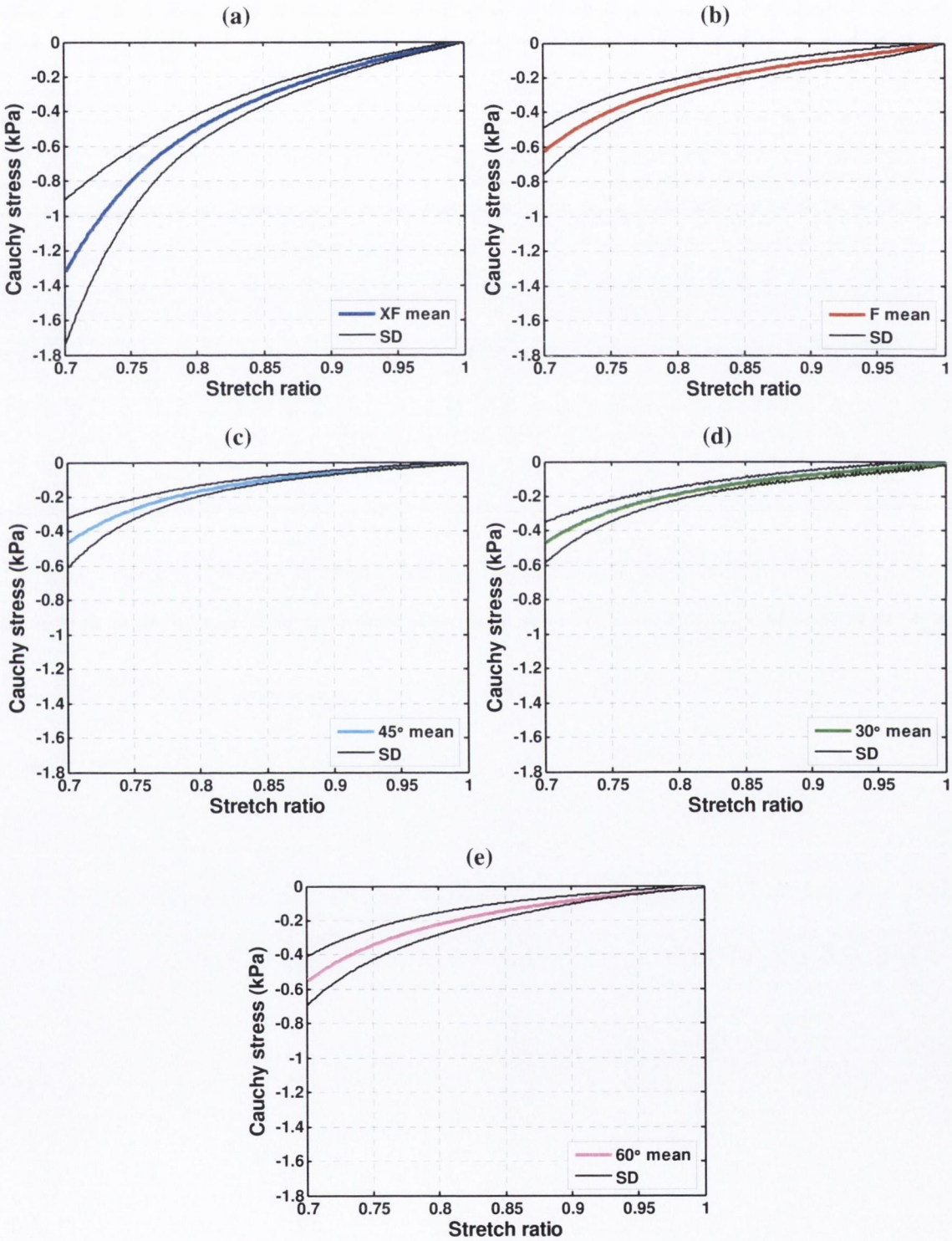


Figure 3-8: Compression tests on fresh porcine samples.

(a) cross-fibre direction, (b) fibre direction, (c) 30°, (d) 45° and (e) 60° from the fibre direction – mean curves with standard deviation.

The amount of variation present in the results increases with the level of compression. Table 3-1 compares mean stresses and standard deviations obtained after 30% compression in all directions of testing.

Table 3-1: Values of stress at 30% compression for fresh porcine samples compressed in various fibre orientations - mean ± SD

	F	30°	45°	60°	XF
$\sigma_{30\%}$(kPa)	-0.626 ±0.137	-0.468 ±0.119	-0.467 ±0.145	-0.553 ±0.142	-1.328 ±0.419

The variation in cross-fibre results is substantially larger than in any other direction. This is due to the presence of three samples with a stiffer response among the 15 samples tested. This might be due to the presence of an increased amount of fat or connective tissues in the samples, or to human error. Figure 3-9 compares results obtained with the original data set and the data set from which the three stiffer samples have been removed (reduced data set). The difference between these results appears to be relatively small; the reduced data set is however in better agreement with results from relaxation tests performed at a later stage (see Chapter 4) and the standard deviation calculated for this data set is closer to values obtained in other directions.

	XF original	XF modified
$\sigma_{30\%}$(kPa)	-1.328±0.419	-1.099±0.170

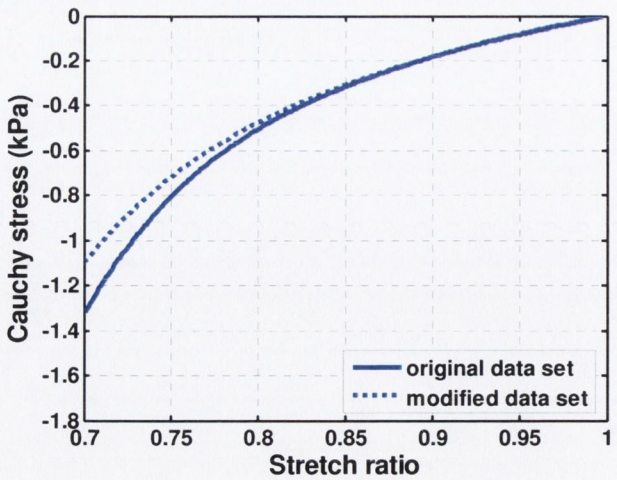


Figure 3-9: Comparison between original and modified data sets for tests on fresh porcine muscle samples in the cross-fibre direction.

From now on, results presented correspond to the reduced data set. Figure 3-10 compares results obtained in the various directions of testing. It shows that, as for the aged tissue, the cross-fibre direction is stiffer than the 45° and the fibre directions. However, the fibre direction is this time stiffer than the 45° direction.

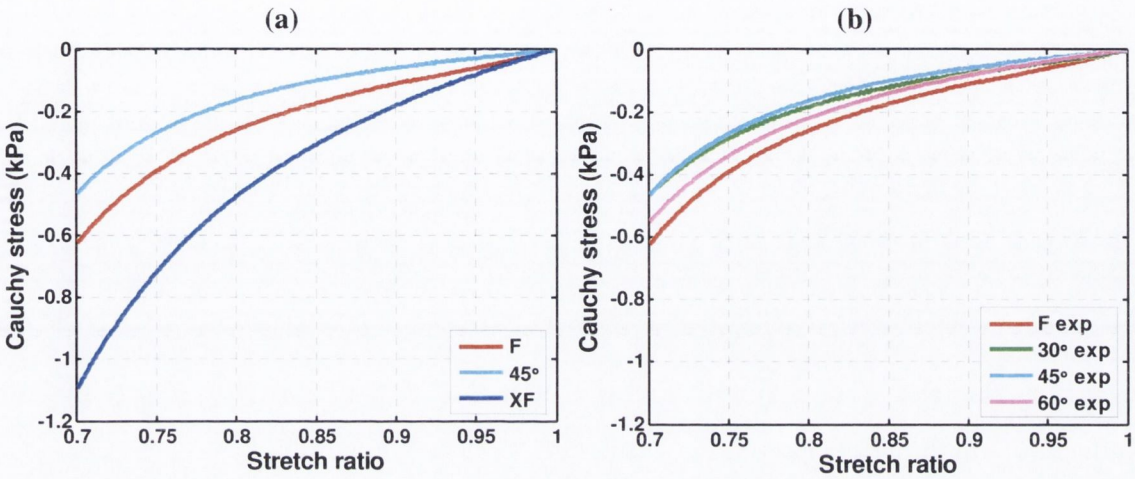


Figure 3-10: Compression tests on fresh porcine samples.

Mean curves comparing results in all directions of testing.

Images recorded during the tests help understand these results. Figure 3-11 illustrates the deformation of a sample with fibres oriented at 45° from the direction of testing.

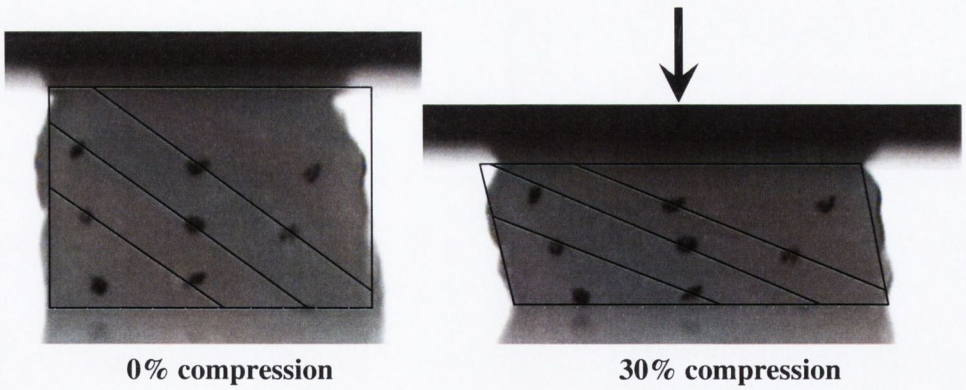


Figure 3-11: Deformation of a porcine sample with fibres oriented at 45° from the direction of testing.

Black lines represent fibres orientation and shape of a sample with perfect geometry.

The black lines superimposed on the image follow the orientation of the muscle fibres during compression and represent the change in geometry for a perfectly box shaped sample.

Shearing is observed between adjacent fibre fascicles leading to a parallelogram-shaped sample after deformation. Shearing is not observed when samples are compressed in the fibre or cross-fibre direction and this explains why muscle tissue is most compliant at 45° from the fibre direction.

Results from the repeated low strain tests are presented in Figure 3-12(a) and (b) for ovine and porcine samples respectively. Significant stiffening of muscle behaviour is noted a few hours after death of the subject: the maximum compressive stress measured at 10% deformation is increased approximately eight-fold for the ovine samples from 2 to 8.5 hours after death. The same type of behaviour was observed in fresh porcine samples with a multiplication factor situated around five between stress values measured after 1 and 16 hours postmortem. This stiffening, due to rigor mortis, emphasises the need to perform tests on fresh tissues.

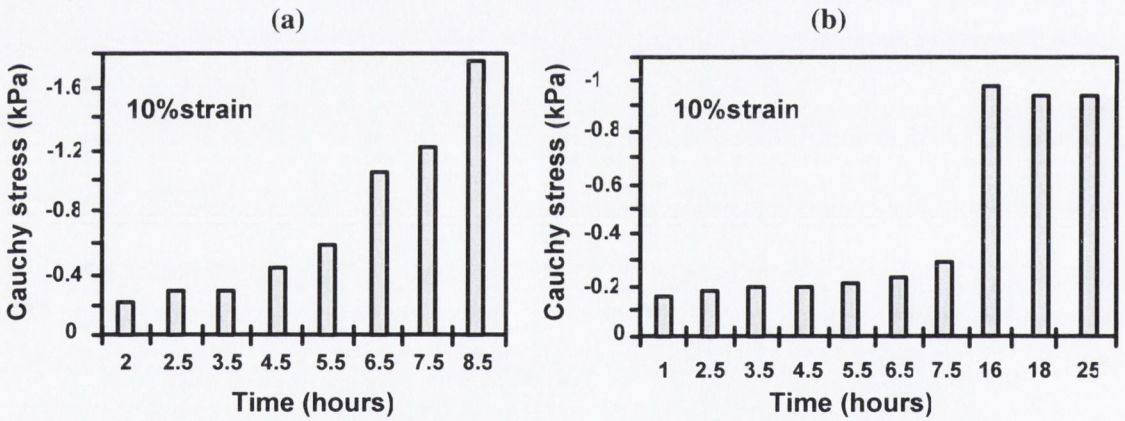


Figure 3-12: Evolution of the maximum compressive stress with time after death for fresh ovine (left) and porcine (right) samples.

3.4 Mathematical modelling

In this section, the ability of two three-dimensional transversely isotropic models to reproduce skeletal muscle quasi-static compressive behaviour is investigated. These models have been presented in section 2.3.2; the first one is the hyperelastic transversely isotropic model developed by Martins *et al.* (1998) for skeletal muscle tissue; the second one is an adaptation of the transversely isotropic, strain dependent Young's moduli (SYM) model developed by Li *et al.* (2001) for aortic heart valves.

3.4.1 Aged tissue

3.4.1.1 Martins' model

Martins *et al.* (1998) developed a model for skeletal muscle including the passive and active properties of the tissue; the active component of the model is however omitted in the following developments as only muscle passive behaviour is considered in this thesis. The strain energy function of the model is defined by:

$$W = W_1(I_1) + W_\alpha(\alpha) \tag{3-2}$$

with I_1 representing the first invariant of the right Cauchy-Green deformation tensor and α the stretch in the fibre direction. The first term of the sum represents the strain energy stored in the isotropic matrix embedding the muscle fibres; the second term represents the strain energy stored in the fibres.

Considering incompressibility, the Cauchy stress tensor takes the form:

$$\boldsymbol{\sigma} = -p\boldsymbol{I} + 2W_1'\boldsymbol{B} + \frac{W_\alpha'}{\alpha}\boldsymbol{F}a_0 \otimes a_0\boldsymbol{F}^T \tag{3-3}$$

with p, $\boldsymbol{I}$, a_0 and $\boldsymbol{B}$ defined as before,

$$W_1' = \partial W / \partial I_1 = c_1 c_2 \exp\left(c_2 (I_1 - 3)\right) \tag{3-4}$$

and

$$W_\alpha' = \partial W / \partial \alpha = \begin{cases} 4T_0 (\alpha - 1)^2, & \text{for } \alpha > 1 \\ 0, & \text{for } \alpha \le 1 \end{cases} \tag{3-5}$$

Parameters c_1 and c_2 correspond to the behaviour of the isotropic matrix. T_0 is the maximum steady-state stress that the muscle can develop under isometric conditions; the muscle fibres are assumed not to bear any load in compression. To determine the model parameters, Martins *et al.* considered that the tension behaviour of muscle tissue was known; expression (3-5) was taken from Chen *et al.* (1992) with $T_0 = 668.8$ kPa. Parameters c_1, c_2 were then determined to approximate the compressive passive behaviour of skeletal muscle without modifying, in a meaningful way, the known tensile behaviour of the tissue. Data published by Grieve and Armstong (1988) from *in vitro* compression tests on porcine muscle tissues were used to obtain c_1, c_2.

In the following developments, a reference frame of rectangular coordinate axes, with basis vectors e_i, $i = 1,2,3$ is considered. In a uniaxial test, with direction *1* as the direction of loading, $\boldsymbol{F}$ and $\boldsymbol{B}$ take the following forms:

$$\boldsymbol{F} = \begin{bmatrix} \lambda_1 & 0 & 0 \\ 0 & \lambda_2 & 0 \\ 0 & 0 & \lambda_3 \end{bmatrix} \quad \text{and} \quad \boldsymbol{B} = \boldsymbol{F}\boldsymbol{F}^T = \begin{bmatrix} \lambda_1^2 & 0 & 0 \\ 0 & \lambda_2^2 & 0 \\ 0 & 0 & \lambda_3^2 \end{bmatrix} \tag{3-6}$$

λ_i ($i = 1,2,3$) representing the stretch ratio along direction e_i.

If muscle fibres are aligned with the direction of testing, the vector defining the fibre orientation is $a_0 = [1 \quad 0 \quad 0]$ and the stretch in the fibre direction coincides with the applied stretch, $\alpha = \lambda_1$.

The components of stress in the principal directions are obtained as:

$$\begin{cases} \sigma_{11} = -p + 2W_1'\lambda_1^2 + \dfrac{W_\alpha'}{\alpha}\lambda_1^2 \\ \sigma_{22} = 0 = -p + 2W_1'\lambda_2^2 \\ \sigma_{33} = 0 = -p + 2W_1'\lambda_3^2 \end{cases} \tag{3-7}$$

with $I_1 = \lambda_1^2 + \lambda_2^2 + \lambda_3^2$ and $\lambda_2 = \lambda_3$ as plane *23* is a plane of isotropy. The incompressibility condition also yields $J = \det \boldsymbol{F} = \lambda_1\lambda_2\lambda_3 = 1 \rightarrow \lambda_2 = \lambda_3 = 1/\sqrt{\lambda_1}$. Equation (3-7.2 or 3-7.3)

leads to $p = 2W_1\lambda_3^2 = 2W_1 / \lambda_1$. The only non-zero stress component, σ_{11}, is thus completely defined as a function of α, c_1, c_2, T_0 .

When compression is considered, $\alpha < 1$, $W'_\alpha = 0$ and σ_{11} takes the form:

$$\sigma_{11} = 2c_1c_2\left(\alpha^2 - \frac{1}{\alpha}\right)\exp\left(c_2\left(\alpha^2 + \frac{2}{\alpha} - 3\right)\right) \tag{3-8}$$

Following the approach by Martins *et al.*, parameters c_1, c_2 were obtained by fitting expression (3-8) to the compressive data obtained for aged bovine and aged porcine muscle tissue in the fibre direction (experimental results presented in Figure 3-5). Fitting was performed using the built in Matlab function *lsqnonlin*; this function minimises the sum of squared differences between model and experimental results using a Levenberg-Marquardt algorithm. Values obtained for c_1, c_2 are presented in Table 3-2 along with correlation coefficients, R^2, assessing the goodness of fit. Results of the fitting are presented in Figure 3-14.

Table 3-2: Parameters for Martins' model fitted to aged bovine and aged porcine data (see equation 3-8).

	c_1 (kPa)	c_2	R^2
Bovine	0.58 ±0.05	0.77 ±0.05	0.97
Porcine	0.68 ±0.005	1.32 ±0.008	0.99

When the muscle fibres are aligned with e_2, perpendicular to the direction of loading, developments become more complicated. In this configuration, $a_0 = [0 \quad 1 \quad 0]$ and the components of stress in directions *1*, *2* and *3* are defined as:

$$\begin{cases} \sigma_{11} = -p + 2W'_1\lambda_1^2 \\ \sigma_{22} = 0 = -p + 2W'_1\lambda_2^2 + \dfrac{W'_\alpha}{\alpha}\lambda_2^2 \\ \sigma_{33} = 0 = -p + 2W'_1\lambda_3^2 \end{cases} \tag{3-9}$$

In this configuration, $\lambda_2 \neq \lambda_3$ due to the material anisotropy. From equation (3-9.3), $p = 2W_1'\lambda_3^2$. Then using the expression for p from equation (3-9.2) and the incompressibility condition, a relationship between λ_1, λ_2 and λ_3 may be established:

$$2W_1'\lambda_3^2 - 2W_1'\lambda_2^2 + W_\alpha'\lambda_2^2 = 0 \quad \text{with} \quad \lambda_2 = 1/(\lambda_1\lambda_3) \tag{3-10}$$

This expression cannot be solved analytically; it is instead possible to numerically determine λ_3 as a function of λ_1, once parameters c_1, c_2 and T_0 are given. The Matlab function *fsolve* was used to solve expression (3-10) and the relationship between λ_1, λ_2 and λ_3 is presented in Figure 3-13.

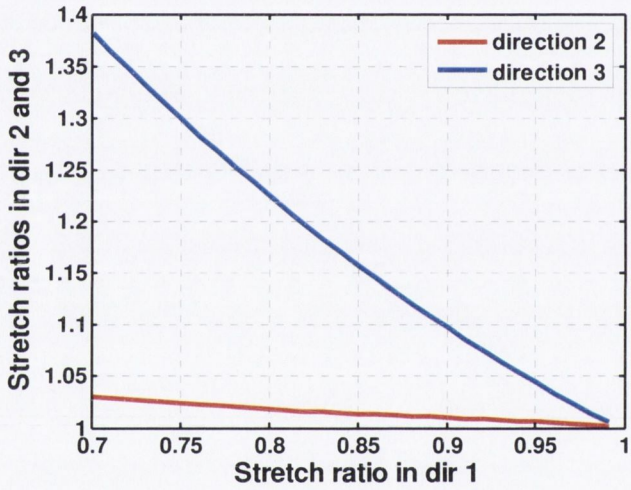


Figure 3-13: Relationship between stretch ratios in directions 1, 2 and 3.
Values obtained with Martins' model for a uniaxial compression test in direction 1 ≡ cross-fibre direction. Direction 2 ≡ fibre direction; direction 3 ≡ cross-fibre direction.

During compression in direction 1 (≡ cross-fibre direction), tensile stretches are observed in directions 2 and 3; Figure 3-13 shows that extension in direction 3 (≡ cross-fibre direction) is much more significant than in direction 2 (≡ fibre direction). This is due to the fact that the fibre direction in the model is much stiffer than the cross-fibre direction during extension.

Results of the fitting are presented in Figure 3-14. The model gives a good fit to data in the fibre direction for both muscle types. The model predictions for compression in the cross-

fibre direction are in good agreement with porcine muscle data but are poor for the data obtained for bovine tissue.

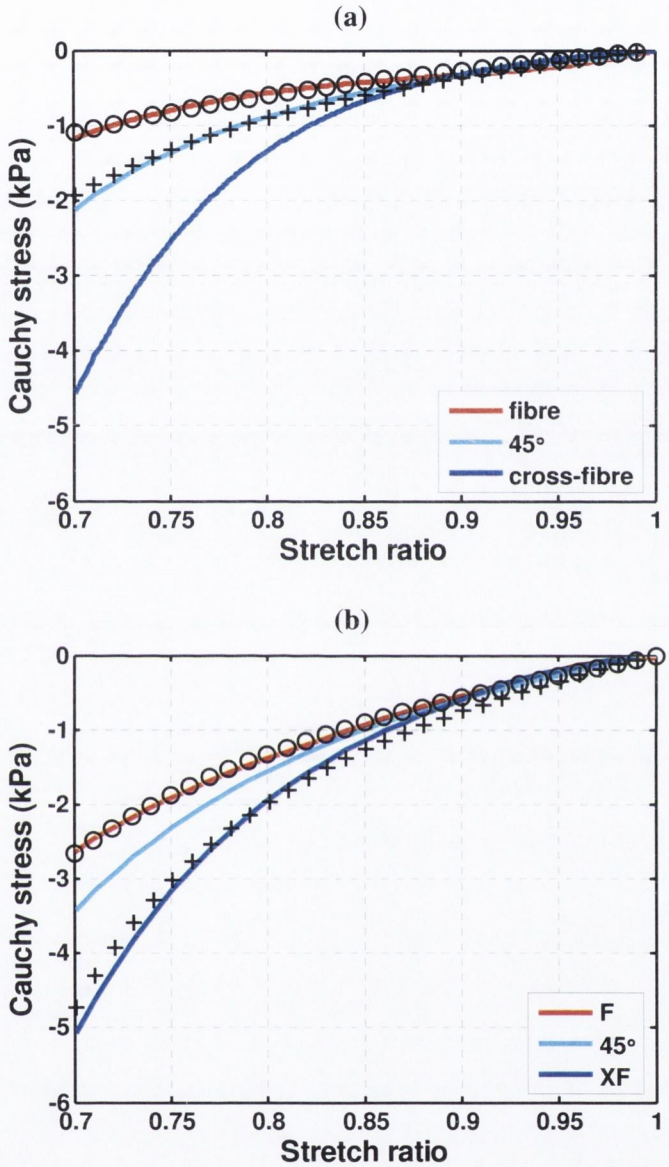


Figure 3-14: Compression tests on (a) aged bovine and (b) aged porcine samples fitted with Martins' model.

Lines denote experimental data, symbols denote model. Symbols in fibre direction (○) represent model fitting; symbols in cross-fibre direction (+) represent model predictions.

The match between experimental data and theoretical values was evaluated using a normalised error calculated as:

$$e_{\%}(\lambda)=\frac{\left|\overline{\sigma}_e(\lambda)-\sigma_t(\lambda)\right|}{\overline{\sigma}_e(\lambda)}\times 100 \tag{3-11}$$

where $\overline{\sigma}_e(\lambda)$ represents mean experimental results; $\sigma_t(\lambda)$ represents theoretical values. Residual errors obtained with Martins' model for bovine and porcine data are presented in Figure 3-15. Graph (b) shows that the error between model and experimental data is higher in the region of small stretches. This is in agreement with the report from Ogden *et al.* (2004) who investigated problems arising during fitting of hyperelastic models to experimental data. It is in part due to the division by small values of the stress when λ is close to 1.

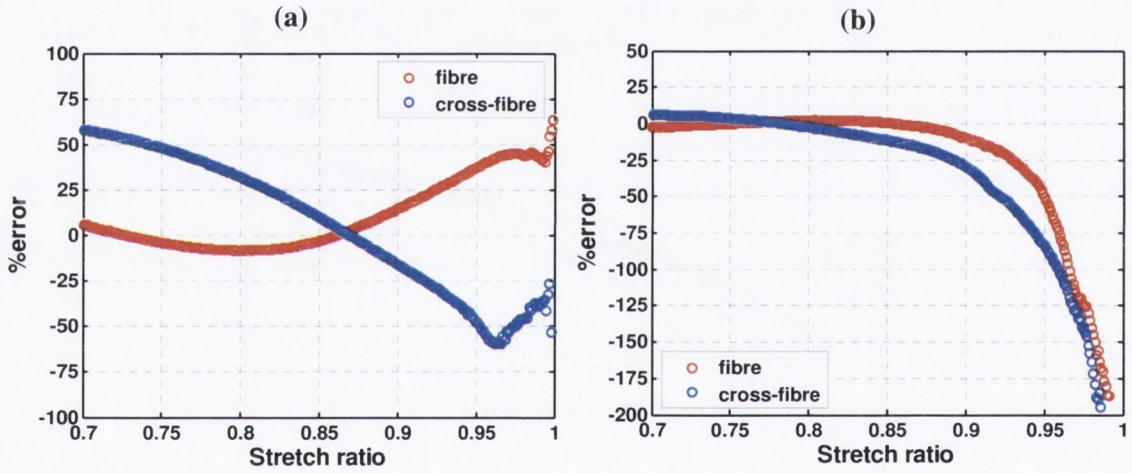


Figure 3-15: Residual errors between experimental data and Martins' model for (a) aged bovine and (b) aged porcine muscle.

For porcine data, the error between model and theoretical values remains below 20% for $\lambda < 0.92$ in the fibre direction and for $\lambda < 0.88$ in the cross-fibre direction.

When the muscle fibres are oriented at 45° from the direction of testing, $a_0 = \left[\frac{\sqrt{2}}{2} \quad \frac{\sqrt{2}}{2} \quad 0\right]$.

The components of stress in directions *1*, *2* and *3* are defined as:

$$\begin{cases} \sigma_{11} = -p + 2W_1'\lambda_1^2 + 0.5\dfrac{W_\alpha'}{\alpha}\lambda_1^2 \\ \sigma_{22} = 0 = -p + 2W_1'\lambda_2^2 + 0.5\dfrac{W_\alpha'}{\alpha}\lambda_2^2 \\ \sigma_{33} = 0 = -p + 2W_1'\lambda_3^2 \end{cases} \tag{3-12}$$

To obtain the relationship between λ_1, λ_2 and λ_3, the following expression needs to be solved numerically:

$$2W_1'\lambda_3^2 - 2W_1'\lambda_2^2 - 0.5\,W_\alpha'\lambda_2^2 = 0 \quad \text{with} \quad \lambda_2 = 1/(\lambda_1\lambda_3) \tag{3-13}$$

This leads to a stretch ratio in the fibre direction $\alpha < 1 \rightarrow W_\alpha' = 0$, $\lambda_2 = \lambda_3$ and the response of the material with fibres oriented at 45° from the direction of testing is the same as the response obtained when fibres are aligned with the direction of testing. This contradicts experimental results, which show that the 45° direction (—) is stiffer than the fibre direction (—) (Figure 3-14).

In view of these developments, the reader can appreciate the mathematical difficulties involved with the use of such a model when only uniaxial data are available. Uniaxial compression data is not sufficient to fully characterise the material parameters and the assumption of known values for muscle tensile properties is made to overcome this limitation (see equation (3-5)). For aged bovine data, successful fitting of the model can be obtained in the fibre direction; however, the model prediction in the cross-fibre direction contradicts experimental results (Figure 3-14a). The model is in good agreement with the behaviour observed experimentally for aged porcine muscle samples in the fibre and the cross-fibre directions (Figure 3-14b); however, it does not predict muscle behaviour when compression at 45° from the fibre direction is considered.

3.4.1.2 SYM model

In the strain dependent Young's moduli (SYM) model the relationship between stress and strain tensors is expressed by equations (2-36) and (2-37). When a uniaxial test in direction j is considered, the Cauchy stress in this direction can be expressed as:

$$\sigma_j = E_j \tilde{\varepsilon}_j \tag{3-14}$$

where E_j is the Young's modulus in direction j and $\tilde{\varepsilon}_j = \ln(\lambda_j)$ the logarithmic strain, used to account for large deformations.

As mentioned previously, five independent elastic constants have to be determined to fully characterise the material, i.e. two Young's moduli (E_L and E_T), two Poisson's ratios ($\nu_{TT'}$ and ν_{LT}) and one shear modulus (G_{LT}). (L denotes the longitudinal direction, T and T' denote the two transverse directions).

To account for material nonlinearities, Li *et al.* (2001) adopted an exponential form for strain dependent Young's moduli in the fibre direction (E_L) and in the cross-fibre direction (E_T). Second order polynomials were chosen in this thesis for E_L and E_T:

$$E_L = k_{1L} + k_{2L}\tilde{\varepsilon}_L + k_{3L}\tilde{\varepsilon}_L^{\,2} \quad \text{and} \quad E_T = k_{1T} + k_{2T}\tilde{\varepsilon}_T + k_{3T}\tilde{\varepsilon}_T^{\,2} \tag{3-15}$$

Parameter k_{1L}, k_{2L}, k_{3L} are determined by fitting to the data in the fibre direction. k_{1T}, k_{2T}, k_{3T} are determined by fitting to the data in the cross-fibre direction. Their values are presented in Table 3-3 for aged bovine and porcine muscle tissues respectively.

Table 3-3: Parameters (in kPa) for the SYM model fitted to aged bovine and aged porcine data (see equation 3-15) - mean ± standard error.

	k_{1L}	k_{2L}	k_{3L}	k_{1T}	k_{2T}	k_{3T}
Bovine	4.74 ±0.03	20.18 ±0.28	45.76 ±0.60	2.75 ±0.02	8.22 ±0.20	102.90 ±0.42
Porcine	3.54 ±0.02	-13.53 ±0.16	-9.08 ±0.34	3.72 ±0.02	-10.82 ±0.19	52.08 ±0.40

Values of 0.45 are used for the Poisson's ratios to account for quasi-incompressibility of the tissue.

The shear modulus is calculated as:

$$G_{LT} = \frac{E_L E_T}{E_T(1+2\nu_{LT}) + E_L} \tag{3-16}$$

This formula was established for transversely isotropic rocks (Lekhnitskii, 1981) and is applied here as a first approximation.

Figure 3-16 presents results of fitting to the experimental data in the fibre and cross-fibre directions. Model predictions at 45° from the fibre direction are also represented.

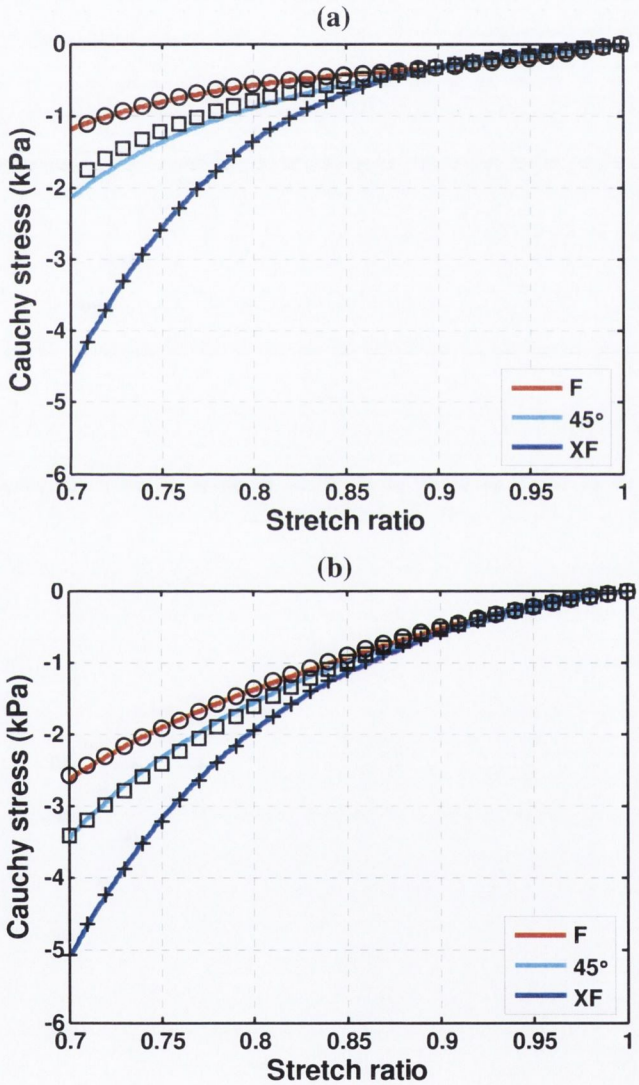


Figure 3-16: Compression tests on (a) aged bovine and (b) aged porcine samples fitted with the SYM model.

Lines denote experimental data, symbols denote model. Symbols in fibre direction (○) and in cross-fibre direction (+) represent model fitting; symbols at 45° from the fibre direction (□) represent model predictions.

The SYM model gives a very good fit to the experimental data in both the fibre and cross-fibre directions for the range of deformations considered. The model also yields a good prediction of muscle behaviour at 45° from the fibre direction. Residual errors calculated using equation (3-11) are presented in Figure 3-17.

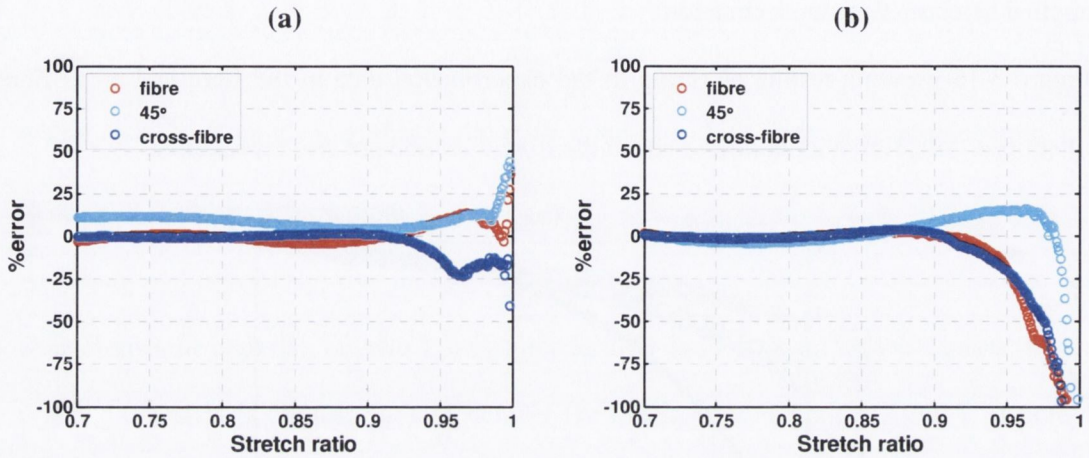


Figure 3-17: Residual error between experimental data and SYM model for (a) aged bovine and (b) aged porcine muscle.

As mentioned in the previous section, errors between model and experimental data are higher in regions of small stretches. However, when values of $\lambda < 0.95$ are considered, Figure 3-17 shows that the errors remain small across the deformation range considered. Correlations coefficients and maximum errors for $\lambda < 0.95$ are presented in Table 3-4.

Table 3-4: Correlation coefficients and max error ($\lambda < 0.95$) for SYM model fitted to aged bovine and aged porcine data.

	Aged bovine tissue	Aged porcine tissue
R^2 fibre fitting	0.998	0.999
R^2 for cross-fibre fitting	1.000	0.999
Max $e_{\%}$ for fibre fitting	9.9	20
Max $e_{\%}$ for 45° prediction	12	15.7
Max $e_{\%}$ for cross-fibre fitting	12.7	20

3.4.2 Fresh tissue

3.4.2.1 Martins' model

Using the method described in section 3.4.1.1, Martins' model was fitted to the data obtained from fresh porcine tissue compressed in the fibre direction (equations 3-8). Values obtained for c_1, c_2 are presented in Table 3-5 along with correlation coefficients, R^2, assessing the goodness of fit. Results of the fitting are presented in Figure 3-18.

Table 3-5: Parameters for Martins' model fitted to fresh porcine data (equation (3-8)).

	c_1 (kPa)	c_2	R^2
Fresh porcine tissue	0.68±0.005	1.32±0.008	0.99

Using these parameters and equations 3-9 and 3-10, the model predictions for compression in the cross-fibre direction were calculated.

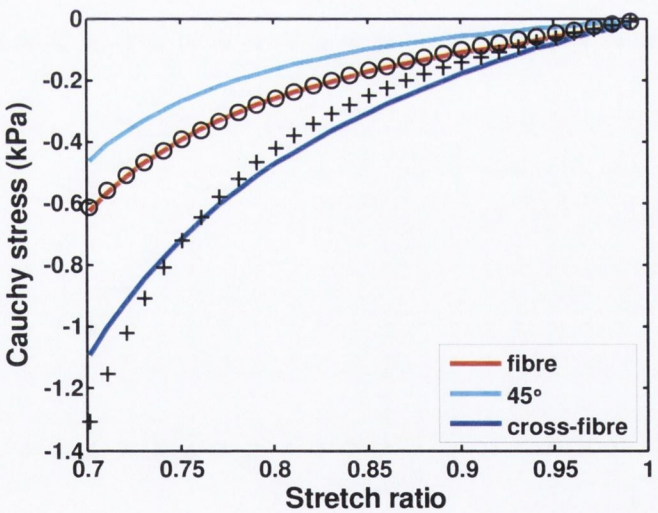


Figure 3-18: Compression tests on fresh porcine samples fitted with Martins' model. *Lines denote experimental data, symbols denote model. Symbols in fibre direction (○) represent model fitting; symbols in cross-fibre direction (+) represent model predictions.*

Figure 3-18 shows that the model can be successfully fitted to the fibre direction data; the model prediction in the cross-fibre direction also remains close to the experimental data.

Figure 3-19 presents the percentage error between theoretical and experimental values; it shows that the error between model and theoretical values remains below 20% for stretch ratios below 0.95.

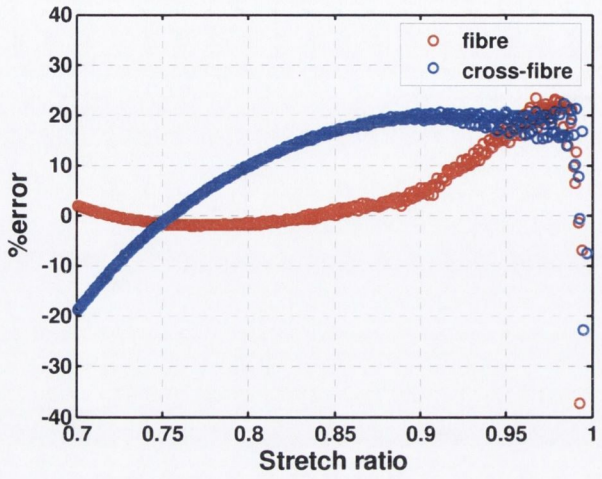


Figure 3-19: Residual errors between experimental data and Martins' model for fresh porcine muscle.

When the muscle fibres are aligned at 45° from the direction of compression, equation 3-13 has to be solved numerically to obtain the relationship between λ_1, λ_2 and λ_3. Then, the stress developed can be calculated using equation 3-12. This leads to a stretch ratio in the fibre direction $\alpha < 1 \rightarrow W_\alpha^{'} = 0$, $\lambda_2 = \lambda_3$ and the response of the material with fibres oriented at 45° from the direction of testing is the same as the response obtained when fibres are aligned with the direction of testing. This contradicts experimental results, which show that the fibre direction (—) is stiffer than the 45° direction (—) (Figure 3-18).

3.4.2.2 SYM model

For the fresh porcine tissues, the displacement of markers placed on the samples was recorded during the tests (Figure 3-20). This provides additional information to calculate values of Poisson's ratios characterising the material, i.e.:

- v_{LT} and $v_{LT'}$, characterising extension in one of the transverse directions (T or T') when compression is applied in the longitudinal direction (L); $v_{LT} = v_{LT'}$ as directions T and T' are assumed to be equivalent;
- $v_{TT'}$, characterising extension in one of the transverse directions (T) when compression is applied in the other transverse direction (T');
- v_{TL} and $v_{T'L}$, characterising extension in the longitudinal direction when compression is applied in one of the transverse directions (T or T'); v_{TL} and $v_{T'L}$ as $T \equiv T'$.

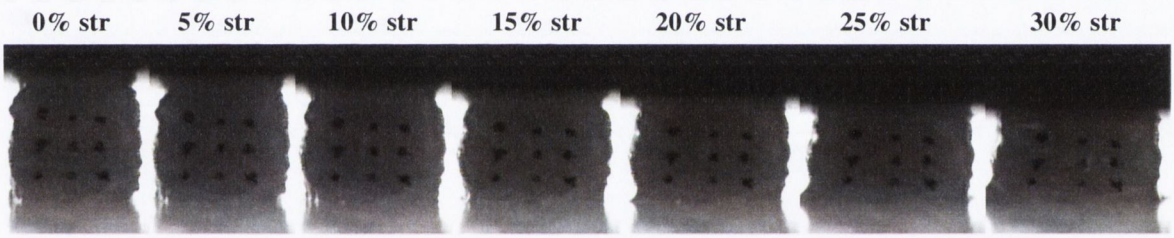


Figure 3-20: Markers displacements during compression tests.

The various Poisson's ratios were calculated by measuring the relative horizontal and vertical displacements of the markers during tests performed in the cross-fibre and fibre directions. Figure 3-21 schematically illustrates the method used. For $i,j = L,T \text{ or } T'$, Poisson's ratio v_{ij} is calculated as:

$$v_{ij} = -\frac{\tilde{\varepsilon}_j}{\tilde{\varepsilon}_i} \tag{3-17}$$

with $$\tilde{\varepsilon}_i = \frac{1}{2}\left(\ln\left(\frac{L_{i1}}{L_{0i1}}\right) + \ln\left(\frac{L_{i2}}{L_{0i2}}\right)\right) \quad \text{and} \quad \tilde{\varepsilon}_j = \frac{1}{2}\left(\ln\left(\frac{L_{j1}}{L_{0j1}}\right) + \ln\left(\frac{L_{j2}}{L_{0j2}}\right)\right) \tag{3-18}$$

$\tilde{\varepsilon}_i$ and $\tilde{\varepsilon}_j$ are the logarithmic strains in direction i and j respectively; they are calculated as the mean of two measurements made on different markers.

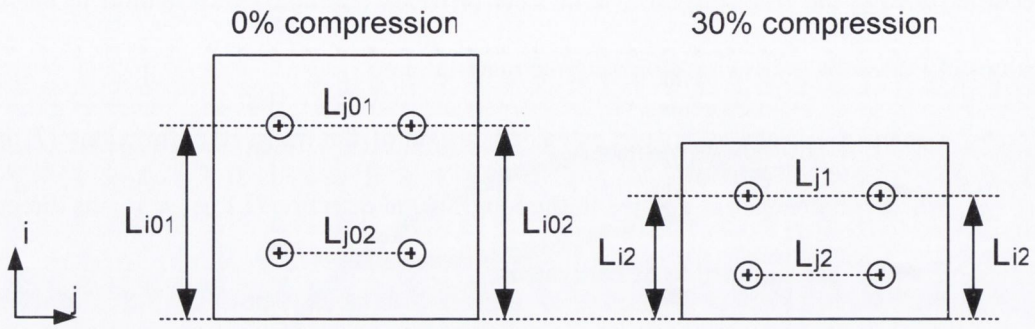


Figure 3-21: Illustration of the method used to calculate the values of Poisson's ratios v_{ij} ($i,j = L,T$ or T').

L_{i01} and L_{i02} characterise the initial horizontal distances between the markers; L_{j01} and L_{j02}, the initial vertical distances. L_{i1} and L_{i2} characterise the horizontal distances between the markers after compression; L_{j1} and L_{j2} the vertical distances. ε_i and ε_j are the logarithmic strains in direction i and j respectively.

A routine was first developed in Matlab to automatically measure the marker displacements during compression; however, due to the poor contrast between markers and samples, this technique could not be applied. Therefore, the markers position was evaluated by manually picking their centre. Increments of 5% compression were considered but no significant variation was observed in v_{ij} values with compression. Table 3-6 summarises the results. Data were collected from 8 muscle samples for each value of v_{ij} ; Figure 3-22 shows the variation obtained.

Table 3-6: values of Poisson's ratios - mean ± standard deviation

$v_{LT} = v_{LT'}$	$v_{TT'}$	v_{TL}
0.50 ± 0.04	0.65±0.05	0.36±0.07

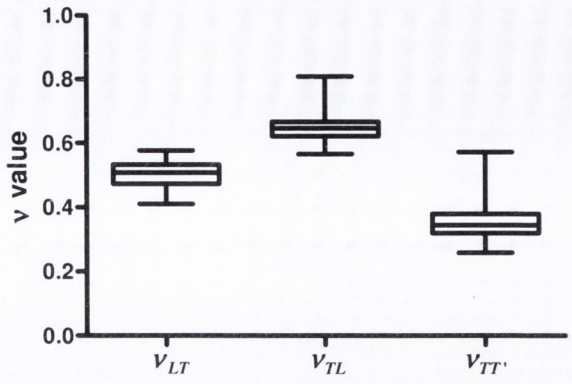


Figure 3-22: Box and whiskers plot for Poisson's ratios of fresh porcine muscle tissue.

To explain the values obtained, muscle anisotropy and incompressibility have to be considered. During an unconfined compression test performed in the muscle cross-fibre direction (*T*), both the fibre (*L*) and the other cross-fibre direction (*T'*) will expand. If the material was isotropic and incompressible, the amount of expansion would be the same in the fibre and in the cross-fibre directions and the Poisson's ratios would all have a value of 0.5. However, for muscle tissue, the fibre direction is stiffer than the cross-fibre direction in expansion so the material will expand less in the fibre than in the cross-fibre direction, leading to $v_{TL} < v_{TT'}$ and to a value greater than 0.5 for $v_{TT'}$.

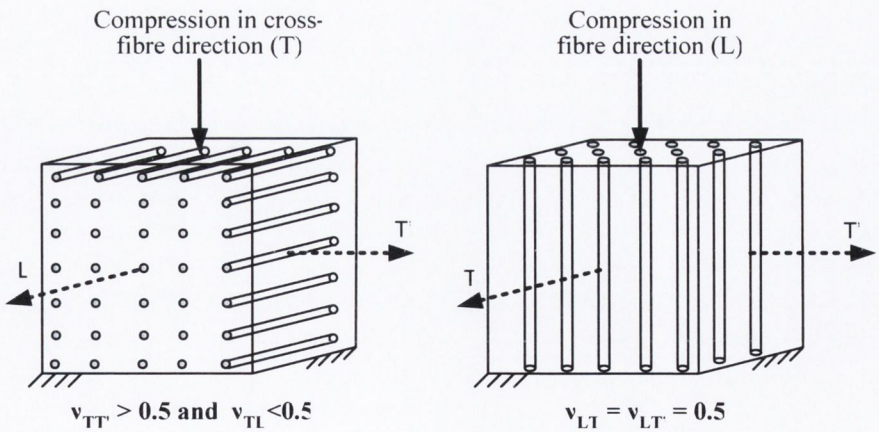


Figure 3-23: Schematic explaining the values of Poisson's ratios for muscle tissue in compression.

$v_{LT} = 0.5$; $v_{TT'} = 0.65$; $v_{TL} = 0.36$. The dashed arrows represent the extension occurring in directions perpendicular to the compression direction.

As previously, parameters k_{1L}, k_{2L}, k_{3L} are determined by fitting to the data in the fibre direction. While k_{1T}, k_{2T}, k_{3T} are determined by fitting to the data in the cross-fibre direction. Their values are presented in Table 3-7.

Table 3-7: Parameters (in kPa) for the SYM model fitted on fresh porcine and ovine data - mean ± standard error.

	k_{1L}	k_{2L}	k_{3L}	k_{1T}	k_{2T}	k_{3T}
porcine	1.306 ±0.007	3.886 ±0.060	14.280 ±0.126	1.681 ±0.010	1.184 ±0.089	14.130 ±0.188
ovine	3.460 ±0.017	12.090 ±0.149	41.770 ±0.313	3.914 ±0.036	12.860 ±0.316	92.630 ±0.663

Experimental results from tests performed at 45° from the fibre direction show that aged and fresh tissues present a different shearing behaviour. For fresh tissues, the 45° orientation is the most compliant of all directions due to shearing appearing between adjacent fibre fascicles. Expression (3-16), used to calculate the shear modulus of aged muscle tissues, leads the fibre direction to be the most compliant direction. This expression is therefore not suitable for fresh tissue and a new form has to be established for G_{LT}.

For transversely isotropic materials, the relationship existing between the properties in any directions and those in the longitudinal and transverse directions can be expressed as:

$$\frac{1}{E_\omega} = \frac{1}{E_L}\cos^4\omega + \left(\frac{1}{G_{LT}} - 2\frac{\nu_{LT}}{E_L}\right)\sin^2\omega\cos^2\omega + \frac{1}{E_T}\sin^4\omega \qquad (3\text{-}19)$$

where ω represents the angle from the longitudinal direction. This expression has been obtained by transformation of elastic constants when the coordinate system is rotated (see Lekhnitskii, 1981). Now considering uniaxial test at 45° from the fibre direction ($\omega = 45°$), equation (3-19) can be rearranged to express G_{LT} as:

$$\frac{1}{G_{LT}} = 4\frac{\tilde{\varepsilon}_{45}}{\sigma_{45}} - \frac{1-2\nu_{LT}}{E_L} - \frac{1}{E_T} \qquad (3\text{-}20)$$

with $\dfrac{\tilde{\varepsilon}_{45}}{\sigma_{45}} = \dfrac{1}{E_{45}}$.

For ease of calculation, an expression similar to E_L and E_T, was used for E_{45}; i.e. $E_{45} = k_{145} + k_{245}\tilde{\varepsilon}_{45} + k_{345}\tilde{\varepsilon}_{45}^{\,2}$.

Parameter k_{145}, k_{245}, and k_{345} were determined by fitting to the data obtained at 45° from the fibre direction. Values obtained for fresh porcine and fresh ovine muscle tissue are presented in Table 3-8.

Table 3-8: Parameters (in kPa) resulting from the fitting of fresh porcine and ovine data at 45° from the muscle fibre direction - mean ± standard error.

	k_{145}	k_{245}	k_{345}
porcine	0.663 ±0.005	2.095 ±0.047	10.730 ±0.099
ovine	2.431 ±0.015	6.571 ±0.128	16.590 ±0.269

Once G_{LT} is calculated theoretical curves corresponding to uniaxial tests at any angle from the fibre direction can be obtained using equation (3-19).

As illustrated in Figure 3-24 for ovine muscle tissue and in Figure 3-25 for porcine muscle, this model gives a very good fit to the experimental data in fibre, cross-fibre and at 45° from the fibre direction.

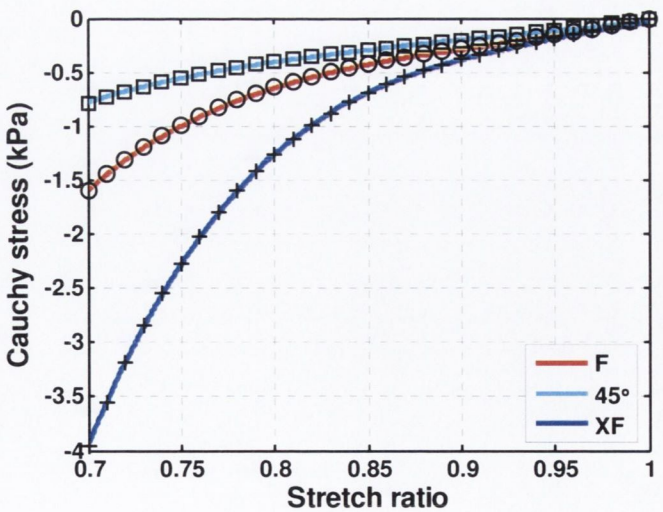


Figure 3-24: Compression tests on fresh ovine muscle samples fitted with the SYM model.

Lines denote experimental data, symbols denote model fitting.

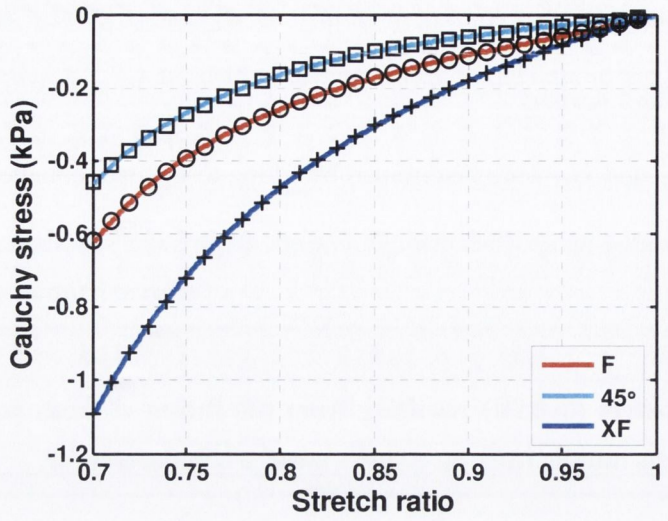


Figure 3-25: Compression tests on fresh porcine muscle samples fitted with the SYM model.

Lines denote experimental data, symbols denote model fitting.

Figure 3-26 compares model predictions and experimental results for tests performed at 30° and 60° from the fibre direction on porcine muscle tissue. It shows that the model also yields a good prediction of muscle behaviour at 30° and 60° from the fibre direction.

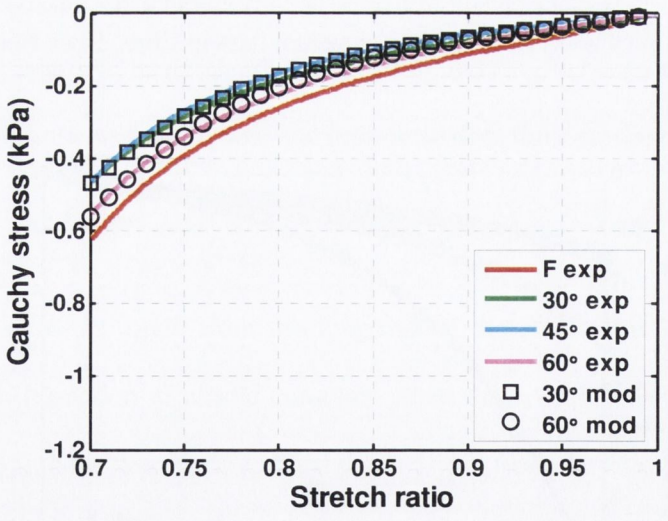


Figure 3-26: Compression tests on fresh porcine samples - Comparison between experimental data and theoretical predictions using the SYM model.

Lines denote experimental data, symbols denote model predictions.

R^2 values and residual errors assessing the goodness of the match between experimental and theoretical curves are presented in Table 3-9 and Figure 3-27.

In view of these results, the SYM model is proposed to represent skeletal muscle compressive behaviour.

Table 3-9: Correlation coefficients and maximum error ($\lambda < 0.95$) for fresh ovine and porcine data

	Fresh ovine tissue	Fresh porcine tissue
R^2 fibre fitting	0.999	0.999
R^2 for 45° fitting	0.999	0.999
R^2 for cross-fibre fitting	0.998	0.999
Max $e_{\%}$ for fibre fitting	5	3.9
Max $e_{\%}$ for 30° prediction	-	22.4
Max $e_{\%}$ for 45° fitting	5.5	18.3
Max $e_{\%}$ for 60° prediction	-	12.2
Max $e_{\%}$ for cross-fibre fitting	3.5	7.7

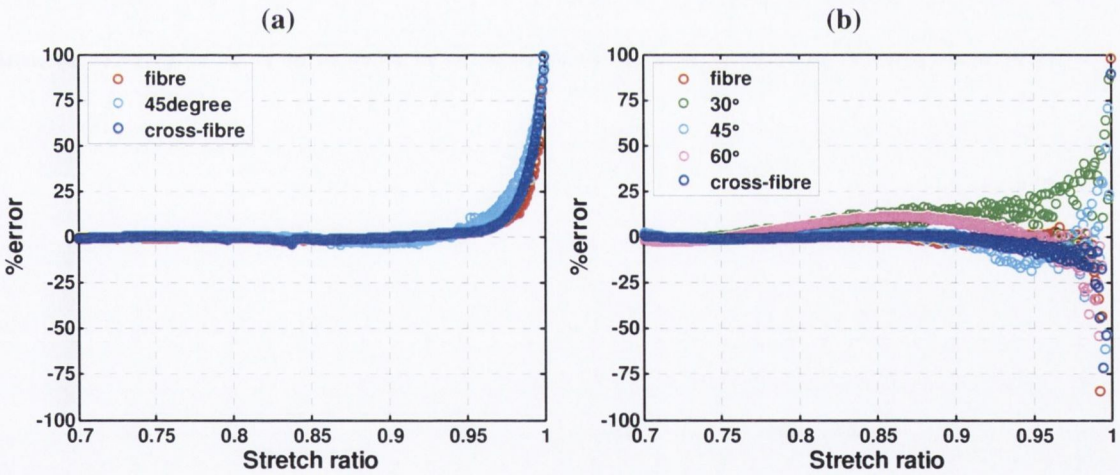


Figure 3-27: Residual error between experimental data and SYM model for fresh porcine muscle.

Finally, Figure 3-28 compares the evolution with stretch of shear moduli and Young's moduli (in fibre, cross-fibre and 45° from the fibre direction) calculated with the SYM model for aged and fresh porcine muscle tissue.

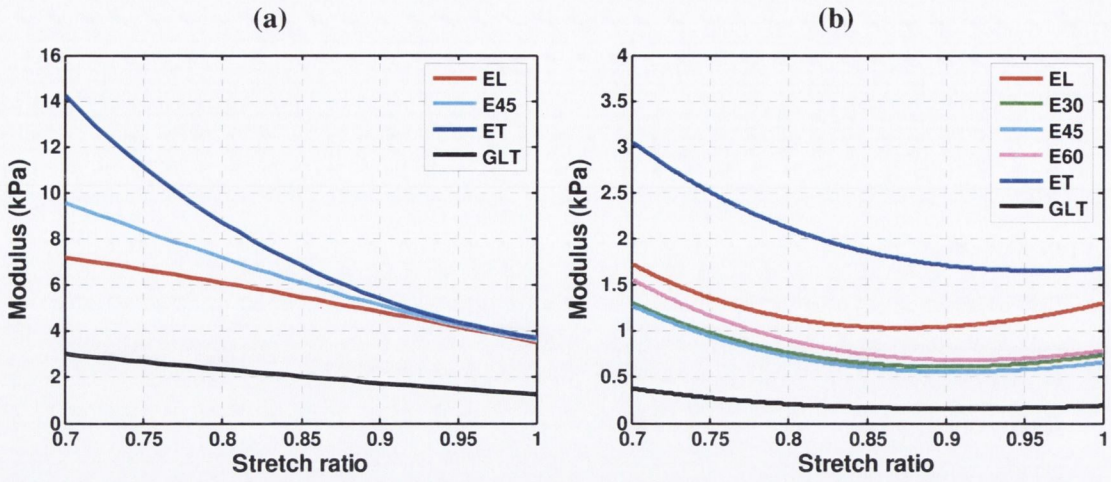


Figure 3-28: Evolution with the stretch ratio of the shear modulus and Young's moduli (in fibre, cross-fibre and 45° from the fibre direction) for (a) aged and (b) fresh porcine muscle.

It shows that shear and Young's moduli are all significantly higher for aged than for fresh tissue. Properties present a rather linear evolution with stretch ratio for aged tissue; the evolution is however nonlinear for fresh muscle. When small deformations are considered, aged tissue Young's moduli present similar values in the three fibre orientations considered; fresh tissues present different properties in the three orientations, even for small deformations.

Data published in the literature often consider muscle tissue as a linear elastic material; in order to establish a comparison with these data, mean values were calculated for the various coefficients represented in Figure 3-28 (see Table 3-10).

Table 3-10: Mean values (± SD) of Young's and shear moduli calculated for aged and fresh porcine muscle tissue (in kPa).

	Aged porcine tissue	Fresh porcine tissue
E_L	5.46±1.07	1.21±0.17
E_{45}	6.27±1.76	0.73±0.20
E_T	7.55±3.03	2.03±0.40
G_{LT}	2.06±0.52	0.21±0.06

3.5 Discussion

3.5.1 General remarks

As described in the literature review, little experimental data is available to characterise skeletal muscle tissue in compression and significant variation is observed between published data. In this chapter, an *in vitro* experimental procedure and a three-dimensional model are proposed to characterise the elastic behaviour of passive skeletal muscle under compressive loading.

Data obtained from aged and fresh animal muscle tissue, tested at various orientations of the muscle fibres have been presented. Results from these tests clearly demonstrate the anisotropy and nonlinearity of mammalian skeletal muscle when submitted to compressive loading. A significant difference in behaviour is observed between aged and fresh muscle tissue, emphasising the need to perform tests on tissues obtained soon after death. From the observations on the fibre dependency of muscle properties, the hypothesis of transverse isotropy was formulated and a nonlinear elastic, transversely isotropic model was proposed to represent skeletal muscle elastic behaviour. The model developed (SYM) provides a very good fit to the data in the cross-fibre direction, the fibre direction and at 45° from the fibre direction (R^2=0.99). It also predicts well the behaviour of muscle tissue at 30° and 60° from the fibre direction. Skeletal muscle elastic properties can therefore be characterised as nonlinear, transversely isotropic with the axis of symmetry running along the direction of the muscle fibres; the most compliant properties being observed at 45° from the fibre direction due to a small shear modulus value.

3.5.2 Choice of experimental parameters and tissue tested

It has long been recognised that the characterisation of the mechanical properties of living tissues should be accomplished *in vivo*; the excision of samples from a tissue or an organ causes the loss of the condition of homeostasis that applies to living tissues and disrupts their

structural integrity. However, due to the lack of reliable non-invasive techniques for direct *in vivo* stress and strain measurements, most of the knowledge on living tissue properties has been derived from *in vitro* experiments. As suggested by others (Quaglini, 2000; Brouwer *et al.* 2001), *in vivo* and *in vitro* techniques should be considered complementary to each other in the measurement of soft tissue properties; *in vivo* conditions provide information about the tissue behaviour in its physiological state, while *in vitro* conditions allow better control over experimental parameters. The tests considered in this thesis to characterise skeletal muscle properties were performed *in vitro* on samples with a well defined geometry. This was considered as a first, fundamental step in the characterisation of muscle mechanical behaviour under compressive loading given the lack of available data in the literature. The technique developed led to the characterisation of the tissue properties dependency on fibre orientation; it also led to data presenting relatively little scatter (10 to 15% on average for fresh porcine muscle tissues). This can be attributed to the use of samples with repeatable geometry, coming from animals of the same origin, same gender and same age. The data obtained will be used as initial information on muscle compressive behaviour for further *in vivo* research conducted in our group.

Due to the difficulty of obtaining human tissue, animal muscles were used for testing. The use of rodents was first envisaged; the muscles obtained were however too small to provide samples large enough for the type of tests performed. Porcine muscles appeared large enough to obtain samples; they also presented fibres large enough to be easily distinguished by eye. Besides, pigs share important anatomic and physiologic characteristics with humans and are often used as surrogate in research on the mechanical properties of human soft tissues (e.g. ligaments and tendons, Woo *et al.,* 2000; kidneys, Snedeker *et al.*, 2005; brain tissue, Miller and Chinzei, 1997; skin, Bischoff, 2006; aortic heart valve, Doehring *et al.*, 2004). Young animals (10 to 12 weeks) were chosen for their small size; this might influence the results as discussed later on.

Strain rate is a critical issue when performing quasi-static testing of soft tissues. It has to be sufficiently low to eliminate viscoelastic effects. However, results show that it is important

to perform tests as quickly as possible after death of the animal to exclude stiffening of the tissue due to rigor mortis; lower strain rates lead to longer testing times which reduces the amount of samples that can be tested with each animal. In the study of soft tissue compressive behaviour, various strain rates have been used in the literature to performed quasi-static tests: $0.1\%s^{-1}$ and $0.01\%s^{-1}$ used for human calcaneal fat pad (Miller-Young *et al.*, 2002), $0.64x10^{-3}$ $\%s^{-1}$ used for brain tissue (Miller and Chinzei, 1997), $0.1x10^{-3}$ $\%s^{-1}$ used for pig skin (Wu *et al.*, 2004). A strain rate of 0.05% s^{-1} was adopted and considered as a good compromise between measurement of truly elastic properties and test duration (600s to attain 30% compression). A certain amount of viscoelastic effect was measured this way. When deformation is maintained constant after compression and samples are allowed to relax, some relaxation is noticed.

Finally, the tests performed were uniaxial; this is a limitation to fully characterise muscle behaviour in three-dimensions. Biaxial information was however obtained on sample deformation using imaged recorded during the tests.

3.5.3 Comparison of experimental results with published data

As mentioned in the general introduction, particular difficulties are associated with the study of soft tissue mechanical properties due to their complex structure; their sensitivity to external parameters such as hydration, temperature, time of test after death; the influence of parameters such as species, gender and age; and for skeletal muscle, the presence of active and passive force components. Along with the type of test performed, all these parameters contribute to the variations observed among published data.

This section compares data published in the literature on muscle compressive properties (section 2.2.2 of the literature review) and experimental results obtained in this study during quasi-static compression of aged and fresh porcine muscle tissue; only results obtained in the muscle transverse direction are considered as data in other directions have not been published in the literature for compressive loading. Figure 3-29 presents stress-stretch ratio curves obtained by various authors.

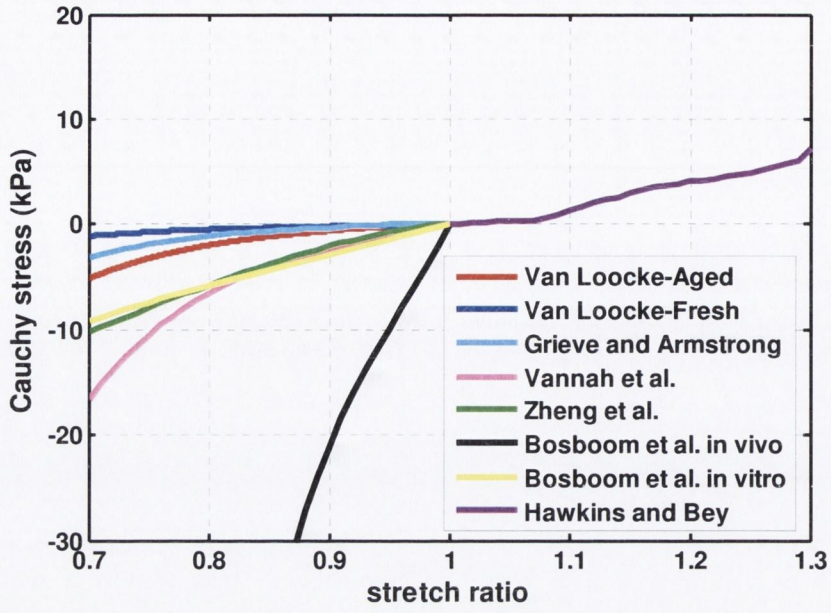


Figure 3-29: Elastic properties of skeletal muscle tissue in compression - comparison between data obtained in this study and data published in the literature.

The blue and red curves correspond to data from this study obtained respectively from fresh and aged porcine tissue; the compression rate was $0.05\%.s^{-1}$. The cyan curve was published by Grieve and Armstrong (1988) who performed similar tests on aged porcine samples *in vitro*; the compression rate was also $0.05\%.s^{-1}$. The magenta and green curves were respectively obtained by Vannah *et al.* (1996) and Zheng *et al.* (1999); they correspond to *in vivo* indentation tests on human limbs using an ultrasound indentation technique. The yellow and black curves were obtained by Bosboom *et al.* who conducted respectively *in vitro* (2001a) and *in vivo* (2001b) compression tests on rat tibialis anterior muscles in the transverse direction; the curves represented in Figure 3-29 were calculated from the quasi-static part of the model adopted by Bosboom *et al.* to fit their experimental results (see section 2.4.3.3 for details). Finally, the purple curve was obtained by Hawkins and Bey (1994) during extension tests performed *in vivo* on rat tibialis anterior muscles in the fibre direction. It is represented to give an idea of the range of values where muscle tensile properties are situated.

Globally, the various results presented show nonlinear, concave characteristics for muscle compressive behaviour; the main difference between them being the stiffness of the tissue.

Results from Grieve and Armstrong (1988) are in good agreement with the tests performed in this study, approximately situated half way between fresh and aged porcine data (the difference between these is addressed in the next section). *In vivo* indentation data published by Vannah *et al.* (1996) and by Zheng *et al.* (1999) lead to stiffer muscle characteristics. These tests were performed on bulk muscular tissue; therefore, the properties of skin and fat surrounding muscle tissue were also included in the measurements. A relaxed muscle state was specified for the experiments; however, non-anesthetised human subjects were tested and muscle activity was only assessed qualitatively. Deformation rate could also be influential: data from Vannah *et al.* (1996) correspond to quasi-static measurements but deformation rate is not specified; Zheng *et al.* used compression rates ranging approximately from 4 to 40%s^{-1}, which is 80 to 800 times faster than the tests performed in this study; Zheng *et al.* reported however that the tissue properties appeared to be rate-insensitive in the range tested.

In vitro tests by Bosboom *et al.* agree with the Zheng *et al.* results. *In vivo* tests by Bosboom *et al.* suggest however a much stiffer behaviour, which leads one to wonder if, although the test animal was anesthetised, some involuntary muscle activity was present during the *in vivo* tests.

In *in vivo* indentation studies, bulk muscular tissue has often been considered as isotropic linear elastic and values of Young's modulus ranging from 6.2 to 145kPa are reported (see Table 2-2). Mean values of 7.55kPa and 2.03kPa have been obtained in this study respectively for aged and fresh porcine muscle tissue.

Using non-invasive ultrasound and MRI techniques and considering linear elastic behaviour (see section 2.3.3), values ranging from 0.92kPa to 39.2kPa have been reported for human muscle shear modulus, measured at rest. Mean values of 2.06kPa and 0.21kPa have been obtained in this study respectively for aged and fresh porcine muscle tissue.

Results obtained in this study with fresh porcine tissue appear thus to be less stiff than other published results. This can probably be attributed to the young age – and therefore small fibre size – of the animals used for the tests.

3.5.4 Differences observed between the various tissues tested

Even though the same technique was used to perform all the tests in this study, differences were observed between the various types of muscle tested. Differences not only in stiffness but also in behaviour were observed between post-mortally aged and fresh tissues. These differences can be attributed to the young age of animals used for tests on fresh tissues (10 to 12 weeks). The difference in behaviour that was observed with fibre orientation between aged and fresh tissue might also be explained by the greater amount of fluid present in the fresh (unbled) samples, leading to a greater mobility of the connection between the fibres and resulting in shearing between adjacent fibre fascicles during compression. Aged muscles, where less fluid is present, show an increase in stiffness with an increase of angle from the fibre direction. Fresh tissues show however that the weaker direction is at 45° from the fibre direction, where shearing has its most significant contribution. Quaglini, (2000) describes soft tissues as composites, constituted of a network of collagen and elastin fibres embedded in the water-polysaccharides matrix. The mechanical properties and configuration of collagen give the tissue strength and flexibility; in association with proteoglycans, water provided the lubrication and spacing that are crucial to the gliding function at the fibre-matrix interface. Muscle tissue is made approximately of 80% water (Vignos *et al.*, 1959). Reports from the meat industry indicate that water loss in the tissue can attain 8.5% of the initial muscle weight 0 to 72 hours post mortem (Toldrá, 2003).

This difference in behaviour as well as the stiffening noticed soon after death emphasise the need to perform tests within a few hours after death of the subject in order to obtain data representative of living tissue properties.

Differences were also observed between aged bovine and aged porcine tissues. Cross-fibre results are quite similar for both tissues; data obtained in the fibre direction and at 45° from the fibre direction appear however to be stiffer for porcine than for bovine tissue. This can illustrate a difference in species. However, these were preliminary results and no control over age, method of storage etc. was available.

Finally, the differences in stiffness observed between the fresh porcine and fresh ovine tissues can also be attributed to the difference in species, age of the animal and therefore fibre size. It should also be noted that tests performed on ovine tissues were started later after death than the porcine tests and rigor mortis could have influenced the results.

This of course leads to question the relationship between animal and human muscle properties. No answer can unfortunately be provided from this study. The author believes that qualitatively, human and animal muscle tissues behave similarly under compressive loading. Quantitative differences are however probably present between both tissues. However, it is believed that these quantitative differences can also be observed between the various muscles of the same subject and are related to the geometry and composition of the tissue, i.e. fibre size, amount of connective and fatty tissues.

3.5.5 Choice of a model

Following the observations made during the experiments, the hypothesis of transverse isotropy was formulated to characterise skeletal muscle elastic behaviour. Two nonlinear, transversely isotropic models were fitted to the experimental data: a hyperelastic model previously applied by Martins *et al.* for muscle tissue and a strain dependant Young's moduli (SYM) model developed for aortic valves. Particular mathematical difficulties are involved with Martins' model when only uniaxial data are considered. Fitting of the model to aged porcine muscle data in the fibre and the cross-fibre directions was successfully achieved; however, the model could not predict muscle behaviour when compression at 45° from the fibre direction was considered.

In contrast, the SYM model parameters could be determined readily from uniaxial tests performed in three orientations of muscle fibres. The model provides a very good fit to the data in the cross-fibre direction, the fibre direction and at 45° from the fibre direction (R^2=0.99). It also predicts well the behaviour of muscle tissue at 30° and 60° from the fibre direction. Moreover, the SYM model uses engineering constants which have a direct physical interpretation.

3.5.6 Tensile behaviour of the tissue

This thesis investigates the mechanical properties of muscle tissue under compressive loading. A transversely isotropic model is proposed, with a set of parameters characterising the tissue behaviour in compression. Another set of parameters is however required to characterise the tensile behaviour of the tissue as skeletal muscle presents different properties in tension and in compression. The main function of skeletal muscle is to act as an actuator and produce force along its fibre direction; along this direction, the properties of the tissue will therefore be stiffer in tension than in compression. The other important role of muscle tissue is to protect the skeleton by absorbing shocks. These solicitations occur mainly in the cross-fibre direction and the tissue presents therefore stiffer characteristics in compression than in tension in the cross-fibre direction.

The hypothesis of transverse isotropy and the SYM model are probably adequate to characterise the tensile behaviour of the tissue. Further tests are however necessary to derive the tensile parameters of the model.

Chapter 4 - Study of muscle viscoelastic properties

4.1 INTRODUCTION 97

4.2 MATERIALS AND METHODS 98

4.2.1 RELAXATION TESTS 98

4.2.2 CYCLIC TESTS 99

4.2.3 SUMMARY OF TESTS PERFORMED 102

4.3 RELAXATION TESTS 103

4.3.1 EXPERIMENTAL RESULTS 103

4.3.1.1 Evolution of muscle compressive behaviour with deformation rate and fibre orientation 103

4.3.1.2 Evolution of muscle relaxation behaviour with deformation rate and fibre orientation 108

4.3.1.3 Evolution of muscle relaxation behaviour with compression level 114

4.3.2 MATHEMATICAL MODELLING 117

4.3.2.1 Quasi-linear viscoelastic SYM model – Unidirectional approach 117

4.3.2.2 Quasi-linear viscoelastic SYM model – Introduction of fibre dependency 130

4.4 CYCLIC TESTS 134

4.4.1 EXPERIMENTAL RESULTS 134

4.4.1.1 Low amplitude, low frequency tests 134

4.4.1.2 High amplitude, low frequency tests 138

4.4.1.3 High amplitude, high frequency tests 145

4.4.1.4 Evolution of the stress cycles amplitude and hysteresis ratio with frequency 150

4.4.2 MATHEMATICAL MODELLING 152

4.4.2.1 Quasi-linear viscoelastic SYM model 152

4.4.2.2 Nonlinear viscoelastic SYM model 158

4.5 DISCUSSION 165

4.5.1 SUMMARY OF EXPERIMENTAL RESULTS 165

4.5.1.1 Skeletal muscle compressive behaviour 165

4.5.1.2 Skeletal muscle relaxation behaviour 167

4.5.1.3 Skeletal muscle cyclic behaviour 168

4.5.2 COMPARISON OF EXPERIMENTAL RESULTS WITH PUBLISHED DATA 170

4.5.3 LIMITATIONS OF THE EXPERIMENTAL PROCEDURE 175

4.5.4 MODELLING OF MUSCLE VISCOELASTIC PROPERTIES USING THE QLV THEORY 176

4.5.5 MODELLING OF MUSCLE VISCOELASTIC PROPERTIES USING A NONLINEAR VISCOELASTIC MODEL 178

4.1 Introduction

As discussed in Chapter 2, the viscoelastic properties of skeletal muscle have rarely been investigated and most published studies remain limited to muscle relaxation behaviour (Best *et al.*, 1994; Bosboom *et al.*, 2001a, b). In contrast, ligament and tendon viscoelasticity has been studied more extensively (Abramowitch *et al.*, 2004; Bonifasi-Lista *et al.*, 2005; Kwan *et al.*, 1993; Provenzano *et al.*, 2001; Schatzmann *et al.*, 1998; Shibata *et al.*, 2006; Weiss *et al.*, 2002).

The viscoelastic behaviour of ligaments has widely been recognised as an important factor that mediates normal joint functions; understanding the viscoelastic properties of tissue can therefore help understand injury and repair processes. Similar mechanisms may apply to skeletal muscle and understanding its viscoelastic behaviour presents particular interests to prevent injuries to the tissue, such as strain injuries.

Tendons/Ligaments tensile properties show time/history-dependent behaviour resulting from complex interactions between collagen, other surrounding proteins and ground substances contained in the tissue. Stress relaxation illustrates the time-dependency; the force required to maintain a constant deformation on a ligament/tendon reduces with time. Hysteresis illustrates the history dependency; during cyclic stretching of ligaments, the nonlinear loading and unloading curves follow different paths, called hysteresis. It has also been observed that during cyclic elongation, the peak load decreases with an increasing number of cycles, which is termed cyclic stress relaxation.

Similarly to tendons/ligaments, skeletal muscle is made of various proportions of collagen, muscle proteins and ground substances. It is thus expected that muscle tissue will also display time- and history dependent behaviour.

In this chapter, the results of stress-relaxation and cyclic tests performed on porcine muscle tissue are presented.

In both types of tests, fibre orientation, strain levels and strain rates were varied in order to answer the following questions:

- Is muscle viscoelastic behaviour dependent on fibre orientation?
- Is muscle time-dependent behaviour (relaxation) strain and/or strain rate dependent?
- Is muscle history-dependent behaviour (hysteresis) strain rate dependent?

Using the quasi-linear viscoelasticity framework, the SYM formulation presented in the previous chapter was extended with Prony series to model muscle viscoelastic behaviour. Results from the stress-relaxation tests were used to derive the model parameters; cyclic tests were used to check the predictive capabilities of the model. A nonlinear viscoelastic approach was also investigated.

4.2 Materials and methods

4.2.1 Relaxation tests

The experimental conditions applied during these tests are very similar to the conditions used for quasi-static testing, described in section 3.1. The tissues tested were fresh porcine muscles excised from the pelvic limb of male pigs aged 10-12 weeks. From these, cubic samples oriented in the fibre direction, the cross-fibre direction, at 45° and 60° from the fibre direction were cut. Samples were kept at room temperature in airtight containers prior to testing, which started within two hours post-mortem. Uniaxial unconfined compression tests were performed on a Z005 Zwick machine (Zwick GmbH & Co. Ulm, Germany), equipped with a 5N load cell for force measurement. Samples were compressed up to 30% of their original length at deformation rates of 0.5, 1, 5 and 10%s^{-1}; following the ramp, compression was held constant for 300s to allow for relaxation. Force and displacement were recorded for the duration of the tests. Similar tests were also performed with compression levels of 10 and 20% at a rate of 1%s^{-1}; the deformation history applied to the samples during these tests is illustrated in Figure 4-1.

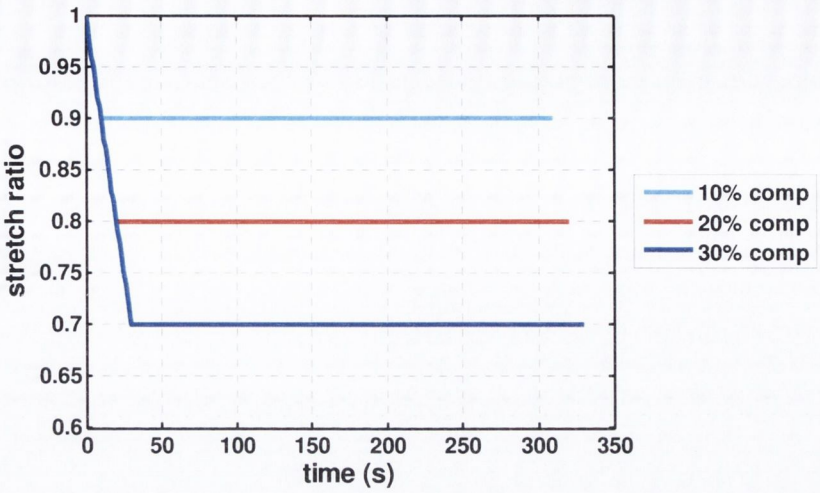


Figure 4-1: Deformation history applied to samples during relaxation tests at 1%str.s^{-1} up to 10, 20 and 30% compression.

4.2.2 Cyclic tests

Low and high amplitude cyclic tests were also performed on the Zwick machine. In the low amplitude tests, samples oriented in the fibre and cross-fibre directions were compressed up to 25% of their original length at a rate of 1%s^{-1}; cycles of 2% amplitude were then performed at the same rate for a duration of 250s. A frequency of 0.25Hz should be obtained in these conditions. However, a small time delay is observed when changes in the direction of the sawtooth deformation waves delivered by the Zwick machine occurred, leading to a frequency of 0.22Hz. Tests were also performed in which samples were subjected to a mean compression level of 19% at a rate of 2%s^{-1}; cycles of 2% amplitude were then performed at the same rate; this resulted in a frequency of 0.4Hz.

In high amplitude tests, samples were submitted to a mean compression level of 25% at compression rates of 5 and 10%s^{-1}; cycles of 10% amplitude were then performed at similar rates for 250s. These tests resulted respectively in frequencies of 0.22 and 0.44Hz. Figure 4-2 illustrates the deformation history applied to the sample during these tests (only the first four cycles are shown).

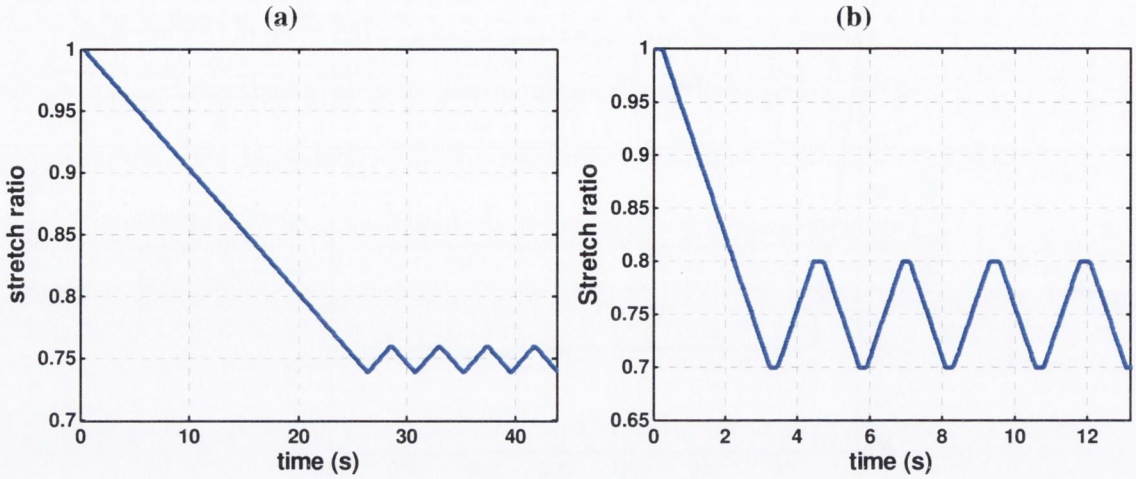


Figure 4-2: Deformation history applied to samples during cyclic tests with (a) 2% and (b) 10% amplitude.

The sawtooth waves delivered by the Zwick machine are limited to low frequencies. In order to investigate muscle behaviour at higher frequencies, a new dynamic testing rig was developed (Figure 4-3). In this uniaxial testing device, samples are compressed between two stainless steel platens. Sinusoidal displacement waves are provided to the bottom platen by an electro-dynamic shaker and various levels of compression are achieved by displacement of the top platen. The device is equipped with a Linear Variable Differential Transformer (LVDT) measuring the displacement of the bottom platen; a static load cell (strain gauge type transducer) mounted on the top platen measures the force; a dynamic load cell (piezoelectric force sensor) is also mounted on the bottom platen in order to account for inertial effects. Further details on these measuring devices are provided in Appendix B.

Using this uniaxial device, fresh porcine samples were cyclically tested at frequencies of 5, 20 and 80Hz. Cycles of 10% amplitude were performed around a mean compression level of 25% for a duration of 250s; this is similar to the deformation applied in high amplitude cyclic tests performed at lower frequency (0.44Hz) on the Zwick machine. At these frequencies, the compression rates were approximately of $200\%s^{-1}$ at 5Hz, $800\%s^{-1}$ at 20Hz and $3200\%s^{-1}$ at 80Hz.

The mean compression level is applied to the samples by displacement of the top platen. The total value of the displacement, which is manually controlled, is recorded; however, its history with time is not recorded as the LVDT measures the displacement of the bottom platen only. This does not influence the results; it only requires an approximation to be made when experimental data are compared to theoretical results (see section 4.4.2).

The analog signals from the displacement and force measuring transducers were acquired on a personal computer using a 16-bit data acquisition card (National Instruments PCI 6036E) and a custom-written Labview interface. Sampling rates of 500, 2000 and 8000Hz were used for tests performed respectively at 5, 20 and 80Hz; this corresponded to the acquisition of 100 data points per cycle. The raw data acquired were then digitally filtered in Matlab using a first order lowpass Butterworth filter (built-in Matlab functions *butter* and *filtfilt*).

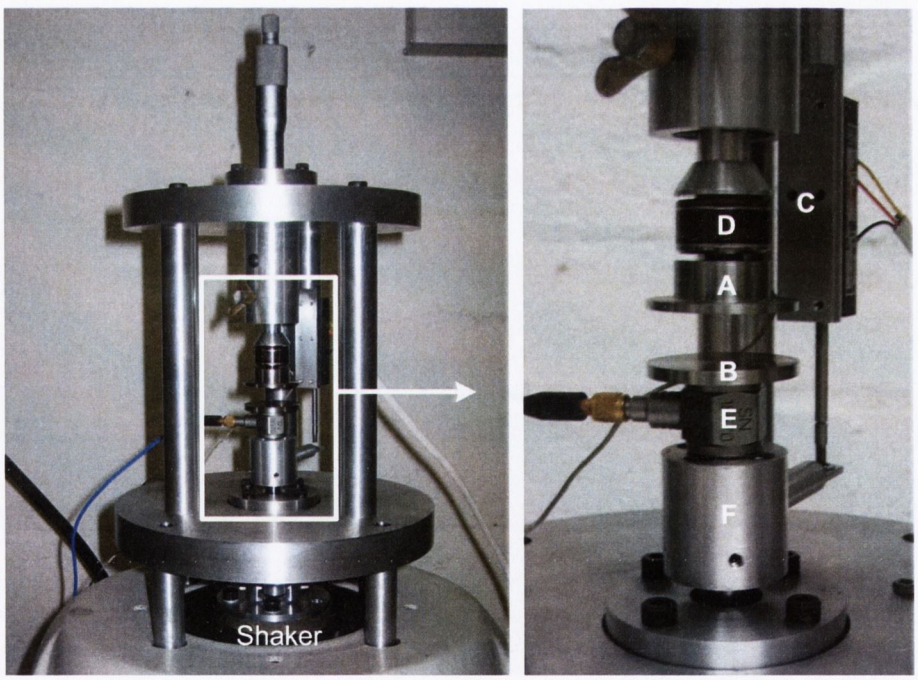


Figure 4-3: Custom built high speed cyclic testing rig.

(A) Top platen; (B) Bottom platen; (C) LVDT transducer; (D) Static load cell; (E) Dynamic load cell; (F) Connection with shaker.

4.2.3 Summary of tests performed

	Type of test	Test direction	# samples in each direction
Quasi-static (chapter3)	Ramp @ 0.05%str.s^{-1} up to 30% compression	F, 30°, 45°, 60°, XF	15
Relaxation	Ramp @ 0.5% str.s^{-1} up to 30% compression & Hold 300s	F, 45°, 60°, XF	6
	Ramp @ 1% str.s^{-1} up to 10, 20 and 30% compression & Hold 300s	F, 45°, 60°, XF	6
	Ramp @ 5% str.s^{-1} up to 30% compression & Hold 300s	F, 45°, 60°, XF	6
	Ramp @ 10% str.s^{-1} up to 30% compression & Hold 300s	F, 45°, 60°, XF	6
Cyclic	2% amp cycles @ 0.22 and 0.4Hz	F, XF	6
	10% amp cycles @ 0.22 and 0.4Hz	F, 45°, 60°, XF	6
	10% amp cycles @ 5, 20 and 80Hz	F, 45°, 60°, XF	6

4.3 Relaxation tests

As in Chapter 3, only mean experimental results are presented in the following sections; complete data sets from which these mean results are derived are presented in Appendix C. Cauchy stress (σ) and stretch ratio (λ) are calculated as previously (equation 3-1).

The deformation applied to samples during relaxation tests consisted of ramp and hold functions performed at various rates and strain levels (Figure 4-1). In the following section, results from both parts of the deformation history are examined separately. Muscle behaviour under compressive ramps performed at various rates is considered first. The stress-relaxation behaviour following these compressive ramps is then examined.

In graphs comparing results obtained at various orientations of the muscle fibres, the colour convention adopted is as before: red for fibre direction, cyan for 45° direction, magenta for 60° direction and blue for cross-fibre direction. This convention is however not respected in graphs comparing results obtained at various deformation rates for a specific fibre orientation.

4.3.1 Experimental results

4.3.1.1 Evolution of muscle compressive behaviour with deformation rate and fibre orientation

This section examines the behaviour of muscle tissue during the ramp part of the tests. Figure 4-4 presents experimental stress-stretch curves obtained during compression of samples at various compression rates (0.05, 0.5, 1, 5 and 10%s^{-1}) in all directions of testing (fibre ≡ 0°, 45°, 60° and cross-fibre ≡ 90° from the fibre direction). Results at 0.05%str.s^{-1} correspond to results from quasi-static tests presented in the previous chapter.

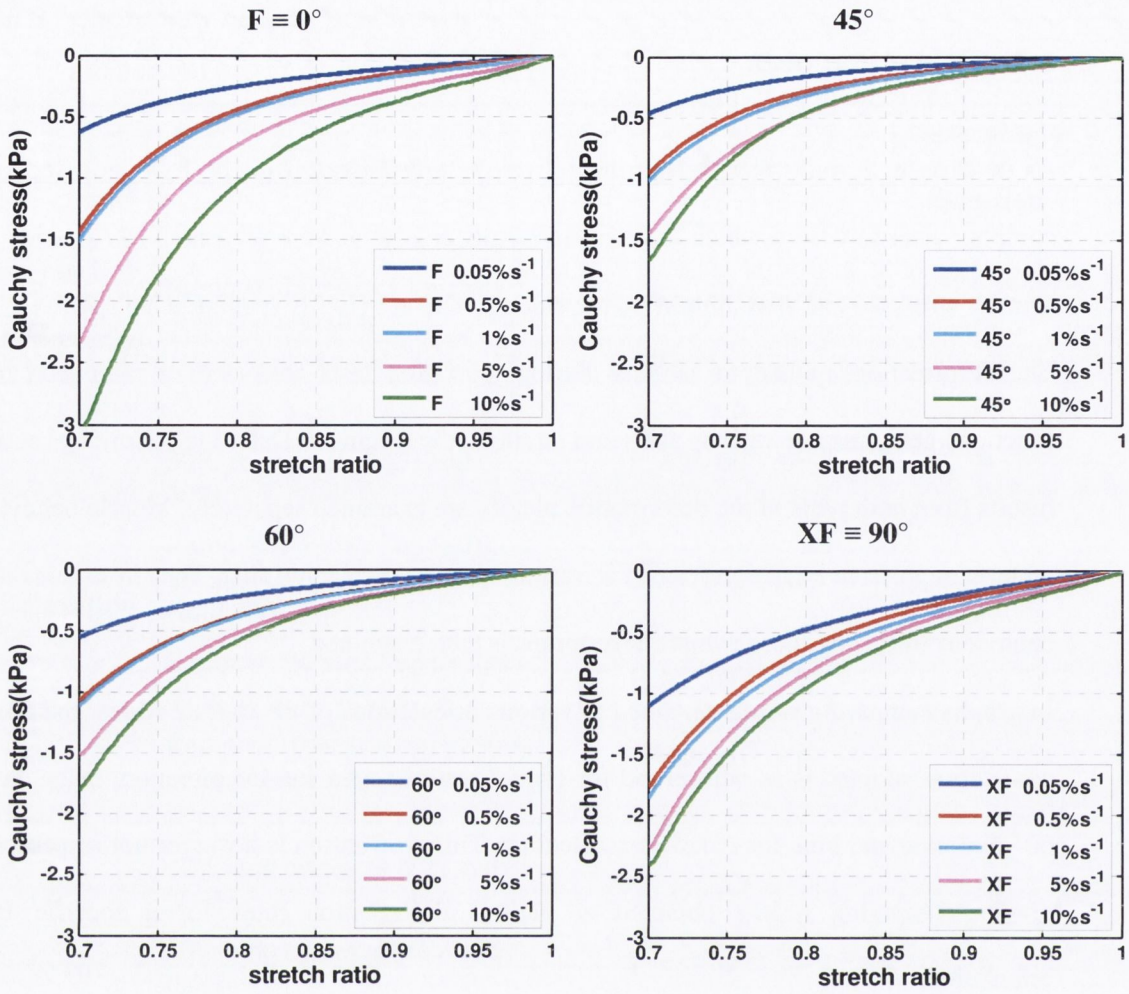


Figure 4-4: Stress-stretch curves comparing porcine muscle compressive behaviour at various rates and various orientations of the muscle fibres.

As expected, a stiffening effect with compression rate is observed in all directions of testing; faster rates give higher peak loads at a given deformation level. The increase in stiffness with compression rate is however more significant in directions closer to the fibre direction. This is illustrated in Figure 4-5 which presents the evolution with compression rate of the stress reached after 30% compression in the various fibre orientations considered. It shows that during quasi-static tests (0.05%str.s^{-1}), the cross-fibre direction (blue) is much stiffer than the fibre direction (red). However, when compression rate increases, the difference in stiffness between both directions diminishes. When a rate of 5%str.s^{-1} is reached the trend is inverted; the fibre direction becomes stiffer than the cross-fibre direction.

The bar chart of Figure 4-5 was constructed from mean values and standard deviations presented in Table 4-1.

Table 4-1: Evolution with deformation rate of the stress reached after 30% compression in various orientations of the muscle fibres - mean ± SD.

	Peak stress at 30% compression ± SD (in kPa)				
	0.05%str.s^{-1}	**0.5%str.s^{-1}**	**1%str.s^{-1}**	**5%str.s^{-1}**	**10%str.s^{-1}**
F	-0.63±0.14	-1.44±0.09	-1.51±0.12	-2.32±0.15	-3.09±0.29
45°	-0.47±0.15	-0.96±0.05	-1.01±0.03	-1.42±0.07	-1.65±0.06
60°	-0.55±0.14	-1.07±0.04	-1.11±0.05	-1.50±0.05	-1.80±0.05
XF	-1.10±0.17	-1.77±0.09	-1.85±0.07	-2.24±0.13	-2.40±0.19

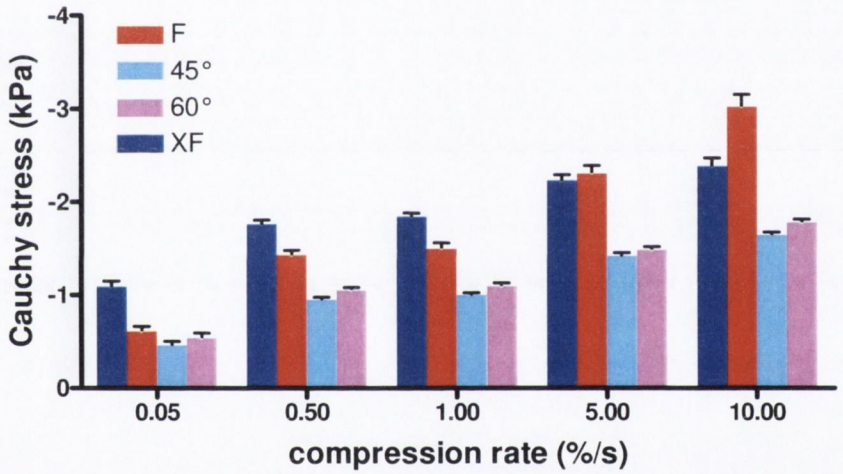


Figure 4-5: Evolution with deformation rate of the stress reached after 30% compression in various orientations of the muscle fibres.
Mean values with standard deviations.

Figure 4-6 compares fibre and cross-fibre results for the complete deformation history (Figure 4-5 compared only peak stresses). It shows that at 5%str.s^{-1}, the fibre direction (—) becomes stiffer than the cross-fibre direction (—) only when high levels of deformation are reached. At 10%str.s^{-1}, the fibre (•••) and the cross-fibre (•••) directions present similar properties up to 15% compression; the fibre direction then becomes stiffer at higher compression levels.

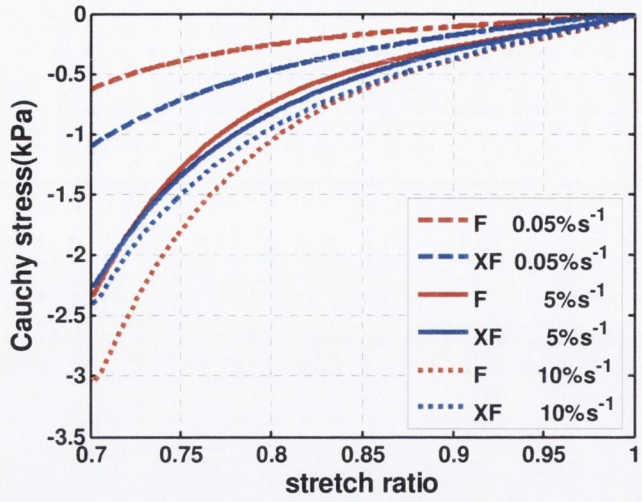


Figure 4-6: Stress-stretch curves comparing muscle compression behaviour at 0.05, 5 and 10%str.s^{-1} in fibre (—) and cross-fibre (—) directions.

During a relaxation test, the peak stress reached after the ramp can be considered as the sum of a long term elastic and a viscoelastic contribution as illustrated in Figure 4-7.

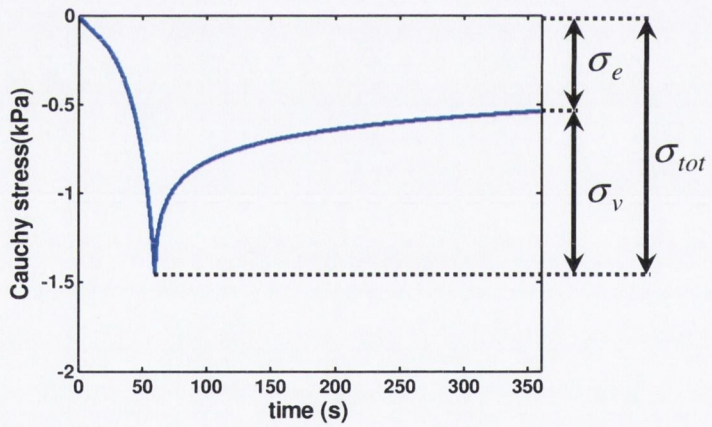


Figure 4-7: Typical stress-relaxation curve illustrating the contribution to the total stress (σ_{tot}) of elastic (σ_e) and viscoelastic (σ_v) components.

The relative contribution of the viscoelastic component to the total stress can be calculated as:

$$\frac{\sigma_v}{\sigma_{tot}} = \frac{\sigma_{tot} - \sigma_e}{\sigma_{tot}} \tag{4-1}$$

Table 4-2 presents the ratios (σ_v/σ_{tot}) calculated at 30% compression for the various deformation rates considered in the experiments. Values for the elastic component were taken from quasi-static tests results (maximum stress reached at 30% compression with a rate of 0.05%s^{-1}) so that σ_v is zero at 0.05%str.s^{-1}. Figure 4-8 summarises these results graphically. It shows that an increase in compression rate leads to an increase in the viscoelastic contribution to the total stress; it also shows that the viscoelastic component has a greater influence in directions closer to the muscle fibres.

Table 4-2: Relative contribution of the viscoelastic component to the total stress reached at 30% compression at various strain rates and fibre orientations.

	Viscoelastic contribution (%)				
	0.05%str.s^{-1}	**0.5%str.s^{-1}**	**1%str.s^{-1}**	**5%str.s^{-1}**	**10%str.s^{-1}**
F ≡ 0°	0	57	59	73	79
45°	0	51	54	67	72
60°	0	48	50	63	69
XF ≡ 90°	0	38	41	51	54

Angle ↓ ; ↑ σ_v

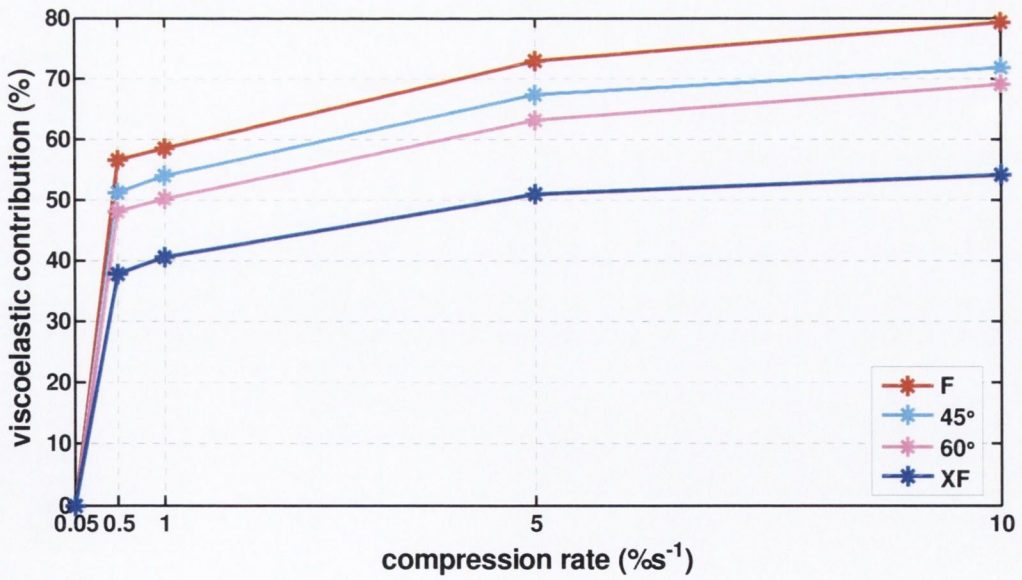


Figure 4-8: Relative contribution of the viscoelastic component to the total stress reached at 30% compression at various strain rates and fibre orientations.

Values obtained using equation (4-1) with σ_e = quasi-static values.

Finally, it should be emphasised that the contribution of the viscoelastic component to muscle behaviour is substantial even for very low strain rates; for a rate of $0.5\%s^{-1}$, σ_v represents respectively 38% and 57% of the total stress reached in the cross-fibre and fibre directions.

4.3.1.2 Evolution of muscle relaxation behaviour with deformation rate and fibre orientation

This section considers muscle behaviour when the deformation is held constant after the ramp. Figure 4-9 compares mean stress-relaxation curves obtained at various compression rates in each direction of testing.

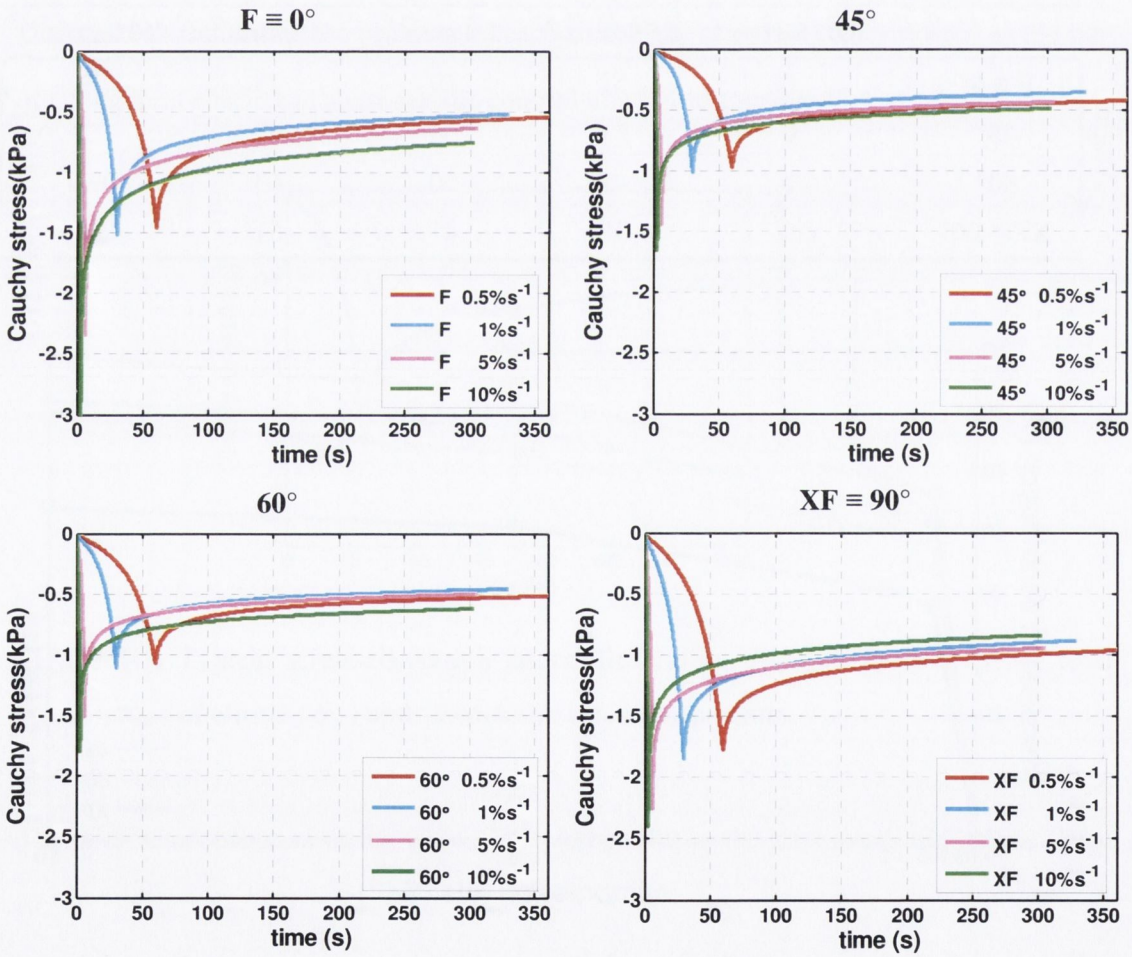


Figure 4-9: Stress-relaxation curves obtained at various compression rates and orientations of the muscle fibres.

Results show that a significant amount of stress-relaxation occurs when deformation is held constant after a compressive ramp, with the main part of the stress reduction happening within the first hundred seconds after the ramp. To quantify this drop, the percentage of stress relaxation is defined as the difference between the peak stress reached after the ramp and the current value of stress, normalised by the peak stress. Figure 4-10 presents the evolution with time of the relaxation amount for each testing direction and strain rate considered. Curves were shifted so that time zero corresponds to the beginning of relaxation. For each fibre orientation considered, Figure 4-10 shows an increase in the amount of relaxation when the compression rate is increased. This behaviour is as expected because higher peaks loads are reached during faster ramps, and the tissue needs to relax by a greater amount to reach its equilibrium value. Also, analysis of the data shows that over 80% of the total relaxation amount occurs within 100s.

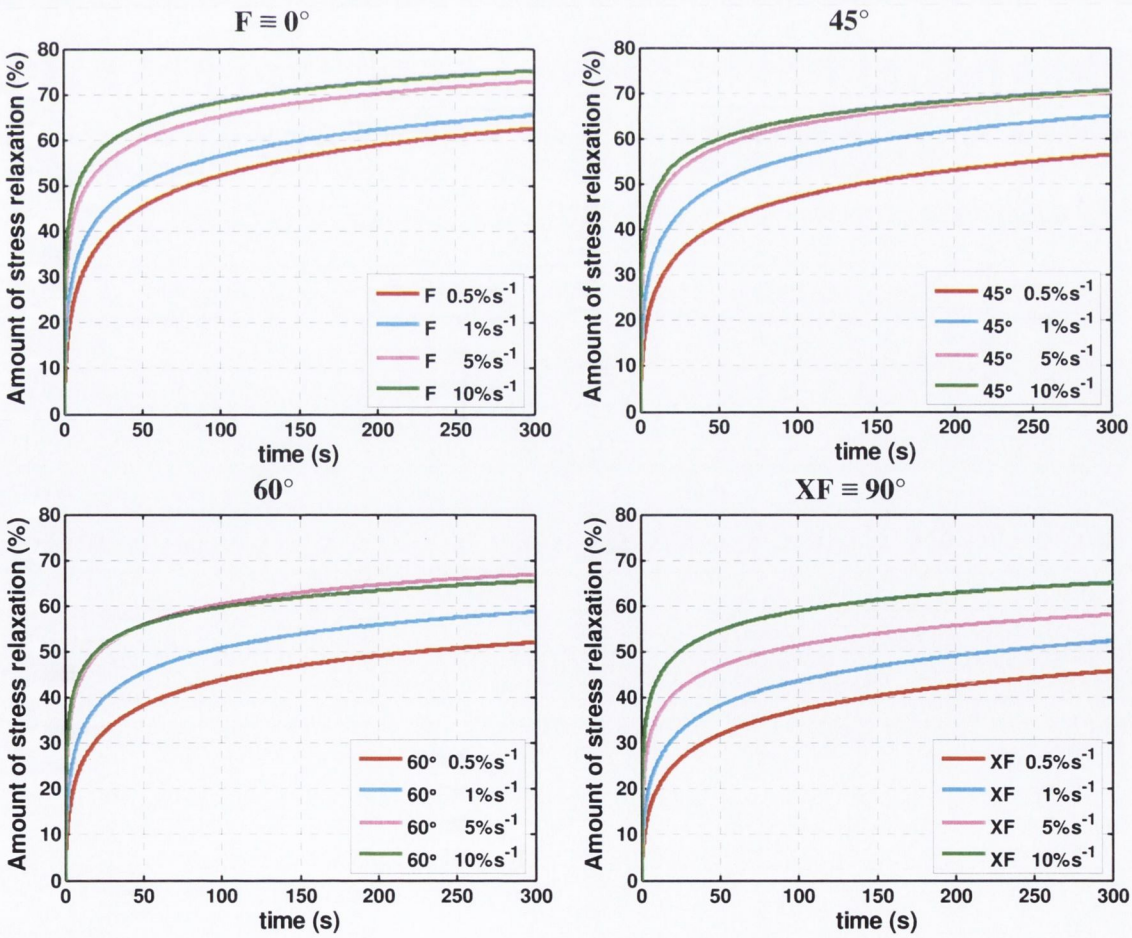


Figure 4-10: Evolution with time of the amount of stress relaxation. Comparison between results obtained at various compression rates.

Table 4-3 presents total amounts of relaxation observed 300s after the ramp.

Table 4-3: Amount of stress relaxation following compressive ramps at various rates and orientations of the muscle fibres – values taken 300s after the ramp.

		Amount of stress relaxation (%)			
		0.5%str.s^{-1}	**1%str.s^{-1}**	**5%str.s^{-1}**	**10%str.s^{-1}**
Angle ↓	**F ≡ 0°**	63	66	73	75
	45°	57	65	70	71
	60°	52	59	67	65
	XF ≡ 90°	46	52	58	65
					↑ $\dot{\varepsilon}_V$

When each compression rate is considered individually, Table 4-3 shows an increase in the amount of relaxation for tests performed in directions closer to the muscle fibres.

Table 4-4 reports mean values of stress reached after 300s relaxation for the various rates and fibre orientations considered; values of stress reached during quasi-static tests are also reported.

Table 4-4: Values of stress at 30% compression in quasi-static and relaxation tests (values taken after 300s relaxation)

	Relaxed stress at 30% compression ± SD (in kPa)					
	0.05%str.s^{-1}	**0.5%str.s^{-1}**	**1%str.s^{-1}**	**5%str.s^{-1}**	**10%str.s^{-1}**	**mean**
F	-0.63±0.14	-0.54±0.04	-0.52±0.04	-0.62±0.06	-0.75±0.12	-0.61±0.11
45°	-0.47±0.15	-0.41±0.02	-0.35±0.02	-0.42±0.02	-0.48±0.06	-0.42±0.05
60°	-0.55±0.14	-0.51±0.04	-0.46±0.03	-0.49±0.06	-0.62±0.03	-0.52±0.07
XF	-1.10±0.17	-0.96±0.05	-0.88±0.03	-0.94±0.09	-0.84±0.04	-0.90±0.05

For each fibre orientation, differences are observed between relaxed values reached at various rates. No pattern is however seen and this might be attributed to variability present between specimens tested. Differences are also noticed between quasi-static and relaxed values, relaxed values being smaller than quasi-static values for most tests. A one-way analysis of variance was conducted to assess the statistical significance of these differences; where significance was detected ($p < 0.05$), Tukey's post-hoc test was used for multiple

comparisons. Figure 4-11 presents a graphical summary of the results; statistically significant differences are denoted with a *. For each orientation considered, most relaxed values do not appear to be significantly different from each other. In view of this, it is reasonable to consider that samples relax to the same equilibrium value independently of the compression rate, for each orientation of the muscle fibres considered individually. A mean relaxed muscle state is defined as the mean between relaxed values obtained at various rates (last column of Table 4-4).

Comparisons between quasi-static and relaxed values show that significant differences appear only in the cross-fibre direction.

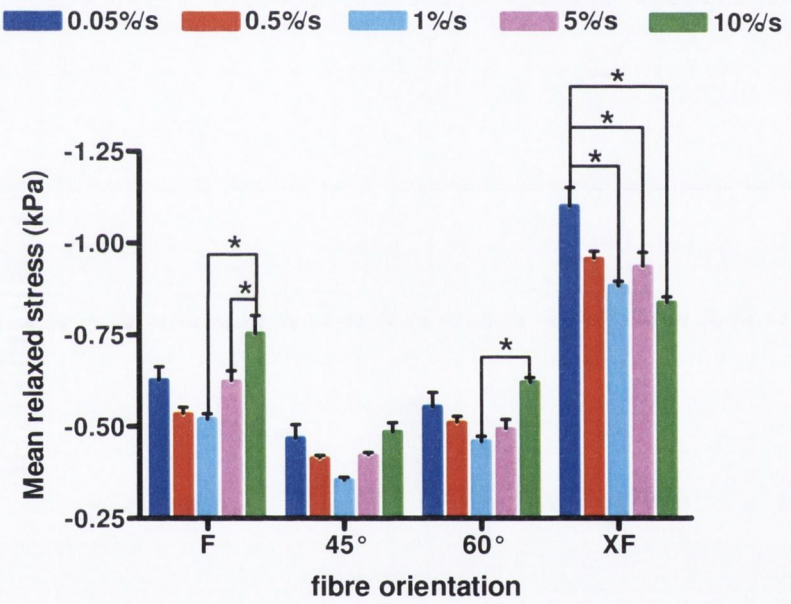


Figure 4-11: Comparison between mean values of stress obtained during quasi-static tests (■) and relaxed values obtained after compressive ramps performed at various rates.

** denotes pairs of values between which a statistical significance is observed ($p<0.05$). Comparisons are established for each fibre orientation individually.*

In Figure 4-12, a comparison is established between muscle relaxation behaviour in various orientations of the muscle fibres, for each compression rate considered (in Figure 4-10 the comparison was established between results obtained at various rates, for each orientation considered individually). It shows that relative amounts of relaxation increase with an

increase in angle from the fibre direction, indicating again muscle anisotropic viscoelastic behaviour and the greater influence of the viscoelastic component in directions closer to the muscle fibres.

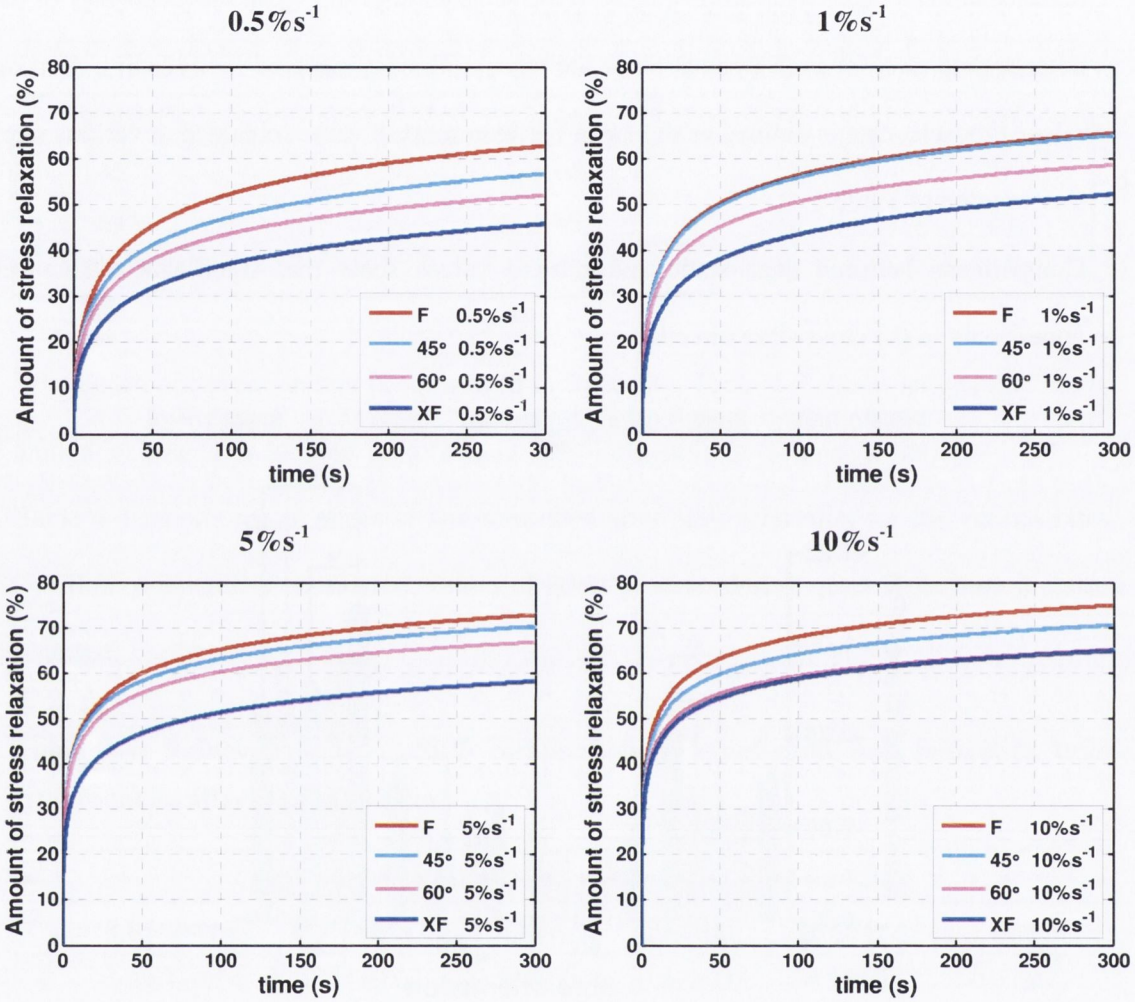


Figure 4-12: Evolution with time of the amount of stress relaxation. Comparison between results obtained at various orientations of the muscle fibres

In the previous section, values for the relative viscoelastic stress contribution to the total stress were calculated using quasi-static values for the elastic stress (see Figure 4-7, Table 4-2 and equation (4-1)). These can now be recalculated using the mean values obtained after relaxation for the elastic stress. Table 4-5 presents the values obtained; Figure 4-13 offers a graphical summary of the results.

Comments are similar to those made for Figure 4-8 (where σ_e was equal to quasi-static values); viscoelastic contribution to the total stress increases with compression rate and the viscoelastic component has a greater influence in directions closer to the muscle fibres. The main difference is the presence here of a relatively minor viscoelastic contribution to the stress obtained from quasi-static testing (rate of 0.05%s^{-1}). This is due to the differences observed between quasi-static and relaxed values (Table 4-4); further comments will be made on this point in the discussion section.

Table 4-5: Relative contribution of the viscoelastic component to the total stress reached at 30% compression at various strain rates.

	Viscoelastic contribution (%)				
Angle ↓	0.05%str.s^{-1}	0.5%str.s^{-1}	1%str.s^{-1}	5%str.s^{-1}	10%str.s^{-1}
F ≡ 0°	2.8	58	60	74	80
45°	10	56	59	71	75
60°	5.6	51	53	65	71
XF ≡ 90°	18	49	51	60	62

↑ σ_v

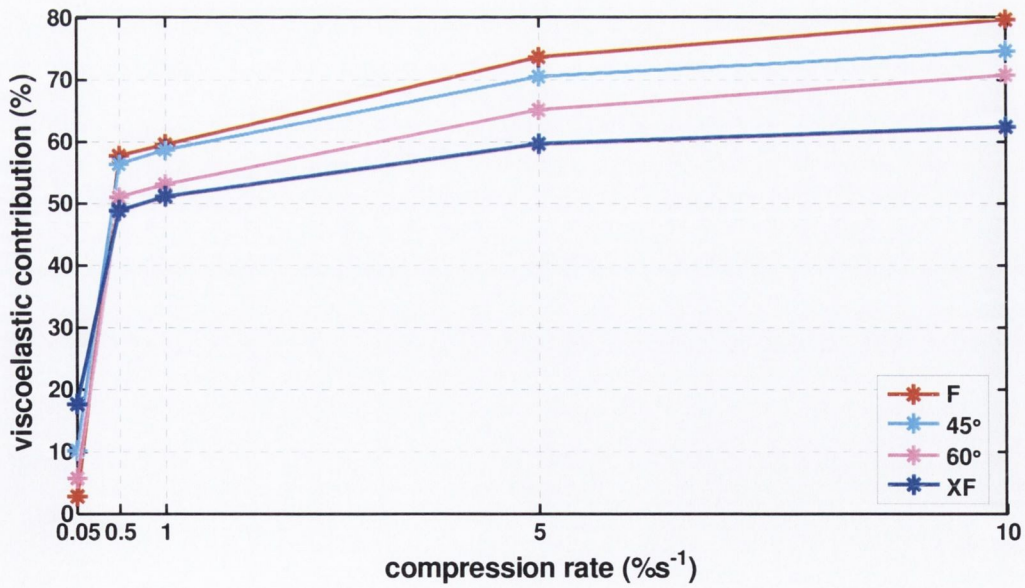


Figure 4-13: Relative contribution of the viscoelastic component to the total stress reached at 30% compression at various strain rates and fibre orientations.

Values obtained using equation (4-1) with σ_e = mean relaxed values

4.3.1.3 Evolution of muscle relaxation behaviour with compression level

Figure 4-14 presents results of relaxation tests performed in the fibre and cross-fibre directions at a compression rate of $1\%s^{-1}$ up to three levels of compression, i.e. 10, 20 and 30%.

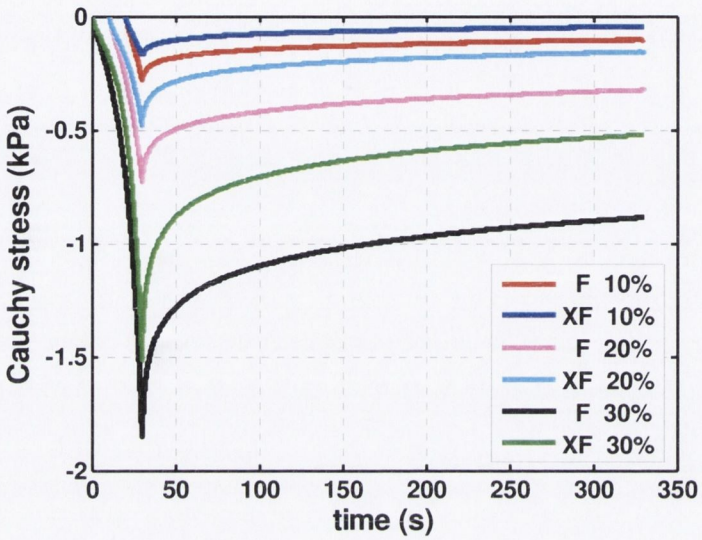


Figure 4-14: Stress relaxation curves in fibre and cross-fibre directions after 10, 20 and 30% compression at a rate of $1\%s^{-1}$.

For clarity in the presentation of the results, curves obtained at 10 and 20% compression were shifted on the x-axis. At the rate considered, the cross-fibre direction remains stiffer than the fibre direction and a substantial amount of stress relaxation is observed at all compression levels as illustrated in Figure 4-15. The amount of relaxation increases when the compression level decreases. For tests performed at finite compression rates, this can be explained by the fact that the material relaxes not only during the relaxation phase but also during the ramp phase of the test; more time is allowed for relaxation during the ramp when a higher level of compression is reached. Results are qualitatively similar in the fibre and cross-fibre directions, however it can be seen that, at all levels of compression, the amount of relaxation is greater by about 10% in the fibre than in the cross-fibre direction.

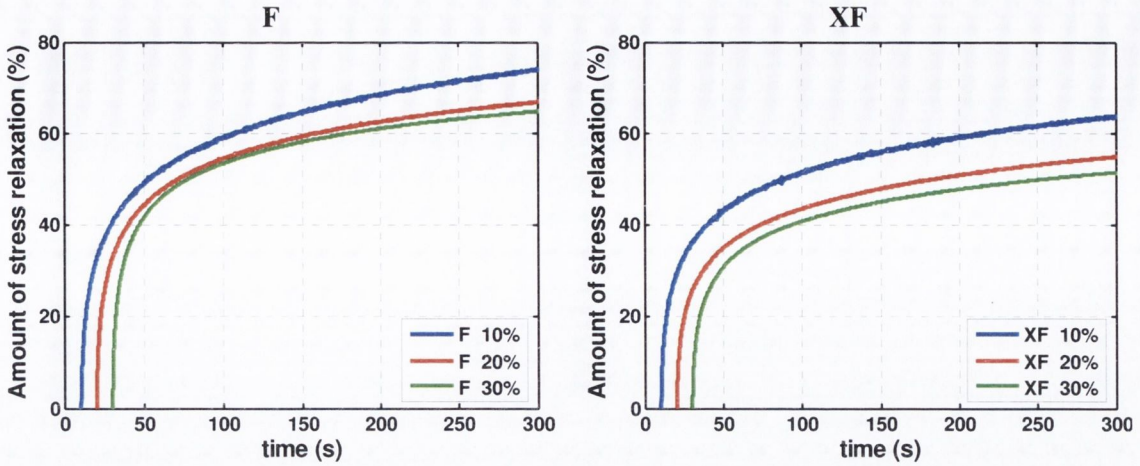


Figure 4-15: Evolution with time of the amount of stress relaxation obtained in the fibre and the cross-fibre directions after 10, 20 and 30% compression; compression rate of 1%s^{-1}.

When stress relaxation curves are plotted using logarithmic scales, a linear relationship is observed aside from the initial relaxation response in the first 10 s (Figure 4-16). A power law can be used for curve fitting,

$$\sigma(t) = \exp(a)\, t^{m} \tag{4-2}$$

where a and m are parameters of fit.

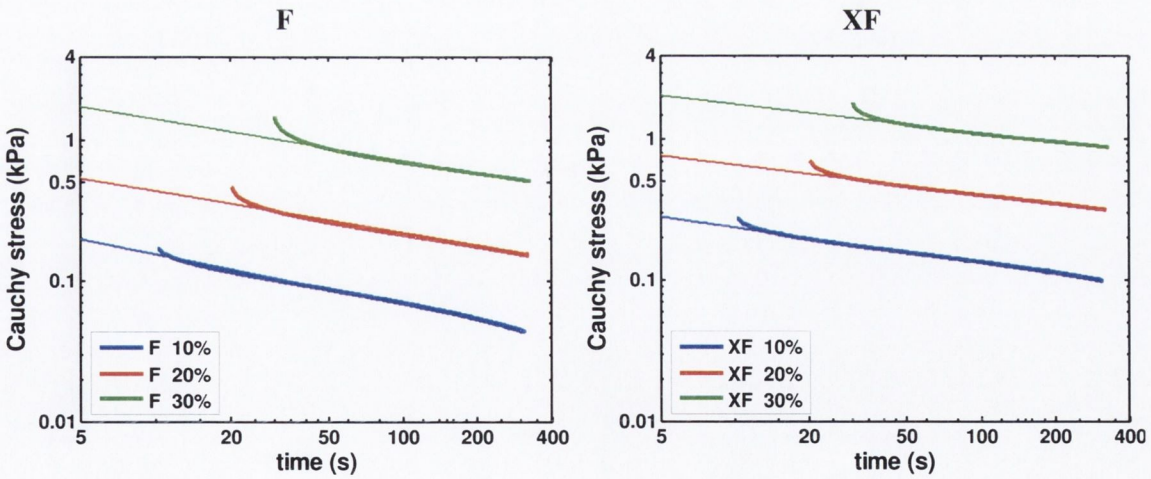


Figure 4-16: Stress-relaxation curves on logarithmic scales illustrating the linear trend of the stress decay.

Thick lines represent experimental results; thin lines represent power-law fitting.

Values obtained for parameters *a* and *m* at various levels of compression in the fibre and cross-fibre directions are presented in Table 4-6. *m* is the parameter of interest here, it represents the slope of the line on a log-log plot and is considered as the rate of relaxation.

Table 4-6: Parameters *m* and *a* for power-law fitting of stress-relaxation curves obtained at various levels of compression in fibre and cross-fibre directions.

		10%	20%	30%
m	F	-0.356±0.045	-0.298±0.019	-0.298±0.018
	XF	-0.252±0.048	-0.217±0.032	-0.208±0.015
a	F	-1.039±0.214	-0.120±0.079	1.052±0.092
	XF	-0.855±0.141	-0.103±0.162	1.068±0.084

The rate of relaxation (*m*) appears to increase when the level of compression decreases. A one-way analysis of variance was conducted to assess the statistical significance of the differences observed; when significance was detected ($p < 0.05$), Tukey's post-hoc test was used for multiple comparisons. Figure 4-17 presents a graphical summary of the results; statistically significant differences are denoted with a *.

Even though a statistically significant difference appears only in the fibre direction, results seem to indicate that muscle relaxation behaviour is dependent on deformation level.

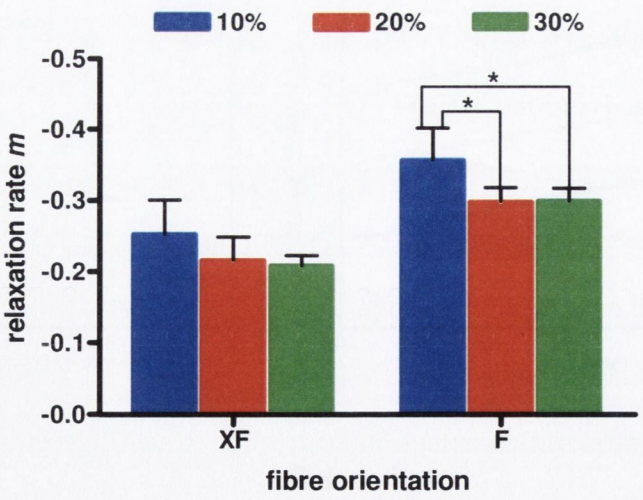


Figure 4-17: Evolution of the relaxation rate (*m*) with compression level.

** denotes pairs of values between which a statistical significance is observed ($p<0.05$).*

4.3.2 Mathematical modelling

This section investigates the use of a quasi-linear viscoelastic model to represent skeletal muscle viscoelastic properties. The model proposed is an extension with Prony series of the SYM model, which successfully represents muscle elastic properties (Chapter 3).

Results from relaxation tests indicate that skeletal muscle has anisotropic properties, not only in its elastic behaviour but also in its viscoelastic behaviour; an anisotropic viscoelastic model is thus required. A unidirectional approach is however first investigated; fitting of the model is performed individually for each orientation of the muscle fibres considered. Viscoelastic anisotropy is then considered and a relationship between fibre orientation and viscoelastic properties is established, following a similar approach as for elastic properties.

4.3.2.1 Quasi-linear viscoelastic SYM model – Unidirectional approach

Considering a uniaxial state of stress, the Cauchy stress in direction j for a quasi-linear viscoelastic material can be expressed as:

$$\sigma_j(t) = \int_0^t G\ (t-\tau)\frac{\partial \sigma_j^e[\tilde{\varepsilon}_j(\tau)]}{\partial \tau} d\tau \tag{4-3}$$

or

$$\sigma_j(t) = \sigma_j^e(0+)G_j(t) + \int_0^t G_j(t-\tau)\frac{\partial \sigma_j^e\left[\tilde{\varepsilon}_j(\tau)\right]}{\partial \tau} d\tau \tag{4-4}$$

$G_j(t)$ is the reduced relaxation function and σ_j^e the instantaneous elastic stress, i.e. the maximum stress in response to an instantaneous step input of deformation; $\tilde{\varepsilon}_j = \ln(\lambda_j)$ to account for large deformations.

Using a Prony series expansion for the reduced relaxation function, $G_j(t) = p_{\infty j} + \sum_{i=1}^{N} p_{ij} \exp(-\frac{t}{\tau_{ij}})$ leads to:

$$\sigma_j(t) = p_{\infty j}\sigma_j^e(t) + \sum_{i=1}^{N} \int_0^t p_{ij} \exp\left(\frac{-(t-\tau)}{\tau_{ij}}\right)\frac{\partial \sigma_j^e[\tilde{\varepsilon}_j(\tau)]}{\partial \tau} d\tau \tag{4-5}$$

p_{ij} and τ_{ij} are parameters characterising the viscoelastic behaviour in direction j;

$p_{\infty j} = 1 - \sum_{i=1}^{N} p_{ij}$.

The SYM formulation was then introduced for the long term elastic stress, $\sigma_{\infty j} = p_{\infty j}\sigma_j^e = k_{1j}\tilde{\varepsilon}_j + k_{2j}\tilde{\varepsilon}_j^2 + k_{3j}\tilde{\varepsilon}_j^3$; k_{1j} , k_{2j} and k_{3j} are the SYM parameters characterising elastic behaviour in the direction considered (Chapter 3).

This model was implemented in the Mathworks software Matlab using the recursive formula presented in section 2.3.3.3. Equation (4-5) can be expressed as:

$$\sigma_j(t) = p_{\infty j}\sigma_j^e(t) + \sum_{i=1}^{N} s_{ij}(t) \tag{4-6}$$

where $$s_{ij}(t) = \int_0^t p_{ij} \exp\left(\frac{-(t-\tau)}{\tau_{ij}}\right) \frac{\partial \sigma_j^e[\tilde{\varepsilon}_j(\tau)]}{\partial \tau} d\tau \tag{4-7}$$

Now considering the time interval (t_n, t_{n+1}), the stress at time t_{n+1} can be calculated as:

$$\sigma_j(t_{n+1}) = p_{\infty j}\sigma_j^e(t_{n+1}) + \sum_{i=1}^{N}\left(\exp\left(-\frac{\Delta t}{\tau_{ij}}\right) s_{ij}(t_n) + p_{ij} \frac{1-\exp\left(-\frac{\Delta t}{\tau_{ij}}\right)}{\frac{\Delta t}{\tau_{ij}}} \left[\sigma_j^e(t_{n+1}) - \sigma_j^e(t_n)\right] \right) \tag{4-8}$$

with $\Delta t = t_{n+1} - t_n$.

Individual fitting to relaxation data obtained at various compression rates was first performed in order to assess the appropriateness of the model to represent muscle behaviour. When parameters obtained from quasi-static testing are used for k_{1j}, k_{2j} and k_{3j}, fitting to ramp and hold tests could not be achieved successfully. This is due to the fact that the rate used for quasi-static tests was not small enough to measure strictly long term elastic properties but a small amount of viscoelastic component was also measured during the tests (see Figure 4-13). Elastic parameters obtained from quasi-static testing are thus slightly too high and were reduced to agree with mean relaxed values obtained in Table 4-4. In order to respect the transversely isotropic relationship established in chapter 3, a similar ratio was adopted for each fibre orientation.

A five term Prony series showed the best fitting results and was adopted for the viscoelastic formulation. Ten parameters have then to be determined for each orientation considered, $p_{1j,\ldots,5j}$ and $\tau_{1j,\ldots,5j}$. Fitting was performed using the built in Matlab function *lsqnonlin* as before (see Chapter 3). The Matlab code used to perform the fitting is provided in Appendix D. Fitting was performed using the complete deformation history as an input; this has been shown to provide the best results for parameters estimation when fitting quasi-linear viscoelastic models to stress-relaxation data (Doehring *et al.*, 2004; Abramowitch and Woo, 2004). Figure 4-18 shows that individual fitting to relaxation data obtained at the various strain rates provides very good results. However, the set of parameters obtained at any specific rate has poor predictive capabilities when other deformation rates are considered.

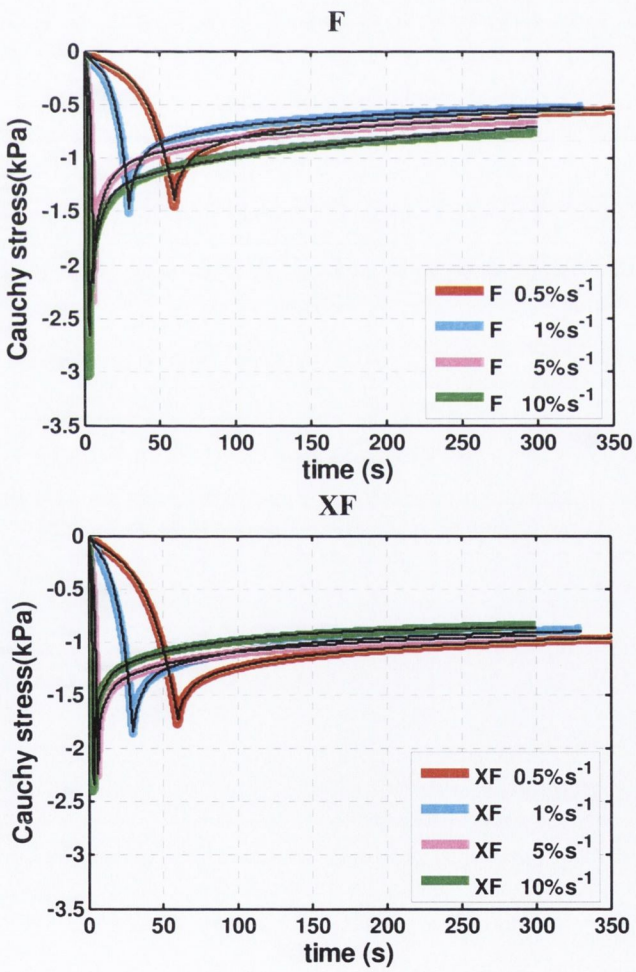


Figure 4-18: Comparison between experimental data and viscoelastic SYM model fitting - Individual fitting at each rate.

F, Fibre direction; XF, Cross-fibre direction. Thick lines represent experimental data; thin lines represent model fitting.

Simultaneous fitting to data obtained at various rates was then performed in order to obtain a global set of parameters representative of muscle relaxation behaviour.

It is however important to understand how the model works to appreciate the difficulty associated with the determination of a single set of parameters to provide a good match to data obtained at various compression rates.

In the model, the total stress is the sum of a long term elastic response and a series of viscoelastic contributions. The long term elastic response corresponds to muscle response after relaxation, $\sigma_{\infty j} = k_{1j}\tilde{\varepsilon}_j + k_{2j}\tilde{\varepsilon}_j^2 + k_{3j}\tilde{\varepsilon}_j^3$; it is a function of the material elastic response only and is independent of the deformation rate. Due to experimental variability however, relaxed values of stress are different in tests performed at different rates (Table 4-4).

The peak stress reached after the ramp is a function of the time taken to perform the ramp; it increases with deformation rate. This is due to the fact that the material also relaxes during the ramp; less time is allowed for relaxation in ramps performed at a higher rate.

The maximum value of stress that can be reached is:

$$\sigma_j^e = (k_{1j}\tilde{\varepsilon}_j + k_{2j}\tilde{\varepsilon}_j^2 + k_{3j}\tilde{\varepsilon}_j^3)/(1 - \sum_{i=1}^{n} p_{ij}) \qquad (4\text{-}9)$$

It corresponds to the instantaneous elastic stress reached if deformation was applied at an infinite rate. σ_j^e depends on elastic parameters (k_{ij}) and viscoelastic parameters (p_{ij}). Simultaneous fitting to data obtained at various rates therefore represents a compromise to match peak and relaxed values of stress reached at each rate.

Individual fitting showed that the five time constants τ_{ij}, characterising muscle relaxation behaviour, ranged from 0.6 to 300s. In order to reduce the number of variables during fitting, the τ_{ij} values were therefore fixed at 0.6, 6, 30, 60 and 300s, independently of deformation rate or fibre orientation. 300s corresponds to the time allowed for relaxation during the experiments; 6, 30 and 60s respectively correspond to the duration of the ramp in tests performed at compression rates of 5, 1 and 0.5%s^{-1}.

The only remaining parameters are the five multiplicative factors p_{ij}, characterising the amplitude of each viscoelastic component; they were obtained by simultaneous fitting to experimental data obtained at compression rates of 0.5, 1 and 10%s^{-1}.

Figures 4-19 to 4-22 present results of the fitting in the fibre direction, at 45° and 60° from the fibre direction and in the cross-fibre direction.

Fibre direction

Parameters values				
k_{1L} (kPa)	k_{2L} (kPa)	k_{3L} (kPa)	-	-
1.005	2.989	10.985		
p_{1L}	p_{2L}	p_{3L}	p_{4L}	p_{5L}
0.465	0.200	0.057	0.066	0.089
τ_{1L} (s)	τ_{2L} (s)	τ_{3L} (s)	τ_{4L} (s)	τ_{5L} (s)
0.6	6	30	60	300

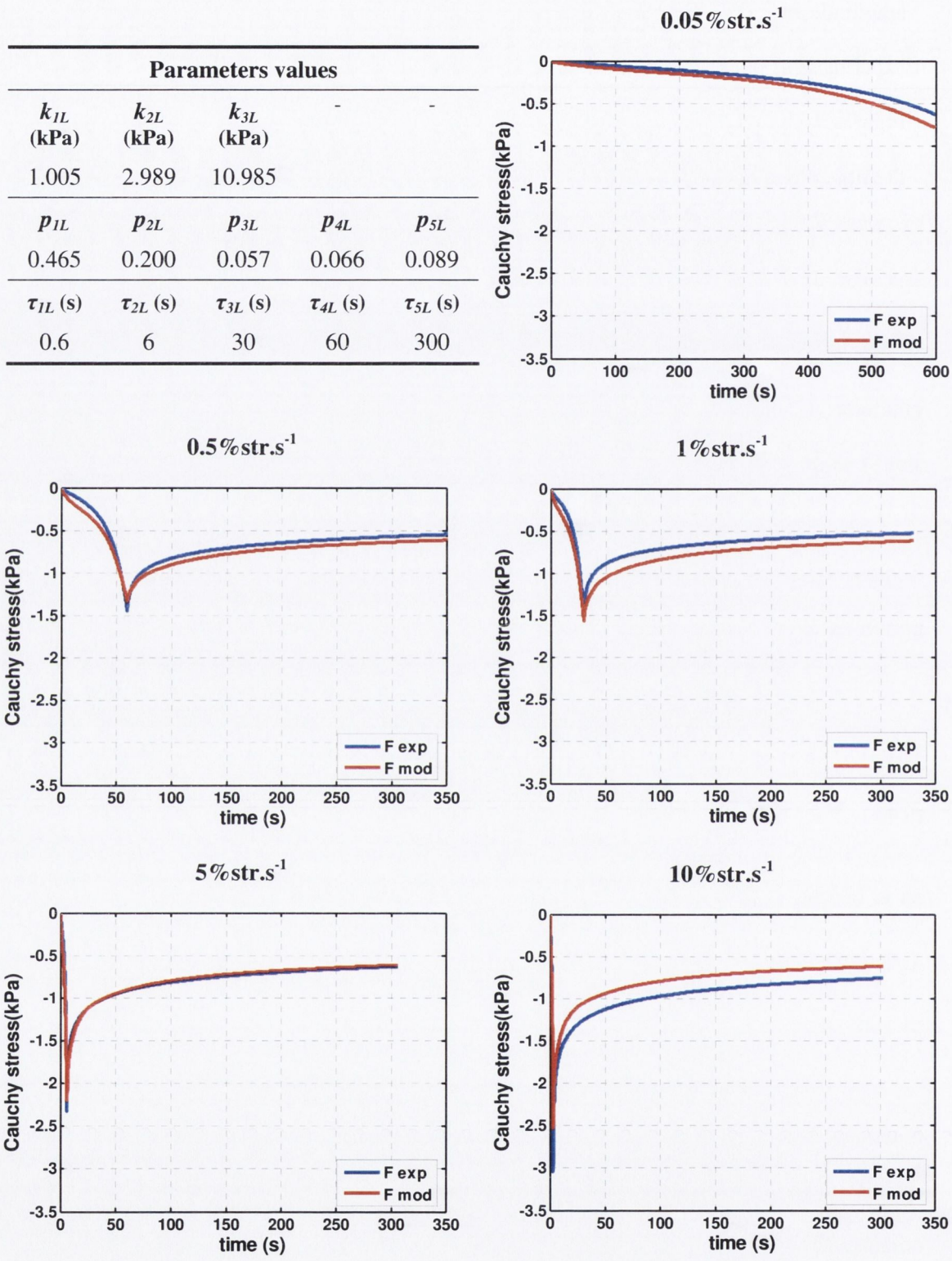


Figure 4-19: Comparison between experimental stress-relaxation results (—) and viscoelastic SYM model fitting (—) in fibre direction.

Simultaneous fitting to data at 0.5, 1 and 10%s^{-1}.

45° from the fibre direction

Parameters values				
k_{145} (kPa)	k_{245} (kPa)	k_{345} (kPa)	-	-
0.510	1.611	8.254		
p_{145}	p_{245}	p_{345}	p_{445}	p_{545}
0.419	0.200	0.057	0.072	0.088
τ_{145} (s)	τ_{245} (s)	τ_{345} (s)	τ_{445} (s)	τ_{545} (s)
0.6	6	30	60	300

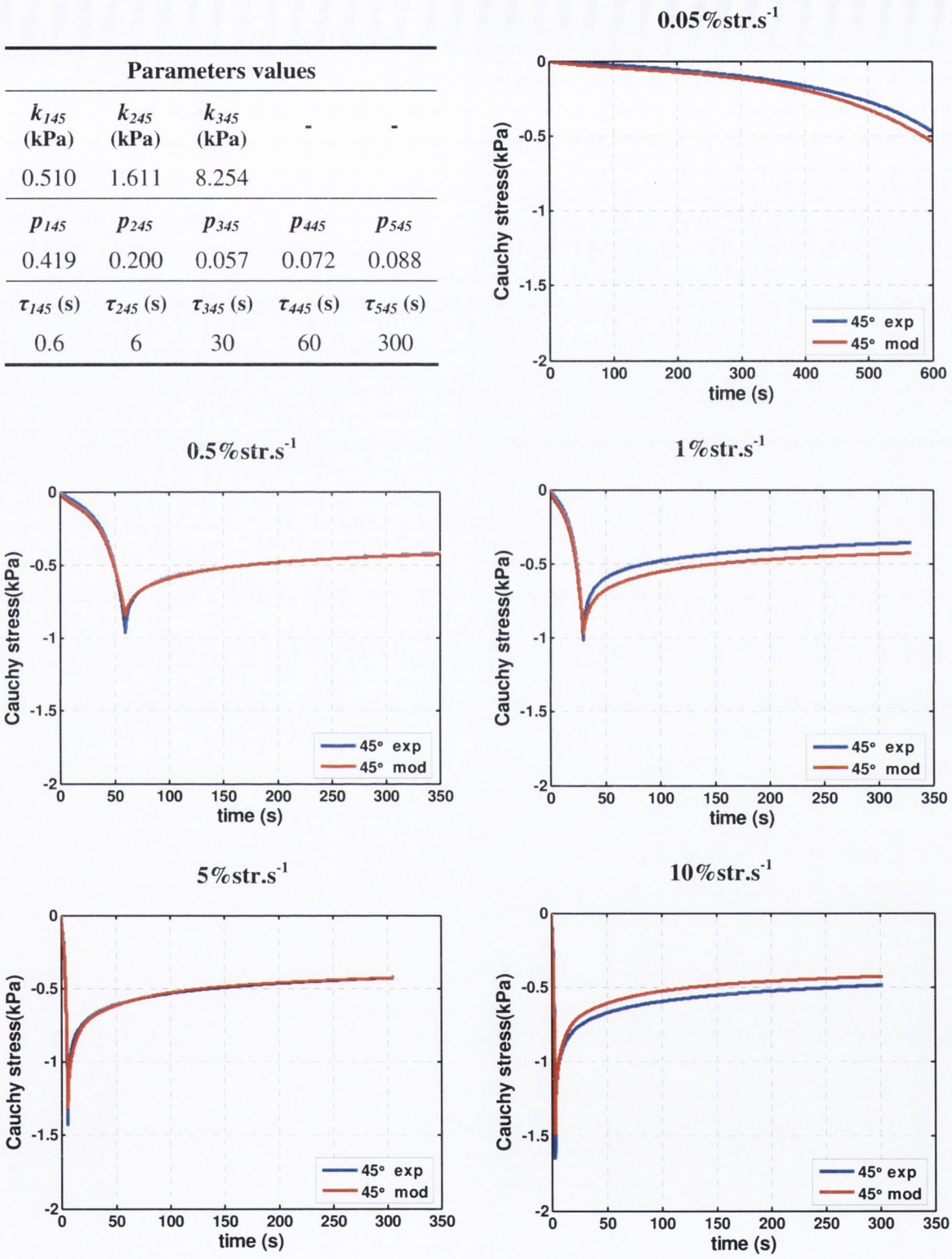


Figure 4-20: Comparison between experimental stress-relaxation results (—) and viscoelastic SYM model fitting (—) at 45° from the fibre direction

Simultaneous fitting to data at 0.5, 1 and 10%s^{-1}.

60° from the fibre direction

Parameters values				
k_{160} (kPa)	k_{260} (kPa)	k_{360} (kPa)	-	-
0.631	1.126	7.395		
p_{160}	p_{260}	p_{360}	p_{460}	p_{560}
0.409	0.181	0.103	0.0001	0.128
τ_{160} (s)	τ_{260} (s)	τ_{360} (s)	τ_{460} (s)	τ_{560} (s)
0.6	6	30	60	300

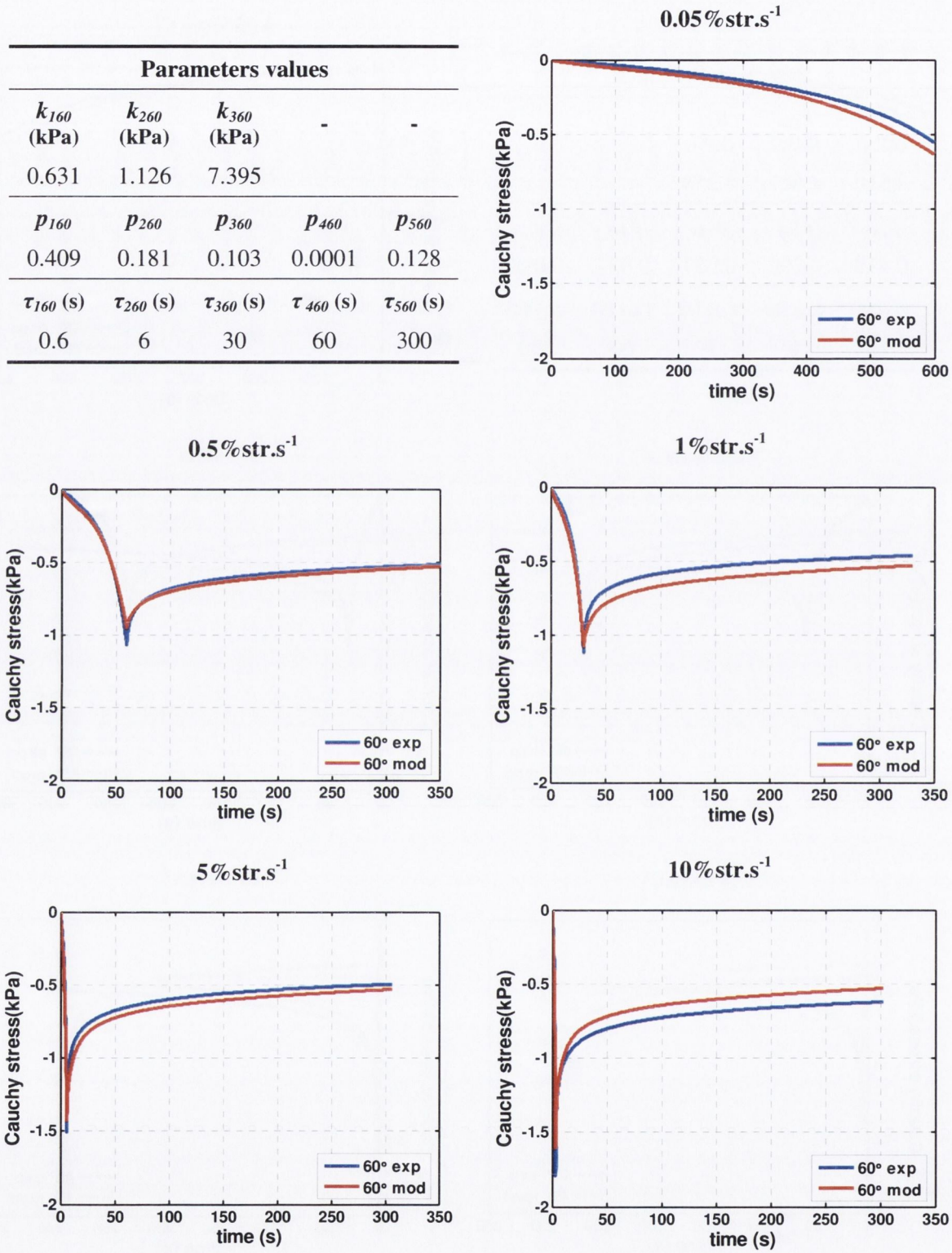


Figure 4-21: Comparison between experimental stress-relaxation results (—) and viscoelastic SYM model fitting (—) at 60° from the fibre direction.

Simultaneous fitting to data at 0.5, 1 and 10%s^{-1}.

Cross-fibre direction

Parameters values				
k_{1T} (kPa)	k_{2T} (kPa)	k_{3T} (kPa)	-	-
1.293	0.911	10.869		
p_{1T}	p_{2T}	p_{3T}	p_{4T}	p_{5T}
0.467	0.120	0.026	0.100	0.056
τ_{1T} (s)	τ_{2T} (s)	τ_{3T} (s)	τ_{4T} (s)	τ_{5T} (s)
0.6	6	30	60	300

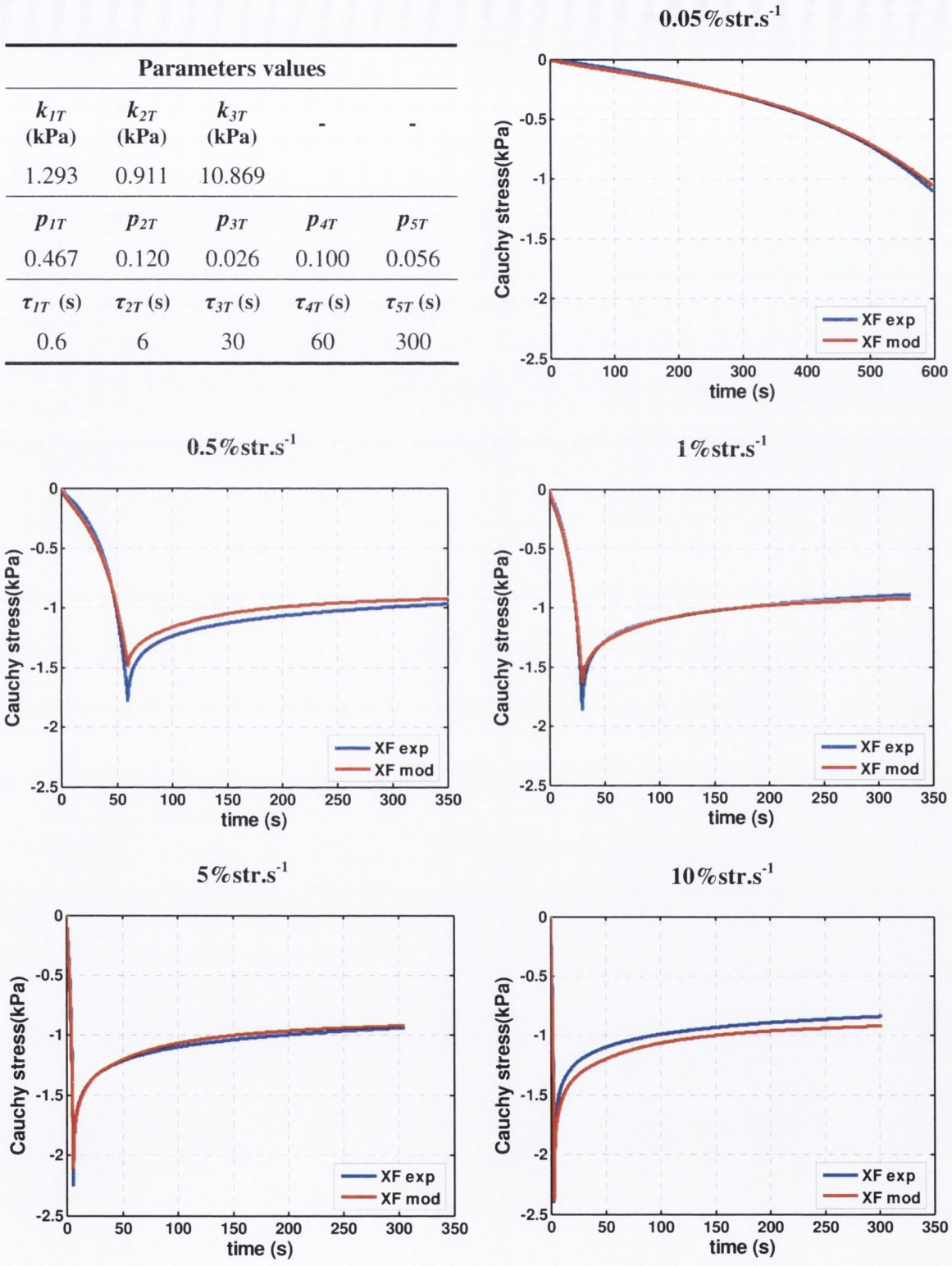


Figure 4-22: Comparison between experimental stress-relaxation results (—) and viscoelastic SYM model fitting (—) in cross-fibre direction.

Simultaneous fitting to data at 0.5, 1 and 10%s^{-1}.

Bearing in mind that variability is observed within experimental data, the model provides a good fit to data obtained at a compression rate of 0.5, 1 and 10%s^{-1} as well as a good prediction of muscle behaviour at 0.05 and 5%s^{-1}.

Figure 4-23 compares experimental and theoretical relaxed values of stress (measured after 300s relaxation). Minimum, maximum and median experimental values are presented; it illustrates the variability presents within experimental relaxed stresses. As mentioned earlier, the model relaxes to a unique value, independently of the compression rate; this value is situated in the middle of the range of relaxed stresses observed experimentally. This explains why differences appear between experimental and theoretical relaxed values of stress.

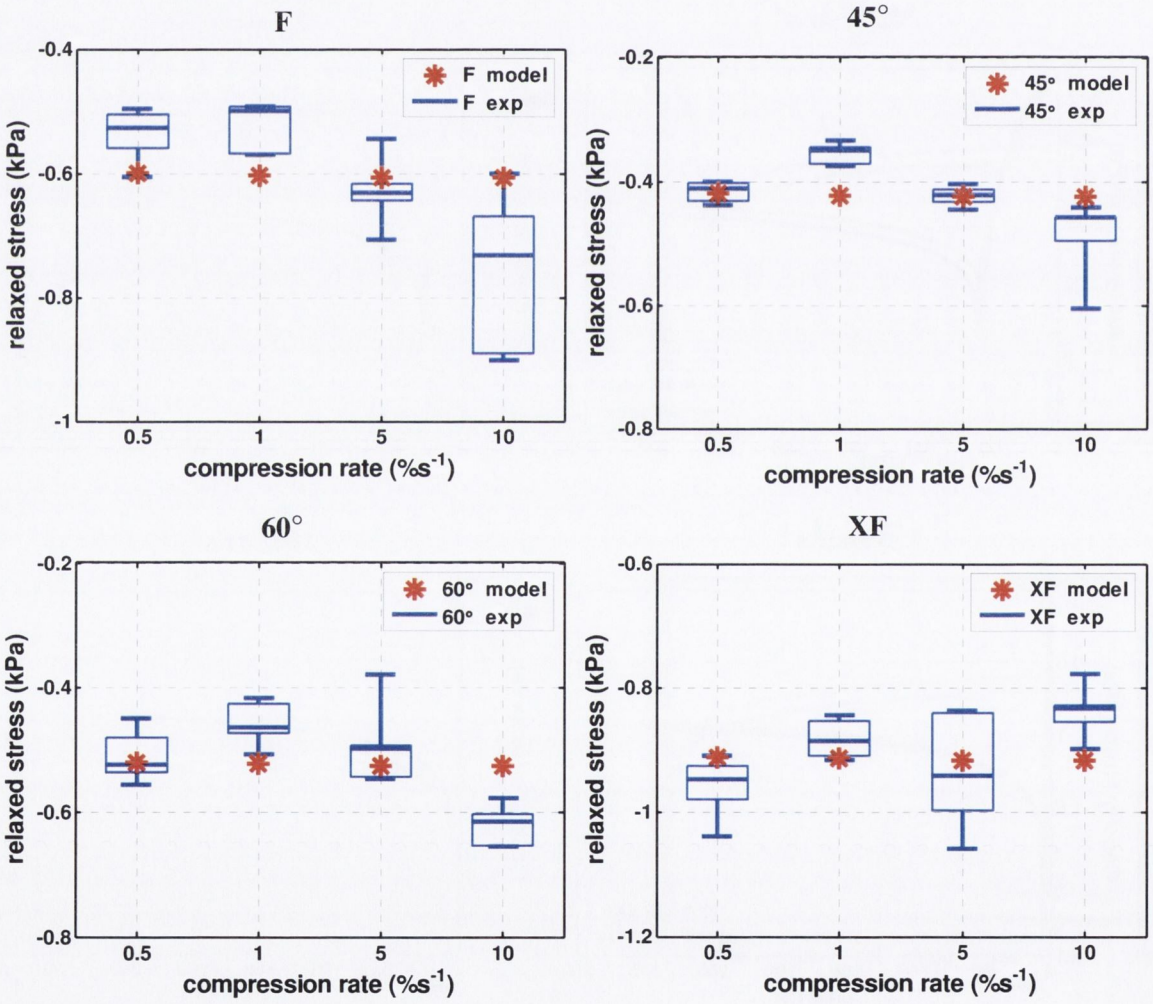


Figure 4-23: Comparison between experimental and theoretical relaxed stresses.

Box and whiskers correspond to experimental values; Stars represent theoretical values.

Figure 4-24 compares experimental and theoretical peak stresses. Experimental and theoretical values are in good agreement in most cases considered; where differences appear, the model generally under-predicts peak stresses limits. Percentage errors between experimental and theoretical relaxed stresses are presented in Figure 4-25 (a). It shows that the errors remain below 25% at all rates and fibre orientations considered. Percentage errors between experimental and theoretical peak stress are presented in Figure 4-25(b). Again, errors remain below 25% at all rates and fibre orientations considered.

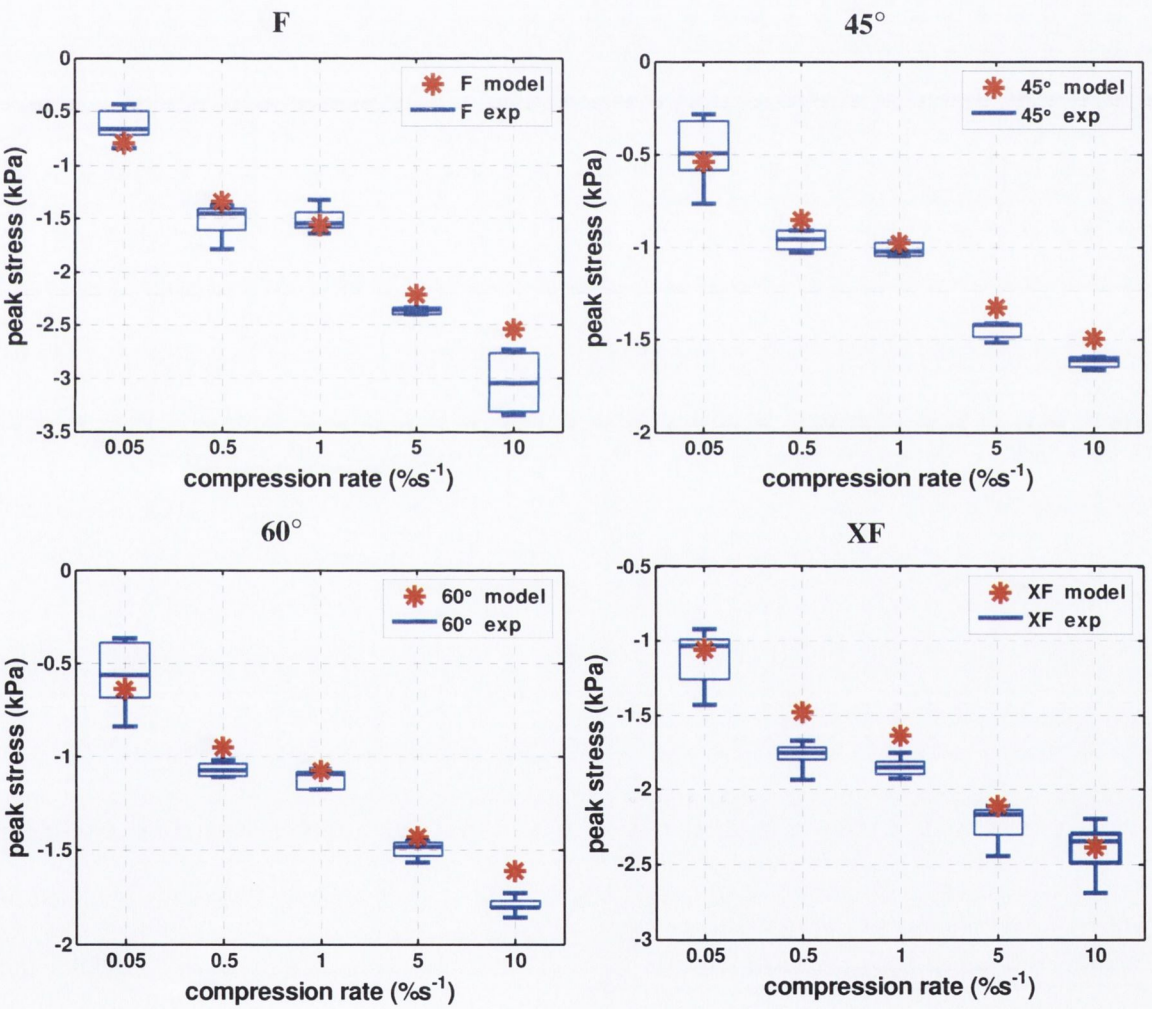


Figure 4-24: Comparison between experimental and theoretical peak stresses.

Box and whiskers correspond to experimental values; Stars represent theoretical values.

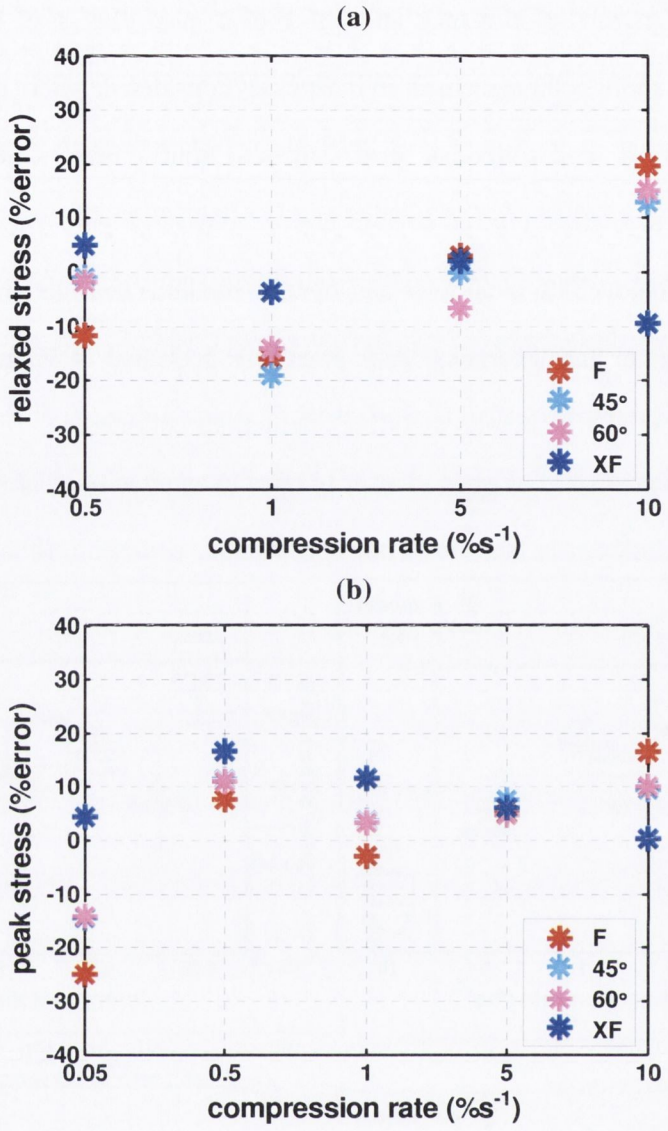


Figure 4-25: Percentage errors between experimental and theoretical (a) relaxed stresses, (b) peak stresses.

Finally, Figure 4-26 compares experimental and theoretical stress-relaxation behaviour for tests performed up to 10, 20 and 30% compression, at a rate of 1% s^{-1}. Results obtained in the fibre and cross-fibre directions are presented. Logarithmic scales are used to compare the rate of decay of stress with time.

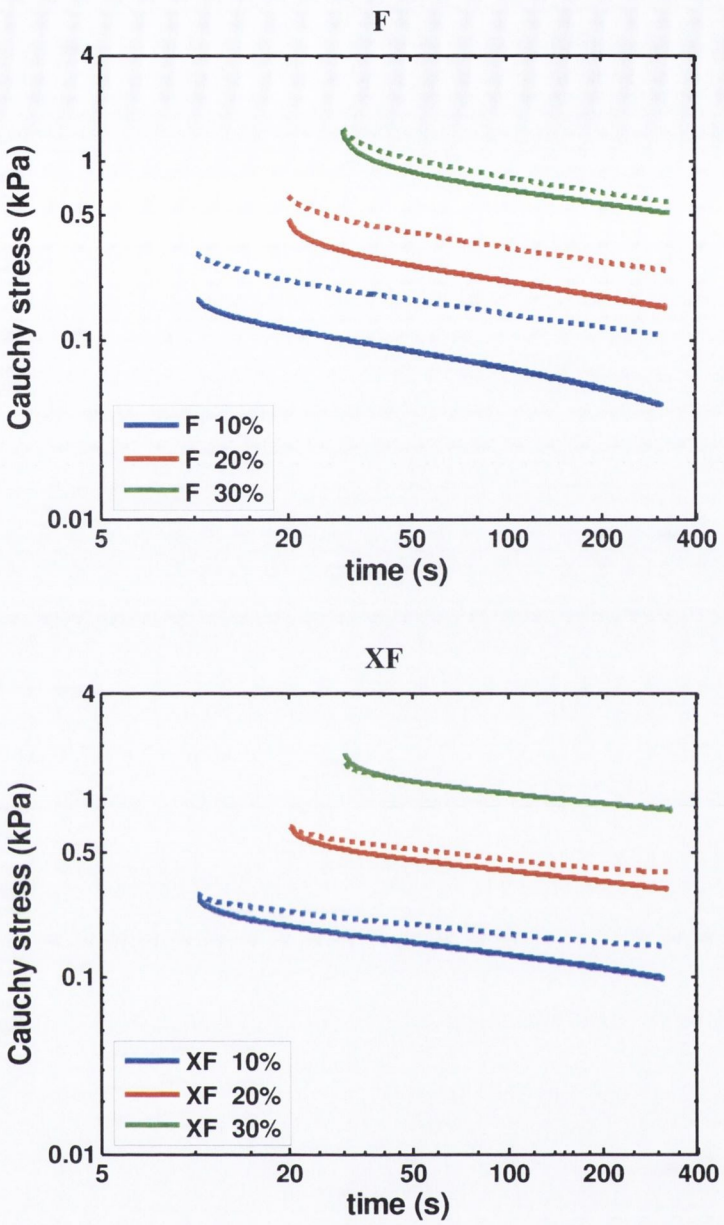


Figure 4-26: Comparison between experimental and theoretical stress-relaxation behaviour at 10, 20 and 30% compression.

Continuous curves represent experimental data; dashed curves represent theoretical data.

In the cross-fibre direction, good agreement is obtained between experimental and theoretical stress levels. Experimental results show a greater rate of decay at lower compression levels; this is however not captured by the model, in which relaxation behaviour is independent of deformation level. In the fibre direction, greater discrepancies are observed between experimental and theoretical stress values; this is due to the fact that

the globally fitted model slightly over predicts muscle behaviour at a rate of $1\%s^{-1}$ (see Figure 4-19).

4.3.2.2 Quasi-linear viscoelastic SYM model – Introduction of fibre dependency

In the previous section, individual fitting to relaxation data obtained at various orientations of the muscle fibres was performed. Identical values were adopted in all directions for the time constants τ_{ij}, characterising muscle relaxation behaviour. The multiplicative factors p_{ij} appeared however to be different in all directions; this is due to the anisotropy of the tissue observed in the experiments. Using a similar approach as for muscle elastic properties, it was hypothesised that muscle viscoelastic properties are transversely isotropic.

In the SYM formulation, five independent elastic constants have to be determined to fully characterise the material, i.e. two Young's moduli (E_L and E_T), two Poisson's ratio ($\nu_{TT'}$ and ν_{LT}) and one shear modulus (G_{LT}). (L again denotes the longitudinal direction, T and T' the two transverse directions).

E_L and E_T were determined by fitting to data obtained respectively in the fibre and in cross-the fibre directions.

The shear modulus G_{LT} was calculated using data obtained at 45° from the fibre direction and:

$$\frac{1}{G_{LT}} = 4\frac{\tilde{\varepsilon}_{45}}{\sigma_{45}} - \frac{1-2\nu_{LT}}{E_L} - \frac{1}{E_T} \tag{4-10}$$

with $\frac{\tilde{\varepsilon}_{45}}{\sigma_{45}} = E_{45}$.

Young's modulus at any angle from the fibre direction was then calculated using the following expression:

$$\frac{1}{E_\omega} = \frac{1}{E_L}\cos^4\omega + \left(\frac{1}{G_{LT}} - 2\frac{\nu_{LT}}{E_L}\right)\sin^2\omega\cos^2\omega + \frac{1}{E_T}\sin^4\omega \tag{4-11}$$

where ω represents the angle from the longitudinal direction.

Replacing the instantaneous elastic stress by the long term elastic stress in equation (4-5), the stress in direction j can be expressed as:

$$\sigma_j(t) = \sigma_{\infty j}(t) + \sum_{i=1}^{N} \int_0^t \frac{p_{ij}}{p_{\infty j}} \exp\left(\frac{-(t-\tau)}{\tau_{ij}}\right) \frac{\partial \sigma_{\infty j}[\tilde{\varepsilon}_j(\tau)]}{\partial \tilde{\varepsilon}_j(\tau)} \frac{\partial \tilde{\varepsilon}_j(\tau)}{\partial \tau} d\tau \tag{4-12}$$

or

$$\sigma_j(t) = E_j \tilde{\varepsilon}_j(t) + \int_0^t E_j^v \frac{\partial \tilde{\varepsilon}_j(\tau)}{\partial \tau} d\tau \tag{4-13}$$

where $E_j = k_{1j} + k_{2j}\tilde{\varepsilon}_j + k_{3j}\tilde{\varepsilon}_j^2$, represents the elastic Young's modulus in direction j and $E_j^v = \sum_{i=1}^{5} \frac{p_{ij}}{p_{\infty j}} \exp\left(\frac{-(t-\tau)}{\tau_{ij}}\right) \frac{\partial \sigma_{\infty j}[\tilde{\varepsilon}_j(\tau)]}{\partial \tilde{\varepsilon}_j(\tau)}$, is the viscoelastic Young's modulus in direction j.

E_L^v and E_T^v were determined by fitting to stress-relaxation data obtained respectively in the fibre and in the cross-fibre directions.

The shear modulus G_{LT}^v was calculated using data obtained at 45° from the fibre direction and:

$$\frac{1}{G_{LT}^v} = \frac{4}{E_{45}^v} - \frac{1-2\nu_{LT}}{E_L^v} - \frac{1}{E_T^v} \tag{4-14}$$

An expression similar to equation (4-11) was then used to calculate the viscoelastic Young's modulus at any angle ω from the fibre direction:

$$\frac{1}{E_\omega^v} = \frac{1}{E_L^v}\cos^4\omega + \left(\frac{1}{G_{LT}^v} - 2\frac{\nu_{LT}}{E_L^v}\right)\sin^2\omega\cos^2\omega + \frac{1}{E_T^v}\sin^4\omega \tag{4-15}$$

Comparison between experimental results and theoretical values calculated with $\omega = 60°$ are presented in Figure 4-27.

60° from the fibre direction – model predictions

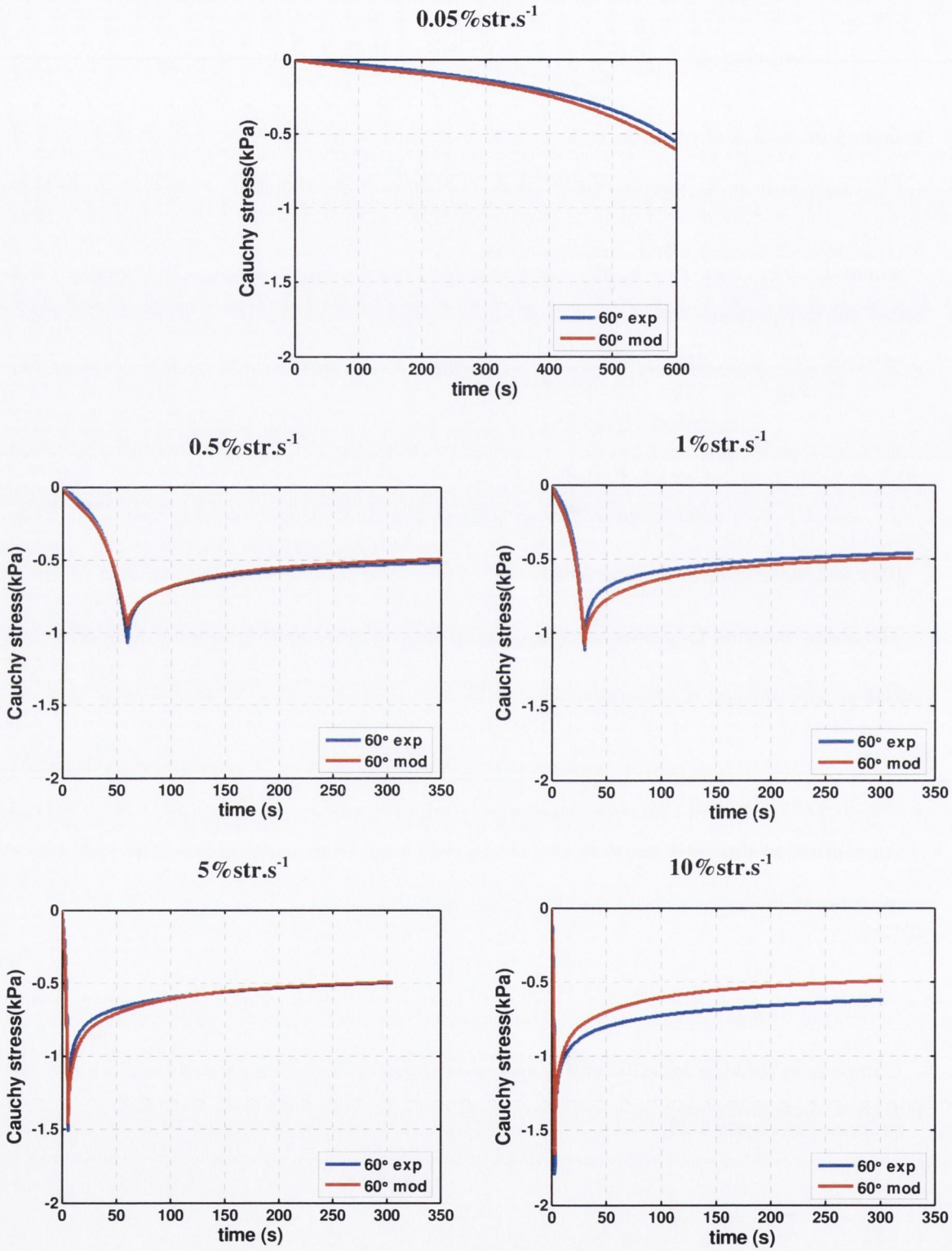


Figure 4-27: Comparison between experimental stress-relaxation results (—) and viscoelastic SYM model predictions (—) at 60° from the fibre direction.

Figure 4-28 compares experimental and theoretical peak and relaxed stresses; percentage errors are presented in Figure 4-29. Results show that model predictions are in good agreement with experimental stress-relaxation data obtained at 60° from the fibre direction; errors between experimental and theoretical peak and relaxed stresses remain below 25% at all rates considered. These results indicate that anisotropy observed in muscle viscoelastic behaviour can be captured by the transversely isotropic viscoelastic model developed.

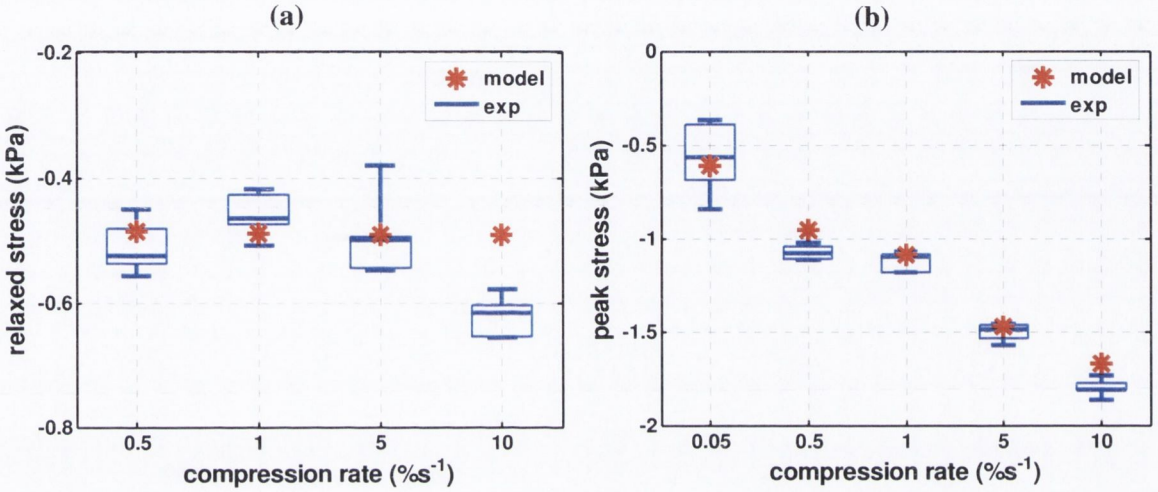


Figure 4-28: Comparison between experimental and theoretical (a) relaxed stresses, (b) peak stresses.

Box and whiskers correspond to experimental values; Stars represent theoretical values.

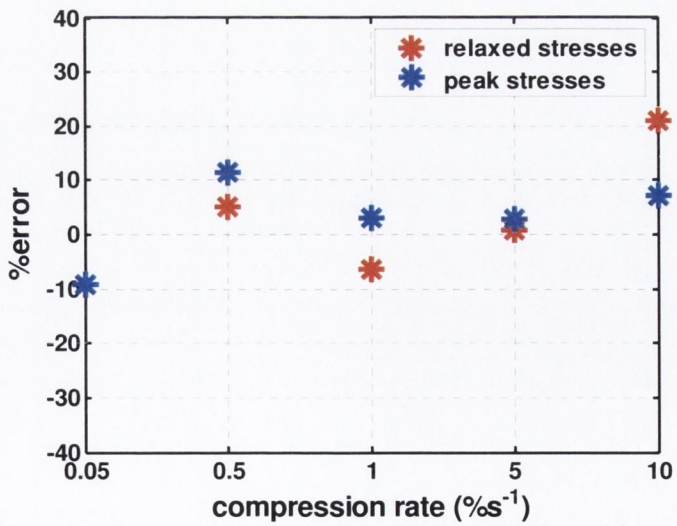


Figure 4-29: Percentage errors between experimental and theoretical relaxed and peak stresses.

4.4 Cyclic tests

4.4.1 Experimental results

In this section, results from cyclic compression tests performed at various amplitudes and frequencies are presented. These tests were conducted to investigate muscle history-dependent behaviour (evolution of hysteresis with frequency). They also provide information on muscle tissue at higher strain rates than the ramp and hold tests performed. Finally, results from the cyclic tests were used to investigate the predictive capabilities of the QLV model, using the parameters derived from relaxation tests (section 4.3.2.1).

Low frequency tests (sections 4.4.1.1 and 4.4.1.2) were performed on the Zwick machine (Z005). Due to small variations in the deformation histories delivered by the machine, mean curves could not be calculated; the results presented correspond to typical curves taken in the range of data observed experimentally. These variations affected the repeatability but not the accuracy of the measurements. Complete date sets are provided in Appendix E. For high frequency tests, performed on the custom made dynamic rig, mean curves were calculated and are presented in section 4.4.1.3.

4.4.1.1 Low amplitude, low frequency tests

Figures 4-30 and 4-31 present results of low amplitude cyclic tests performed on fresh porcine muscle samples in the fibre and cross-fibre directions. In a first series of tests, samples were cyclically compressed between 24 and 26% of their original length at a frequency of 0.22Hz (graphs (a) and (c)). In a second series of tests, samples were cyclically compressed between 18 and 20% of their original length at a frequency of 0.4Hz (graphs (c) and (d)). The frequencies of 0.22 and 0.4Hz respectively correspond to compression rates of $1\%s^{-1}$ and $2\%s^{-1}$ as explained in the methods section of this chapter (section 4.2.2).

Figure 4-30 (a) and (b) present the deformation history applied to the samples during the tests. Figure 4-30 (b) and (d) present stress-time curves; they illustrate the cyclic stress-

relaxation of the tissue; i.e. peak and valley stresses decrease with an increasing number of cycles. Qualitatively, fibre and cross-fibre results are similar with the cross-fibre direction being stiffer than the fibre direction.

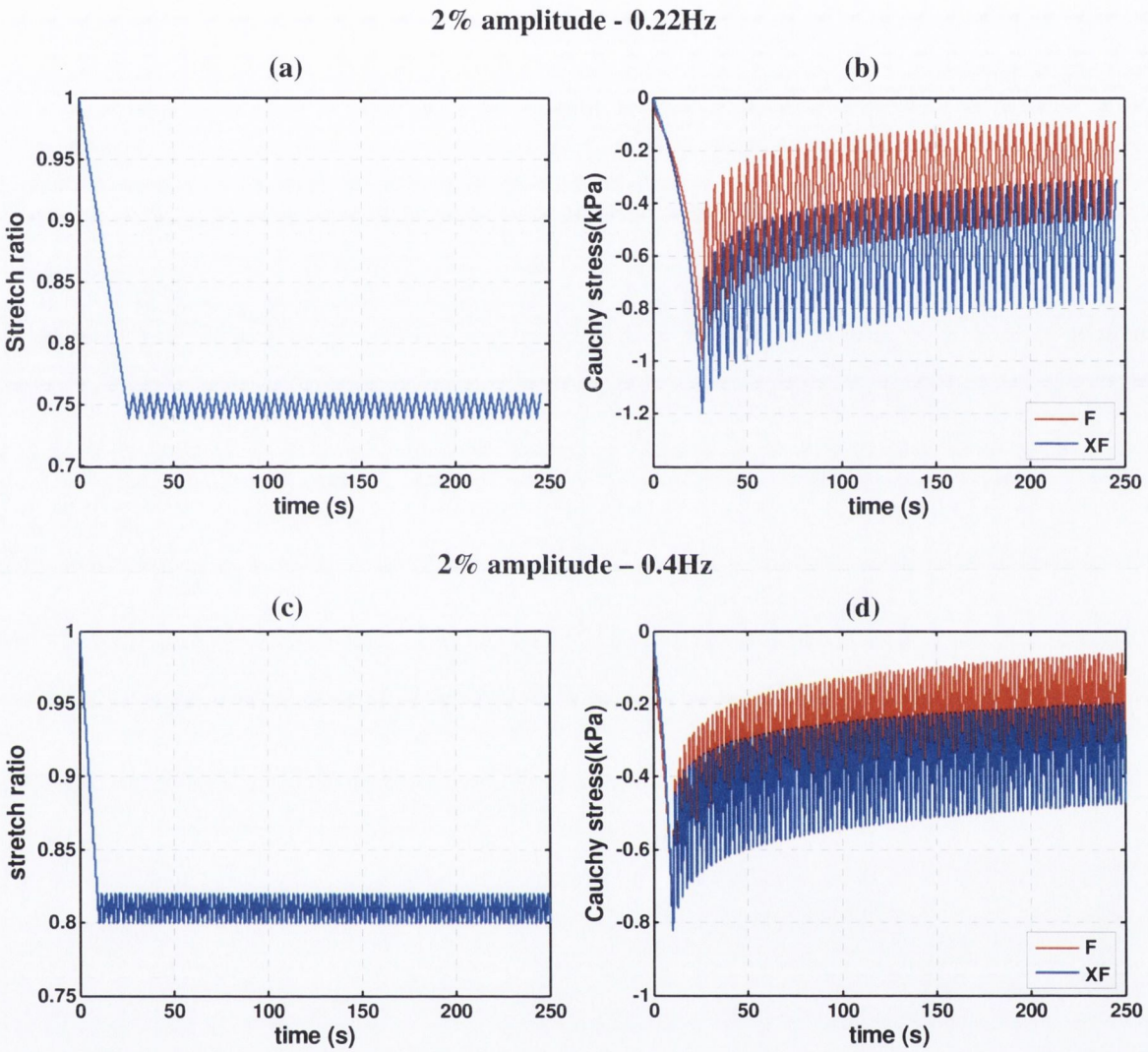


Figure 4-30: (a) and (c) Deformation history applied to porcine samples during low amplitude cyclic compression tests performed respectively at 0.22 and 0.4Hz. (b) and (d) Corresponding cyclic stress-relaxation curves obtained in fibre and cross-fibre directions.

Figure 4-31 present stress-stretch curves obtained in the cross-fibre direction. The complete deformation history is represented in graphs (a) and (c); the first two and last twenty cycles are represented in graphs (b) and (d). It illustrates the history dependence of the tissue (hysteresis), i.e. the loading and unloading curves follow different paths from one cycle to

another. The area enclosed by the loop represents the mechanical energy absorbed during the deformation cycle. The size of the hysteresis loop decreases when the number of cycles increases; during the last twenty cycles hysteresis is constant and relaxation is almost completed.

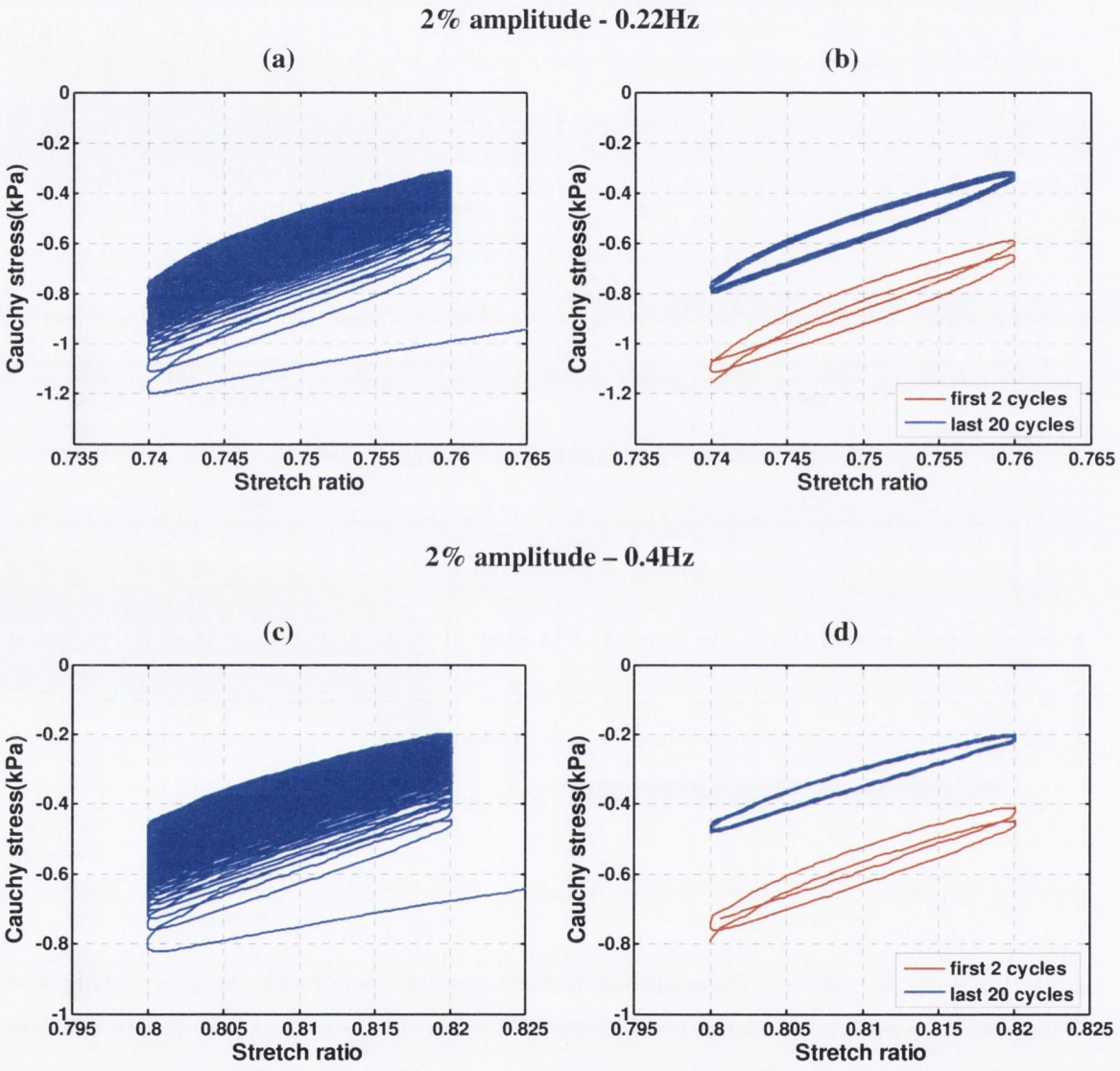


Figure 4-31: (a) and (c) Stress-stretch curves obtained during low amplitude cyclic compression tests of porcine muscle samples performed respectively at 0.22 and 0.4Hz (cross-fibre results). (b) and (d) Corresponding plots of the first two and last twenty cycles.

The hysteresis ratio for a typical loading–unloading cycle is defined as:

$$h_r = 100\frac{(A_l - A_u)}{A_l} \tag{4-16}$$

where A_l is the area below the load/deformation curve during tissue loading, and A_u is the area below the load/deformation curve during unloading (Holzapfel *et al.*, 2004). This is graphically illustrated in Figure 4-32. h_r represents the ratio of the energy dissipated to the energy required to deform the tissue during a cycle.

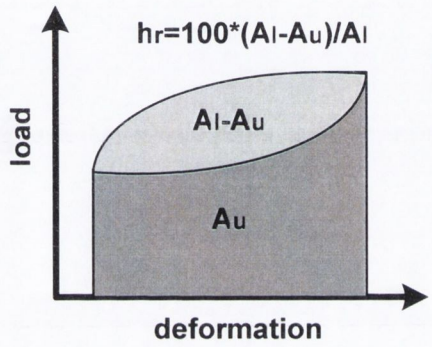


Figure 4-32: Definition of the hysteresis ratio h_r. A_l and A_u represent respectively the loading and unloading areas.

Table 4-7 presents values of hysteresis ratio and stress cycle amplitude calculated at the end of the test. The areas A_l and A_u were calculated using numerical integration. Results show that in the fibre direction approximately 18% of the loading energy is dissipated during each cycle; only 13% is dissipated in the cross-fibre direction. Values are similar for both frequencies considered. The amplitude of the cycles imposed to the samples was the same for both frequencies (2% of their original length); however, the mean compression level was of 25% for the 0.22Hz tests and of 19% for the 0.4Hz tests. Higher stress cycle amplitudes are observed for the 0.22Hz tests (column 4 of Table 4-7); this illustrates again the dependency of muscle behaviour on the compression level.

Table 4-7: Hysteresis ratio (h_r) and stress cycle amplitude calculated after 240s for low amplitude, low frequency tests.

Frequency	Test direction	Hysteresis (%)	Amp ± SD (kPa)
0.22Hz	**F**	17.14 ± 1.01	0.38 ± 0.04
	XF	13.67 ± 0.73	0.48 ± 0.02
0.4Hz	**F**	18.59 ± 2.68	0.30 ± 0.03
	XF	12.83 ± 1.99	0.29 ± 0.01

4.4.1.2 High amplitude, low frequency tests

This section presents results from higher amplitude cyclic tests performed on fresh porcine muscle samples at various orientations of the muscle fibres. In these tests, samples were cyclically compressed between 20 and 30% of their original length at frequencies of 0.22Hz (Figure 4-33) and 0.44Hz (Figure 4-34). These frequencies correspond respectively to compression rates of 5 and $10\%s^{-1}$. 0.22Hz tests were performed only in the fibre and cross-fibre directions; 0.44Hz tests were also performed at 45° and 60° from the fibre direction. In both figures, graph (a) presents the deformation history applied to the samples; the following graphs present stress-time curves obtained in the various orientations considered.

Again, cyclic stress-relaxation of the tissue is observed. Peak stresses decrease gradually with an increasing number of cycles; valley stresses however appear to be completely relaxed over a small number of cycles. It can also be observed that, within each cycle, the amplitude of the cycle is sufficient to bring the stress back to a value close to zero, even though samples are still submitted to a compression level of 20%.

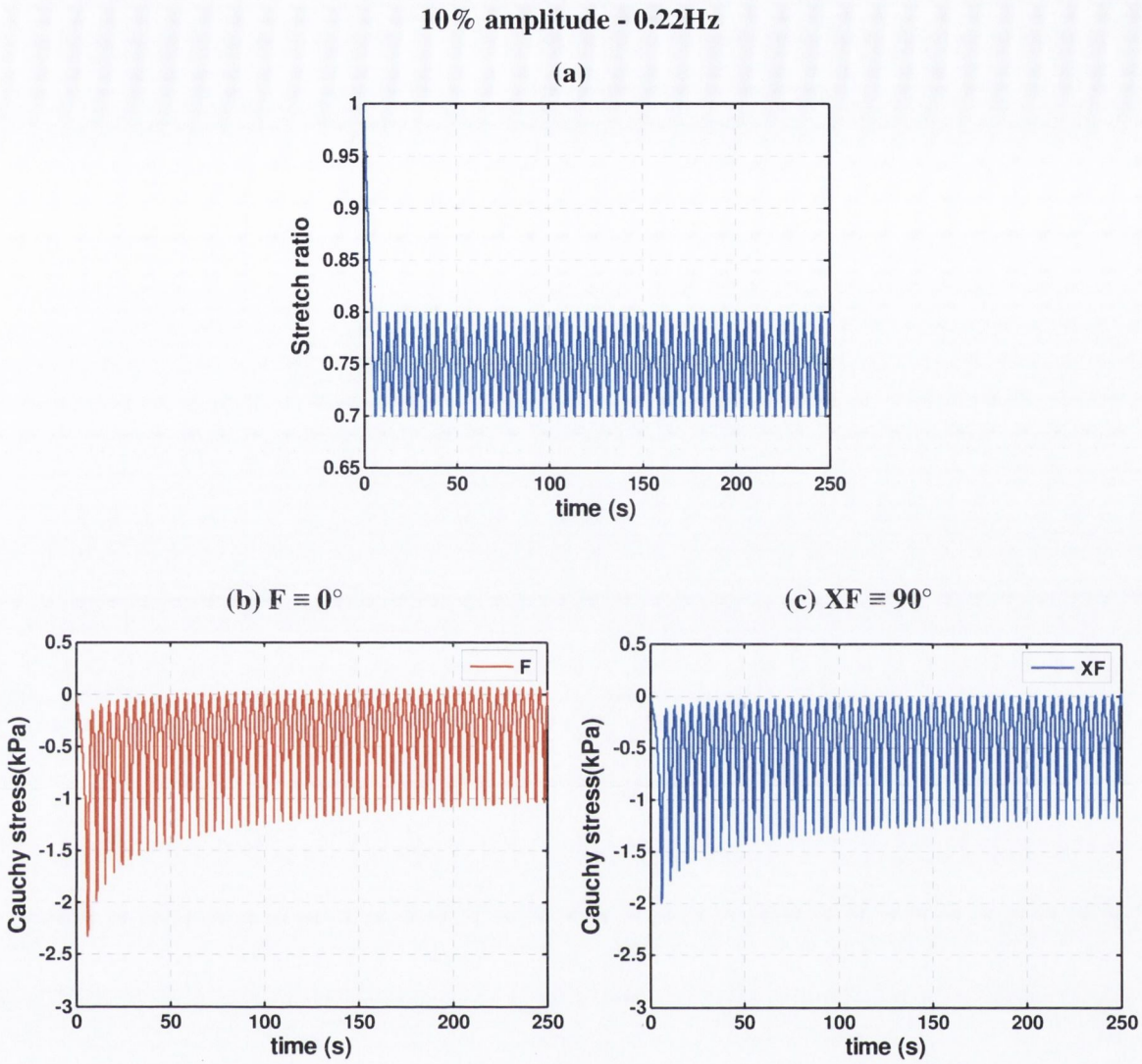


Figure 4-33: (a) Deformation history applied to fresh porcine samples during high amplitude cyclic compression tests performed at 0.22 Hz. (b) and (c) Corresponding cyclic stress-relaxation curves obtained in fibre and cross-fibre directions.

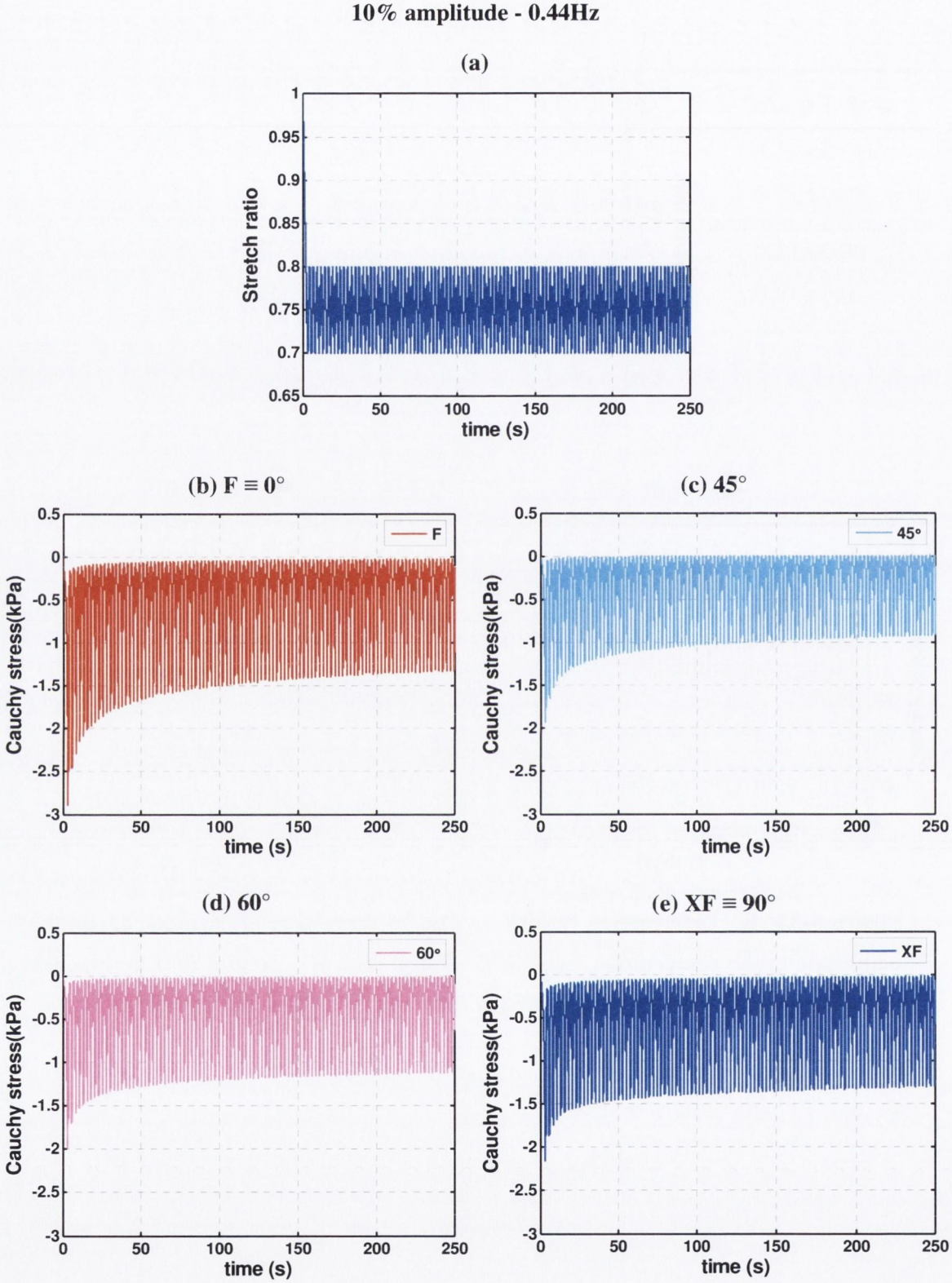


Figure 4-34: (a) Deformation history applied to fresh porcine samples during high amplitude cyclic compression tests performed at 0.44 Hz. (b) to (e) Corresponding cyclic stress-relaxation curves obtained in fibre and cross-fibre directions.

Figure 4-35 presents a close-up view of stress-time curves obtained at 0.44Hz at the beginning (compression ramp and first few cycles) and at the end of the tests. It shows that after the compressive ramp performed at a rate of $10\%s^{-1}$, the fibre direction is the stiffest of all directions, then followed by the cross-fibre results; 45° and 60° results appear to be almost identical. After cyclic relaxation however, the fibre and cross-fibre results become nearly identical and the 45° direction is now the least stiff; therefore a greater amount of stress-relaxation has occurred in the fibre and the 45° directions. This can also be qualitatively observed comparing Figure 4-34 (b) to (e). It confirms results obtained during static stress-relaxation experiments; the viscoelastic component has a greater influence in directions closer to the muscle fibres.

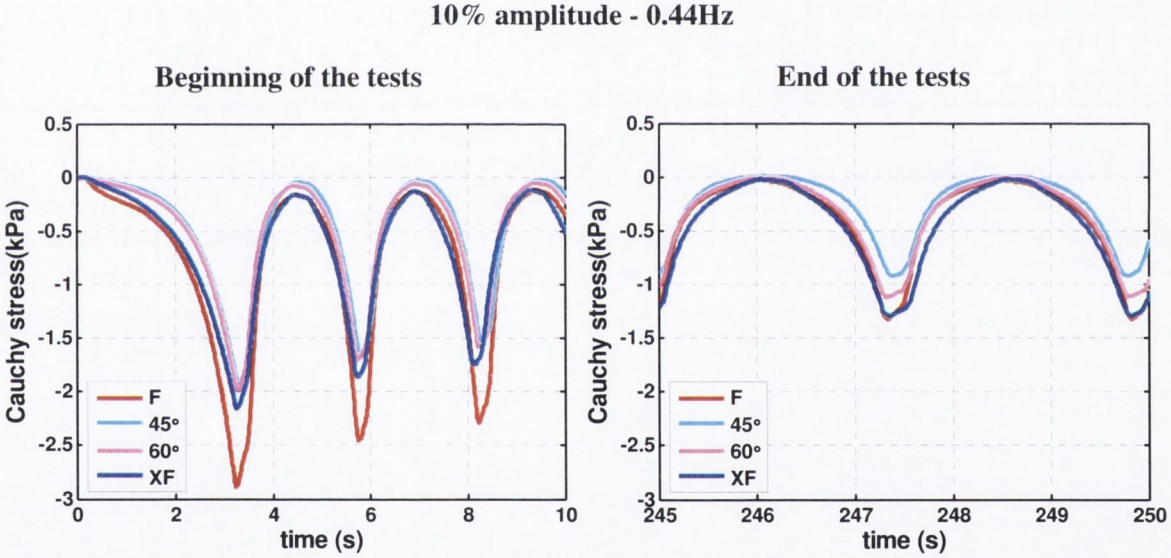


Figure 4-35: Close-up comparing stress-time curves at various orientations of the muscle fibres for high amplitude, low frequency cyclic tests.

Figure 4-36 presents stress-stretch ratio curves obtained in the cross-fibre direction for both frequencies considered. The complete deformation history is represented in graphs (a) and (c); the first two and last twenty cycles are represented in graph (b) and (d). As during low amplitude tests, the size of the hysteresis loop decreases when the number of cycles increases; during the last twenty cycles hysteresis remains constant.

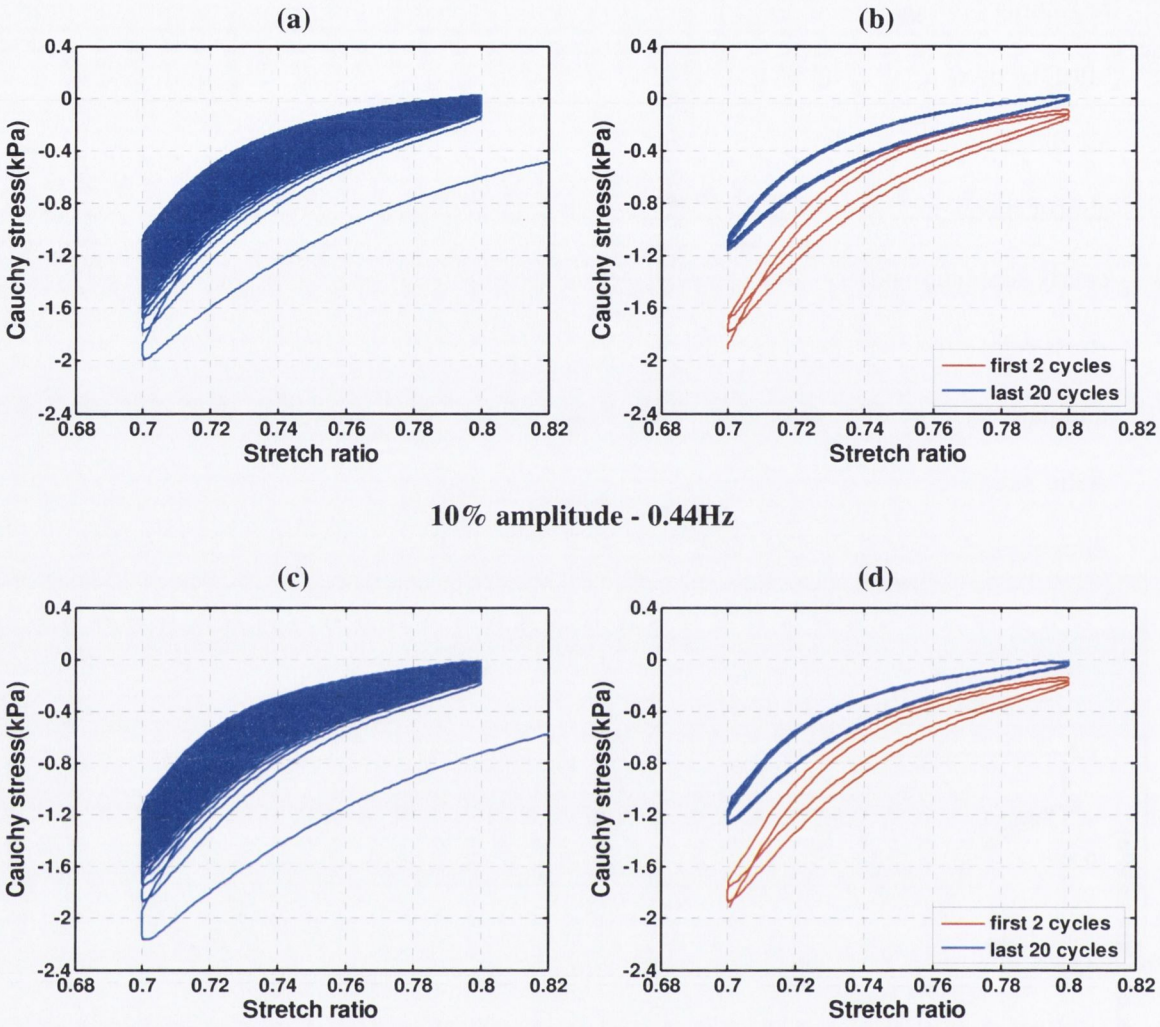


Figure 4-36: (a) and (c) Stress-stretch curves obtained during high amplitude cyclic compression tests of porcine muscle samples performed respectively at 0.22 and 0.44 Hz (cross-fibre results). (b) and (d) Corresponding plots of the first two and last twenty cycles.

Table 4-8 presents values of hysteresis ratio and stress cycle amplitude calculated at the end of the test. Results show that in the fibre and 45° directions approximately 34% of the loading energy is dissipated during each cycle; approximately 38% is dissipated in the cross-fibre and 60° directions. A one-way analysis of variance showed however that the differences observed have no statistical significance. No differences are observed between both frequencies considered for the hysteresis; the amplitude of the stress cycles is slightly higher at 0.44 than at 0.22Hz.

Table 4-8: Hysteresis ratio (h_r) and cycles amplitude calculated after 240s for high amplitude, low frequency tests.

Frequency	Test direction	Hysteresis (%)	Amp ± SD (kPa)
0.22Hz	F	34.48 ± 1.42	1.15 ± 0.08
	45°	-	-
	60°	-	-
	XF	37.89 ± 6.14	1.19 ± 0.01
0.44Hz	F	34.76 ± 6.65	1.28 ± 0.21
	45°	34.69 ± 3.15	0.87 ± 0.19
	60°	39.37 ± 3.26	1.00 ± 0.07
	XF	38.05 ± 7.25	1.29 ± 0.09

Tests with various cycle amplitudes were performed to further investigate the observations showing that the stress reaches a value close to zero during unloading and that only a few cycles are sufficient to achieve relaxation. In these tests, samples were compressed up to 30% of their original length and cycles of 2, 10, 20 and 30% amplitude were performed. The deformation applied to the samples is presented in Figure 4-37 (a). Figure 4-37 (b) compares the corresponding stress-time curves obtained. Only 10s of the total test duration are presented to better visualise the results; results from 2 and 20% amplitude tests are presented in Figure 4-37 (c) and (d) for the complete test duration. Figure 4-37 (b) shows that cycles with 10% amplitude are sufficient to bring the stress back to almost zero even though samples are still under 20% compression; positive (tensile) stresses are observed when cycles of 20 and 30% amplitude are performed.

In 2% amplitude tests, relaxation behaviour is similar for loading and unloading; in tests with higher amplitudes, the unloading stress relaxes less and faster than the loading stress.

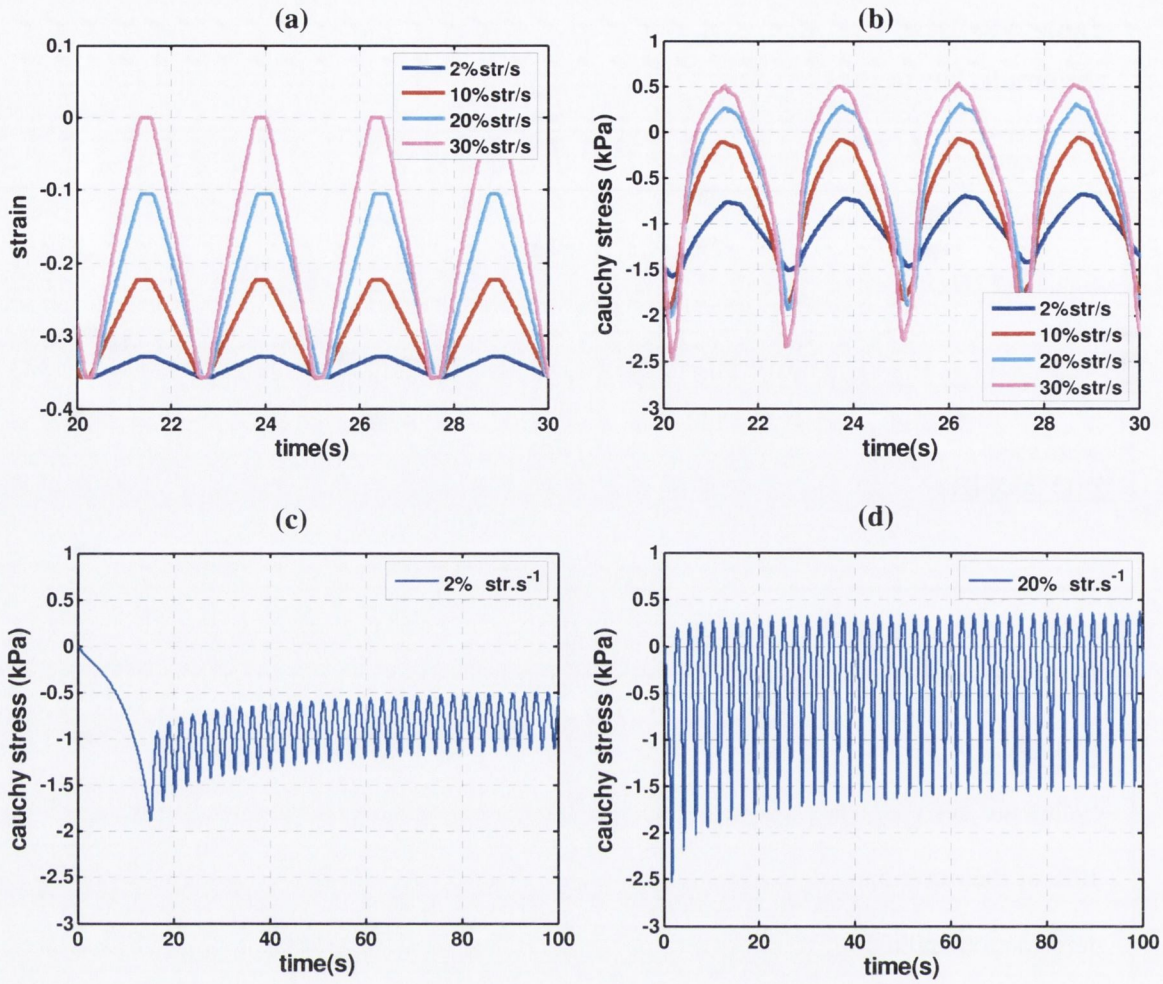


Figure 4-37: Comparison between cyclic relaxation tests with 2, 10, 20 and 30% amplitude.

(a) Deformation history applied to the samples (only 10s represented); (b) Corresponding stress-time curves; (c) and (d) Stress-time curve obtained for cycles of 2 and 20% amplitude (complete test duration represented).

4.4.1.3 High amplitude, high frequency tests

Figures 4-38 to 4-40 present results from high amplitude cyclic tests performed at frequencies of 5, 20 and 80Hz on porcine muscle samples oriented at 0°, 45°, 60° and 90° from the fibre direction. These tests were conducted on the custom made dynamic rig (Figure 4-3). As in high amplitude, low frequency tests (previous section), samples were cyclically compressed between 20% and 30% of their original length; the deformation was however applied in these tests using sine waves and not saw tooth waves due to technical constraints. The frequencies used correspond approximately to compression rates of 200%s^{-1} at 5Hz, 800%s^{-1} at 20Hz and 3200%s^{-1} at 80Hz.

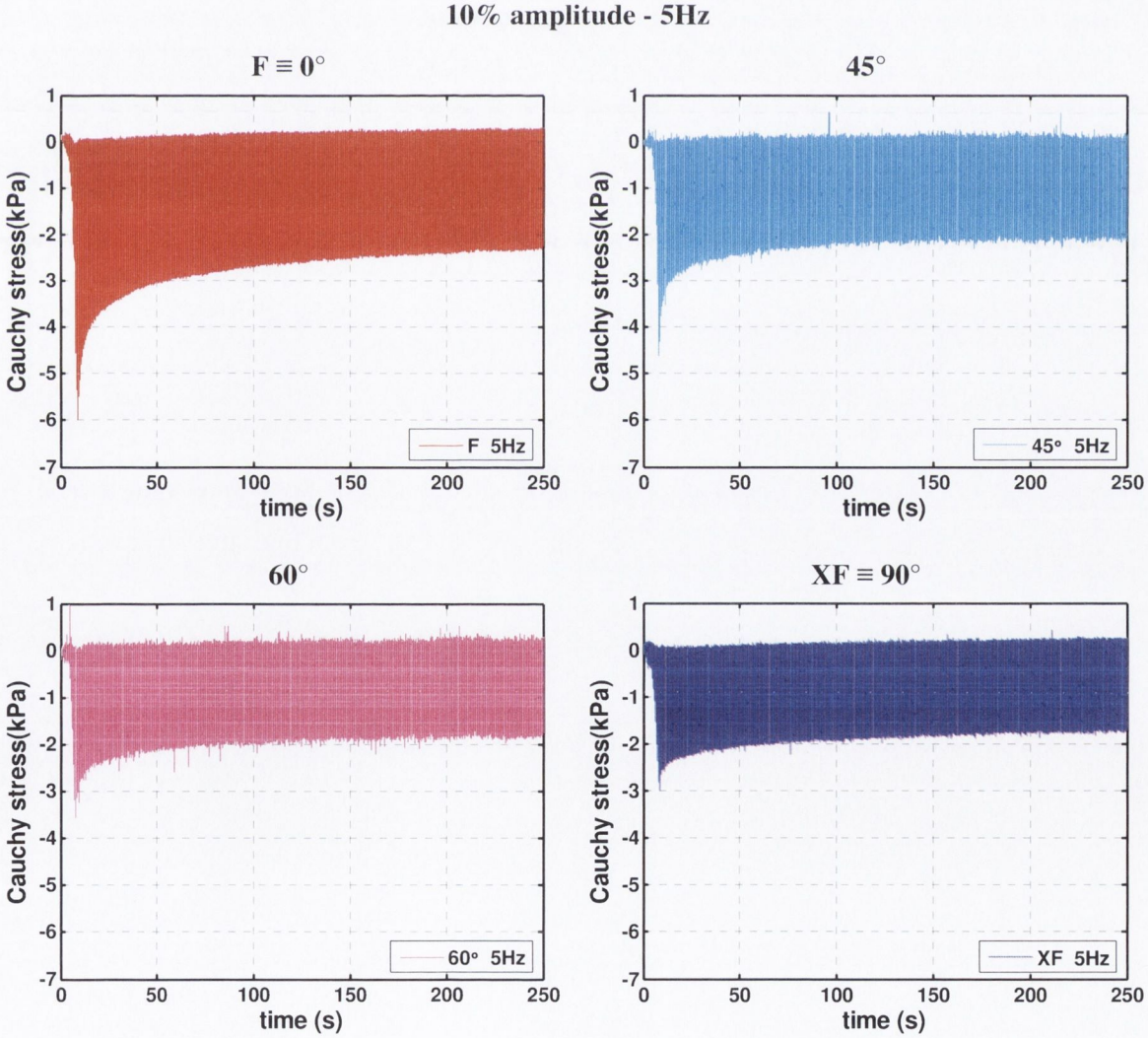


Figure 4-38: Cyclic stress-relaxation curves obtained during high amplitude cyclic compression tests performed at 5Hz, at 0°, 45°, 60° and 90° from the fibre direction.

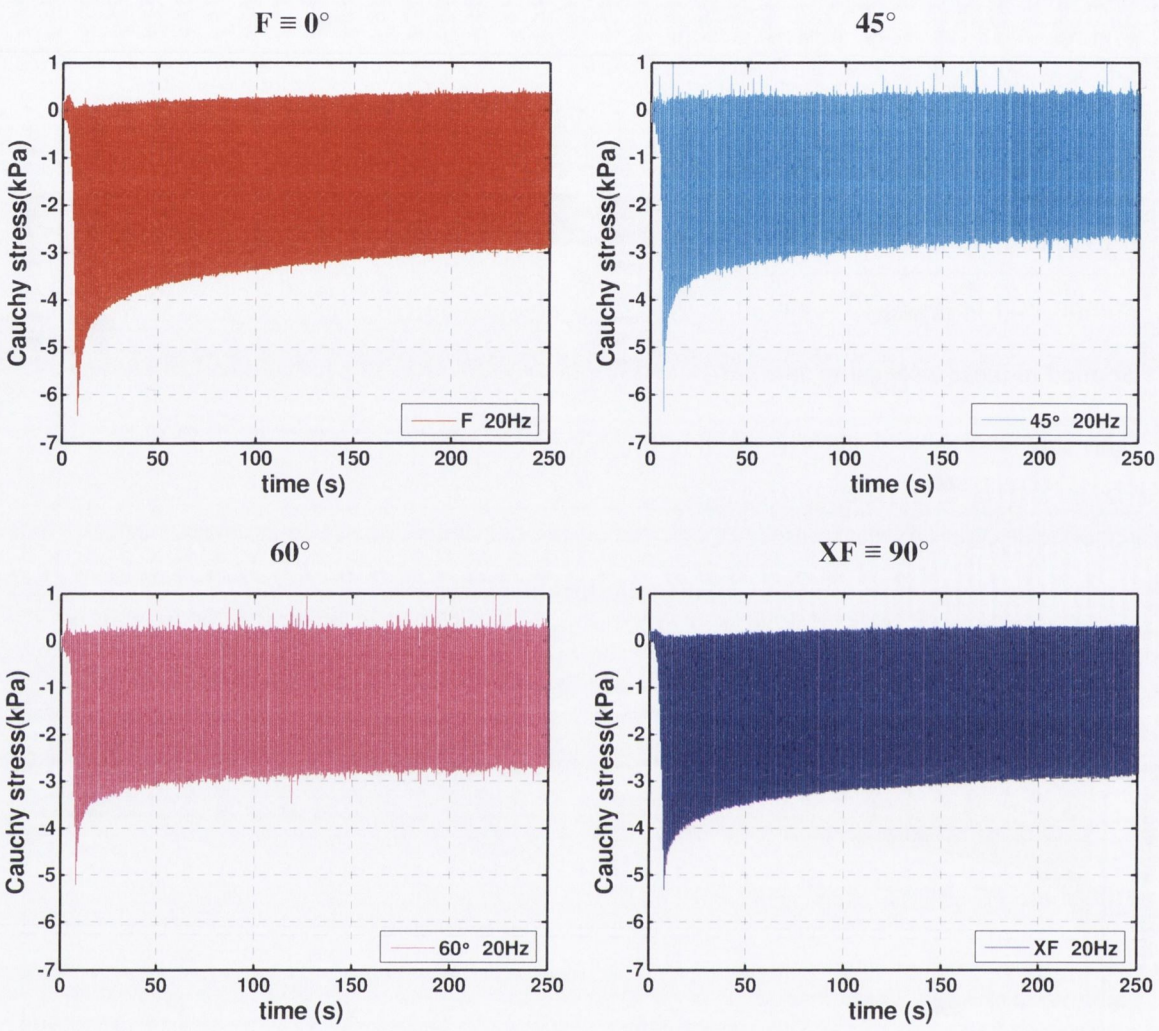


Figure 4-39: Cyclic stress-relaxation curves obtained during high amplitude cyclic compression tests performed at 20Hz, at 0°, 45°, 60° and 90° from the fibre direction.

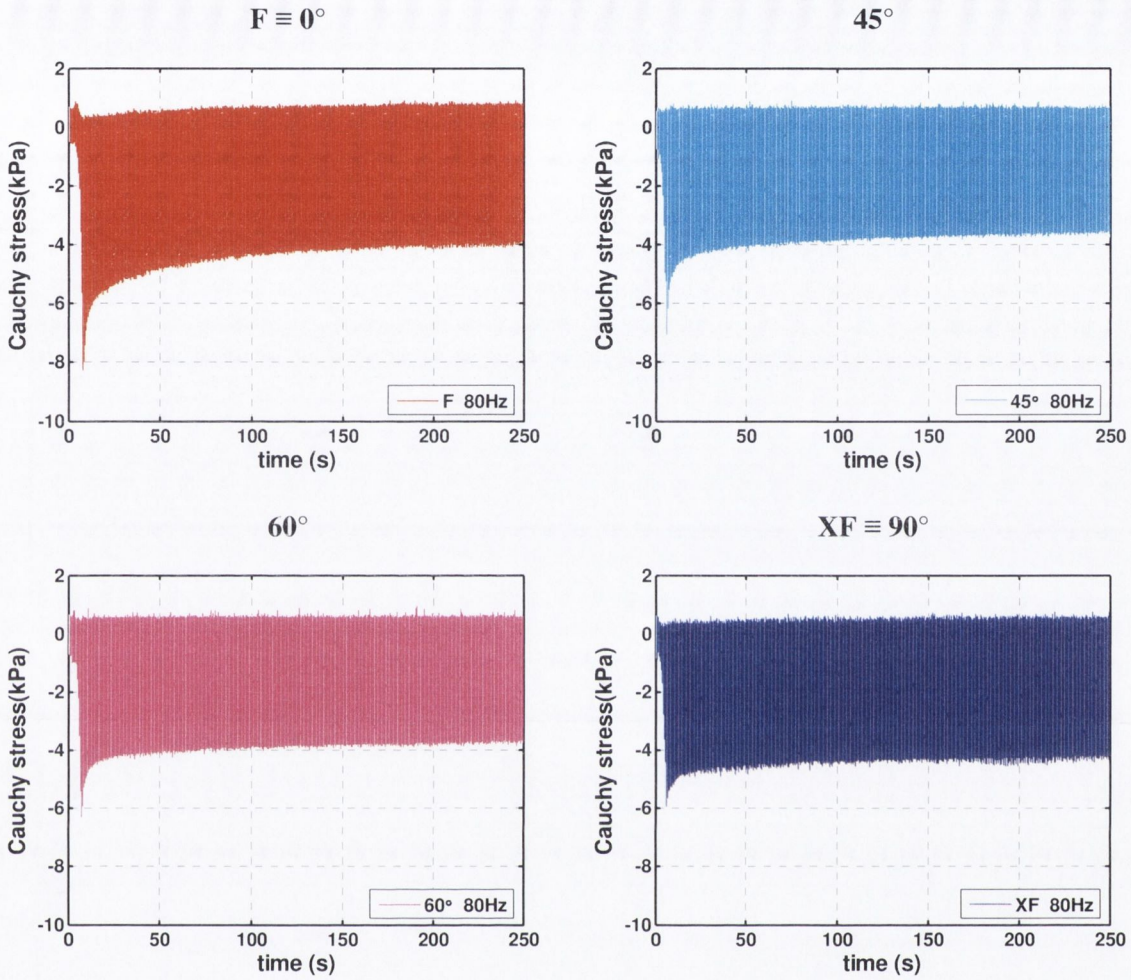


Figure 4-40: Cyclic stress-relaxation curves obtained during high amplitude cyclic compression tests performed at 80Hz, at 0°, 45°, 60° and 90° from the fibre direction.

Figures 4-38 to 4-40 present signals from which inertia effects have been subtracted. The force signal measured by the load cell corresponds indeed to the sum of the force due to the sample compression and inertia effects due to the displacement of the sample. The acceleration signal corresponding to each test was calculated by numerical differentiation of the displacement signal; the inertia due to the sample displacement was then calculated by multiplying the mass of the sample by the acceleration. The inertia obtained was then subtracted from the readings of the load cell. At 5Hz, inertia effects were negligible compared to the force due to the sample compression; the order of magnitude of these effects was of 0.05kPa at 20Hz and of 0.6kPa at 80Hz.

Figure 4-41 presents a close-up view of stress-time curves at the beginning and at the end of the tests for the three frequencies considered.

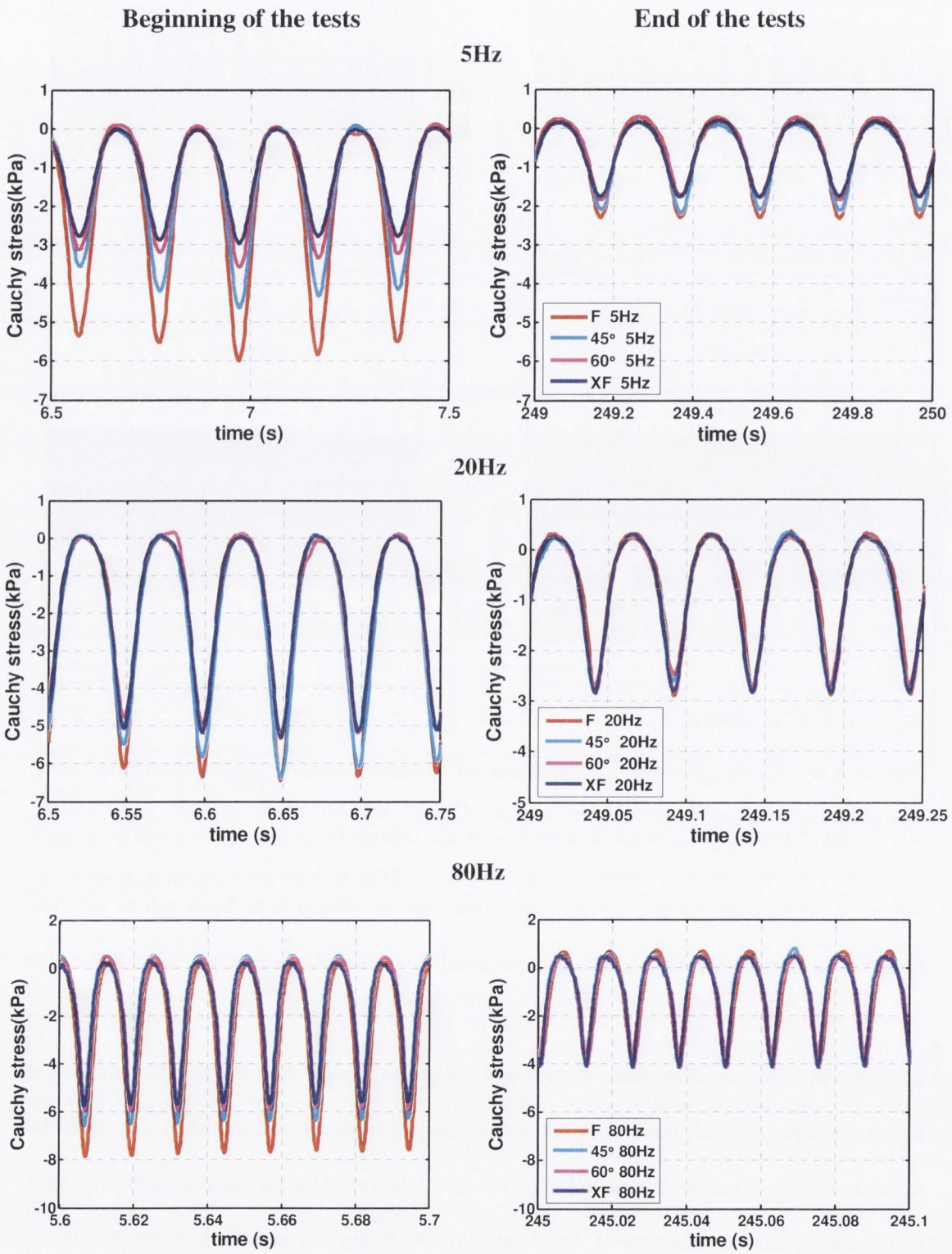


Figure 4-41: Close-up comparing stress-time curves at various orientations of the muscle fibres for high amplitude, high frequency cyclic tests.

Similarly to the tests performed at 0.44Hz, it can be observed that a greater amount of stress-relaxation occurs in the fibre and 45° directions. At the beginning of the test (just after the compressive ramp), the fibre direction is the stiffest of all directions. After cyclic relaxation however, results in all directions become nearly identical. This can also be qualitatively observed in Figures 4-38 to 4-40.

Table 4-9 presents values of hysteresis ratio and stress cycle amplitude calculated at the end of the test. Results indicate an increase in the stress cycle amplitude with frequency. The cycle amplitude appears to be higher in the fibre direction; however, values are very close for the various fibre orientations considered.

The influence of the frequency and fibre orientation on the hysteresis is not clear due to the variations observed in the results. These variations are due to noise and vibrations present in the system at the high frequency considered (80Hz); the quality of the signal measured is thus poorer than at lower frequencies.

Table 4-9: Hysteresis ratio (h_r) and stress cycles amplitude calculated after 240s for high amplitude, high frequency tests.

Frequency	Test direction	Hysteresis (%)	Amp ± SD (kPa)
5Hz	**F**	39.33±9.76	2.68±0.17
	45°	43.05±7.93	2.21±0.21
	60°	49.65±7.64	2.13±0.16
	XF	46.95±10.46	2.06±0.08
20Hz	**F**	44.12±5.15	3.39±0.43
	45°	40.94±6.51	3.29±0.09
	60°	45.83±6.01	3.10±0.15
	XF	60.61±4.49	3.25±0.28
80Hz	**F**	49.13±9.98	4.88±1.04
	45°	49.63±11.03	4.54±0.36
	60°	46.10±10.41	4.44±0.36
	XF	68.92±1.46	4.80±0.35

4.4.1.4 Evolution of the stress cycles amplitude and hysteresis ratio with frequency

This section compares the results obtained during the 10% amplitude cyclic tests performed at 0.22, 0.44, 5, 20 and 80Hz (results presented in sections 4.4.1.2 and 4.4.1.3). Figures 4-42 and 4-43 present respectively the evolution with frequency of the stress cycles amplitude and of the hysteresis ratio for the various fibre orientations considered. These values were taken after 240s of cyclic relaxation.

For each frequency considered individually, Figure 4-42 shows that the amplitude of the stress cycles is approximately the same in all orientations of the muscle fibres. At these frequencies, the influence of fibre orientation on muscle properties (i.e. the anisotropy) is thus reduced when a steady state of the tissue is considered (i.e. after cyclic relaxation).

For each orientation considered, it can also be observed that the amplitude of the stress cycles increases with the test frequency; the stress cycles amplitude is multiplied approximately five fold from 0.22 to 80Hz.

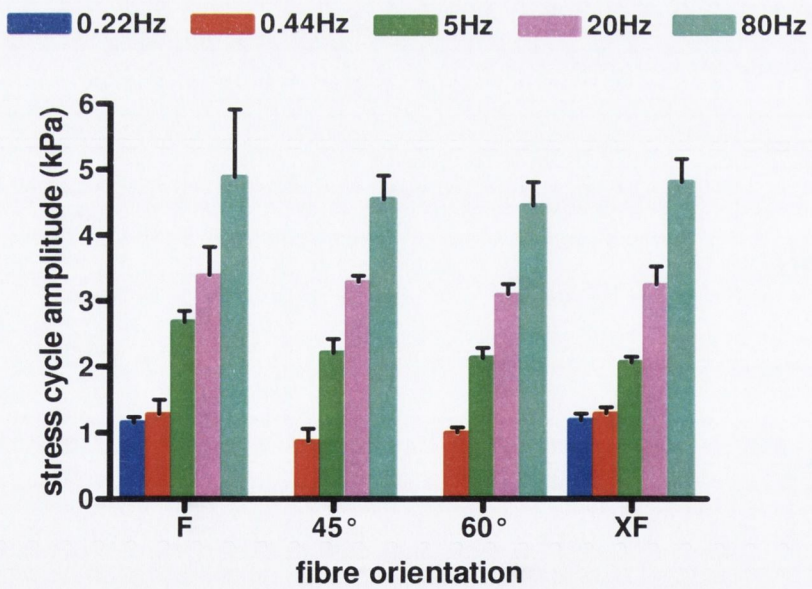


Figure 4-42: Evolution of the stress cycle amplitude with frequency for 10% amplitude cyclic tests performed on fresh porcine muscle samples.

For the hysteresis ratio, the trend in the results is not as clear due to relatively high variations. Figure 4-43 indicates however an increase in the hysteresis ratio with frequency.

Also, hysteresis ratio seems to presents higher values in the cross-fibre direction. This observation contradicts other results showing that the viscoelastic component is more influential in the fibre direction. Additional investigation is required to comment further on this point.

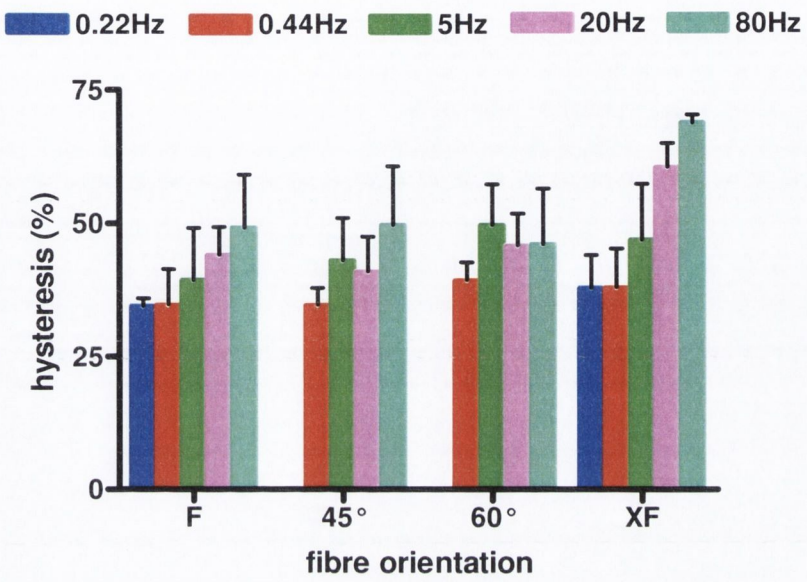


Figure 4-43: Evolution of the hysteresis with frequency for 10% amplitude cyclic tests performed on fresh porcine muscle samples.

4.4.2 Mathematical modelling

4.4.2.1 Quasi-linear viscoelastic SYM model

In this section, experimental results from cyclic tests are compared to theoretical results obtained with the quasi-linear viscoelastic SYM model. This model, which consists of a nonlinear transversely isotropic formulation extended with Prony series, has been successfully fitted to stress-relaxation data obtained at various rates and orientations of the muscle fibres (section 4.3.2). Using the parameters obtained from this fitting, theoretical predictions of muscle behaviour were calculated for low and high amplitudes cyclic tests. Figures 4-44 and 4-45 compare experimental and theoretical results obtained for 2% amplitude cyclic tests performed respectively at 0.22 and 0.4Hz.

Results show that, qualitatively, the model provides a good prediction of muscle cyclic-relaxation behaviour for cycles of low amplitude. Quantitatively, it can however be observed that the model tends to under-estimate the stress amplitude of the cycles. Nonetheless, the match between theory and experimental results can still be qualified as very good, accounting for the experimental variability and bearing in mind that the theoretical results presented in Figures 4-44 and 4-45 (—) correspond to predictions made with the model – i.e. using parameters obtained from the fitting to relaxation data (see section 4.3.2.1).

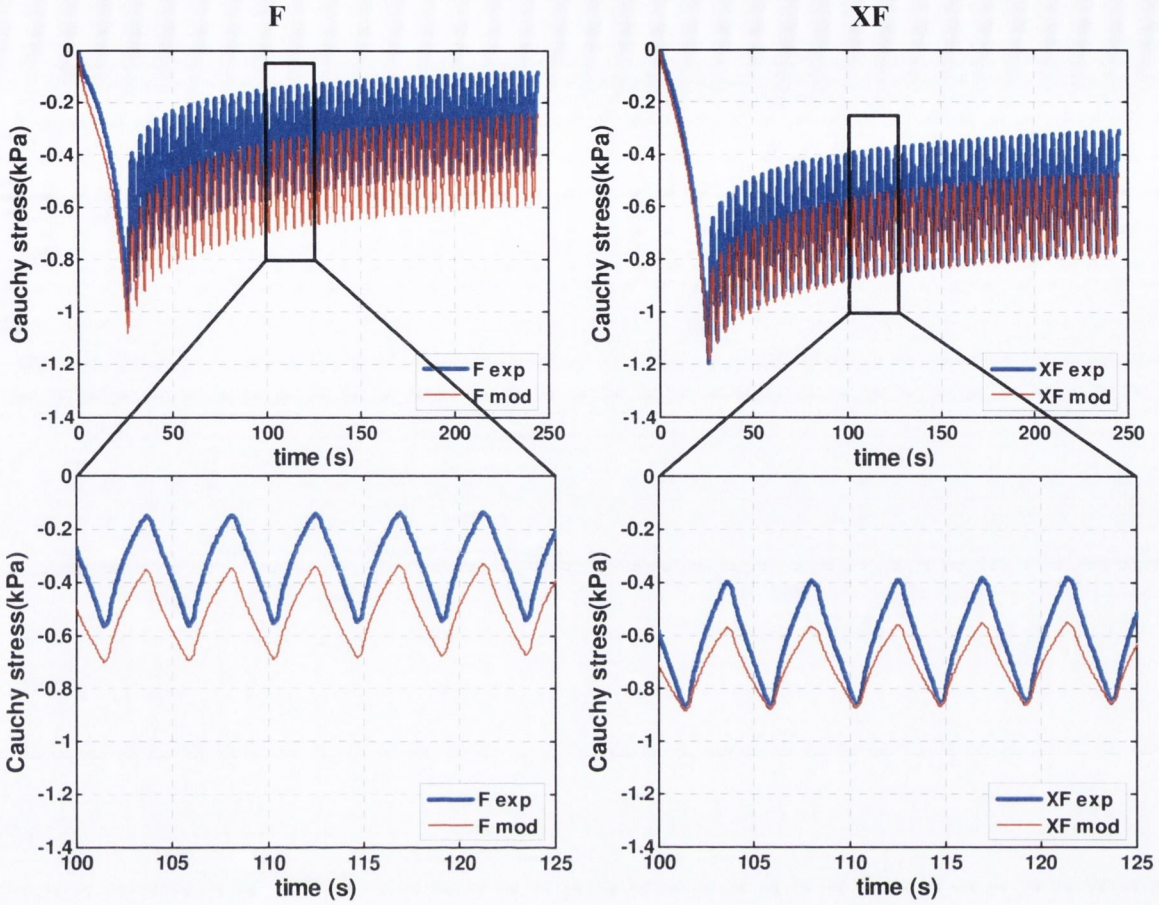


Figure 4-44: Comparison between experimental results (—) and viscoelastic SYM model predictions (—) for low amplitude cyclic compression tests performed in (left) fibre and (right) cross-fibre directions at 0.22Hz.

(left) Fibre and (right) cross-fibre results are presented; the bottom graphs represent a close-up view of the results (black box area).

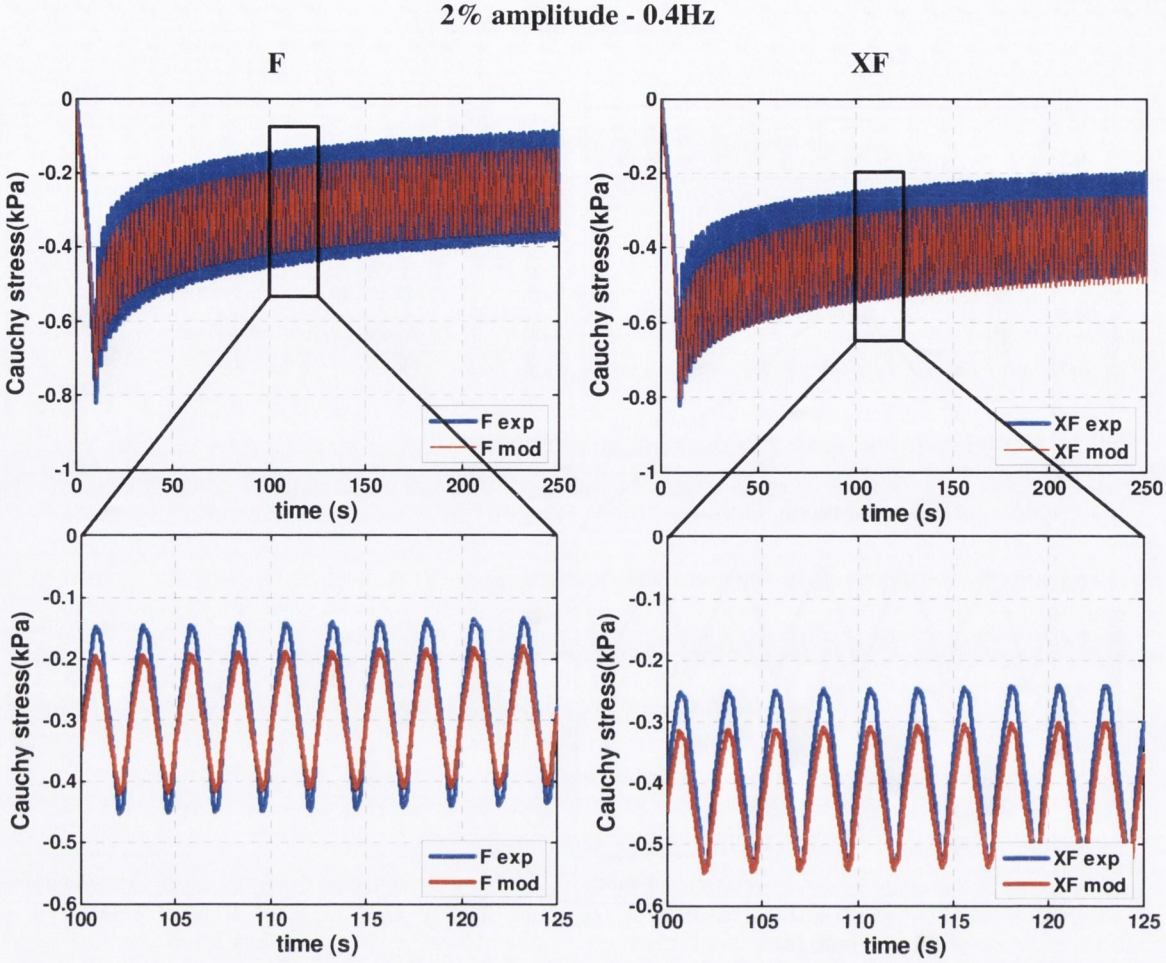


Figure 4-45: Comparison between experimental results (—) and viscoelastic SYM model predictions (—) for low amplitude cyclic compression tests performed in (left) fibre and (right) cross-fibre directions at 0.4Hz.

(left) Fibre and (right) cross-fibre results are presented; the bottom graphs represent a close-up view of the results (black box area).

Figure 4-46 compares experimental and theoretical results obtained for 10% amplitude cyclic tests performed at 0.44Hz. It shows that the model does not fully predict the behaviour observed experimentally for high amplitude cyclic tests. Graphs (c) and (d) show that the model predicts relatively well muscle behaviour for the ramp and the first few cycles. The difference between theory and experiment increases however when the number of cycles increases. The model predicts similar relaxation behaviour during loading and unloading leading to cycles of constant amplitude; faster and smaller relaxation was however observed experimentally for the unloading stress.

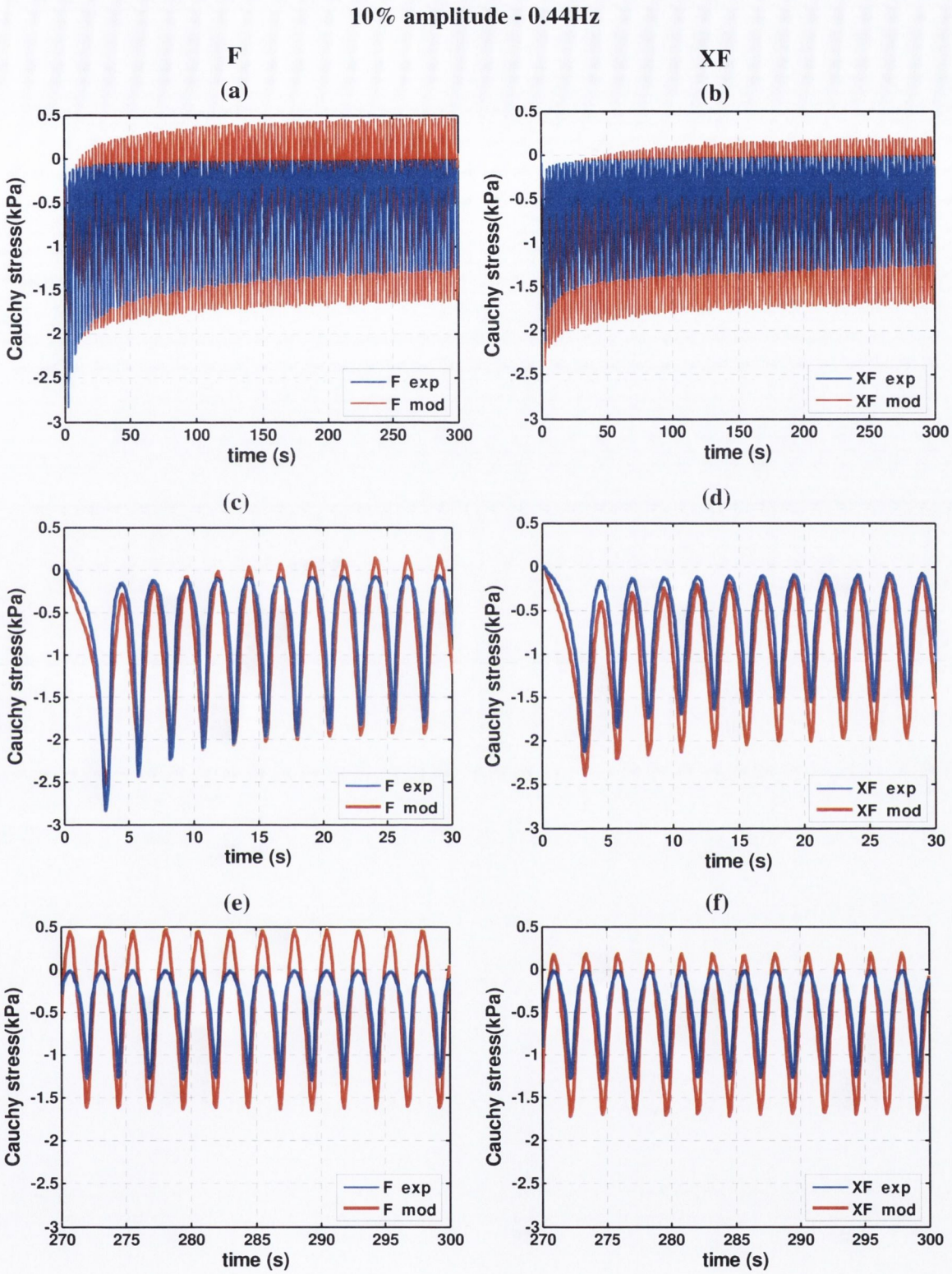


Figure 4-46: Comparison between experimental results (—) and viscoelastic SYM model predictions (—) for high amplitude cyclic compression tests performed in (left) fibre and (right) cross-fibre directions at 0.44Hz.

(left) Fibre and (right) cross-fibre results are presented; the bottom graphs represent a close-up view of the results (c and d) at the beginning and (e and f) at the end of the tests.

The discrepancies between muscle behaviour and theoretical predictions are more significant in the fibre than in the cross-fibre direction; this is due to the fact that a higher peak stress and a greater amount of cyclic stress relaxation are observed in the fibre direction.

Figures 4-47 and 4-48 compare experimental and theoretical results obtained for 10% amplitude cyclic tests performed at 5 and 20Hz in the fibre and cross-fibre directions. As explained previously (section 4.2.2), the mean compression level applied to the samples was controlled manually and the displacement history was not recorded during the first few second of the tests; it was therefore approximated to calculate the model response.

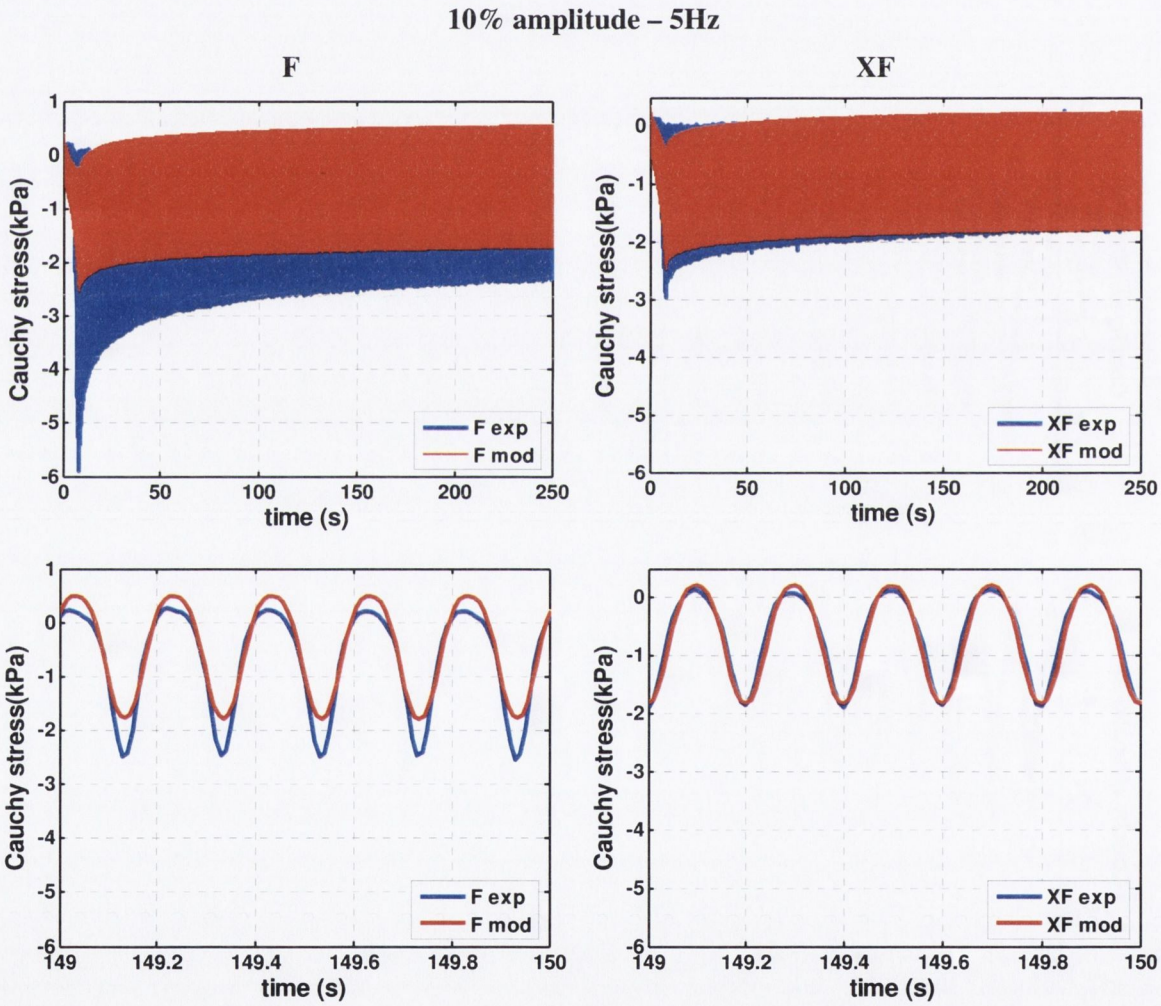


Figure 4-47: Comparison between experimental results (—) and viscoelastic SYM model predictions (—) for high amplitude cyclic compression tests performed in (left) fibre and (right) cross-fibre directions at 5Hz.

The bottom graphs represent a close-up view of the results around 150s.

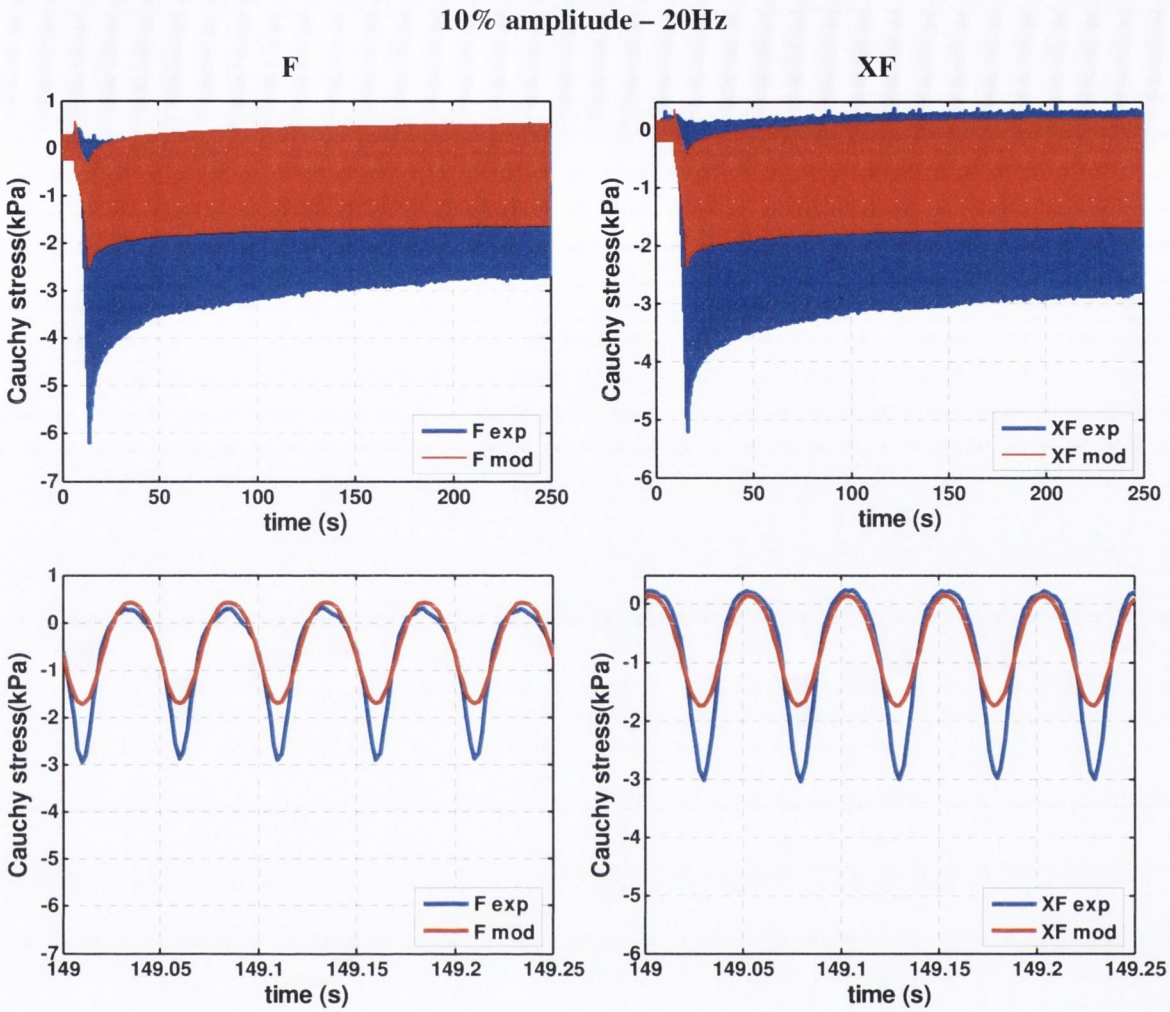


Figure 4-48: Comparison between experimental results (—) and viscoelastic SYM model predictions (—) for high amplitude cyclic compression tests performed in (left) fibre and (right) cross-fibre directions at 20Hz.

The bottom graphs represent a close-up view of the results around 150s.

Results from cyclic tests (section 4.4.1) showed that the stress cycles amplitude increases with frequency for muscle tissue. It was also observed that higher peak stresses are reached in the fibre than in the cross-fibre direction after the compressive ramp. A greater amount of stress relaxation is however observed in the fibre direction. The amplitude of the stress cycles is therefore approximately the same in both directions after cyclic relaxation.

Figure 4-47 shows that the model predicts relatively well results obtained in the cross-fibre direction at 5Hz. In the fibre direction however, the model predictions are poor; the peak stress observed experimentally cannot be reached.

Figure 4-48 shows similar results for the tests performed at 20Hz in both directions; the model cannot predict the increase in stiffness observed experimentally with frequency.

Nearly identical stress amplitudes are in fact obtained with the model at 5, 20 and 80Hz. At these high frequencies, the maximum value of stress that can be predicted by the model has been reached (see equation (4-9)).

This is a limitation of the model, which has been outlined by previous authors interested in the modeling of ligaments viscoelasticity (Pioletti *et al.*, 1998; Woo *et al.*, 1981). To address this limitation of the QLV theory, Pioletti *et al.* (2000) developed a model in which stress-relaxation and the strain rate effect are discriminated according to the time scale of their effects (see section 2.4.3.4). The stress relaxation corresponds to the long time memory and can be described with the QLV theory for example; the strain rate dependence corresponds to the short time memory and requires the introduction of an explicit strain rate dependent term. The addition of such a term in the QLV SYM model proposed could provide an answer to the limitation of the model at higher strain rates; further investigations are required on this point.

4.4.2.2 Nonlinear viscoelastic SYM model

The previous section showed that the quasi-linear viscoelastic approach could not capture the nonlinear behaviour observed for muscle tissue during high amplitude cyclic tests. In this section, the nonlinear approach developed by Schapery (1969) is considered to represent skeletal muscle viscoelasticity. Schapery's model is here briefly presented, further details are provided in the literature review (section 2.4.3.5).

Schapery's formulation is a nonlinear generalisation of Boltzmann superposition principle:

$$\sigma(t) = h_e G_\infty \varepsilon(t) + h_1 \int_0^t \Delta G(\rho - \rho') \frac{dh_2 \varepsilon(\tau)}{d\tau} d\tau \qquad (4\text{-}17)$$

with the reduced time, ρ, defined as

$$\rho = \int_0^t \frac{dt'}{a_\tau[\varepsilon(t')]} \quad \text{and} \quad \rho' = \rho(\tau) = \int_0^\tau \frac{dt'}{a_\tau[\varepsilon(t')]} \qquad (4\text{-}18)$$

$G_\infty = G_n(\infty)$ represents the equilibrium value of the relaxation modulus and $\Delta G(t)$ the transient component of the modulus. The terms h_e, h_1, h_2, and a_τ are strain-dependent material properties; they account for nonlinearities of the elastic properties (h_e and h_2) and the viscoelastic properties (h_1 and a_τ).

Poon *et al.* (1998) extended Shapery's one-dimensional model to a three-dimensional anisotropic formulation; using the index notation, the stress components are expressed as:

$$\sigma_{ij}(t) = h_e\left[\sum_k\sum_l G^{\infty}_{ijkl}\varepsilon_{kl}\right] + h_1\int_0^t\sum_k\sum_l\left[\Delta G_{ijkl}(\xi_{ijkl} - \xi'_{ijkl})\frac{d}{d\tau}(h_2\varepsilon_{kl})\right]d\tau \qquad (4\text{-}19)$$

where the scalar functions h_e, h_1, h_2 are dependent on the strain tensor. The reduced time is influenced by the mechanical strain via:

$$\xi_{ijkl} = \int_0^t \frac{dt}{a_{\tau ijkl}(\boldsymbol{E}(t'))} \qquad (4\text{-}20)$$

Poon *et al.* proposed Prony series to describe the stress relaxation behaviour and polynomials for the strain dependent expressions h_e, h_1, h_2 and a_τ.

In this thesis, the model was adapted to include the SYM formulation for the elastic behaviour of muscle tissue. The quasi-linear SYM model developed in section 4.3.2.1 already included nonlinearities for the elastic behaviour of the tissue – the SYM formulation taking the role of h_e and h_2 in equation 4-17. The viscoelastic component was however linear; terms h_1 and a_τ were then introduced in equation (4-4) to account for viscoelastic nonlinearities (h_1 and a_τ are respectively denoted h_j and a_j in the following equations).

The Cauchy stress in direction j can therefore be expressed as:

$$\sigma_j(t) = \sigma^e_j G_j(t) + h_j(\tilde{\varepsilon}_j)\int_0^t G_j(\xi_j - \xi'_j)\frac{\partial\sigma^e_j[\tilde{\varepsilon}_j(\tau)]}{\partial\tau}d\tau \qquad (4\text{-}21)$$

with

$$\xi_j = \int_0^t \frac{dt'}{a_j[\tilde{\varepsilon}_j(t')]} \qquad (4\text{-}22)$$

h_j and a_j were chosen as

$$\begin{cases} h_j(\tilde{\varepsilon}_j) = h_{1j}\tilde{\varepsilon}_j + h_{2j}\tilde{\varepsilon}_j^2 \\ a_j(\tilde{\varepsilon}_j) = 1 - a_{1j}\tilde{\varepsilon}_j + a_{2j}\tilde{\varepsilon}_j^2 \end{cases} \quad (4\text{-}23)$$

A Prony series expansion is adopted for the reduced relaxation function, $G_j(t) = p_{\infty j} + \sum_{i=1}^{N} p_{ij} \exp(-\frac{t}{\tau_{ij}})$ and the SYM formulation is introduced for the elastic stress, $\sigma_j^e = \frac{\sigma_{\infty j}}{p_{\infty j}} = \frac{k_{1j}\tilde{\varepsilon}_j + k_{2j}\tilde{\varepsilon}_j^2 + k_{3j}\tilde{\varepsilon}_j^3}{p_{\infty j}}$.

This leads to:

$$\sigma_j(t) = p_{\infty j}\sigma_j^e(t) + h_j(\tilde{\varepsilon}_j)\sum_{i=1}^{N}\int_0^t p_{ij}\exp\left(\frac{-(\xi_j - \xi_j')}{\tau_{ij}}\right)\frac{\partial\sigma_j^e[\tilde{\varepsilon}_j(\tau)]}{\partial\tau}d\tau \quad (4\text{-}24)$$

Poon *et al.* also developed a method to perform the integration and implemented the model into a finite element analysis; using this recursive formula, the model was implemented in Matlab. Similar to the QLV approach, a fitting procedure was developed using the built in Matlab function *lsqnonlin*; the code used to perform the fitting is provided in Appendix F. The model was first fitted to the high amplitude (10%), low frequency (0.44Hz) data. Table 4-10 presents values of the parameters for fibre and cross-fibre data.

Table 4-10: Parameters for the nonlinear viscoelastic SYM model fitted to high amplitude cyclic data obtained at 0.44Hz on fresh porcine muscle tissue in fibre (left) and cross-fibre (right) directions.

F					XF				
k_{1L} (kPa)	k_{2L} (kPa)	k_{3L} (kPa)	-	-	k_{1T} (kPa)	k_{2T} (kPa)	k_{3T} (kPa)	-	-
1.005	2.989	10.985			1.293	0.911	10.869		
p_{1L}	p_{2L}	p_{3L}	p_{4L}	p_{5L}	p_{1T}	p_{2T}	p_{3T}	p_{4T}	p_{5T}
0.374	0.285	0.077	0.078	0.101	0.097	0.532	0.072	0.000	0.086
τ_{1L} (s)	τ_{2L} (s)	τ_{3L} (s)	τ_{4L} (s)	τ_{5L} (s)	τ_{1T} (s)	τ_{2T} (s)	τ_{3T} (s)	τ_{4T} (s)	τ_{5T} (s)
0.6	6	30	60	300	0.6	6	30	60	300
h_{1L}	h_{2L}	a_{1L}	a_{2L}	-	h_{1T}	h_{2T}	a_{1T}	a_{2T}	-
2.337	12.532	2.337	12.532	-	0.858	9.771	0.858	9.771	-

Results of the fitting are presented in Figure 4-49. It shows that the model provides a good fit to the experimental data and is able to capture the nonlinear behaviour observed during these cyclic tests.

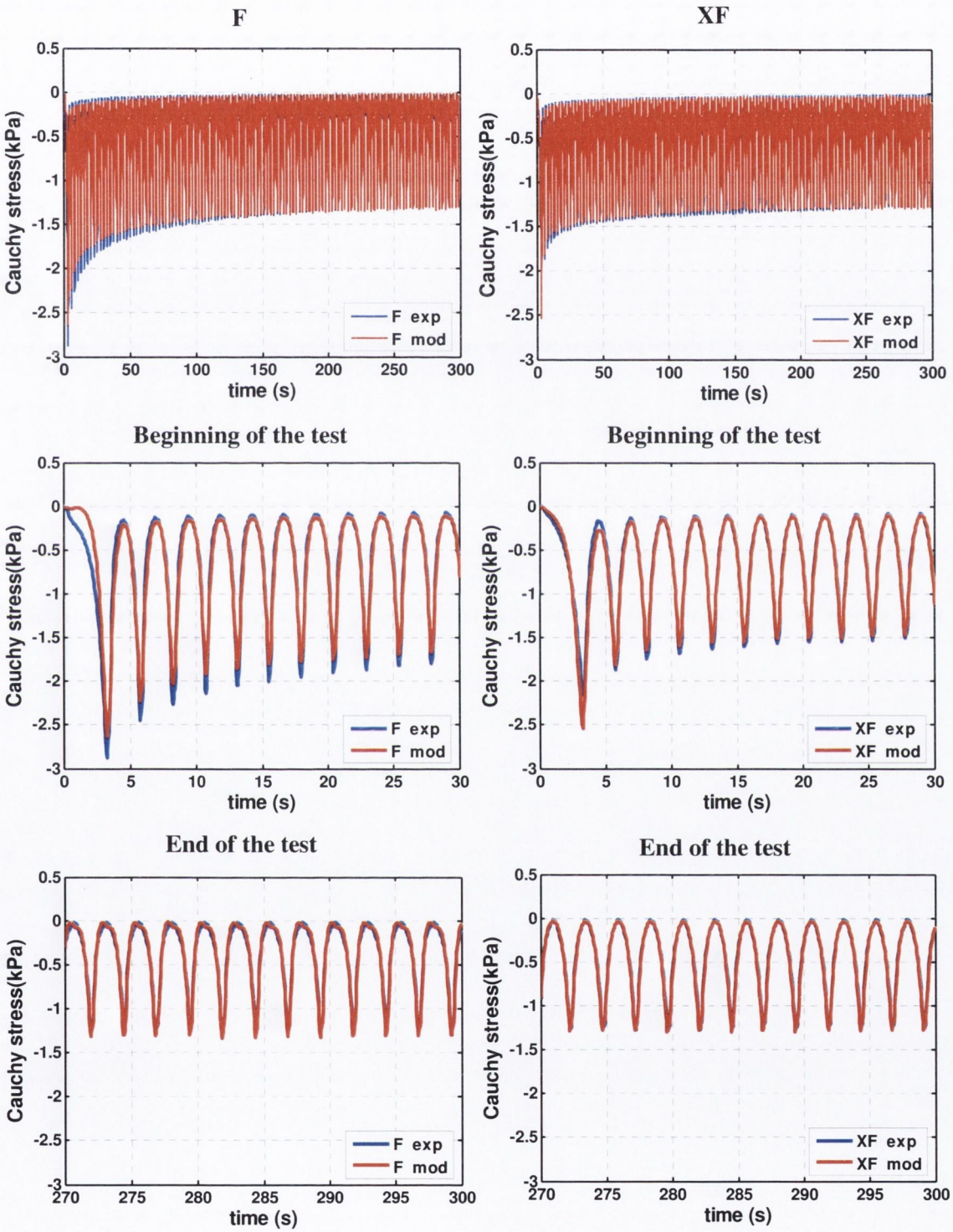


Figure 4-49: Comparison between experimental results (—) and nonlinear viscoelastic SYM model fitting (—) for high amplitude cyclic compression tests performed in fibre (left) and cross-fibre (right) directions at 0.44Hz.

The match between experiments and theory is very good overall; discrepancies can however be observed during the ramp part of the test. This is due to the multiplication of the viscoelastic terms by a second order polynomial (h_j in equation 4-21).

When cyclic tests performed at higher frequencies (5 to 80Hz) are considered, this model presents similar limitations as the quasi-linear model; it cannot predict the increase in stiffness observed with frequency for muscle tissue as illustrated in Figure 4-50 for results obtained at 5Hz in the fibre direction.

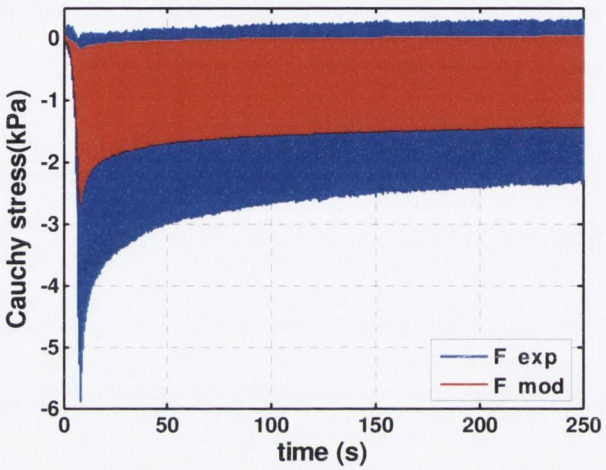


Figure 4-50: Comparison between experimental results (—) and nonlinear viscoelastic SYM model predictions (—) for high amplitude cyclic compression tests performed in the fibre direction at 5Hz.

Figure 4-51 shows the evolution with deformation of h_j and a_j corresponding to fitting in the cross-fibre direction ($j \equiv XF$). In the model, the amplitude of the viscoelastic terms is multiplied by h_j and the time constants characterising the relaxation behaviour are multiplied by a_j. Therefore, Figure 4-51 indicates that the amplitude of the viscoelastic terms is reduced at lower compression levels (h_{XF} decreases) and the value of time constants are reduced at higher compression levels (a_{XF} decreases).

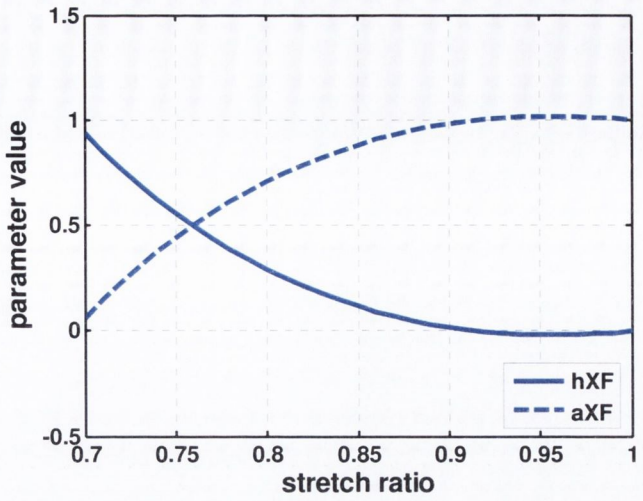


Figure 4-51: Evolution with stretch ratio of expressions h_j and a_j, $j \equiv XF$ (see equation 4-21) obtained from fitting to cyclic data in the cross-fibre direction.

Using the parameters obtained from fitting to the cyclic data, the nonlinear model was then used to predict muscle relaxation behaviour. Results obtained are compared to experimental data in Figure 4-52. It shows that the response obtained with this nonlinear model is not as good as the response obtained with the quasi-linear model for what concerns relaxation behaviour. Theoretical and experimental results remain relatively close; however, the model relaxes faster than muscle tissue and under-predicts the peak stresses reached after compression. This is due to the influence of the nonlinear term a_j, which reduces the value of the relaxation constants at higher compression levels (see Figure 4-51).

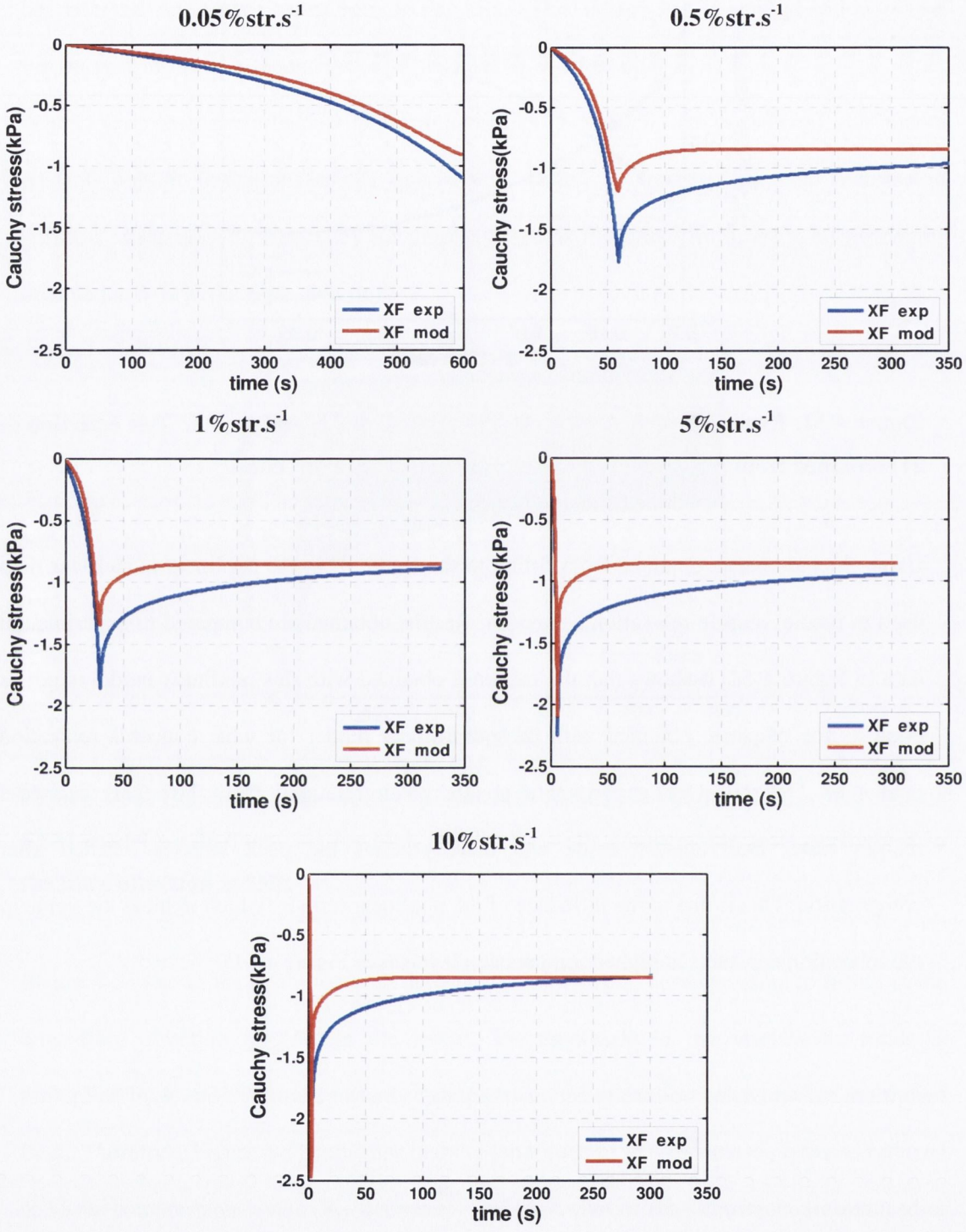


Figure 4-52: Comparison between experimental stress-relaxation results (—) and nonlinear viscoelastic SYM model predictions (—) in the cross- fibre direction.

4.5 Discussion

4.5.1 Summary of experimental results

This chapter aimed to investigate the viscoelastic behaviour of skeletal muscle tissue under compressive loading. Uniaxial stress-relaxation and cyclic compression tests were performed on fresh porcine muscle tissue *in vitro*. Samples were tested at various orientations of the muscle fibres, various strain levels and various strain rates in order to investigate if muscle viscoelastic behaviour depends on fibre orientation, strain and/or strain rate.

4.5.1.1 Skeletal muscle compressive behaviour

In chapter 3, the long term elastic properties of muscle tissue were investigated by means of uniaxial unconfined compression tests performed at a rate of $0.05\%s^{-1}$; these tests were mainly conducted in the fibre, the cross-fibre and at 45° from the fibre direction. Results showed that muscle elastic behaviour is transversely isotropic; the stiffest direction being the cross-fibre direction, followed by the fibre and the 45° direction. In this chapter, similar tests performed at compression rates ranging from 0.5 to $10\%s^{-1}$ are also described. During these tests, a stiffening effect with compression rate was observed in all directions of testing; faster rates give higher peak loads at a given deformation level. The increase in stiffness with compression rate is however more significant in directions closer to the fibre direction. During quasi-static tests ($0.05\%str.s^{-1}$), the cross-fibre direction appears to be much stiffer than the fibre direction; however, when the compression rate increases, the difference in stiffness between both directions diminishes. Figure 4-53 summarises these observations.
The influence of the viscoelastic component is then greater in directions closer to the muscle fibres.

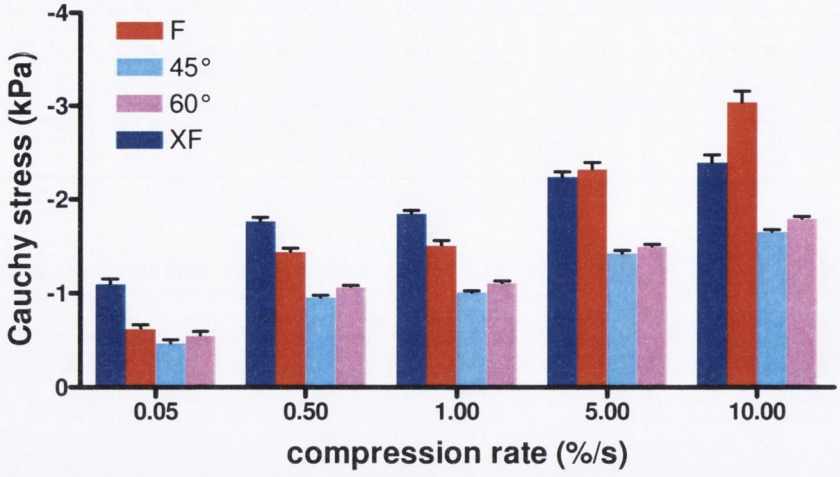
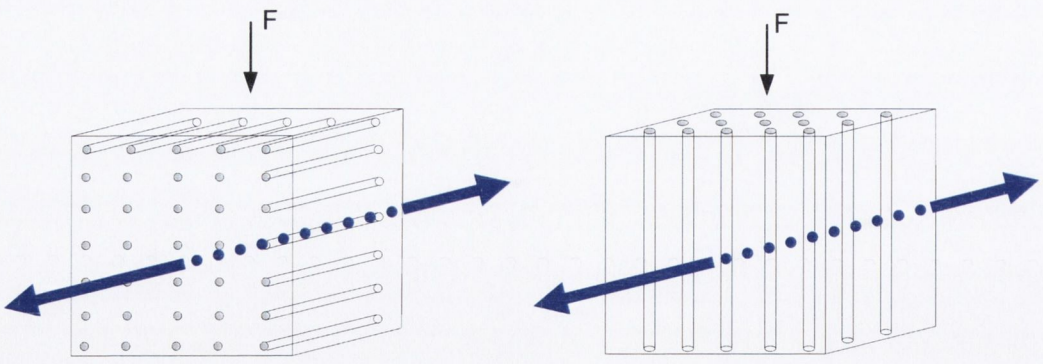


Figure 4-53: Evolution with deformation rate of the stress reached after 30% compression in various orientations of the muscle fibres.

Mean values with standard deviations.

To explain this behaviour, muscle tissue can be considered as made of "bags" (fibre fascicles) filled with fluid (Figure 4-54). The movement of the fluid component appears to be easier along the fibres. When compression takes place in the cross-fibre direction (a), the fluid is free to rearrange itself; whereas during compression in the fibre direction (b), the fluid is "trapped" between the compression plates and higher stress levels are reached. It has to be emphasised that no expulsion of fluid from the specimens was observed during these tests.



(a) **(b)**

Figure 4-54: Illustration of the influence of the fluid component on muscle viscoelastic behaviour during compression in (a) cross-fibre and (b) fibre directions.

Skeletal muscle compressive behaviour is thus dependent on fibre orientation (anisotropic) and compression rate. Results indicate that above a very small compression rate, the viscoelastic component plays a significant role on muscle mechanical properties; this is graphically summarised in Figure 4-55.

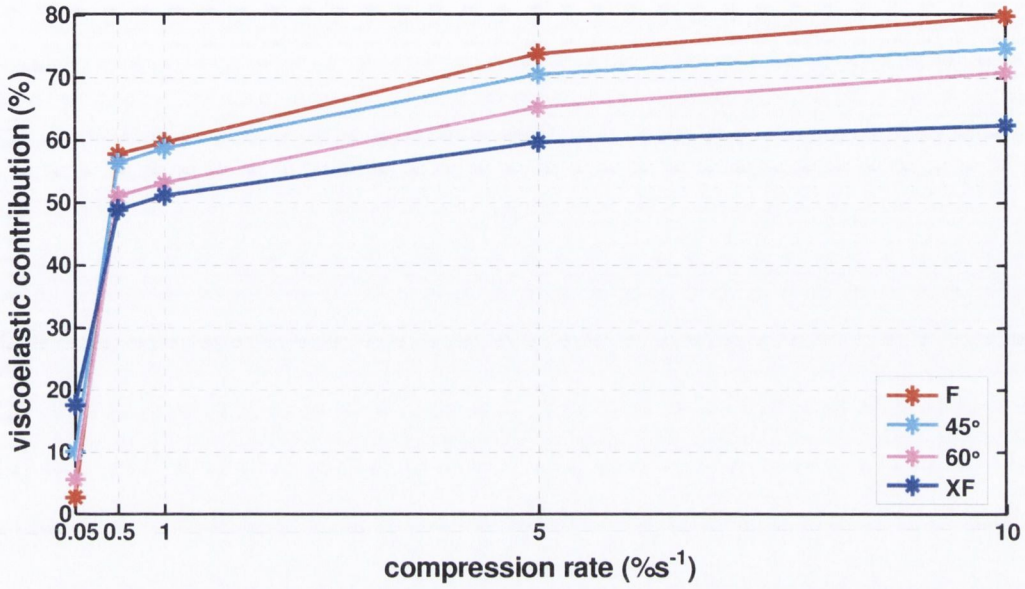


Figure 4-55: Relative contribution of the viscoelastic component to the total stress reached at 30% compression at various strain rates and fibre orientations.
Values obtained using equation (4-1) with σ_e = mean relaxed values

4.5.1.2 Skeletal muscle relaxation behaviour

Following the compressive ramp performed at various rates, deformation was held constant for 300s to allow for relaxation of the tissue. Results show that a significant amount of stress-relaxation occurs: over 45% and over 60% stress-relaxation are respectively observed in the cross-fibre and fibre directions for tests performed at $0.5\%s^{-1}$. The data also show that over 80% of the total relaxation amount occurs within 100s after the ramp.

After analysis, it was considered that muscle relaxation behaviour is independent on compression rate; samples relax to the same equilibrium value independently of the compression rate.

An increase in the relative amounts of stress-relaxation was observed with an increase in angle from the fibre direction, indicating again muscle anisotropic viscoelastic behaviour and the greater influence of the viscoelastic component in directions closer to the muscle fibres.

Finally, relaxation tests were performed in the fibre and cross-fibre directions up to three levels of compression, i.e. 10, 20 and 30%. Results from these tests indicate that the rate of relaxation increases when the level of compression decreases. Even though a statistically significant difference appears only in the fibre direction, results seem to indicate that muscle relaxation behaviour is dependent on the compression level.

4.5.1.3 Skeletal muscle cyclic behaviour

In order to investigate muscle dynamic behaviour, cyclic tests were performed on fresh porcine muscle samples with various cycles amplitudes (2 or 10%) and frequencies (0.22 to 80Hz, corresponding to compression rates ranging from 1 to 3200%s^{-1}).

During the low amplitude (2%), low frequency (0.22Hz and 0.44Hz) tests, muscle tissue displayed a linear viscoelastic behaviour. As expected, cyclic relaxation (i.e. a decrease in peak stresses with an increasing number of cycles) and hysteresis (i.e. different paths followed by the loading and unloading curves) were observed in the results. Qualitatively, fibre and cross-fibre results were similar, with the cross-fibre direction being stiffer than the fibre direction. In the fibre direction approximately 18% of the loading energy was dissipated during each cycle; only 13% was dissipated in the cross-fibre direction.

However, during higher amplitude (10%) tests, muscle tissue displayed a nonlinear behaviour. Cyclic stress-relaxation of the tissue and hysteresis were again observed. Peak stresses decreased gradually with an increasing number of cycles; valley stresses however appeared to be completely relaxed over a small number of cycles. Also, the cycle amplitudes were sufficient to return the stress to a value close to zero, even though samples were still submitted to a compression level of 20%. In 2% amplitude tests, relaxation behaviour was identical for loading and unloading; in tests with higher amplitudes, the unloading stress relaxed both less and faster than the loading stress.

Results also show that a greater amount of cyclic stress-relaxation occurs in the fibre and 45° directions. This confirms the observation made during static stress-relaxation experiments; the viscoelastic component has a greater influence in directions closer to the muscle fibres.

For high amplitude tests performed at higher frequencies (5 to 80Hz), results are qualitatively similar to results obtained at lower frequencies, the main difference being the amplitude of the stress cycles. An increase in the amplitude of the stress cycles is indeed observed with the frequency; Figure 4-56 (a) summarises the results obtained in all directions of testing. It shows that at the frequencies considered, the amplitude of the stress cycles is relatively independent on the fibre orientation (for values measured after cyclic relaxation).

The hysteresis ratio, i.e. the energy dissipated per cycle, also increases with the frequency. Results obtained at higher frequencies present however higher variability and further tests would be required to draw definite conclusions on this point.

Figure 4-56 (b) summarises the findings.

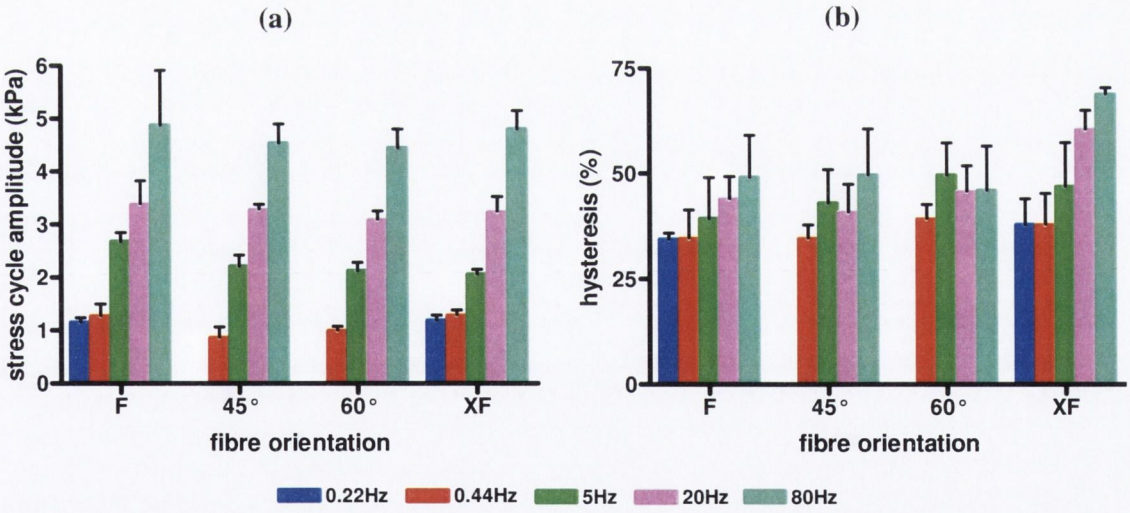


Figure 4-56: Evolution of (a) the stress cycle amplitude and (b) the hysteresis with frequency for 10% amplitude cyclic tests performed on fresh porcine muscle samples.

4.5.2 Comparison of experimental results with published data

When compressive loading is considered, chapter 1 of this thesis showed that the literature on muscle elastic behaviour was sparse; muscle viscoelastic behaviour has even been less investigated.

In 2001, Bosboom *et al.* presented results of compression tests conducted *in vivo* on rat tibialis anterior (TA) muscles in the transverse direction. Each TA was compressed following a ramp and hold function, with a ramp speed of $0.25mm.s^{-1}$ and a hold phase of 20s only; muscle relaxation behaviour could thus not be fully captured. Due to the non-uniform geometry of the muscle tested, stress-strain curves could not be obtained and a direct comparison with these experimental data is not possible. Bosboom *et al.* fitted their experimental data with a viscoelastic hyperelastic model. They implemented viscoelasticity by means of a single term Prony series expansion; the multiplication factor of the Prony series had a value of 0.549 and the time constant a value of 6.01s. This corresponds to one of the five time constants adopted in this thesis to characterise muscle relaxation behaviour.

Zheng *et al.* (1999) performed *in vivo* indentation tests performed on human bulk muscular tissues. They used indentation rates ranging approximately from 4 to $40\%s^{-1}$ and reported that the tissue properties appeared to be rate-insensitive in the range tested. This contradicts our findings which show a dependency of muscle compressive behaviour to compression rate.

Silver-Thorn *et al.* (1999) also performed *in vivo* indentation tests performed on human muscular tissues. They reported that limb bulk soft tissues undergo substantial relaxation: after indenting the tissue at $5mm.s^{-1}$, 95% relaxation was observed on average; the majority of this relaxation (85%) occurring within the first five seconds after indentation. Equilibrium was typically reached in less than 60 s. These values are higher than the values observed during our tests; approximately 50% relaxation was obtained in the cross-fibre direction and 80% of this amount occurred in 100s.

As mentioned previously, *in vivo* indentation tests measure bulk muscular properties (skin, fat and muscle tissue); muscle activity was only assessed qualitatively in the tests. These factors could influence the results and explain the differences observed.

Grieve and Armstrong (1988) performed *in vitro* measurements of aged porcine muscle tissues compressive properties at various strain rates. As mentioned in chapter 3, results obtained by Grieve and Armstrong at a quasi-static rate are slightly stiffer than the results obtained in this work on fresh muscle tissue. However, an increase in stiffness with compression rate was also observed in their experiments. The stress reached after 30% compression is approximately doubled from 0.05 to 2.5%str.s^{-1}; this is similar to the observations made in this thesis (Figure 4-53).

McElhaney (1966) and Van Sligtenhorst et *al.* (2006) also measured muscle compressive properties. However, very high compression levels (up to 80%) and very high strain rates (up to 2300s^{-1}) were considered in these studies and the results are presented in such a way that data cannot be read for the deformation levels and compression rates considered in this thesis. McElhaney reported that the maximum compressive stress measured at 75% strain is multiplied by only 2.6 from tests performed at 0.001 to 1000str.s^{-1}. In the data published by Van Sligtenhorst et *al.* (2006), a multiplication factor of 4.5 was observed between data measured at 1000 and 2300str.s^{-1}, at 30% compression.

Finally, Song *et al.* (Article in Press) also performed *in vitro* compression tests on porcine muscle tissue at strain rates ranging from 0.007 to 3700 s^{-1}. Again the very high strain rates considered and the presentation of the data does not allow a direct comparison with the data obtained in this thesis. Results obtained in the fibre and cross-fibre directions are presented in Figure 4-57. Song *et al.* concluded that porcine muscle compressive response is nonlinear and strongly strain-rate sensitive. Figure 4-57 shows however that data obtained at strain rates of 0.007s^{-1} and 0.07s^{-1} are identical and the strain-rate effect remains small for strain rates below 540s^{-1}. This contradicts the findings by Grieve and Armstrong (1988) as well as the data obtained in this thesis and leads to question the sensitivity of the tests performed on the SHPB apparatus. Song *et al.* comment that the strain-rate sensitivity appears to be more

significant in the cross-fibre direction. Figure 4-57 indicates however that this observation holds only for data obtained at 3700 s^{-1} in the cross-fibre direction; below this strain rate, the strain-rate sensitivity appears to be more significant in the fibre direction.

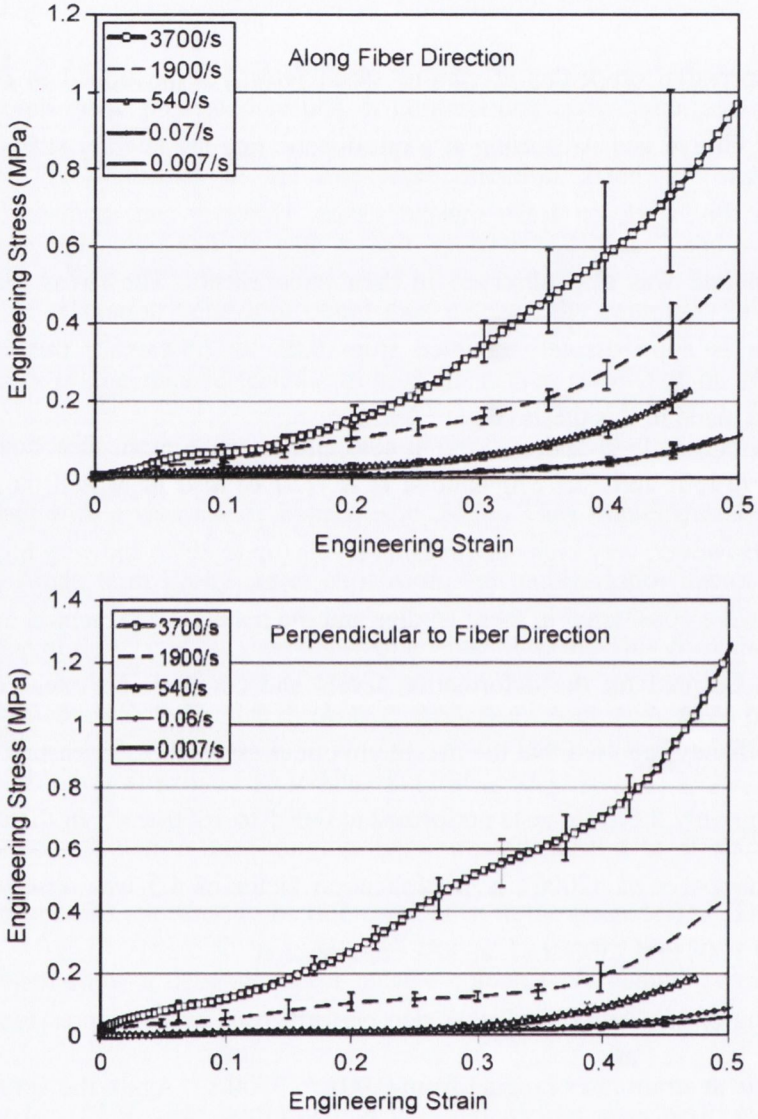


Figure 4-57: Results from compression tests performed on porcine muscle tissue at various strain rates, in fibre and cross-fibre directions (reproduced from Song *et al.*, Article in press).

The studies published confirm the results obtained in this thesis, i.e. skeletal muscle compressive properties are dependent on the deformation rate. Quantitative comparisons are however difficult to establish due to differences in the experimental protocols used. An attempt was however made to globally characterise the increase in stiffness observed with

compression rate. Three sets of data were considered: compression tests (single stroke) performed in this thesis at rates ranging from 0.05 to 10%s^{-1}, 10% amplitude cyclic compression tests performed at rates ranging from 5 to 3200%s^{-1} and compression tests (single stroke) performed by Song *et al.* at rates ranging from 7 to 3700.10^2 %s^{-1}. Data obtained in the fibre direction were considered. Numerical values are provided in Table 4-11. For single stroke tests, the value of stress obtained at 30% compression was taken to establish the comparison; for cyclic tests, the amplitude of the stress cycles was considered (Absolute stress in Table 4-11). For each type of test, the value of stress obtained at the smaller rate was taken as a reference and the ratios between this value and values obtained at higher rates were calculated (Stress ratios by test type in Table 4-11). These ratios were then combined to show the increase in stress from a compression rate of 0.05%s^{-1} (ratio of 1) to a rate of 3700.10^2 %s^{-1} (Global stress ratios in Table 4-11). Results are graphically presented in Figure 4-58 (a logarithmic scale was used to better visualise the results).

Table 4-11: Numerical values used to characterise the increase in stress with compression rate for skeletal muscle tissue.

Type of test	Compression rate (%s^{-1})	Absolute stress value (kPa)	Stress ratios by test type	Global stress ratios
Ramp – Van Loocke	0.05	-0.6	**1**	**1**
	0.5	-1.4	2.3	2.3
	1	-1.5	2.5	2.5
	5	-2.3	3.8	3.8
	10	-3.0	5	5
Cyclic – Van Loocke	5	-1.2	**1**	-
	10	-1.3	1.1	4.1
	200	-2.7	2.2	8.6
	800	-3.4	2.8	10.9
	3200	-4.9	4.1	15.7
Ramp – Song *et al.*	7	-15.4	**1**	-
	540.10^2	-52.1	3.4	12.9
	1900.10^2	-155.8	10.1	38.8
	3700.10^2	-339.6	22.1	84.5

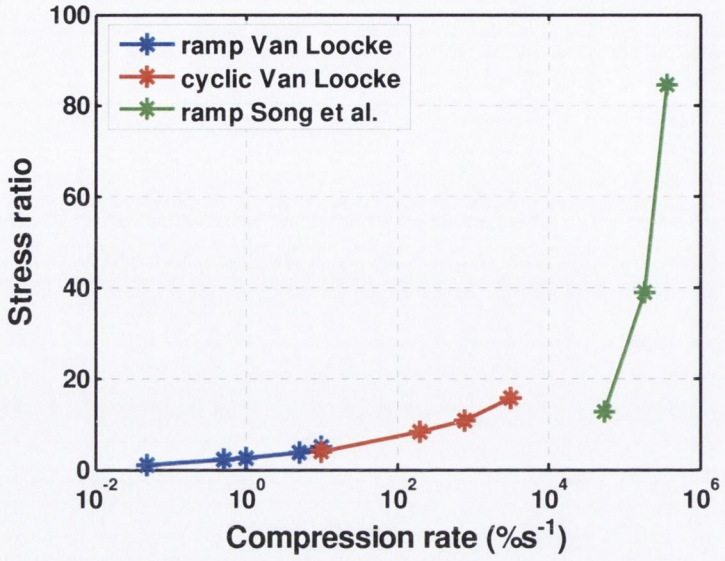


Figure 4-58: Relative increase in stress with compression rate for skeletal muscle tissue. *Values calculated from tests performed in this thesis (compressive ramp — and cyclic —) and compression tests by Song et al. (In Press) (—).*

Even though different types of tests were performed, an almost continuous evolution is observed in the results. Figure 4-58 indicates that skeletal muscle compressive behaviour depends strongly on the rate of deformation applied, more so than the compression rate increases.

The dependency of the rate of relaxation on the level of deformation, observed during tests performed at various compression levels, was also observed for ligaments (Provenzano *et al.*, 2001). The tests performed on muscle tissue up to 10, 20 and 30% compression showed a decrease in the rate of relaxation when the level of compression increases. Provenzano *et al.* (2001), performed tensile tests on medial collateral ligaments and made similar observations. Provenzano *et al.* speculate that the decrease in relaxation rate with increasing strain could be the result of larger strains causing greater water loss during the tests. No fluid loss was however observed during the tests performed on muscle tissue for this thesis.

Concerning results from the cyclic tests and the observations made on muscle hysteresis, a direct comparison cannot be established given the lack of published data.

Best *et al.* (1994) performed *in vivo* tensile tests on rabbits tibialis anterior muscles. The experimental protocol consisted of a relaxation test followed by six constant velocity tests at rates ranging from 0.01 to 2Hz; details on strain histories are however not provided. A value of 39.3 ± 5.4% is reported for the average hysteresis energy, which appears to be insensitive to the deformation rate. This value is in good agreement with the values of hysteresis measured in the fibre direction for 10% amplitude cyclic tests: 35% at 0.22 and 0.44Hz, and 39% at 5Hz. The lack of details concerning the tests performed by Best *et al.* does however not allow one to draw further conclusions.

4.5.3 Limitations of the experimental procedure

A critical point in the measurement of a materials' relaxation behaviour is the choice of the cut-off time for the experiment. The values of stress reached after 300s were here considered as steady-state, relaxed values even though a small amount of relaxation still occurred after the end of the tests. Over 80% of the total relaxation amount occurred however within 100s after the ramp and the 300s allowed for relaxation was considered as a good compromise between measurement of "truly relaxed" muscle properties and test duration. The time allowed for testing was limited by rigor mortis appearing in the tissue a few hours after death and leading to stiffer mechanical properties.

Small differences were observed between values of stress obtained during quasi-static tests and values of stress obtained from ramp and hold tests, after relaxation. These values should be similar as they both correspond to the long term elastic properties of the tissue. This is probably due to the fact that the compression rate adopted for quasi-static tests was not small enough to measure only long term elastic properties. As mentioned in section 3.4, 0.05%str.s^{-1} was however chosen as a compromise between test duration and measurement of true, long term elastic properties of the tissue.

Comparisons between quasi-static and relaxed values show that significant differences appear only in the cross-fibre direction. Even though no expulsion of fluid was noticed during the tests, this effect could be explained by the fact that fluid has the possibility to

freely rearrange itself during tests in the cross-fibre direction and come to the surface of the material, reducing the stress in this way.

In tests performed at high frequencies (20 and 80Hz), higher levels of variation were observed compared to lower frequencies tests. This is due to vibrations and noise appearing in the system at those high frequencies, which diminishes the quality of the signals measured. Qualitatively, the results obtained are representative of the behaviour of muscle tissue; quantitatively, however, results are not as accurate as tests performed at lower frequencies.

4.5.4 Modelling of muscle viscoelastic properties using the QLV theory

The quasi-linear viscoelastic theory developed by Fung remains the most widely used approach to represent soft tissue viscoelasticity. The applicability of this model (in a discretised form) to represent skeletal muscle viscoelastic properties was therefore investigated. The model proposed is an extension with Prony series of the SYM model, which successfully represents the nonlinear elastic, transversely isotropic properties of muscle tissue (Chapter 3).

A unidirectional approach was first investigated; fitting of the model was performed individually for each orientation of the muscle fibres considered. A five term Prony series was adopted for the viscoelastic formulation. The viscoelastic time constants were fixed at 0.6, 6, 30, 60 and 300s; the multiplicative viscoelastic parameters were calculated by simultaneous fitting to relaxation data obtained at compression rates of 0.5, 1 and $10\%s^{-1}$.

Results show that the model provides a good fit to the data considered as well as a good prediction of muscle behaviour at rates of 0.05 and $5\%s^{-1}$.

Anisotropy was then considered and a relationship between fibre orientation and viscoelastic properties was established. Using a similar approach as for muscle elastic properties, it was hypothesised that muscle viscoelastic properties are transversely isotropic. Parameters of the model were obtained by fitting to stress-relaxation data obtained in the fibre, the cross-fibre

and the 45° direction; the model was then successfully used to predict stress-relaxation behaviour at 60° from the fibre direction.

The first limitation of the model appears in the prediction of muscle relaxation behaviour at various strain levels. Results from relaxation tests performed at 10, 20 and 30% compression indicate that the rate of relaxation increases when the level of compression decreases. This cannot be captured by the model; however, the magnitude of the theoretical results remains close to experimental data.

When muscle cyclic tests are considered, the quasi-linear viscoelastic model provides good predictions of muscle behaviour for cycles of low amplitude (2%). However, when higher amplitude cycles are performed, the model cannot fully capture muscle behaviour which is nonlinear.

Finally, when higher strain rates are considered, the model is not adequate to capture the increase in stiffness observed for muscle tissue. The maximum value of stress that can be reached with the model is $\sigma_j^e = (k_{1j}\tilde{\varepsilon}_j + k_{2j}\tilde{\varepsilon}_j^2 + k_{3j}\tilde{\varepsilon}_j^3)/(1 - \sum_{i=1}^{n} p_{ij})$. Theoretically, it corresponds to the instantaneous elastic stress that would be reached if deformation was applied at an infinite rate. In practice however, the deformation rate does not have to be infinite to attain this value, the stress reached during tests performed at a rate of $10\%s^{-1}$ is close to this maximum value. Therefore, the model cannot fully capture the increase in stiffness characteristic of muscle behaviour when higher strain rates are considered.

Further improvement of the model needs to be made to address this limitation. The approach by Pioletti *et al.* (2000) is recommended for future research; an explicit strain-rate dependent term should be introduced in the quasi-linear viscoelastic SYM model proposed in order to represent adequately muscle behaviour at higher deformation rates. This approach is however not straightforward and requires further investigations which fell beyond the timeframe of this thesis.

4.5.5 Modelling of muscle viscoelastic properties using a nonlinear viscoelastic model

Finally, a nonlinear viscoelastic approach was envisaged to capture the nonlinearities observed during high amplitude cyclic tests. The basis of this formulation remains the extension of the SYM formulation with a five terms Prony series. Compared to the quasi-linear model, two strain dependent terms were introduced; one acting on the amplitude of the viscoelastic components and the other one acting on the value of the viscoelastic time constants.

The model provides a good fit to the experimental data and is able to capture the nonlinear behaviour observed during high amplitude cyclic tests.

When cyclic tests performed at higher frequencies (5 to 80Hz) are considered, this model presents similar limitations as the quasi-linear model; it cannot predict the increase in stiffness observed with frequency for muscle tissue.

The nonlinear model was then used to predict muscle relaxation behaviour. The response of this nonlinear model is not as good as the response obtained with the quasi-linear model. Theoretical and experimental results remain relatively close; however, the model relaxes faster than muscle tissue and under-predicts the peak stresses reached after compression. This is due to the influence of the nonlinear term, which reduces the value of the relaxation constants at higher compression levels

The limitation concerning the strain rate dependency is also present with this formulation and requires the introduction of an additional strain-rate dependent term at higher compression rates.

Chapter 5 - Conclusions

5.1 MAIN EXPERIMENTAL RESULTS OF THE THESIS 180

5.2 MODEL PROPOSED TO REPRESENT SKELETAL MUSCLE BEHAVIOUR IN COMPRESSION 184

5.3 GUIDELINES FOR FUTURE WORK 188

5.4 CONCLUDING REMARK 189

5.1 Main experimental results of the thesis

This thesis was aimed to further advance the knowledge of passive skeletal muscle properties in compression. The stated objectives (chapter 1) were to provide an experimental as well as a mathematical characterisation of passive skeletal muscle properties under compressive loading.

Given the paucity of published data concerning muscle compressive behaviour and the complexity of skeletal muscle structure and physiological behaviour, a fundamental experimental approach was adopted. Only the passive properties of the tissue were considered; tests were performed *in vitro* using specimens with regular geometry; all samples were obtained from animals of the same species, age and gender; the same muscle was considered in each subject. These experimental restrictions were addressed in the discussion chapters; they brought limitations in the results obtained but also led to reliable data, presenting small variations.

The mechanical properties of the tissue were investigated using uniaxial unconfined compression tests performed up to 30% deformation, at various orientations of the muscle fibres and various compression rates. These parameters were varied to characterise the nonlinearity and anisotropy of skeletal muscle elastic and viscoelastic properties in compression.

Tests performed at the quasi-static rate of $0.05\%s^{-1}$ showed that the elastic compressive behaviour of muscle tissue is nonlinear, transversely isotropic with the axis of symmetry running along the direction of the muscle fibres. The stiffest characteristics are observed in the cross-fibre direction of the tissue and the most compliant properties are observed at 45° from the fibre direction, due to low shearing properties (Figure 5-1).

Significant differences in stiffness appear between the three orientations considered; muscle tissue is strongly anisotropic and it is therefore important to consider this anisotropy when modelling muscle elastic properties.

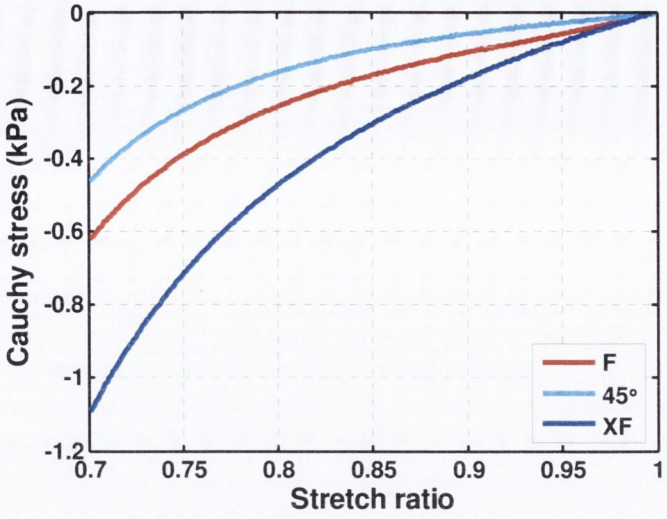


Figure 5-1: Elastic properties of fresh porcine muscle tissue under compressive loading in three orientations of the muscle fibres.

Little data are available in the literature to compare and validate the results obtained in this work. Data published on muscle properties appear however to be stiffer than the properties measured in this thesis on fresh porcine tissue. Amongst other parameters, this could be attributed to the young age of the animals used for the tests and this factor should be further investigated in future.

Tests performed at compression rates ranging from 0.05 to 10%s^{-1} answered one of the questions raised at the beginning of this project concerning the significance of deformation rate on muscle mechanical properties. During these tests, a stiffening effect with compression rate was observed in all directions of testing (Figure 5-2). This stiffening is due to the viscoelastic component which plays a significant role on muscle mechanical behaviour from a very low compression rate as illustrated in Figure 5-3.

Skeletal muscle viscoelastic properties must therefore be taken into account when modelling the tissue behaviour, even in applications where strain rates remain small (e.g. modelling of surgical procedures).

Figure 5-3 also illustrates that the influence of the viscoelastic component is greater in directions closer to the muscle fibres; skeletal muscle also presents anisotropic viscoelastic behaviour.

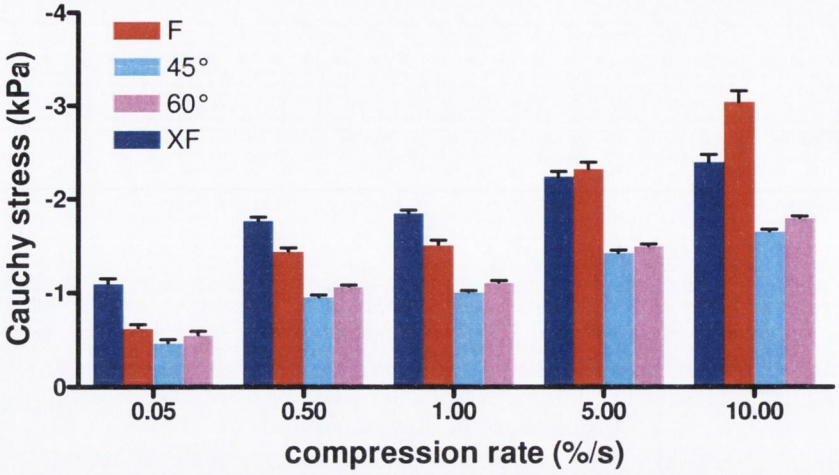


Figure 5-2: Evolution with deformation rate of the stress reached after 30% compression in various orientations of the muscle fibres.

Mean values with standard deviations.

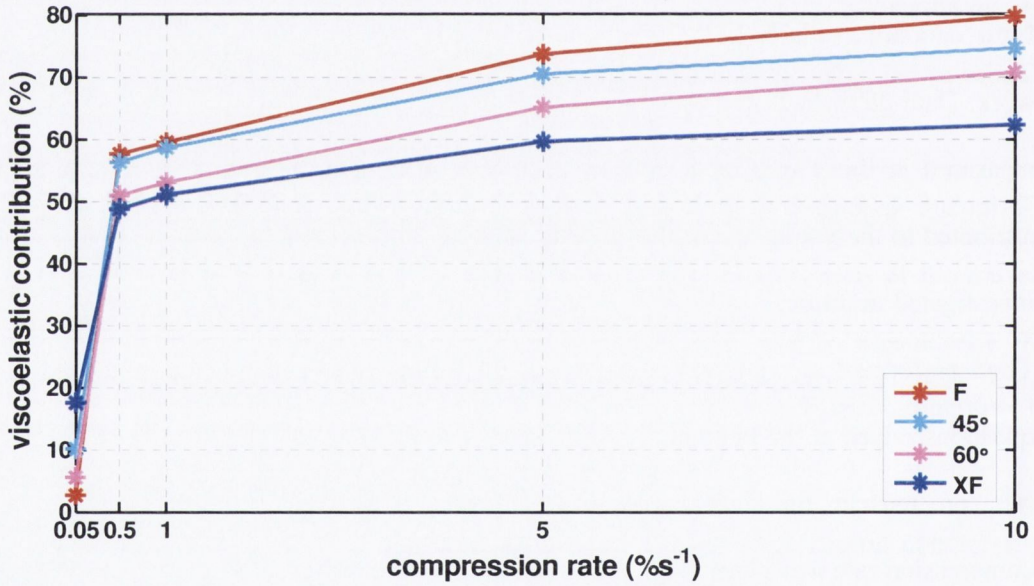


Figure 5-3: Relative contribution of the viscoelastic component to the total stress reached at 30% compression at various compression rates and fibre orientations.

Muscle relaxation behaviour was also investigated. A substantial amount of stress-relaxation occurred when deformation was held constant after a compressive ramp, with the main relaxation happening within the first 100s after the ramp.

Results indicated that muscle relaxation behaviour was independent of compression rate. A dependency on compression level was however observed; the rate of relaxation increased

(moderately) when the level of compression decreased; similar behaviour has previously been observed for ligaments but no satisfactory explanation has yet been provided.

Under low amplitude, low frequency cyclic deformation, muscle tissue displayed a linear viscoelastic behaviour. When higher amplitude cycles and higher frequencies were considered, nonlinearity was however observed in the tissue behaviour.

Cyclic stress relaxation and hysteresis characterised the tissue response during these tests. An increase in the amplitude of the stress cycles with an increase in frequency was also observed during the 10% amplitude tests cyclic tests which were performed at frequencies of 0.22, 0.44, 5, 20 and 80 Hz, corresponding to compression rates of 5, 10, 200%s^{-1}, 800%s^{-1} and 3200%s^{-1} (see Figure 5-4).

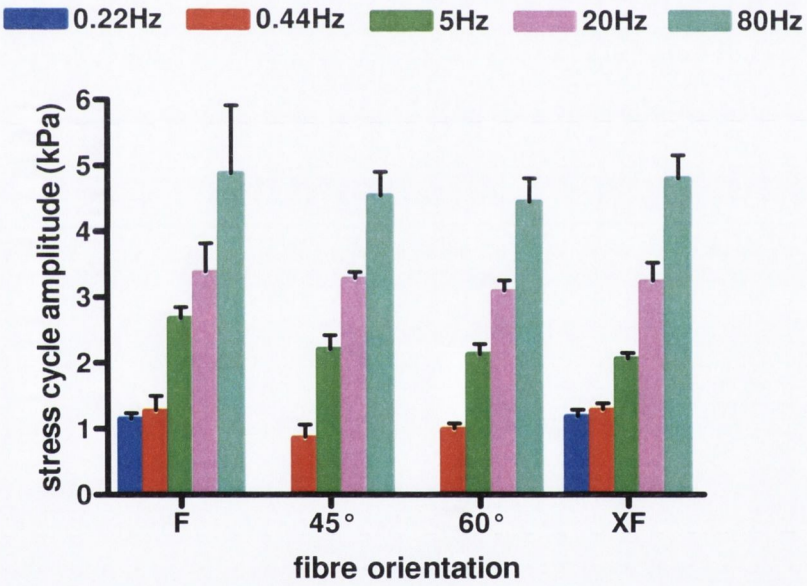


Figure 5-4: Evolution of the stress cycle amplitude with frequency for 10% amplitude cyclic tests performed on fresh porcine muscle samples (values taken after cyclic relaxation).

In order to globally characterise the stress increase observed for muscle tissue with compression rate, data obtained in this thesis during single ramp and cyclic compression tests, as well as data obtained at very high strain rates by Song *et al.* (at press) were considered. The relative increase in stress was calculated, taking the value of stress obtained at the quasi-static rate of 0.05%s^{-1} as a reference (see section 4.5.2 for details). Figure 5-5

presents the results of this comparison. Even though different types of tests were performed, an almost continuous evolution is observed in the stress increase. Figure 5-5 shows that skeletal muscle behaviour depends strongly on the rate of deformation applied; this dependency becomes even more significant than the compression rate increases.

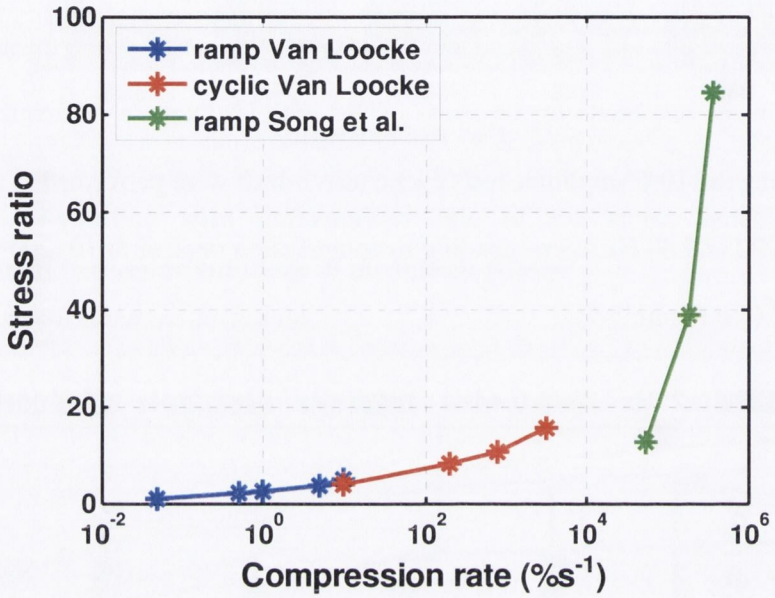


Figure 5-5: Relative increase in stress with compression rate for skeletal muscle tissue. *Values calculated from tests performed in this thesis (compressive ramp — and cyclic —) and compression tests by Song et al. (In Press) —.*

5.2 Model proposed to represent skeletal muscle behaviour in compression

Results obtained during quasi-static tests indicate that skeletal muscle has transversely isotropic elastic properties. The model proposed to represent these properties is a nonlinear, transversely isotropic model, based on the theory of linear elasticity for transversely isotropic bodies and including strain dependent Young's moduli (SYM) to account for nonlinearities in the tissue.

The following equations characterise the SYM model:

$$\begin{vmatrix} \tilde{\varepsilon}_L \\ \tilde{\varepsilon}_T \\ \tilde{\varepsilon}_{T'} \\ \tilde{\varepsilon}_{LT} \\ \tilde{\varepsilon}_{LT'} \\ \tilde{\varepsilon}_{TT'} \end{vmatrix} = \boldsymbol{K} \begin{vmatrix} \sigma_L \\ \sigma_T \\ \sigma_{T'} \\ \sigma_{LT} \\ \sigma_{LT'} \\ \sigma_{TT'} \end{vmatrix} \tag{5-1}$$

$$\text{with} \quad \boldsymbol{K} = \begin{vmatrix} 1/E_L & -\nu_{TL}/E_T & -\nu_{TL}/E_T & 0 & 0 & 0 \\ -\nu_{LT}/E_L & 1/E_T & -\nu_{TT}/E_T & 0 & 0 & 0 \\ -\nu_{LT}/E_L & -\nu_{TT}/E_T & 1/E_T & 0 & 0 & 0 \\ 0 & 0 & 0 & 1/(G_{LT}) & 0 & 0 \\ 0 & 0 & 0 & 0 & 1/(G_{LT}) & 0 \\ 0 & 0 & 0 & 0 & 0 & 2*(1+\nu_{TT})/E_T \end{vmatrix} \tag{5-2}$$

$$E_L = k_{1L} + k_{2L}\tilde{\varepsilon}_L + k_{3L}\tilde{\varepsilon}_L^{\,2} \quad \text{and} \quad E_T = k_{1T} + k_{2T}\tilde{\varepsilon}_T + k_{3T}\tilde{\varepsilon}_T^{\,2} \tag{5-3}$$

and

$$\frac{1}{G_{LT}} = \frac{4}{E_{45}} - \frac{1-2\nu_{LT}}{E_L} - \frac{1}{E_T} \tag{5-4}$$

with $E_{45} = \dfrac{\sigma_{45}}{\tilde{\varepsilon}_{45}}$

Model parameters corresponding to fresh porcine muscle tissue are presented in Table 5-1. This model provides a very good fit to the data in the cross-fibre direction, the fibre direction and at 45° from the fibre direction. It also yields a very good prediction of muscle behaviour at 30° and 60° from the fibre direction.

Table 5-1: Parameters for the SYM model fitted on fresh porcine data

k_{1L} (kPa)	k_{2L} (kPa)	k_{3L} (kPa)	k_{1T} (kPa)	k_{2T} (kPa)	k_{3T} (kPa)
1.31	3.89	14.28	1.68	1.18	14.13
k_{145} (kPa)	k_{245} (kPa)	k_{345} (kPa)	$\nu_{LT} = \nu_{LT'}$	$\nu_{TT'}$	ν_{TL}
0.66	2.09	10.73	0.50	0.65	0.36

In order to account for the tissue viscoelatic properties, a discretised quasi-linear viscoelastic approach was adopted and the SYM model was extended with Prony series. Using a similar approach as for muscle elastic properties, it was hypothesised that muscle viscoelastic properties were transversely isotropic.

The formulation developed is summarised by the equations presented below.

The Cauchy stress in direction j is defined as:

$$\sigma_j(t) = E_j \tilde{\varepsilon}_j(t) + \int_0^t E_j^v \frac{\partial \tilde{\varepsilon}_j(\tau)}{\partial \tau} d\tau \tag{5-5}$$

with

$$E_j = k_{1j} + k_{2j}\tilde{\varepsilon}_j + k_{3j}\tilde{\varepsilon}_j^2 \tag{5-6}$$

$$E_j^v = \sum_{i=1}^{5} \frac{p_{ij}}{p_{\infty j}} \exp\left(\frac{-(t-\tau)}{\tau_{ij}}\right) \frac{\partial \sigma_{\infty j}[\tilde{\varepsilon}_j(\tau)]}{\partial \tilde{\varepsilon}_j(\tau)} \tag{5-7}$$

$$\frac{1}{G_{LT}^v} = \frac{4}{E_{45}^v} - \frac{1-2\nu_{LT}}{E_L^v} - \frac{1}{E_T^v} \tag{5-8}$$

$p_{\infty j} = 1 - \sum_{i=1}^{N} p_{ij}$ and $\sigma_{\infty j} = p_{\infty j}\sigma_j^e = k_{1j}\tilde{\varepsilon}_j + k_{2j}\tilde{\varepsilon}_j^2 + k_{3j}\tilde{\varepsilon}_j^3$.

A five term Prony series was adopted for the viscoelastic formulation. The viscoelatic time constants τ_{ij} were fixed at 0.6, 6, 30, 60 and 300s and the multiplicative viscoelatic parameters p_{ij} were calculated by simultaneous fitting to stress-relaxation data obtained at compression rates of 0.5, 1 and 10%s^{-1}. Parameters of the fitting corresponding to fresh porcine muscle tissue are presented in Table 5-2 for fibre, cross-fibre and 45° data.

Table 5-2: Parameters for the quasi-linear SYM model fitted on fresh porcine data

k_{1L} (kPa)	k_{2L} (kPa)	k_{3L} (kPa)	p_{1L}	p_{2L}	p_{3L}	p_{4L}	p_{5L}
1.005	2.989	10.985	0.465	0.200	0.057	0.066	0.089
k_{1T} (kPa)	k_{2T} (kPa)	k_{3T} (kPa)	p_{1T}	p_{2T}	p_{3T}	p_{4T}	p_{5T}
1.293	0.911	10.869	0.467	0.120	0.026	0.100	0.056
k_{145} (kPa)	k_{245} (kPa)	k_{345} (kPa)	p_{145}	p_{245}	p_{345}	p_{445}	p_{545}
0.510	1.611	8.254	0.419	0.200	0.057	0.072	0.088

A phenomenological approach was used here; the model proposed describes the overall behaviour of muscle tissue by means of mathematical equations which are not related to the microstructure of the material. This type of approach has the advantage of being relatively

simple and easy to implement; it presents however limitations when modelling complex structures such as skeletal muscles in various loading conditions.

Very good agreement between theoretical and experimental results was obtained with this model for what concerns stress-relaxation and low amplitude cyclic tests. When muscle tissue was submitted to cycles of higher amplitudes, the model presented poorer predictive capabilities due to the nonlinearities displayed by the tissue.

Nonlinearities were therefore introduced in the model by means of two additional strain-dependent terms. In this model, the Cauchy stress in direction j is defined as:

$$\sigma_j(t) = p_{\infty j}\sigma_j^e(t) + h_j(\tilde{\varepsilon}_j)\sum_{i=1}^{N}\int_0^t p_{ij}\exp\left(\frac{-(\xi_j - \xi_j')}{\tau_{ij}}\right)\frac{\partial\sigma_j^e[\tilde{\varepsilon}_j(\tau)]}{\partial\tau}d\tau \qquad (5\text{-}9)$$

with

$$\begin{cases} \xi_j = \int_0^t \dfrac{dt'}{a_j[\tilde{\varepsilon}_j(t')]} \\ h_j(\tilde{\varepsilon}_j) = h_{1j}\tilde{\varepsilon}_j + h_{2j}\tilde{\varepsilon}_j^2 \\ a_j(\tilde{\varepsilon}_j) = 1 - h_{1j}\tilde{\varepsilon}_j + h_{2j}\tilde{\varepsilon}_j^2 \end{cases} \qquad (5\text{-}10)$$

Parameters of the model were obtained by fitting to cyclic data and are presented in Table 5-3. Compared to the QLV formulation, p_{ij} were the only parameters modified; $h_{ij} = a_{ij}$ were added parameters.

Table 5-3: Parameters for the nonlinear viscoelastic SYM model fitted on fresh porcine data

h_{1L} (kPa)	h_{2L} (kPa)	p_{1L}	p_{2L}	p_{3L}	p_{4L}	p_{5L}
2.337	12.532	0.374	0.285	0.077	0.078	0.101
h_{1T} (kPa)	h_{2T} (kPa)	p_{1T}	p_{2T}	p_{3T}	p_{4T}	p_{5T}
0.858	9.771	0.097	0.532	0.072	0.000	0.086

This model captured well the nonlinearities observed during high amplitude cyclic tests. The predictions obtained for muscle relaxation behaviour are however poorer than with the quasi-linear approach.

This illustrates again the limitations of the phenomenological approach. The model should therefore be chosen depending on the application and the loading conditions to which the material is submitted.

Finally, the models proposed (quasi-linear or nonlinear) are not able in their current form to fully capture the increase in stiffness characteristic of muscle behaviour when high deformation rates are considered. The addition of an explicit strain-rate dependent term in both models could be an answer to this limitation; however, this is not straightforward and further investigations are required on this point.

5.3 Guidelines for future work

This study has provided new information on skeletal muscle compressive behaviour. Numerous questions have however been raised and remain unanswered. As George Bernard Shaw once said, "*Science never solves a problem without creating ten more.*"

Experimentally, the most challenging aspect of future research will probably be to relate data on animal muscle to human skeletal muscle. Due to the difficulties involved with tests on human tissue, most available data has been obtained on animal muscle. It is well known that differences in muscle properties exist between species. However, differences have also been observed between subjects of the same species and between muscles of the same subject. These variations usually concern the quantitative and not the qualitative behaviour of the tissue, which is related to its structure and is essentially the same for all skeletal muscles. Variations in fibre size or amount of connective tissue present in a specific muscle could explain the differences observed and it would therefore be advantageous to relate skeletal muscle mechanical properties to a structural parameter such as fibre size. This could help bring together past and future research on muscle mechanical behaviour.

Non-invasive techniques, combining *in vivo* measurement of deformation (using MRI for example) and finite element modelling, are probably the most promising tools to obtain accurate information on the behaviour of human skeletal muscle in living conditions. In view of this, one of the future tasks to be performed should be the finite element implementation

of the model proposed. Using the recursive method presented in chapter 2, the implementation of the discretised formulation developed should not present great difficulties. From a modelling point of view, efforts should also be made to further improve the model proposed for applications where high deformation rates are envisaged. On this point of view, it would also be interesting to perform further experiments to characterise muscle behaviour at high compression rates and fill in the gap shown on Figure 5-5 between rates of 3.10^3 and 5.10^4 $\%s^{-1}$.

Finally, the consideration of muscle active properties also leads to a new area of investigations concerning muscle compressive behaviour. Much stiffer properties are observed in tension when skeletal muscle is activated. Does this increase in stiffness influence the transverse isotropy observed in the passive tissue? Does the viscoelastic component still play a significant role in muscle behaviour when activated? How can these changes be modelled?

Despite the advance made in this thesis, the knowledge of skeletal muscle compressive properties still remains unsatisfactory, and numerous perspectives are therefore opened to further investigate the mechanical behaviour of this complex structure.

5.4 Concluding remark

The author of this thesis hopes that useful information has been provided on the behaviour of skeletal muscle under compression and that this information will find adequate use in applications where more accurate human body models are required.

The data presented in this thesis were obtained from tests performed on young porcine skeletal muscle. Given the similarities in structure between human and porcine muscular tissue, it is believed that the model proposed will successfully represent the qualitative behaviour of human muscle. Quantitatively, however, the parameters provided for the model might not be adequate for human muscles. Further efforts should therefore be dedicated to relate animal and human muscle properties, and eventually establish scaling factors relating muscle mechanical behaviour to parameters such as age, muscle type and species.

Finally, the author also hopes that the need to attain more repeatable data and perform more uniform investigations concerning soft tissue properties has been demonstrated and that this thesis will inspire future research on the mechanical properties of soft tissues.

References

Abramowitch, S. D., Woo, S. L. Y., 2004. An improved method to analyze the stress relaxation of ligaments following a finite ramp time based on the quasi-linear viscoelastic theory. Journal of Biomechanical Engineering 126, 92-97.

Abramowitch, S. D., Woo, S. L. Y., Clineff, T. D., Debski, R. E., 2004. An evaluation of the quasi-linear viscoelastic properties of the healing medial collateral ligament in a goat model. Annals of Biomedical Engineering 32, 329-335.

Aimedieu, P., Jr., Mitton, D., Faure, J. P., Denninger, L., Lavaste, F., 2003. Dynamic stiffness and damping of porcine muscle specimens. Medical Engineering & Physics 25, 795-799.

Bensamoun, S. F., Ringleb, S. I., Littrell, L., Chen, Q., Brennan, M., Ehman, R. L., An, K. N., 2006. Determination of thigh muscle stiffness using magnetic resonance elastography. Journal of Magnetic Resonance Imaging 23, 242-247.

Best, T. M., McElhaney, J., Garrett, W. E., Jr., Myers, B. S., 1994. Characterization of the passive responses of live skeletal muscle using the quasi-linear theory of viscoelasticity. Journal of Biomechanics 27, 413-419.

Bischoff, J., 2006. Reduced Parameter Formulation for Incorporating Fiber Level Viscoelasticity into Tissue Level Biomechanical Models. Annals of Biomedical Engineering, 1-9.

Boltzmann, L. 1874. Zur Theorie der elastischen Nachwirkung. Sitzungsberichte der Akademie der Wissenschaften II 70, 275-306.

Bonifasi-Lista, C., Lake, S. P., Small, M. S., Weiss, J. A., 2005. Viscoelastic properties of the human medial collateral ligament under longitudinal, transverse and shear loading. Journal of Orthopaedic Research 23, 67-76.

Borelli, G.A., 1681-1682: 'De motu animalum', On the movement of animals. Translated into English by Paul Mayet, Springer Berlin, 1989.

Bosboom, E. M. H., Thomassen, J. A. M., Oomens, C. W. J., Bouten, C. V. C., Baaijens, F. P. T., 2001a. A numerical experimental approach to determine the transverse mechanical properties of skeletal muscle. In: Middleton, J., Jones, M. L., Shrive, N. G. (Eds.), Computer Methods in Biomechanics and Biomedical Engineering-3. Gordon and Breach Sciences Publishers, 187-192.

Bosboom, E. M., Hesselink, M. K., Oomens, C. W., Bouten, C. V., Drost, M. R., Baaijens, F. P., 2001b. Passive transverse mechanical properties of skeletal muscle under in vivo compression. Journal of Biomechanics 34, 1365-1368.

Brouwer, I., Ustin, J., Bentley, L., Sherman, A., Dhruv, N., Tendick, F., 2001. Measuring in vivo animal soft tissue properties for haptic modeling in surgical simulation. In: Proceedings of Medicine Meets Virtual Reality, IOS Press, 69-74

Brown, I. E., Scott, S. H., Loeb, G. E., 1996. Mechanics of feline soleus: II. Design and validation of a mathematical model. Journal of Muscle Research and Cell Motility 17, 221-233.

Butchal, F., Kaiser, E., Rosenfalk, P., 1951. The rheology of the cross-striated muscle fibre with particular reference to isotonic conditions. Danske Biologiske Meddeleser 21, 1-318.

Chen, D. T., Zeltzer, D., 1992. Pump It Up: Computer animation of a biomechanically based model of the muscle using the finite element method. Computer Graphics 26, 89-98.

Chiba, M., Komatsu, K., 1993. Mechanical responses of the periodontal ligament in the transverse section of the rat mandibular incisor at various velocities of loading in vitro. Journal of Biomechanics 26, 561-570.

Close, R. I., 1972. Dynamic properties of mammalian skeletal muscles. Physiological Reviews 52, 129-197.

Cole, G. K., van den Bogert, A. J., Herzog, W., Gerritsen, K. G., 1996. Modelling of force production in skeletal muscle undergoing stretch. Journal of Biomechanics 29, 1091-1104.

Davis, J., Kaufman, K. R., Lieber, R. L., 2003. Correlation between active and passive isometric force and intramuscular pressure in the isolated rabbit tibialis anterior muscle. Journal of Biomechanics 36, 505-512.

de Jager, M., 2000. Mathematical head-neck models for acceleration impacts. PhD thesis, Technische Universiteit Eindhoven, Eindhoven.

Delp, S. L., Loan, J. P., Hoy, M. G., Zajac, F. E., Topp, E. L., Rosen, J. M., 1990. An interactive graphics-based model of the lower extremity to study orthopaedic surgical procedures. IEEE Transactions on Biomedical Engineering 37, 757-767.

Deng, Y. C., Goldsmith, W., 1987. Response of a human head/neck/upper-torso replica to dynamic loading-I. Physical model. Journal of Biomechanics 20, 471-86.

Doehring, T. C., Carew, E. O., Vesely, I., 2004. The effect of strain rate on the viscoelastic response of aortic valve tissue: a direct-fit approach. Annals of Biomedical Engineering 32, 223-232.

Dortmans, L. J., Sauren, A. A., Rousseau, E. P., 1984. Parameter estimation using the quasi-linear viscoelastic model proposed by Fung. Journal of Biomechanical Engineering 106, 198-203.

Dresner, M. A., Rose, G. H., Rossman, P. J., Muthupillai, R., Manduca, A., Ehman, R. L., 2001. Magnetic resonance elastography of skeletal muscle. Journal of Magnetic Resonance Imaging 13, 269-276.

Forbes, P. A., Cronin, D. S., Deng, Y. C., Boismenu, M., 2005. Numerical human model to predict side impact thoracic trauma. In: Gilchrist, M.D. (Ed.), IUTAM Symposium on Impact Biomechanics: From Fundamental Insights to Applications. Springer, New York, 441-450.

Forcinito, M., Epstein, M., Herzog, W., 1998. Can a rheological muscle model predict force depression/enhancement? Journal of Biomechanics 31, 1093-1099.

Fung, Y. C., 1972. Stress-strain-history relations of soft tissues in simple elongation. In: Fung, Y. C., Perrone, N., Anliker, M. (Eds.), Biomechanics: Its foundations and objectives. Prentice-Hall, Englewood Cliffs, NJ.

Fung, Y. C., 1993. Biomechanics: Mechanical properties of living tissues. Springer-Verlag, New York.

Gareis, H., Solomonow, M., Baratta, R., Best, R., D'Ambrosia, R., 1992. The isometric length-force models of nine different skeletal muscles. Journal of Biomechanics 25, 903-916.

Gennisson, J. L., Cornu, C., Catheline, S., Fink, M., Portero, P., 2005. Human muscle hardness assessment during incremental isometric contraction using transient elastography. Journal of Biomechanics 38, 1543-1550.

Goh, S. M., Charalambides, M. N., Williams, J. G., 2004. Determination of the constitutive constants of non-linear viscoelastic materials. Mechanics of Time-Dependent Materials 8, 255-268.

Grieve, A. P., Armstrong, C. G., 1988. Compressive properties of soft tissues. In: de Groot, G., Hollander, A. P., Huijing, P. A., van Ingen Schenau, G. J. (Eds.), Biomechanics XI-A. International series on biomechanics. Free University Press, Amsterdam, pp. 531-536.

Guccione, J. M., Moonly, S. M., Wallace, A. W., Ratcliffe, M. B., 2001. Residual stress produced by ventricular volume reduction surgery has little effect on ventricular function and mechanics: a finite element model study. Journal of Thoracic and Cardiovascular Surgery 122, 592-599.

Haut, R. C., Little, R. W., 1972. A constitutive equation for collagen fibers. Journal of Biomechanics 5, 423-430.

Hawkins, D., Bey, M., 1994. A comprehensive approach for studying muscle-tendon mechanics. Journal of Biomechanical Engineering 116, 51-55.

Hawkins, D., Bey, M., 1997. Muscle and tendon force-length properties and their interactions in vivo. Journal of Biomechanics 30, 63-70.

Herzog, W., Kamal, S., Clarke, H. D., 1992. Myofilament lengths of cat skeletal muscle: theoretical considerations and functional implications. Journal of Biomechanics 25, 945-948.

Herzog, W. (Ed.), 2000. Skeletal muscle mechanics: from mechanisms to function. Chichester : Wiley.

Herzog, W., Leonard, T. R., 2000. The history dependence of force production in mammalian skeletal muscle following stretch-shortening and shortening-stretch cycles. Journal of Biomechanics 33, 531-42.

Hill, A. V., 1938. The heat of shortening and the dynamic constants of muscle. Proceedings of the Royal Society (London) 126, 136-195

Hof, A. L., Van den Berg, J., 1981. EMG to force processing I: An electrical analogue of the Hill muscle model. Journal of Biomechanics 14, 747-758.

Holzapfel, G. A., 2000. Nonlinear Solid Mechanics. A continuum approach for engineering. John Wiley & Sons Ltd, Chichester.

Holzapfel, G. A., Gasser, T. C., Stadler, M., 2002. A structural model for the viscoelastic behavior of arterial walls: Continuum formulation and finite element analysis. European Journal of Mechanics A/Solids 21, 441-463.

Holzapfel, G. A., Sommer, G., Regitnig, P., 2004. Anisotropic Mechanical Properties of Tissue Components in Human Atherosclerotic Plaques. Journal of Biomechanical Engineering 126, 657-665.

Huijing, P. A., 1999. Muscle as a collagen fiber reinforced composite: a review of force transmission in muscle and whole limb. Journal of Biomechanics 32, 329-45.

Humphrey, J. D., Yin, F. C. P., 1987. On constitutive relations and finite deformations of passive cardiac tissue. I. A pseudostrainenergy function. Journal of Biomechanical Engineering 109, 298-304.

Humphrey, J. D., Strumpf, R. K., Yin, F. C., 1990. Determination of a constitutive relation for passive myocardium: I. A new functional form. Journal of Biomechanical Engineering 112, 333-339.

Huxley, A. F., 1980. Reflections on muscle. Liverpool University Press, Liverpool.

Kardel, T., 1990. Niels Stensens geometrical theory of muscle contractions (1667): A Reappraisal. Journal of Biomechanics 23, 953-965.

Keeve, E., Girod, S., Kikinis, R., Girod, B., 1998. Deformable Modeling of Facial Tissue for Craniofacial Surgery Simulation. Computer Aided Surgery 3, 228-238.

Kjær, M., 2004. Role of Extracellular Matrix in Adaptation of Tendon and Skeletal Muscle to Mechanical Loading. Physiological Reviews 84, 649–698.

Krouskop, T. A., Muilenberg, A. L., Dougherty, D. R., Winningham, D. J., 1987. Computer-aided design of a prosthetic socket for an above-knee amputee. Journal of Rehabilitation Research and Development 24, 31-38.

Kwan, M. K., Lin, T. H., Woo, S. L., 1993. On the viscoelastic properties of the anteromedial bundle of the anterior cruciate ligament. Journal of Biomechanics 26, 447-52.

Lanir, Y., 1980. A microstructure model for the rheology of mammalian tendon. Journal of Biomechanical Engineering 102, 332-339.

Lekhnitskii, S. G., 1981. Theory of elasticity of an anisotropic body. Mir Publishers, Moscow.

Lemaitre, J., Chaboche, J.-L., 1990. Mechanics of Solid Materials. Cambridge University Press, Cambridge.

Li, J., Luo, X. Y., Kuang, Z. B., 2001. A nonlinear anisotropic model for porcine aortic heart valves. Journal of Biomechanics 34, 1279-1289.

Limbert, G., Middleton, J., 2004. A transversely isotropic viscohyperelastic material: Application to the modeling of biological soft connective tissues. International Journal of Solids and Structures 41, 4237-4260.

Lyon, R. M., Lin, H. C., Kwan, M. K., Hollis, W., Akeson, J. M., Woo, S. L.-Y., 1988. Stress relaxation of the anterior cruciate ligament and the patellar tendon. Transactions of the Orthopaedic Research Society 13, 81

MADYMO User's Manuals, Version 6.0., 2001. TNO Crash-Safety Research Center, Delft, The Netherlands.

Mak, A. F. T., Liu, G. H. W., Lee, S. Y., 1994. Biomechanical assessment of below-knee residual limb tissue. Journal of Rehabilitation Research and Development 31(3), 188-198.

Martins, J. A. C., Pires, E. B., Salvado, R., Dinis, P. B., 1998. A numerical model of passive and active behavior of skeletal muscles. Computer Methods in Applied Mechanics and Engineering 151, 419-433.

Martins, P. A. L. S., Jorge, R. M. N., Ferreira, A. J. M., 2006. A comparative study of several material models for prediction of hyperelastic behavior of silicone-rubber. Strain 42, 135-147.

Maurel, W., Wu, Y., Magnenat Thalmann, N., Thalmann, D., 1998. Biomechanical Models for Soft Tissue Simulation. Springer, Berlin

McElhaney, J. H., 1966. Dynamic response of bone and muscle tissue. Journal of Applied Physiology 21, 1231-1236.

Miller-Young, J. E., Duncan, N. A., Baroud, G., 2002. Material properties of the human calcaneal fat pad in compression: experiment and theory. Journal of Biomechanics 35, 1523-1531.

Miller, K., 1999. Constitutive model of brain tissue suitable for finite element analysis of surgical procedures. Journal of Biomechanics 32, 531-537.

Miller, K., Chinzei, K., 1997. Constitutive modelling of brain tissue: Experiment and theory. Journal of Biomechanics 30, 1115-1121.

Miller, K., Chinzei, K., 2002. Mechanical properties of brain tissue in tension. Journal of Biomechanics 35, 483-490.

Mow, V. C., Kuei, S. C., Lai, W. M., Armstrong, C. G., 1980. Biphasic creep and stress relaxation of articular cartilage in compression? Theory and experiments. Journal of Biomechanical Engineering 102, 73-84.

Muhl, Z. F., 1982. Active length-tension relation and the effect of muscle pinnation on fiber lengthening. Journal of Morphology 173, 285-292.

Myers, B. S., McElhaney, J. H., Doherty, B. J., 1991. The viscoelastic responses of the human cervical spine in torsion: experimental limitations of quasi-linear theory, and a method for reducing these effects. Journal of Biomechanics 24, 811-817.

Nigul, I., Nigul, U., 1987. On algorithms of evaluation of Fung's relaxation function parameters. Journal of Biomechanics 20, 343-352.

Novak, V. P., Yin, F. C., Humphrey, J. D., 1994. Regional mechanical properties of passive myocardium. Journal of Biomechanics 27, 403-412.

Oden, J. T., 1972. Finite Elements of Nonlinear Continua. New York: McGraw-Hill.

Ogden, R. W., 1984. Non-linear elastic deformations. Chichester: Ellis Horwood; New York: Wiley.

Ogden, R. W., Saccomandi, G., Sgura, I., 2004. Fitting hyperelastic models to experimental data. Computational Mechanics 34, 484-502.

Oomens, C. W. J., Bressers, O. F. J. T., Bosboom, E. M. H., Bouten, C. V. C., 2001. Deformation analysis of a supported buttock contact. ASME Summer Bioengineering Conference, Snowbird, Utah, 853-854.

Pinto, J. G., Patitucci, P. J., 1980. Visco-elasticity of passive cardiac muscle. Journal of Biomechanical Engineering 102, 57-61.

Pioletti, D. P., Rakotomanana, L. R., Benvenuti, J. F., Leyvraz, P. F., 1998. Viscoelastic constitutive law in large deformations: application to human knee ligaments and tendons. Journal of Biomechanics 31, 753-757.

Pioletti, D. P., Rakotomanana, L. R., 2000. Non-linear laws for soft biological tissues. European Journal of Mechanics A/Solids 19, 749-759.

Poon, H., Ahmad, M. F., 1998. A material point time integration procedure for anisotropic, thermo rheologically simple, viscoelastic solids. Computational Mechanics V21, 236-242.

Provenzano, P., Lakes, R., Keenan, T., Vanderby, R., 2001. Nonlinear ligament viscoelasticity. Annals of Biomedical Engineering 29, 908-914.

Puso, M. A., Weiss, J. A., 1998. Finite element implementation of anisotropic quasi-linear viscoelasticity using a discrete spectrum approximation. Journal of Biomechanical Engineering 120, 62-70.

Quaglini, V., 2000. Characterization of mechanical properties and identification of constitutive parameters for soft tissues. PhD Thesis, Politecnico di Milano, Milano.

Reynolds, D. P., 1988. Shape design and interface load analysis for below-knee prosthetic sockets. PhD Thesis, University College, London. Cited from Silver-Thorn, 1996.

Rousseau, E. P. M., Sauren, A. A. H. J., van Hout, M. C., van Steenhoven, A. A., 1983. Elastic and viscoelastic material behaviour of fresh and glutaraldehyde-treated porcine aortic valve tissue. Journal of Biomechanics 16, 339-341.

Sacks, M. S., Chuong, C. J., 1993. A constitutive relation for passive right-ventricular free wall myocardium. Journal of Biomechanics 26, 1341-1345.

Sauren, A. A., van Hout, M. C., van Steenhoven, A. A., Veldpaus, F. E., Janssen, J. D., 1983. The mechanical properties of porcine aortic valve tissues. Journal of Biomechanics 16, 327-337.

Schapery, R. A., 1969. On the characterization of nonlinear viscoelastic materials. Polymer Engineering and Science 9, 295-310.

Schatzmann, L., Brunner, P., Staubli, H. U., 1998. Effect of cyclic preconditioning on the tensile properties of human quadriceps tendons and patellar ligaments. Knee Surgery, Sports Traumatology, Arthroscopy 6 Suppl 1, S56-61.

Shibata, T., Botsis, J., Bergomi, M., Mellal, A., Komatsu, K., 2006. Mechanical behavior of bovine periodontal ligament under tensioncompression cyclic displacements. European Journal of Oral Sciences 114, 74-82.

Silver-Thorn, M. B., Steege, J. W., Childress, D. S., 1996. A review of prosthetic interface stress investigations. Journal of Rehabilitation Research and Development 33, 253-266.

Silver-Thorn, M. B., 1999. In Vivo indentation of lower extremity limb soft tissues. IEEE Transactions on Rehabilitation Engineering 7(3), 268-277.

Simo, J. C., Hughes, T. J. R., 1998. Computational inelasticity. Springer, New York.

Snedeker, J. G., Niederer, P., Schmidlin, F. R., Farshad, M., Demetropoulos, C. K., Lee, J. B., Yang, K. H., 2005. Strain-rate dependent material properties of the porcine and human kidney capsule. Journal of Biomechanics 38, 1011-1021.

Stensen, N., 1667. Elementorum myologiae specimen, cited from Kardel, 1990.

Song, B., Chen, W., Weerasooriya, T. Dynamic and quasi-static compressive response of porcine muscle. Journal of Biomechanics, Article in Press.

Spencer, A. J. M., 1984. Continuum Theory of the Mechanics of Fiber Reinforced Composites. Springer-Verlag, New York.

Squire, J. M., 1990. Molecular mechanisms in muscular contraction. Basingstoke: Macmillan.

Steege, J. W., Schnur, D. S., Childress, D. S., 1987. Finite element prediction of pressure at the below-knee socket interface. In: Biomechanics of normal and prosthetic gait. ASME, New York. BED-4, 39-44.

Tanaka, T. T., Fung, Y. C., 1974. Elastic and inelastic properties of the canine aorta and their variation along the aortic tree. Journal of Biomechanics 7, 357-70.

Taylor, R. L., Pister, K. S., Goudreau, G. L., 1970. Thermomechanical analysis of viscoelastic solids. International Journal for Numerical Methods in Engineering 2, 45-59.

Ticker, J. B., Bigliani, L. U., Soslowsky, L. J., Pawluk, R. J., Flatow, E. L., Mow, V. C., 1996. Inferior glenohumeral ligament: Geometric and strain-rate dependent properties. Journal of Shoulder and Elbow Surgery 5, 269-279.

Toldrá, F., 2003. Muscle foods: water, structure and functionality. Food Science and Technology International 9(3), 173-177.

van Rooij L., Bours R., van Hoof J., Mihm J. J., Ridella S. A., Bass C. R., Crandall J. R., 2003. The development, validation and application of a finite element upper extremity model subjected to airbag loading. Stapp Car Crash Journal 47.

Van Sligtenhorst, C., Cronin, D. S., Wayne Brodland, G., 2006. High strain rate compressive properties of bovine muscle tissue determined using a split Hopkinson bar apparatus. Journal of Biomechanics 39, 1852-1858.

Vannah, W. M., Childress, D. S., 1996. Indentor tests and finite element modeling of bulk muscular tissue in vivo. Journal of Rehabilitation Research and Development 33, 239-252.

Verver, M. M., van Hoof, J., Oomens, C. W. J., Wismans, J. S. H. M., Baaijens, F. P. T., 2004. A finite element model of the human buttocks for prediction of seat pressure distributions. Computer Methods in Biomechanics and Biomedical Engineering 7, 193-203.

Vignos, P. J., Jr., Lefkowitz, M., 1959. A biochemical study of certain skeletal muscle constituents in human progressive muscular dystrophy. The Journal of Clinical Investigation 38, 873-881.

Ward, E. E., Kleinverger, M., Lennon, A. M., Roberts, J. C., 2005. Modelling the effects of blast on the human thorax using high strain rate viscoelastic properties of human tissue. In: Gilchrist, M.D. (Ed.), IUTAM Symposium on Impact Biomechanics, Springer, 17-24.

Weiss, J. A., Maker, B. N., Govindjee, S., 1996. Finite element implementation of incompressible, transversely isotropic hyperelasticity. Computational Methods in Applied Mechanics and Engineering 135, 107-128.

Weiss, J. A., Gardiner, J. C., Bonifasi-Lista, C., 2002. Ligament material behavior is nonlinear, viscoelastic and rate-independent under shear loading. Journal of Biomechanics 35, 943-950.

Winters, J. M., Stark, L., 1988. Estimated mechanical properties of synergistic muscles involved in movements of a variety of human joints. Journal of Biomechanics 21, 1027-1041.

Winters, J. M., 1990. Hill-Based Muscle Models: A Systems Engineering Perspective. In: Winters, J. M., Woo S. L.-Y. (Ed.). Multiple muscle systems: Biomechanics and movemement organization. Springer-Verlag, New York, pp. 69-93.

Woittiez, R. D., Huijing, P. A., Boom, H. B., Rozendal, R. H., 1984. A three-dimensional muscle model: a quantified relation between form and function of skeletal muscles. Journal of Morphology 182, 95-113.

Woo, S. L., Gomez, M. A., Akeson, W. H., 1981. The time and history-dependent viscoelastic properties of the canine medical collateral ligament. Journal of Biomechanical Engineering 103, 293-298.

Woo, S. L. Y., Debski, R. E., Zeminski, J., Abramowitch, S. D., Chan Saw, M. S. S. S., Fenwick, J. A., 2000. Injury and repair of ligaments and tendons. Annual Review of Biomedical Engineering 2, 83-118.

Wu, J. Z., Dong, R. G., Schopper, A. W., 2004. Analysis of effects of friction on the deformation behavior of soft tissues in unconfined compression tests. Journal of Biomechanics 37, 147-55.

Zajac, F. E., 1989. Muscle and tendon: properties, models, scaling, and application to biomechanics and motor control. Critical Reviews in Biomedical Engineering 17, 359-411.

Zheng, Y., Mak, A. F., 1999. Effective elastic properties for lower limb soft tissues from manual indentation experiment. IEEE Transactions on Rehabilitation Engineering 7, 257-267.

http://jan.ucc.nau.edu/~jrc1/exs%20490/EXS%20490%20MusSkRev1.pdf (accessed in January 2004)

http://www.visualhistology.com/Visual_Histology_Atlas , Chapter 3 (accessed in May 2006)

Appendices

The appendices are provided electronically on the cd attached at the back of the thesis. Considering the amount of data obtained in this study, the electronic format was adopted in order to reduce pages number and also to provide data in a directly usable format.

In each folder of the cd, a word document gives details on the data provided.

APPENDIX A: Quasi-static tests results – Complete data set.

APPENDIX B: Details on the dynamic testing rig

APPENDIX C: Relaxation tests results – Complete data set.

APPENDIX D: Matlab code used for the implementation of the quasi-linear viscoelastic SYM model.

APPENDIX E: Cyclic tests results – Complete data set.

APPENDIX F: Matlab code used for the implementation of the nonlininear viscoelastic SYM model.